1996

Pressure fluctuations as a diagnostic tool for fluidized beds

Ethan James Brue
Iowa State University

INFORMATION TO USERS

This manuscript has been reproduced from the microfilm master. UMI films the text directly from the original or copy submitted. Thus, some thesis and dissertation copies are in typewriter face, while others may be from any type of computer printer.

The quality of this reproduction is dependent upon the quality of the copy submitted. Broken or indistinct print, colored or poor quality illustrations and photographs, print bleedthrough, substandard margins, and improper alignment can adversely affect reproduction.

In the unlikely event that the author did not send UMI a complete manuscript and there are missing pages, these will be noted. Also, if unauthorized copyright material had to be removed, a note will indicate the deletion.

Oversize materials (e.g., maps, drawings, charts) are reproduced by sectioning the original, beginning at the upper left-hand corner and continuing from left to right in equal sections with small overlaps. Each original is also photographed in one exposure and is included in reduced form at the back of the book.

Photographs included in the original manuscript have been reproduced xerographically in this copy. Higher quality 6" x 9" black and white photographic prints are available for any photographs or illustrations appearing in this copy for an additional charge. Contact UMI directly to order.

UMI

A Bell & Howell Information Company
300 North Zeeb Road, Ann Arbor MI 48106-1346 USA
313/761-4700 800/521-0600

Pressure fluctuations as a diagnostic tool for fluidized beds

by

Ethan James Brue

A Dissertation Submitted to the

Graduate Faculty in Partial Fulfillment of the

Requirements for the degree of

DOCTOR OF PHILOSOPHY

Department: Mechanical Engineering
Major: Mechanical Engineering

Approved:

Signature was redacted for privacy.

In Charge of Major Work

Signature was redacted for privacy.

For the Major Department

Signature was redacted for privacy.

For the Graduate College

Iowa State University
Ames, Iowa

1996

TABLE OF CONTENTS

ACKNOWLEDGMENTS

I would like to thank my major professor, Dr. Robert C. Brown who has guided my research and provided instruction. Through the balance of criticism and encouragement that he has provided, I have learned much about conducting research and communicating results. I thank Professor Gerald Colver, Professor Thomas Wheelock, Professor Howard Shapiro, and Professor Alan Marcus for serving on my graduate committee. I also want to express thanks to Professor Marcus, Professor Bix, and Professor Thompson, in the department of History. I thoroughly enjoyed my introduction to the study of the history of technology that they provided. I want to express thanks to all my instructors during my Ph.D. program. They taught me the most important lesson; there is so much yet to be learned. The financial support for this study provided by the U.S. Department of Energy grant # DE-FG22-94PC94210 is gratefully acknowledged.

I wish to thank my wife Donna, for her continual love, encouragement, and help. I also want to thank my daughter Kinza. She was unaware that, by sleeping a lot, she was helping her dad finish his dissertation.

Above all, I thank God who has created this marvelous universe and has given us the ability to find joy in creating and discovering.

Soli Deo Gloria!

ABSTRACT

The goal of this research is to determine how spectral analysis of pressure fluctuations can be used as a diagnostic and design tool for both bubbling fluidized beds (BFB) and circulating fluidized beds (CFB). Static pressure fluctuations are measured from two BFB models, two CFB models, and two Pyropower CFB boilers located at the ISU power plant/cogeneration facility. Analyzing the fluctuations using spectral analysis shows that the structure of pressure fluctuations is governed by multiple phenomena. Similarities and differences between the nature of fluctuations in bubbling, turbulent, and fast fluidization regimes are discussed.

The Bode plots of pressure fluctuations under bubbling/turbulent fluidization exhibit the characteristics of an oscillatory second order system. This system is governed by a combination of voidage oscillations and surface eruptions. A theoretical model is developed to predict the frequency of oscillation in fluidized systems, and to explain the second order behavior. A comparison of pressure fluctuation behavior in two geometrically similar BFBs is conducted, which validates previously derived fluidized bed similitude parameters under most operating conditions.

Multiple second order phenomena acting concurrently also govern CFB pressure fluctuations. Phenomena similar to that proposed for BFBs governs pressure fluctuations in the lower dense regions of the CFB. A surface wave phenomena is hypothesized to govern CFB fluctuations above the lower dense bed. Similar pressure dynamics and axial voidage profiles are not observed when currently proposed similitude parameters are matched in two CFBs. By replacing the dimensionless solids flux with a dimensionless riser loading parameter, this modified set of similitude parameters can be used to establish similar hydrodynamics in CFBs . Primarily due to the periodic operation of the coal feed system in the industrial scale CFB Boiler, pressure fluctuation analysis did not result in any definitive hydrodynamic information.

CHAPTER 1. INTRODUCTION AND MOTIVATION

All technology and science come about through a distinct human activity in which the direction of the design or research reflect, in some way, the world view of the engineers or scientists involved. The direction of technological innovation mirrors societies predominant world view [1-4]. At the same time, the activity of technology and the products of technology shape our social interactions and our perceptions of the world. Technology is never neutral. Technology will always embody cultural ideologies while simultaneously augmenting the predominant systems of values and beliefs [5-9]. Understanding this symbiotic relationship between technology and society, it is important that the engineer attempt to recognize the values that motivate a project and evaluate how the end result will benefit society.

The underlying motivation for developing fluidized bed combustion technology is threefold. Fluidized bed combustion can significantly reduce coal combustion emissions harmful to the environment, without the addition of expensive pollution control equipment. Secondly, fluidized bed combustors have unique characteristics that allow for cheaper, more compact construction and lower fuel preparation costs than pulverized fuel boilers. Finally, fluidized bed combustors have the capability to effectively combust (or gasify) a wide variety of fuels from solid waste to biomass. Fluidized beds provide an excellent means of converting waste to energy and utilizing renewable solid fuels such as biomass. Exercising a concern for the environment, and practicing stewardship of finite energy resources are important as we respond to our calling as caretakers of creation. Additionally, our efforts to promote economic stewardship in power plant design should be motivated by an understanding that engineers bear partial responsibility for providing energy to the public at a justifiable and reasonable cost.

Currently, there are many unanswered questions concerning the operation of fluidized bed processes. This study will provide a better understanding of fluidization systems by focusing on the nature of BFB and CFB static pressure fluctuations. Pressure fluctuations provide hydrodynamic information on how the fluidized bed is operating, and can be used as

an easy to implement diagnostic tool in the hot reactive environment of fluidized bed combustors. Secondly, since pressure fluctuations provide important hydrodynamic information about the fluidized system, the analysis of pressure fluctuations can provide a dependent parameter for validating similitude relations in fluidized beds. The design of industrial scale fluidized bed combustors would be aided by the development of a valid set of dimensionless parameters that describes fluidization.

Measurements of static pressure fluctuations are commonly used to characterize flow regimes in fluidized beds. For example, probability density functions and power spectral density functions of pressure fluctuations have previously been employed as dependent parameters in similitude studies of BFB and CFB scale models [10-15]. Analysis of pressure fluctuations has also been the basis for claims that fluidized beds are chaotic hydrodynamic systems [16-21]. However, the origin of these pressure fluctuations has never been fully explained. Until a mechanistic model for this phenomenon is established, the usefulness of pressure measurements in describing CFB hydrodynamics is problematic. The goal of this research is to first relate these pressure fluctuations to fundamental physical processes in the bed. Using spectral analysis, a linear model of the system can be estimated that characterizes the multiple phenomena observed in bubbling fluidized bed models and in the upper and lower regions of a cold-flow CFB riser. Both mechanistic models and qualitative system descriptions are proposed to explain the pressure dynamics. From this understanding of the phenomena governing pressure fluctuation in fluidized beds, experiments are conducted to determine if pressure fluctuations verify the validity of previously proposed BFB and CFB similitude parameters.

CHAPTER 2. FLUIDIZATION BACKGROUND

Definitions and Regime Descriptions

Fluidization occurs when a fluid flows up through a bed of particles. This process gets its name from its ability to transform the bed into a fluid-like gas-solid suspension. This suspension has many of the same properties that we associate with liquids. In fluidized beds, as shown in Figure 2.1, light objects will float, the upper bed surface will remain horizontal, the bed can "leak" out of containment, and the bed will produce a hydrostatic head that depends on the weight of the bed. The onset of this suspension is a result of the balancing of gravitational and drag forces on the particles.

The establishment of fluidization provides a number of unique characteristics. Of particular interest to the engineer is the excellent gas-solid contacting and gas-solid mixing associated with fluidization. In addition to these hydrodynamic advantages, the heat transfer rates both within the bed and from the bed to any immersed surface are also very high. These high heat transfer coefficients are primarily due to the large bed surface area exposed to the fluidizing gas, allowing the bed to maintain excellent temperature uniformity. The enhanced bed-to-surface heat transfer coefficients allow for smaller heat exchangers and better control of the reactor temperature. Because of these characteristics, fluidized beds are useful for a number of chemical engineering processes such as gasification, synthesis reactions, fluid catalytic cracking, solids drying, and industrial coating methods as described in detail by Kunni [24]. Recent interest has also increased in the use of fluidized beds for a variety of combustion applications with an emphasis on solid fuels such as coal.

Fluidization can be categorized by a number of regimes which are functions of the fluid velocity (superficial velocity), as illustrated in Figure 2.2. As the superficial velocity is slowly increased through a fixed bed, the pressure drop will increase linearly until the bed reaches a state of minimum fluidization typically accompanied by some degree of bed expansion as shown in Figure 2.2b. This point of incipient or minimum fluidization is defined as the point at which the gravitational force balances the drag force on the particles. At this point, the

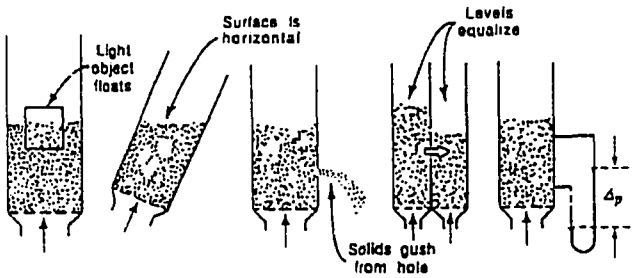

Figure 2.1: Liquid-like behavior of gas fluidized beds [24]

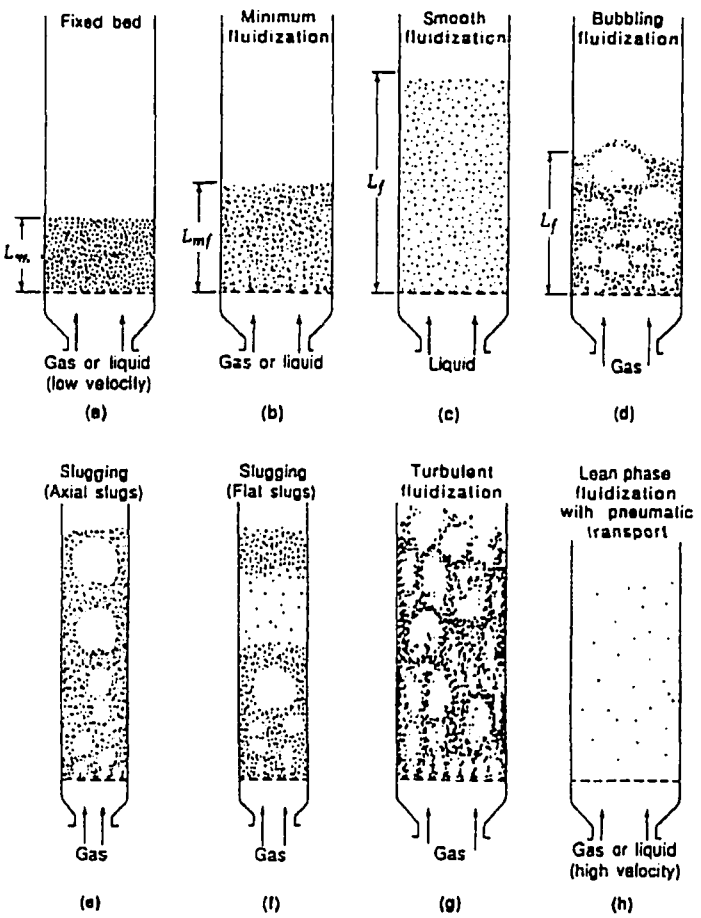

Figure 2.2: Various forms of contacting of a batch of solids by a fluid [24]

pressure drop across any section of the bed nearly equals the weight of the particles within that section for gas fluidization. Increasing the superficial velocity beyond the state of minimum fluidization will not significantly change the average pressure drop in a section from this incipient value. In gas fluidization, the increase of superficial velocity beyond the point of minimum fluidization will cause the bed to either channel, expand, or begin to bubble. Bed behavior at this incipient state is the basis for characterization of fluidized particles.

Geldart's classification of fluidized particles into four groups (A, B, C, and D) based on particle size, particle density, and the fluidizing gas density is shown in Figure 2.3. Group C particles are very fine particles that are generally cohesive and very difficult to fluidize. In many cases, rather than fluidizing the bed, the gas will create vertical jets above the distributor or will tend to develop channels through group C particles. With an increase in superficial velocity, a bed of group A particles expands significantly before the bed reaches a more unstable bubbling regime. In contrast, a bed of group B particles will typically start bubbling immediately after minimum fluidization is reached and will not result in a bed expansion. Large group D particles exhibit a spouting behavior in fluidization which for most applications is not advantageous. Figure 2.4 shows some of these characteristics of bed behavior that may occur after minimum fluidization.

The bubbling regime, illustrated in Figure 2.2d, is observed immediately following minimum fluidization for type B particles,. The magnitude of static pressure fluctuations in the bubbling regime increase significantly compared to conditions of smooth fluidization, as illustrated by Figure 2.2c. As the height of the bed increases, bubbles will grow larger as they rise to the upper bed surface due to bubble coalescence. As the superficial velocity is increased, this coalescence may increase until a bubble extends across the entire cross-section of the bed. This creates a single periodic disruption of the bed surface rather than a boiling motion across the surface. This stage of fluidization is called slugging (Figures 2.2e and 2.2f). For larger particles and higher flow velocities, a portion of the bed above a large bubble will lift up in a piston-like manner. This flat-slug behavior comprises a highly unstable oscillatory motion in the bed.

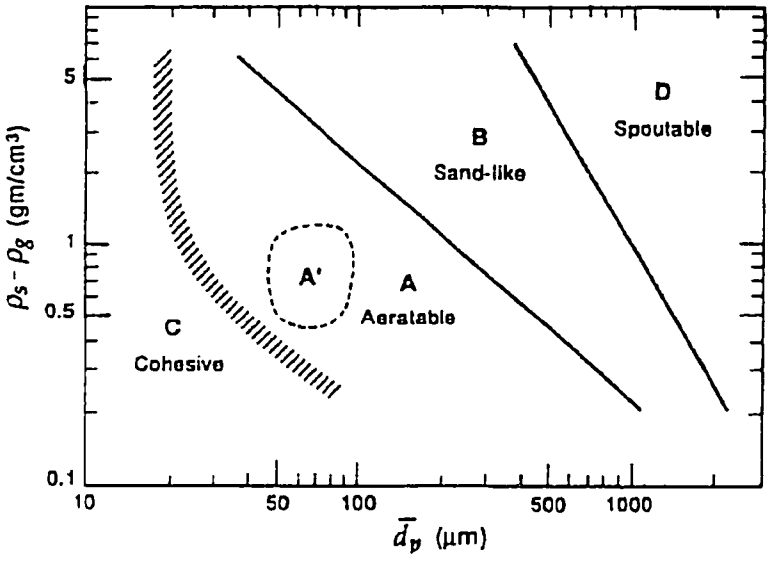

Figure 2.3: Geldart particle classification [25]

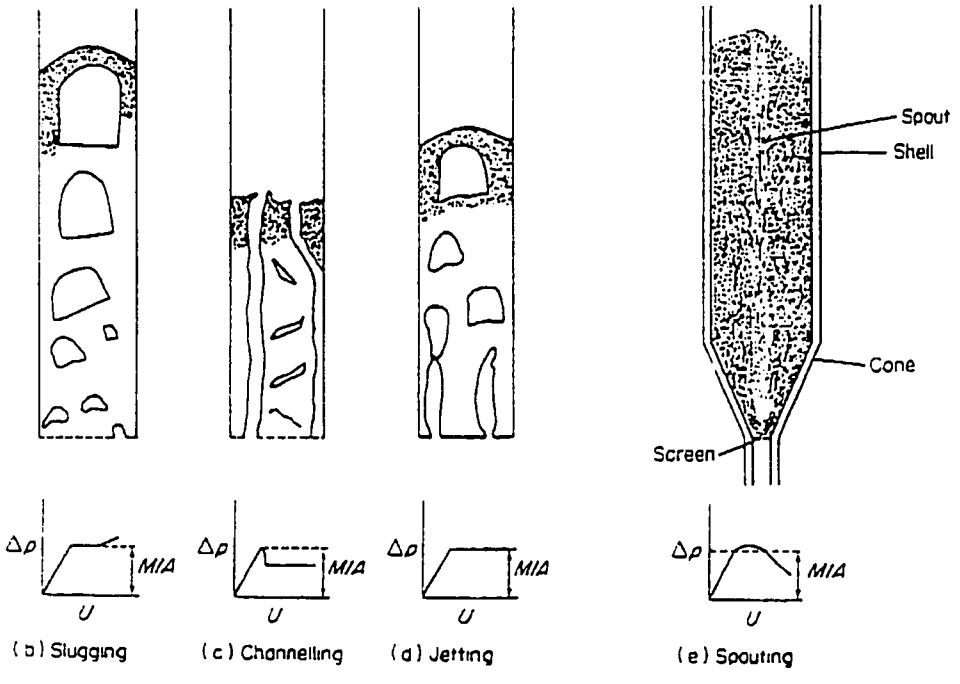

Figure 2.4: Types of fluidization [25]

At gas flow rates approaching the terminal velocity of the particles, bubbling and slugging phenomena disappear and a turbulent bed appears as illustrated in Figure 2.2g. Irregular voids and solid clusters violently mix in this regime, while finer particles may become entrained in the gas flow, leaving the bed surface. The upper surface of a turbulent bed is not well defined. Increasing the flow further for group A or B particles, a large percentage of particles become entrained in the flow and elutriate from the bed. Under these conditions, the bed can be described by one of two regimes depending on the solids loading. With a small concentration of particles in the bed, the velocity of the individual particles will be nearly equal to the difference between the single particle terminal velocity and the superficial velocity. This mode of fluidization is termed pneumatic transport (Figure 2.2h). If the solids loading is increased under these high velocity conditions, the particles will continuously form clusters or loose agglomerates in which single particles will remain inside the wake of preceding particles [26]. This group of fluidized particles has a higher terminal velocity, thus increasing the particle residence time within the bed. This fluidization regime is known as fast fluidization, which is the normal operating regime for circulating fluidized beds. A plot of the dimensionless velocity versus the dimensionless particle diameter, illustrated in Figure 2.5, provides an approximate description of these fluidization regimes. In Figure 2.5:

$$d_p^* = d_p \cdot \left[\frac{\rho_g \cdot (\rho_s - \rho_g) \cdot g}{\mu^2} \right]^{\frac{1}{3}} \quad \text{and} \quad u^* = U \cdot \left[\frac{\rho_g^{\,2}}{\mu \cdot (\rho_s - \rho_g) \cdot g} \right]^{\frac{1}{3}}$$

Circulating Fluidized Beds

A means of collecting the elutriated particles and returning them to the bed for recirculation is necessary for circulating fluidized bed operation. The primary components of a CFB are the riser, the gas-solid separator, the downcomer or standpipe, and a means of transferring particles in the standpipe back into the riser. Most methods to remove entrained particles from the gas flow of a circulating fluidized bed utilize some type of cyclone or other inertial separator. The solids recycle device is typically a non-mechanical valve system such as

a L-valve, V-valve, J-valve, loop seal, or pot seal device. Solids recycle and solids separation devices are described in detail by Basu [26]. As in bubbling fluidized beds, there are many chemical conversion applications of circulating fluidized beds. Of growing interest is the utilization of circulating fluidized beds for combustion and gasification. Circulating fluidized bed boilers in coal based power production are becoming a viable alternative to conventional stoker and pulverized boilers as a result of strict environmental regulations.

Circulating fluidized bed boilers have a number of advantages as summarized by Basu [26]. The first advantage considered by Basu is fuel flexibility. The solid fuel in a CFB boiler is typically a small fraction of the total solids concentration in the bed. As long as the bed can be sustained at a temperature higher than the ignition temperature of the fuel, the addition of the solid fuel will not decrease the temperature of the bed. The solid fuel will almost instantaneously reach its ignition temperature due to excellent mixing and heat transfer. Any fuel that has a heating value sufficient to raise the fluidizing air and the solid fuel above its ignition temperature could be used in a CFB without a secondary fuel or additional modifications. CFB boilers have a higher combustion efficiency than many conventional and bubbling fluidized bed combustors. This is due to higher burning rates, better gas-solids mixing, and the ability to recycle unburned carbon particles back into combustor. Typically a CFB boiler will combust 97 to 99 percent of the fuels carbon content. The efficient reduction of sulfur dioxide emissions is also a characteristic of CFB boilers. Conventional boilers require addition of wet scrubbers to react with the SO_2 in the combustion gases. Fluidized bed combustors allow the introduction of dry sorbent for the removal of sulfur dioxide. Sulfur removal rates of up to 90% can be achieved in fluidized beds. To achieve this rate, bubbling beds require twice as much calcium sorbent as circulating fluidized beds, since finer particles can be effectively utilized in a CFB [27]. NO_x emissions are also kept low in CFB combustors due to relatively low bed temperatures (800 - 900 C) that remain below the temperature at which combustion air is oxidized. Good load-turndown and load-following capabilities in circulating fluidized beds along with excellent heat transfer coefficients (CFB: 200-250 W/m^2K, BFB: 300-500 W/m^2K) are additional advantages of fluidized bed

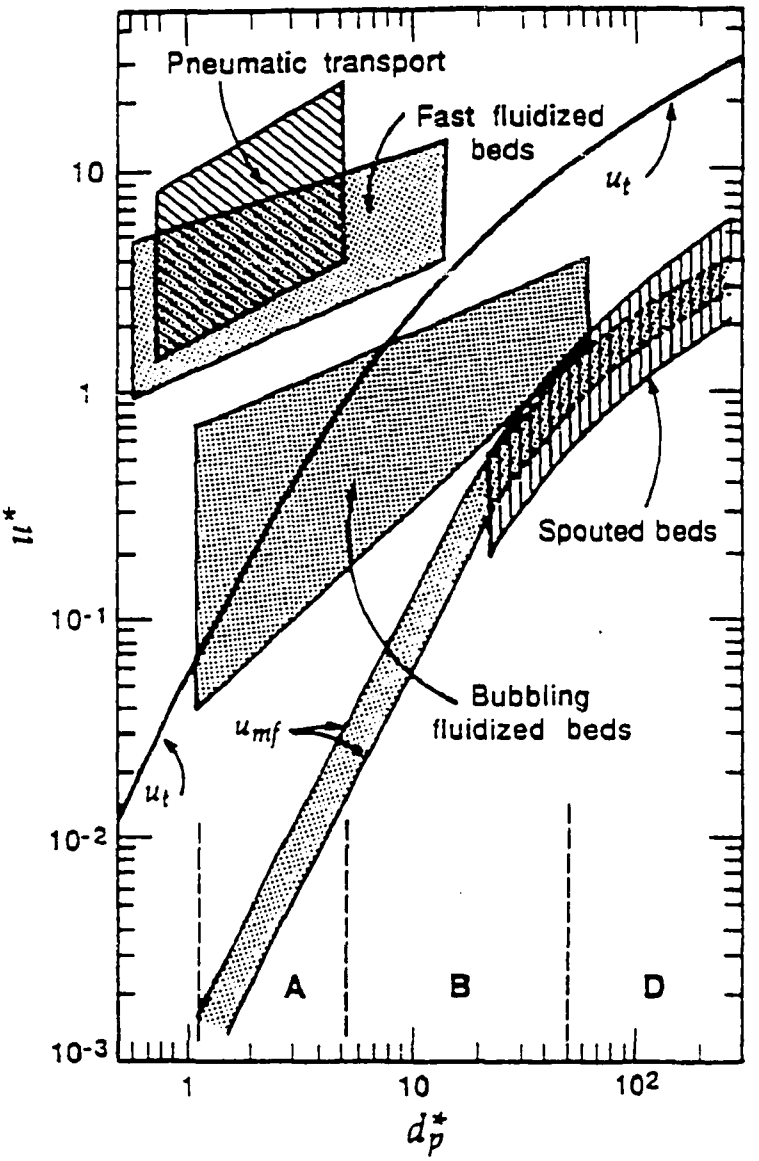

Figure 2.5: Fluidization regime diagram [24]

combustors [28]. A comparison of coal-based boilers is shown in Table 2.1. There are also alternative conceptual methods of complex cycles that combine CFB combustion and CFB gasification in a power production process which could theoretically yield overall efficiencies greater than 50% [29].

Table 2.1: Comparison of coal based boilers [19]

Characteristics:	Stoker	Bubbling	Circulating	Pulverized
Height of burning zone	0.2	1-2	15-40	27-45
Superficial velocity (m/s)	1.2	1.5-2.5	4-8	4-6
Excess air (%)	20-30	20-25	10-20	15-30
Heat release rate (MW/m^2)	0.5-1.5	0.5-1.5	3-5	4-6
Coal size (mm)	6-32	0-6	0-6	< 0.0001
Turn down ratio	4:1	3:1	3-4:1	
Combustion efficiency (%)	85-90	90-96	95-99	99
NOx emission (ppm)	400-600	300-400	50-200	400-600
SO_2 capture in furnace (%)	none	80-90	80-90	small

Circulating Fluidized Bed Hydrodynamics

As discussed previously, increasing the superficial velocity in a fluidized bed system so that it reaches the terminal velocity of the particles results in particle elutriation. With sufficient solids loading at this increased velocity, the bed does not behave as expected. For a single particle in a gas flow, an increase in the superficial velocity beyond its terminal velocity should equal the increase in the particle velocity. This behavior does not occur in fast fluidization since groups of particles are able to sustain a terminal velocity higher than that of individual particles. The concept of slip velocity is another way to present this important

characteristic of fast fluidization. The slip velocity is the local velocity of the gas relative to the particle. It is defined as:

$$U_{slip} = U/\varepsilon - U_S \tag{2.1}$$

where U is the superficial velocity of the gas, ε is the voidage, and U_S is the mean solids velocity. The mean solid velocity can be calculated from the mean solids concentration in the riser, ρ_{SC}, and the solids flux, G:

$$U_S = G / \rho_{SC} \tag{2.2}$$

Fluidization regimes can be qualitatively described in terms of their slip velocities as is shown in Figure 2.7 [30].

For a constant solids loading, fast fluidization is bounded by the transition to pneumatic transport and the transition to a turbulent bed (choking) as described by Takeuchi

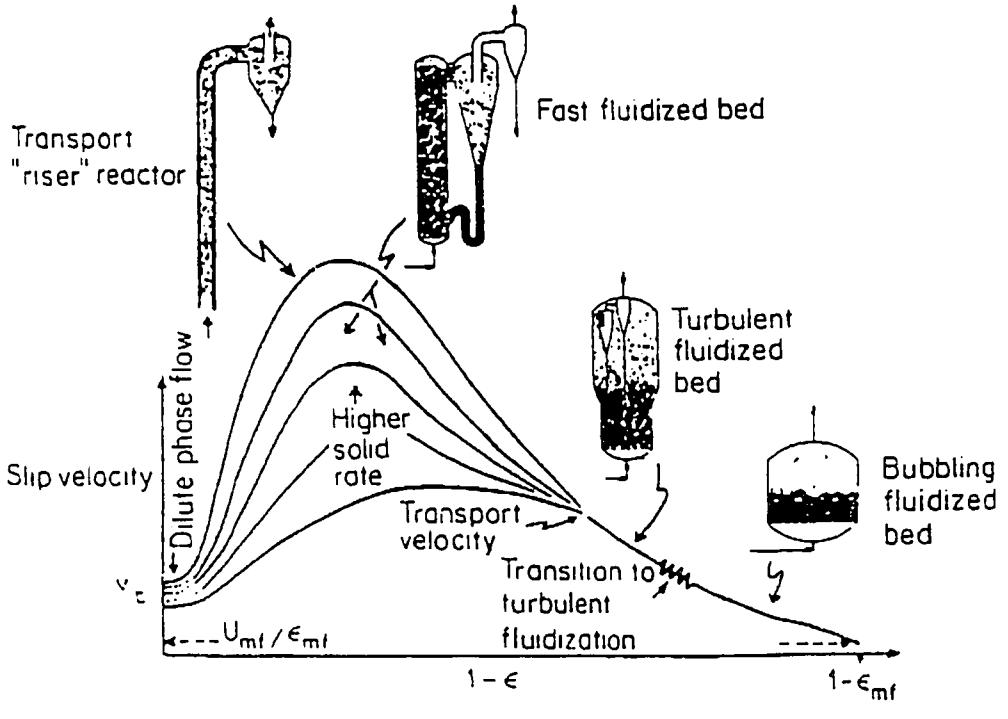

Figure 2.7: The relationship between slip velocity and fluidization regimes [30]

[31] and illustrated in Figure 2.8. The distinction between the pneumatic transport and fast fluidization regimes can be qualitatively described by changes in the static pressure. If the CFB is held at a given solids loading, the bed can maintain pneumatic transport at a significantly high superficial velocity. As this superficial velocity is decreased, the static pressure drop across a section of the riser will also decrease due to frictional effects, just as the longitudinal pressure drop decreases in a water pipe with a decrease in fluid velocity. If the superficial velocity is further reduced at constant solids loading, the solids suspended in the bed will increase and the pressure drop of a section will also increase due to the static head of the particles (the weight of the particles between pressure taps). As defined by Reddy-Karri and Knowlton, this point at which the pressure drop across a section of the bed begins to increase with decreasing superficial velocity is the point that distinguishes fast fluidization from pneumatic transport [32]. Decreasing the superficial velocity even further at this constant solids feeds rate, a very steep rise in the pressure drop across a lower section will occur once the velocity is no longer sufficient to carry the solids up the column. This point is the onset of choking. At this transition, the bed will either change to a slugging bed (in small diameter beds) or a turbulent bed. This change produces an increase in the magnitude of the pressure fluctuations.

The hydrodynamics of a CFB operating under fast fluidization are very complex and not fully understood. It is common for researchers to describe the circulating bed in two parts: a dense lower section and an upper dilute phase. This distinction has been verified by researchers who have studied axial density or voidage distributions [24, 33]. Figure 2.9 shows the axial density profiles for a variety of fluidized beds. In the lower dense phase, the bed operates in a regime similar to the turbulent regime. Some researchers have even compared the lower CFB to a bubbling bed. From visual observation of the cold laboratory scale circulating fluidized beds, the lower regions appear turbulent with random sheets and particle packets mixing violently, with no evidence of distinct bubble formations. Only under conditions of high solids loading can non-homogeneous upward moving air pockets be observed in the lower riser. Some researchers, such as Werther [34], claim that the lower

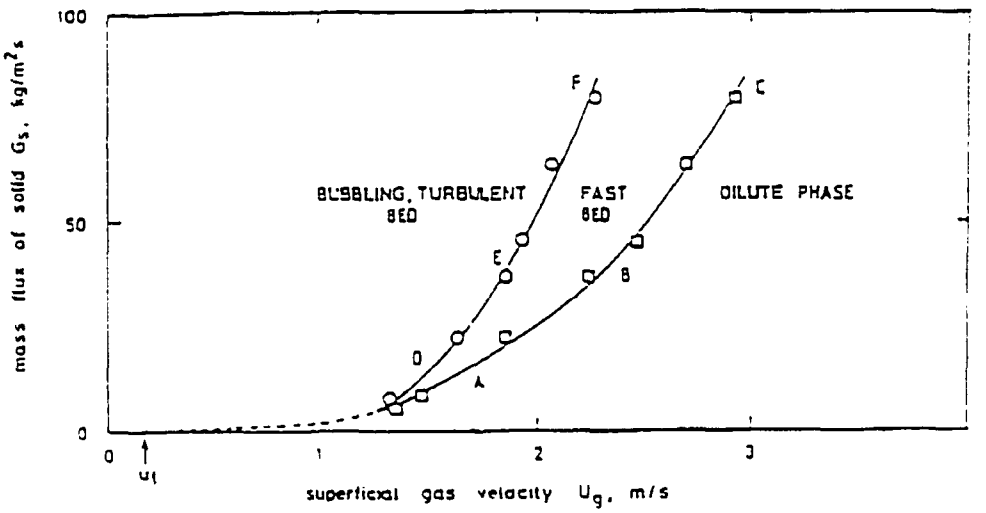

Figure 2.8: The quantitative bounds of fast fluidization [31]

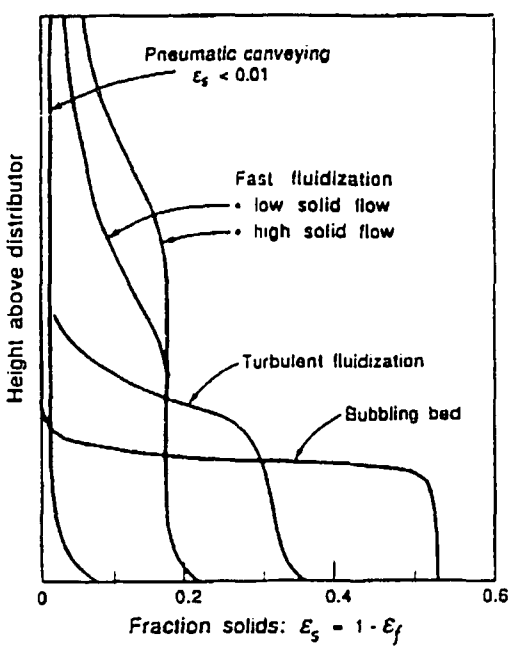

Figure 2.9: Axial solids density profiles [24]

bed in a full-scale CFB does not change from a bubbling regime to a turbulent regime. Werther claims that the existence of the turbulent regime as observed in pressure fluctuation records is a characteristic of small-scale models only. He cites a number of researchers who have characterized the lower CFB in terms of bubble properties using pressure fluctuation data and optical probe signals.

The upper dilute region is seen to operate in a much smoother and consistent manner. Researchers such as Bader, Findlay, and Knowlton [35] claim that this dilute region contains two phases, namely, a dilute core and a dense annulus. They have verified this distinction by measuring radial density profiles in this CFB region. Observation of an upper section of a CFB model shows that solids travel up in the dilute phase and down in a relatively thin annulus at the wall. Further observation shows this upper bed moving in a oscillating manner, as particle clusters break up, drop down the annulus, and reform in the core. Parabolic radial distributions of the solids density in this dilute region, with the highest solids concentration at the wall, have been observed by a number of researchers [36-38]. While the radial density has been shown to vary significantly from the center of the bed to the wall, the radial pressure distribution has been shown by Weinstein and Chen [39] to exhibit a more constant gradient. In their study, the pressure at the wall is at most only 0.5 inches of H_2O (120 Pa) different from the pressure in the center of the bed. Due to the ease of obtaining the static pressure measurement at the wall, most work assumes the fluctuations at this location to be characteristic of the overall hydrodynamics.

CHAPTER 3. LITERATURE REVIEW: PRESSURE FLUCTUATIONS IN FLUIDIZED BEDS

In addition to characterizing fluidized bed hydrodynamics by changes in static pressure drop across the bed, fluidized beds can also be characterized by changes in the relative magnitude of the pressure fluctuations. At a constant superficial velocity, the static pressure drop across a fixed bed will remain constant with very little variation. Static pressure fluctuations begin to appear at the onset of fluidization. The transition from the bubbling regime to the turbulent regime is characterized by an increase in the magnitude of the pressure fluctuations. The static pressure variation during this transition to the turbulent regime is typically larger than any other regime of fluidization [26]. Changing from a turbulent bed to fast fluidization will result in a decrease in the amplitude of the pressure fluctuations. Data presented by Yerushalmi [30] in Figure 3.1 shows this phenomena for various particle types. These fluctuations continue to decrease as the bed approaches pneumatic transport. Many studies have attempted to further relate the pressure fluctuations to features of fluidization hydrodynamics. A large amount of research has focused on the fluctuations of bubbling fluidized beds.

Pressure Fluctuations in Bubbling Beds

Bubbling fluidized beds were developed industrially before a complete description of their governing mechanisms was developed. Determining the operating conditions necessary for good fluidization was usually done by a combination of visual observation and trial and error. The need for better techniques for determining "fluidization quality" led to research on bubbling bed pressure fluctuations. Early researchers used techniques that measured changes in the local solids density of the bed. These measured fluctuations were believed to appear due to the random propagation of bubbles. Fluctuations in the local bed voidage were sensed by "capacitance probes" measuring changes in the dielectric constant of bed material between probe plates [40]. Probes that sensed the magnitude of the particle impacts were also used

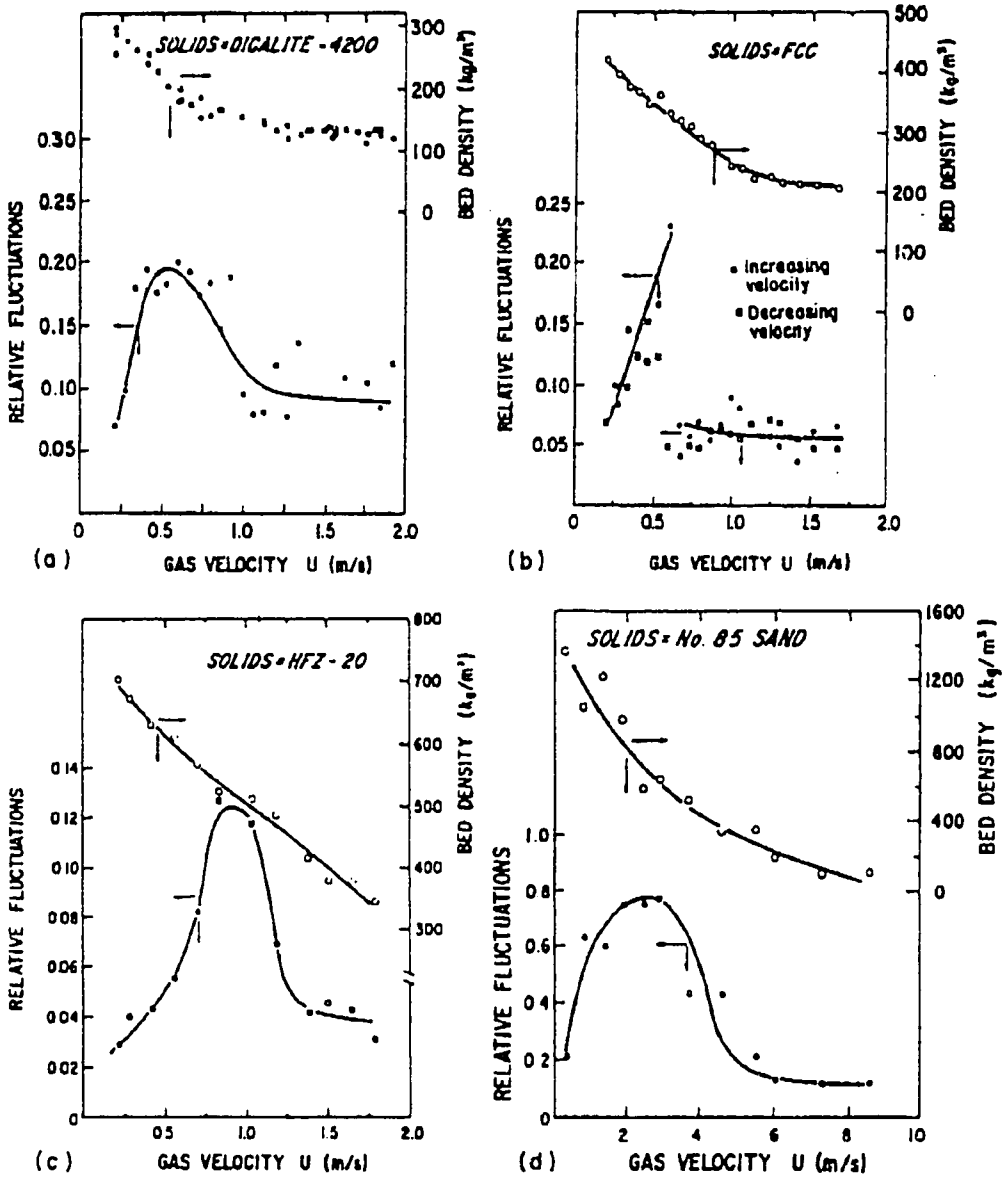

Figure 3.1: Relative pressure fluctuations in fluid beds [30]

[41]. In both studies it was necessary to disturb the bed flow in order to record bed fluctuations.

Shuster and Kisliak were among the first to proposed the use of static pressure fluctuation measurements as an indicator of "fluidization quality" [42]. By measuring the static pressure fluctuations at the wall, any flow disturbances arising from an immersed probe were eliminated. These researchers constructed a strain gage pressure recorder for measuring differential pressure fluctuations at any height in the bed with respect to the plenum. In each of these studies the overall quality of fluidization was related to the magnitude of these fluctuations and quantified by a fluidization index. The fluidization index is the ratio of the fluctuation magnitude to the fluctuation frequency. Good fluidization is achieved when this index is kept small (i.e. low frequency fluctuations of low amplitude). While providing a general indicator of fluidization quality, Shuster does not attempt to explain the processes that govern pressure fluctuations in fluidized beds.

Subsequent studies by several other researchers attempted to correlate pressure fluctuations to bubble properties. These studies were motivated by the work of Davidson, who proposed a theoretical model for the propagation of a single bubble in a fluidized bed. This work described the pressure field that surrounds a bubble [43]. In a related study, Rueter experimentally measured the pressure field of a single bubble [44]. Researchers such as Tamarin and Winter assumed the frequency of the static pressure fluctuations in fluidized beds to originate from bubble propagation. The characteristic low frequency (less than 10 Hz) of bubble phenomena is used by Tamarin to define a modified Froude number. He used this number to develop an empirical relationship to quantify bubbling bed hydrodynamics [45]. Winter utilized the probability density function of the pressure fluctuation signal to characterize overall bed hydrodynamics [46].

Kang [47] was one of the first to use spectral analysis tools, such as the power spectral density function, to analyze bubbling bed pressure fluctuations. Lirag [48] extended this analysis by utilizing not only the power spectral density, but also the auto-correlation, and cross-correlation functions to analyze fluctuations in bubbling beds. Lirag used these tools to

develop relationships for the average bubble size and bed height as functions of the pressure fluctuation frequency. He concluded that pressure fluctuations are caused by bed height fluctuations resulting from the eruption of bubbles at the bed surface. He clearly showed that pressure fluctuations in bubbling fluidized beds are periodic. Sitnai [49] confirmed Lirag's results with further research that related the pressure fluctuation signal to important bubble properties. In similar work, Fan, Ho, and Walawender [50,51] investigated pressure fluctuations using both statistical and spectral methods. They concluded that pressure fluctuations are solely due to bubbles. They related bubble propagation and pressure waves to the pressure fluctuations. To date, one of the most extensive studies on the behavior of pressure fluctuations in fluidized bed systems is by Dhodapkar and Klinzing [52]. While this study describes the effect of particle size, particle density, bed height, bed diameter, superficial velocity, and the location of the pressure taps on the dominant frequencies, it does not propose an explanation of pressure fluctuations.

Until the recent work completed by Kage et al. [53], researchers neglected the complexity of the frequency spectrum and have tried to relate a single phenomenon to the dominant frequencies observed. Kage et al., study pressure fluctuations in the plenum of a bubbling bed. They observe multiple frequency phenomena and relate the numerous dominant frequencies to the natural frequency of the entire bed, the bubble generation frequency, and the bubble eruption frequency at the bed surface. While this study is the first to address the issue of multiple frequency phenomena, the study is lacking the broad range of spectral data needed to adequately support their physical explanations of fluidization frequency phenomena.

While most bubbling bed studies have assumed pressure fluctuations to be the manifestation of a local phenomena (i.e. the propagation of bubbles past the measurement instrument) periodic phenomena have also been observed in non-bubbling fluidization systems. Researchers such as Hiby and Verloop studied pressure fluctuations in incipiently fluidized beds [54,55]. To maintain a homogeneous (non-bubbling) bed, the bed must be shallow and have a height less than the critical length proposed by Verloop. Under this homogeneous condition, periodic pressure fluctuations can occur as the entire bed oscillates in phase. This

periodic phenomena is attributed to the system establishing an equilibrium between the gravitational and the frictional forces on the particles. In a similar study, it has been shown by Roy and Davidson [56] that compression waves are observed in deep incipiently fluidized beds. These waves are similar to the acoustical waves generated in an organ pipe. These wave phenomena studies consider pressure fluctuations to be a global phenomena.

It is evident from the literature reviewed that there is no consensus as to the origin of pressure fluctuations in fluidized beds. Roy and Davidson [56] provide an excellent summary of the proposed theories by grouping the theories into the five categories below:

1) Entire incipiently fluidized bed oscillates in phase [54,55]
2) Vertical oscillations observed in fluidized beds with low resistance distributors [57,58]
3) Oscillations of bed surface analogous to surface water waves [59,60]
4) Fluctuations caused by bubbles rising past a pressure probe [51]
5) Fluctuations caused by a slugging frequency that periodically lifts the surface of the fluidized bed [61,62]

In this outline, only 1) and 3) are important for this study. Phenomena 2) is not observed in our work since high resistance distributor plates are used. Phenomena 4) and 5) are not dealt with in this study since our research has indicated that fluctuations are due to a global phenomena. As discussed previously, Hiby [54] and Verloop [55] propose essentially the same global mechanism although their derivations differ slightly. While Verloop maintains that the entire incipiently fluidized bed oscillates in phase, Hiby proposes a system of oscillating layers being "pulled into tune." The changes in bed voidage as the bed expands and returns to its initial position result in the fluctuations of static pressure drop across the bed. While Verloop focuses on shallow incipiently fluidized beds, Hiby speculates that bubble production may coincide with these voidage oscillations of a BFB.

Baskakov [60] takes a different approach to fluidized bed dynamics. He proposes a direct analogy between fluidized bed dynamics and a hydraulic pendulum (i.e. U-tube manometer). For Baskakov, the changes in voidage (or pressure) are due to changes in the

height of the surface caused by the rise of a single large bubble. As the bubble rises through the bed, it carries along particles, causing the bed surface to rise. The solids return downward along the sides of the bed to restore the bed to its equilibrium condition. This cyclic movement of solids up the center of the bed via bubbles and back down the sides via annular flow constitutes Baskakov's oscillatory pendulum. The primary weakness of Baskakov's theory lies in the validity of the hydraulic pendulum analogy. The simplifying assumptions that go into this analogy are not convincing. The relationship between unbalanced forces in a U-tube and the undulating surface of a fluidized bed is not made explicit.

Noting the many liquid-like characteristics of fluidized beds, Sun et. al [59] propose that surface waves, analogous to surface waves in water, govern fluctuations in fluidized bed systems. In this theory, it is necessary to have an estimate of the wave length (λ). Sun assumes the bubble size at the surface determines the wavelength. For deep beds, the bubble size approaches the diameter of the bed and the wavelength is defined by the bed diameter. The use of bubble diameter to determine wavelength raises numerous questions as to how such a surface wave can be sustained amidst random bubble eruptions at the surface. Not all experimental data agrees well with Sun's hypothesis.

The relations derived for the fluctuation frequency of the bed proposed by the authors above are summarized below:

Hiby (1967)
$$\omega = \sqrt{\frac{g \cdot (1-\varepsilon)}{(0.75 \cdot \pi^2) \cdot H \cdot \varepsilon}} \tag{3.1}$$

Verloop (1974)
$$\omega = \frac{1}{2 \cdot \pi} \sqrt{\frac{g \cdot (2-\varepsilon)}{H \cdot \varepsilon}} \tag{3.2}$$

Baskakov (1986)
$$\omega = \frac{1}{\pi} \sqrt{\frac{g}{H}} \tag{3.3}$$

Sun (1988)
$$\omega = \frac{1}{2 \cdot \pi} \sqrt{\left[\frac{g}{\lambda \cdot 2 \cdot \pi} \cdot \tanh\left(\frac{2 \cdot \pi}{\lambda} \cdot H\right)\right]} \tag{3.4}$$

Using BFB pressure fluctuations to verify hydrodynamic similitude

While pressure fluctuations in bubbling beds have been used to characterize fluidization quality, bubble properties, and wave phenomena, only recently have they been used in similitude and scale-up studies. Glicksman [14,63] derives a set of dimensionless parameters for fluidization from non-dimensionalized equations of motion and the Buckingham Pi theorem. Most researchers have attempted to verify the validity of these parameters by comparing pressure fluctuations after matching dimensionless parameters in two geometrically similar beds of different scales. Many compare the autocorrelation, power spectral density, and probability density functions of the pressure fluctuations in both beds under conditions of similitude. If these statistical and spectral profiles match, it is assumed that the appropriate dimensionless parameters have been used [63-66]. In bubbling beds, use of pressure fluctuations to validate hydrodynamic similitude has been justified on the grounds that bubble phenomena are a function of the hydrodynamic conditions in the bed. However, many of these previous studies have either used an inadequate method of analysis, or have oversimplified the observed dynamics by trying to characterize fluidized bed dynamics with a single frequency.

Pressure Fluctuations in Circulating Fluidized Beds

In contrast to the wealth of research dealing with the pressure fluctuations in bubbling beds, only recently have pressure fluctuations in circulating fluidized beds been studied. Schnitzlein and Weinstein [67] use the probability density function to distinguish between the dilute and dense regions in the circulating fluidized bed. They also utilize a cross-correlation function to determine the pressure wave speed in the dense region of the bed. In this work, the wave speed was recorded as the superficial velocity was increased. This wave speed was then related to the bubble or slug velocity. In the turbulent and fast fluidization regimes, this wave speed no longer varied with superficial velocity.

Currently there is no adequate explanation for the origin of pressure fluctuations in circulating fluidized beds. Some research has been done in an attempt to describe pressure

fluctuations as chaotic systems [16-21]. Others have applied spectral analysis methods to characterize CFB hydrodynamics [13,15,68-72]. These studies have noted dominant frequencies in these pressure fluctuations but have been unable to relate these frequencies to a governing phenomena in circulating fluidized beds. Some of these studies have produced inconsistent results due to improper application of spectral analysis techniques.

Using CFB pressure fluctuations to verify hydrodynamic similitude

Increasing use of industrial circulating fluidized bed combustors has led researchers to work on the relationships needed for proper scale-up. Glicksman extended his development of similitude parameters for bubbling fluidized beds to circulating fluidized beds [68]. In this work, the profiles of the power spectral density, probability density function, and axial density distribution were compared in runs under conditions of similitude [11,68-70]. In a related scale-up study, Louge [12] presented a similar set of dimensionless parameters and utilizes a probability density function of dimensionless pressure to verify that similitude had been achieved. All these similitude studies have assumed that periodic pressure fluctuations characterize the overall bed hydrodynamics. However, it has never been explained why pressure fluctuations should correlate with the hydrodynamic state of the system. To date, no research has been published that definitively validates the CFB similitude parameters proposed by Glicksman.

An important objective of this research is to qualitatively describe the physical processes that govern static pressure fluctuations in circulating fluidized beds using properly applied spectral analysis. The phenomena governing fluctuations in fluidized bed systems must first be understood before pressure fluctuations can be used to validate similitude parameters in bubbling and circulating fluidized beds.

CHAPTER 4. METHODS OF ANALYSIS

Statistical Methods

A variety of statistical and spectral techniques have been used to analyze pressure fluctuations. Early researchers simply used mean and variance to describe fluctuation signals. Others have used the probability density function, which provides a more descriptive representation of the variation (or spread) of the signal from its most probable values. The probability density function is estimated for finite data sets as a histogram. A histogram plots how often the signal yields a value between a given range for all signal values. For a more complete presentation of probability theory and the probability density function, see Jenkins and Watts [73].

Both the probability density function and mean/standard deviation methods are statistical approaches which present similar information. Both methods are the primary tools of analysis for purely random signals. For periodic signals, spectral analysis methods provide a more complete description of the structure of a correlated signal.

Spectral Analysis Methods

Correlation functions are used frequently to characterize periodic signals. A correlation function is described by considering two signal realizations as functions of time. Assuming two functions x(t) and y(t) which are sampled such that x_m and y_m occur simultaneously from m = 0 to m = N (total number of data points), the discrete correlation function is:

$$Rxy_m = \frac{\sum_m x_m \cdot y_m}{N} \tag{4.1}$$

This value represents the correlation at the discrete point m. It is evident that for two zero-mean signals, the correlation will be the greatest if the signals are identical. For two dissimilar signals, the sum of the products will be smaller since some are positive and some will be negative.

Just as correlation can be applied to two different signals, correlation can also be performed on a single signal. This analysis is termed the autocorrelation. Autocorrelation is a method of determining the periodicity of a signal by correlating the function value y(t) to a subsequent function value $y(t + \tau)$. The auto-correlation function can then be calculated as a function of the time shift τ. The autocorrelation function, $R_{yy}(\tau)$, of a continuous system is defined as the average product of the signal value and its time shifted value and can be represented by:

$$R_{yy}(\tau) = \lim_{T\to\infty} \frac{1}{T} \int_{-T/2}^{T/2} y(t) \cdot y(t+\tau) dt \tag{4.2}$$

where T is the total length of the time record. For a sampled data set the discrete representation is:

$$R_{yy}(\tau) = \lim_{N\to\infty} \frac{1}{(2 \cdot N + 1)} \sum_{m=-N}^{N} y_m \cdot y_{m+k} \tag{4.3}$$

where k is an index, such that x_m and x_{m+k} are separated by k·T seconds, with T being the total sampling time. The auto-correlation function is symmetric about $\tau = 0$ with a maximum always at this point. Purely random or white noise signals will yield an autocorrelation function with a sharp peak only at zero since they exhibit no correlation at any other point.

The power spectral density (PSD) function is defined as the Fourier transform of the autocorrelation function. It is the equivalent of the autocorrelation function in the frequency domain. For a stationary process, in which the probability density functions are invariant with time, the power spectral density, Syy(iω), can be related to the autocorrelation function by the Weiner-Khinchin relation:

$$S_{yy}(i\omega) = \Im\{R_{yy}(\tau)\} = \int_{-\infty}^{\infty} R_{yy}(\tau) \cdot e^{-i\cdot\omega\cdot\tau} d\tau \tag{4.4}$$

with ω representing the angular frequency in radians per second. In many cases, instead of the autocorrelation function, only a finite zero-mean data set, T, is available. An estimate of the PSD can be obtained from the following relationship:

$$\int_{-\infty}^{\infty} R_{yy}(\tau) \cdot e^{-i\cdot\omega\cdot\tau} d\tau = \lim_{T\to\infty} E\left\{\frac{1}{2 \cdot T} |\Im(y(t))|^2\right\} \tag{4.5}$$

where

$$\left\{\frac{1}{2\cdot T}\left|\Im(y(t))\right|^2\right\} \tag{4.6}$$

is known as the periodogram and E is the expected value operator. The estimated PSD function is equal to the average periodogram. Ignoring this expected value operator in the definition of the PSD can produced inconclusive results. To calculate a PSD, the Fourier transform of the time domain signal must be obtained. As a continuous function, the Fourier transform is defined as:

$$\Im\{y(t)\} = \int_{-\infty}^{\infty} y(t)\, e^{-i\alpha t}\, dt \tag{4.7}$$

For a sampled data set, a very efficient means of computing the discrete Fourier transform is through the use of the FFT (fast Fourier transform) algorithm:

$$FFT(n) = \sum_{k=0}^{N-1} y(k)\cdot e^{\frac{i\cdot 2\cdot\pi\cdot k\cdot n}{N}} \tag{4.8}$$

for N data points where n = 0, 1, 2 ..., N-1. The FFT can be used, provided that $N = 2^m$ where m is an integer greater than one. Many computational packages such as Matlab, Mathcad, and Mathematica, have built in FFT algorithms. In short, a power spectral density periodogram can be calculated as:

$$PSD(n) = \frac{1}{2\cdot T}E\left[\left|FFT(n)\right|^2\right] = \frac{1}{2\cdot T}E\left[FFT(n)\cdot FFT^*(n)\right] \tag{4.9}$$

Where FFT*(n) denotes the complex conjugate of the FFT(n). The PSD will represent the frequency spectrum from zero to N/2. The variable n can be converted to a frequency in Hertz by dividing by the number of samples and multiplying by the sampling frequency. While the autocorrelation can determine whether a signal is periodic, the power spectral density function will provide a better description of the dominant frequency or frequencies of the periodic components. For a complete derivation of correlation and spectral relations see Lynn and Komo [22,23].

System Identification Methods

While the auto-correlation function and the PSD function have many applications in characterizing periodic systems, these techniques find an extended application in system identification studies. Linear systems can be described in the frequency domain by a transfer function. Knowledge of the output and the input signals will provide the transfer function for a given system. The transfer function, H(s), of a linear system will be described with input X(s) and output Y(s). The relationship between the system transfer function and the power spectral density function of the output is shown in equation 4.10:

$$S_{yy}(s) = |H(s)|^2 \cdot S_{xx}(s) \tag{4.10}$$

where $s = i\cdot\omega$. For a white noise input $S_{XX}(s) = \sigma^2$, where σ is the statistical variance in the input signal. The relationship between the PSD and the transfer function for a white noise input is simply:

$$Syy(s) = |H(s)|^2 \cdot \sigma^2 \tag{4.11}$$

System transfer functions can be represented as Bode plots, which are a convenient graphical means of determining the order and time constants of systems [74,75]. The Bode plot is created by plotting $20\cdot\log|H(s)|$ (decibels) versus the log of the angular frequency (radians/second). The asymptotic slopes of the plot at -20 dB/decade intervals indicate the system order, while the intersection of asymptotes denote the characteristic system time constants. From the above definition of the Bode plot and equation 4.11, the Bode plot for a system with a white noise input can be defined in terms of the PSD. By simple algebraic manipulation the relationship is:

$$20\cdot\log|H(s)| = 10\cdot\log(Syy(s)) - 20\cdot\log\sigma \tag{4.12}$$

Knowledge of the nature of the input signal is not necessary for defining the profile of the Bode plot since changes in the variance of the input signal correspond only to a gain in the frequency response plot. The analysis of systems with white noise input is presented by Lynn and Komo [22,23].

To better understand how Bode plots describe linear systems and to demonstrate the experimental approach of this study, consider a simple first order system in the time domain which can be represented as follows:

$$\frac{d(y(t))}{dt} + k \cdot y(t) = u(t) \tag{4.13}$$

where u(t) = δ(t), the unit impulse or Dirac delta function. This differential equation has the following exponential solution:

$$y(t) = e^{-k \cdot t} \tag{4.14}$$

as shown in Figure 4.1 where k is arbitrarily assigned a value of 5 s^{-1}. Moving from the time domain to the frequency domain using the Laplace transform, this exponential response to an impulse forcing function is represented by the following transfer function:

$$H(i\omega) = \frac{1}{1 + \frac{i \cdot \omega}{k}} \tag{4.15}$$

As a Bode plot presented as 20 log |H(iω)|, this first order system assumes the profile of Figure 4.2. The two important system characteristics can be determined from this plot. First, the plot has an asymptotic slope of -20 dB per decade indicative of a first order system. Secondly, the 0 dB per decade and the -20 dB per decade asymptotes intersect at the characteristic time constant k. Higher order systems would roll-off at -40 dB, -60 dB, and -80 dB per decade for second, third, and fourth order systems respectively.

The experimental approach of this study can be demonstrated using this same first order system example. Using a Matlab simulation, a randomly generated signal (white noise) is used as the system input. The corresponding output is shown in Figure 4.3. Taking the FFT of this signal and multiplying by its complex conjugate, a single PSD periodogram can be produced. This single PSD periodogram is presented as a Bode plot in Figure 4.4. It is evident that no definitive system information can be gained from the spectral analysis of this single realization. In order to observe the important system information, adequate realization averaging is a necessity. Averaging eight realizations from this same first order system and averaging the PSD periodograms results in the Bode plot shown in Fig. 4.5. Although lacking

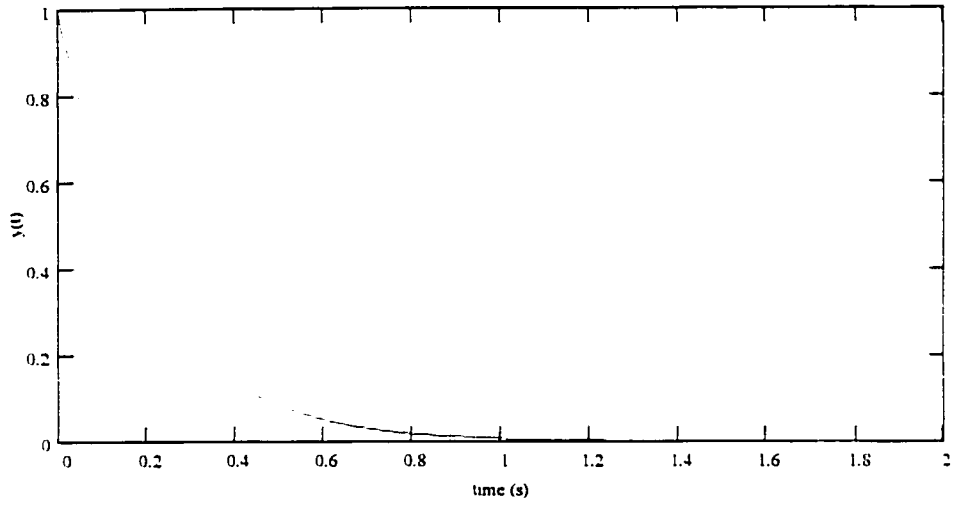

Figure 4.1: Example of spectral analysis - First-order system response in the time domain

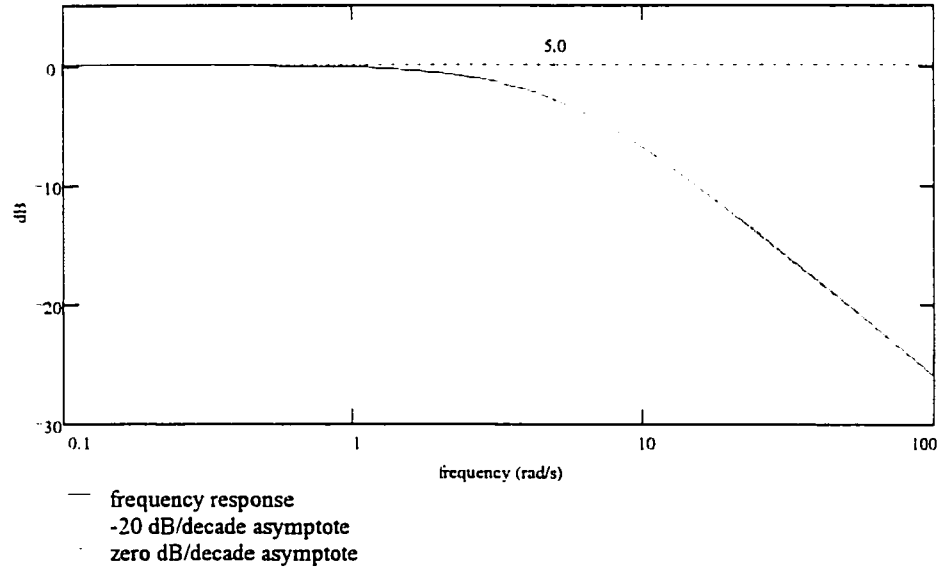

Figure 4.2: Example of spectral analysis - Bode plot of first-order system response

INPUT (white noise)

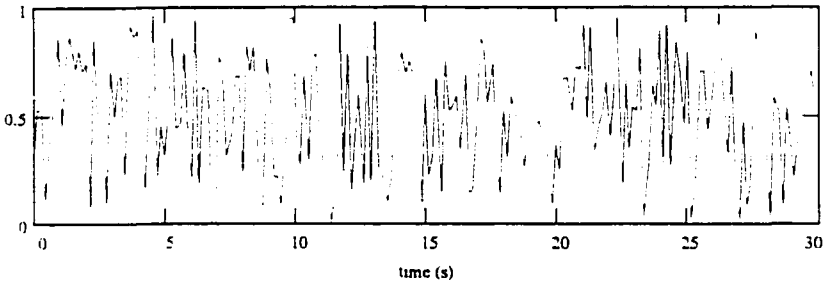

$$H(s) = \frac{5}{s+5}$$

OUTPUT (correlated noise)

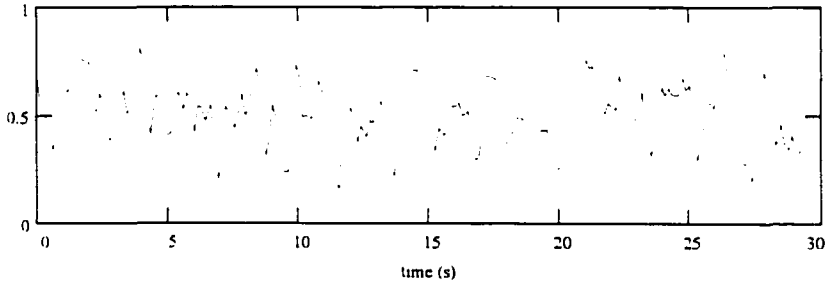

Figure 4.3: White noise input and correlated first order output

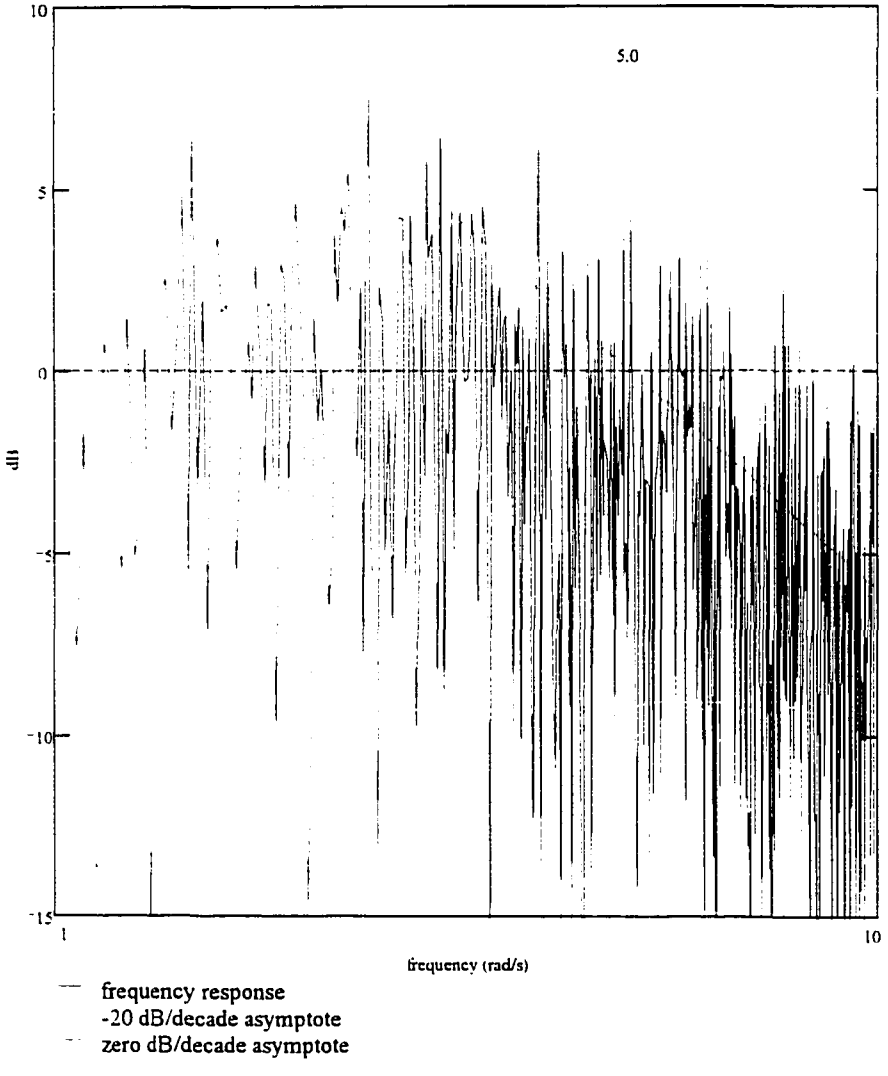

Figure 4.4: Bode plot of first order system with white noise input (without averaging)

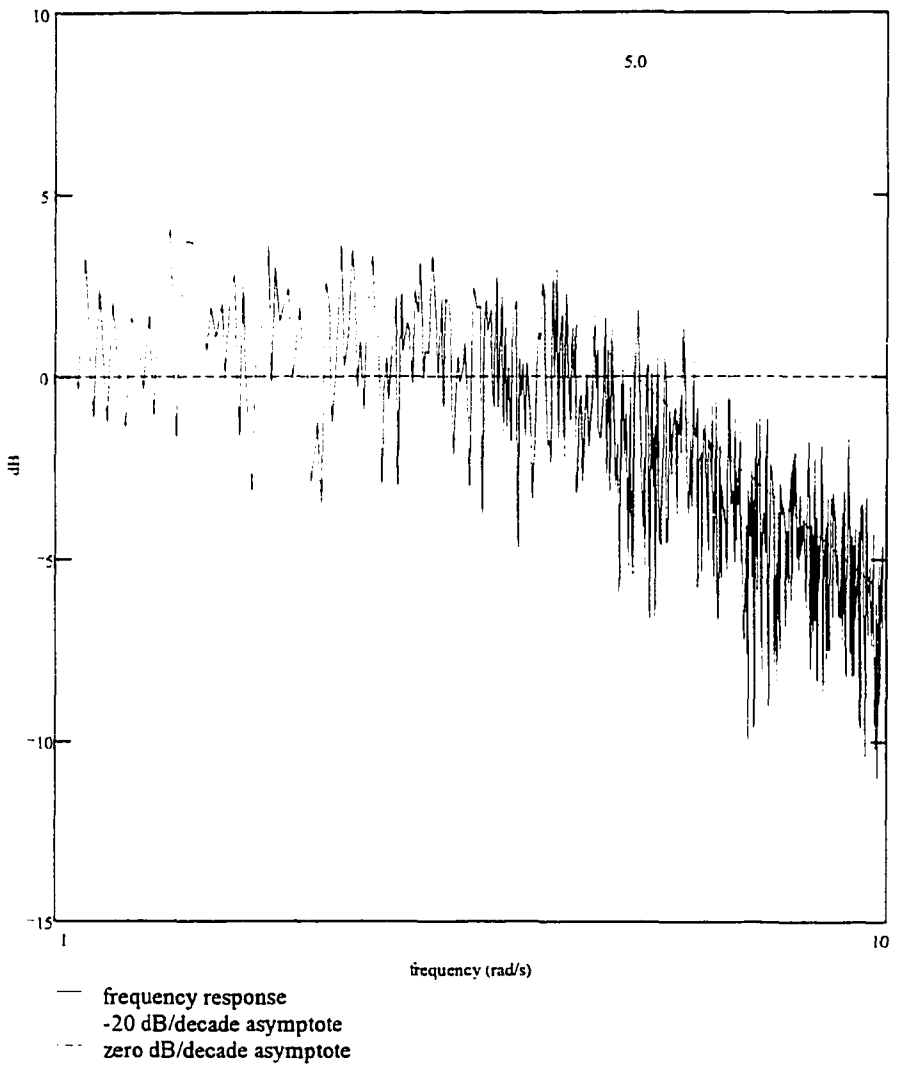

Figure 4.5: Bode plot of first order system with white noise input (with 8 set averaging)

the clarity that would result from averaging additional realizations, the characteristic slope of -20 dB per decade is evident in this Bode plot, along with the cornering frequency of 5 s^{-1}.

The importance of signal averaging and adequate sampling times when analyzing pressure fluctuations in fluidized bed systems cannot be overemphasized. Without signal averaging, system characteristics cannot be accurately estimated from the resulting spectrum. If the sampling frequency is too high and the time period not long enough, there will be too few data points to represent low frequency phenomena on the Bode plots. An example of the inconclusive results that can result when these two analysis guidelines are not observed is shown in Figures 4.6 and 4.7. Using only 1024 data points sampled at 100 Hz and averaging only 4 sets of 256 point realizations as other researchers have done, Figure 4.6 compares the Bode plots of two different runs in the same CFB under identical operating conditions (similitude). Figure 4.7 compares the Bode plots of the same CFB under two completely different modes of operation (non-similitude). By using this insufficient method of analysis, no conclusions can be drawn from similitude studies, since it is evident that the Bode plots yield nearly identical profiles under all operating conditions. None of the important low frequency CFB characteristics can be distinguished in these Bode plots. In the chapters following, it will be apparent that the structure of pressure fluctuations is significantly different under the two different conditions described in Figure 4.7.

In this study of the CFB hydrodynamic system, pressure fluctuations are assumed to be correlated noise arising from white noise input to the system. The origin of this white noise might be random pressure perturbations as air flows through the distributor. Pressure fluctuations between selected pairs of pressure taps were typically recorded at sampling frequencies of 20 Hz for CFBs (40 Hz for BFBs) to obtain 70,000 data points for each run. This sampling rate provided the frequency response information in the range 0-10 Hertz. Computer memory constraints on both the analysis program and data acquisition system limited the total number of data points that could be taken each run. Data was analyzed by dividing the data set into 15 realizations and taking the FFT of each realization. The PSD periodogram for each segment was found from the product of the FFT and its complex

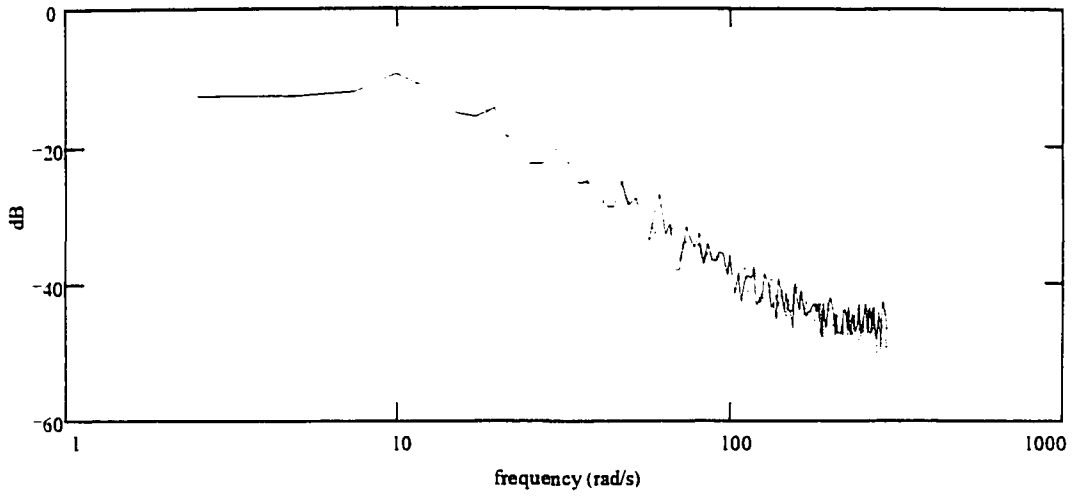

Dotted trace - (Re_p=150, Fr=7700, G_a=0.98·10^{-3})

Solid trace - (Re_p=150, Fr=7700, G_a=0.98·10^{-3})

Figure 4.6: Inconclusive Bode plot of CFB fluctuations under identical conditions

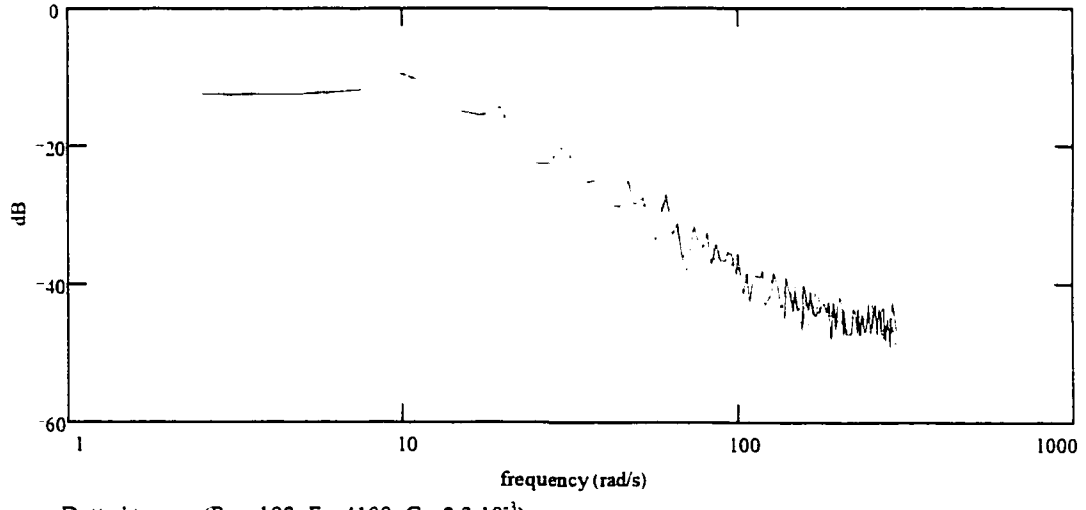

Dotted trace - (Re_p=108, Fr=4100, G_a=2.3·10^{-3})

Solid trace - (Re_p=150, Fr=7700, G_a=0.98·10^{-3})

Figure 4.7: Inconclusive Bode plot of CFB fluctuations under non-similitude conditions

conjugate. These 15 periodograms were averaged to create a smooth characteristic PSD for the run. A Bode plot is produced from this PSD.

The use of Bode plots in combination with the PSD functions has two advantages in this study. While underdamped frequencies are more accurately determine quantitatively on the non-log scale of the PSD, the relative magnitude of the peaks (i.e. the damping of the system) is much easier to visualize from Bode plots. Secondly, the frequency of overdamped peaks is impossible to determine accurately from the PSD alone. The Bode plot brings out these important system characteristics.

CHAPTER 5. EXPERIMENTAL SET-UP AND OPERATION

CFB Models

This study was performed in two geometrically similar cold-flow CFBs, illustrated in Figure 5.1. The riser of the larger unit (prototype) is 10.2 cm in diameter and 3.00 m tall. This unit is fluidized with 0.2, 0.3, and 0.4 mm diameter glass beads. Pressure taps are located at 25.4 cm intervals along the riser, with two additional pressure taps spaced evenly between the first 25.4 cm interval. Each pressure tap is threaded into the CFB so that the tap is flush with the inner wall. The riser, cyclone, and L-valve of both circulating fluidized beds are constructed of aluminum to reduce electrostatic effects. The downcomer and solids flux meter are constructed of Plexiglas to allow visual observation of bed operation. The 10.2 cm diameter CFB has two small Plexiglas sections in the riser to observe solids circulation. This large CFB is designed to be operated only at atmospheric pressure, using air as the fluidizing gas. The smaller unit is a one-half scale model of the larger unit with an inside diameter of 5.08 cm and a height of 1.50 m. The smaller CFB (model) is fluidized with 0.1, 0.15, and 0.2 mm diameter steel shot, for the purpose of conducting hydrodynamic similitude studies between the two beds. Since the fluidizing gas density must be greater in the small bed in order to achieve similitude, it is fluidized with pressurized air (0-200 kPa gage). The range of operating conditions used in this study is shown in Table 5.1.

Table 5.1: Experimental operating conditions

	Solids Flux (kg/m^2s)	Superficial Velocity (m/s)
Large CFB (0.4 mm glass beads)	5 - 29	3 - 5.5
Small CFB (0.2 mm steel shot) @ 0 psig	20 - 50	3 - 8
Small CFB (0.2 mm steel shot) @ 28 psig	15 - 50	2 - 4

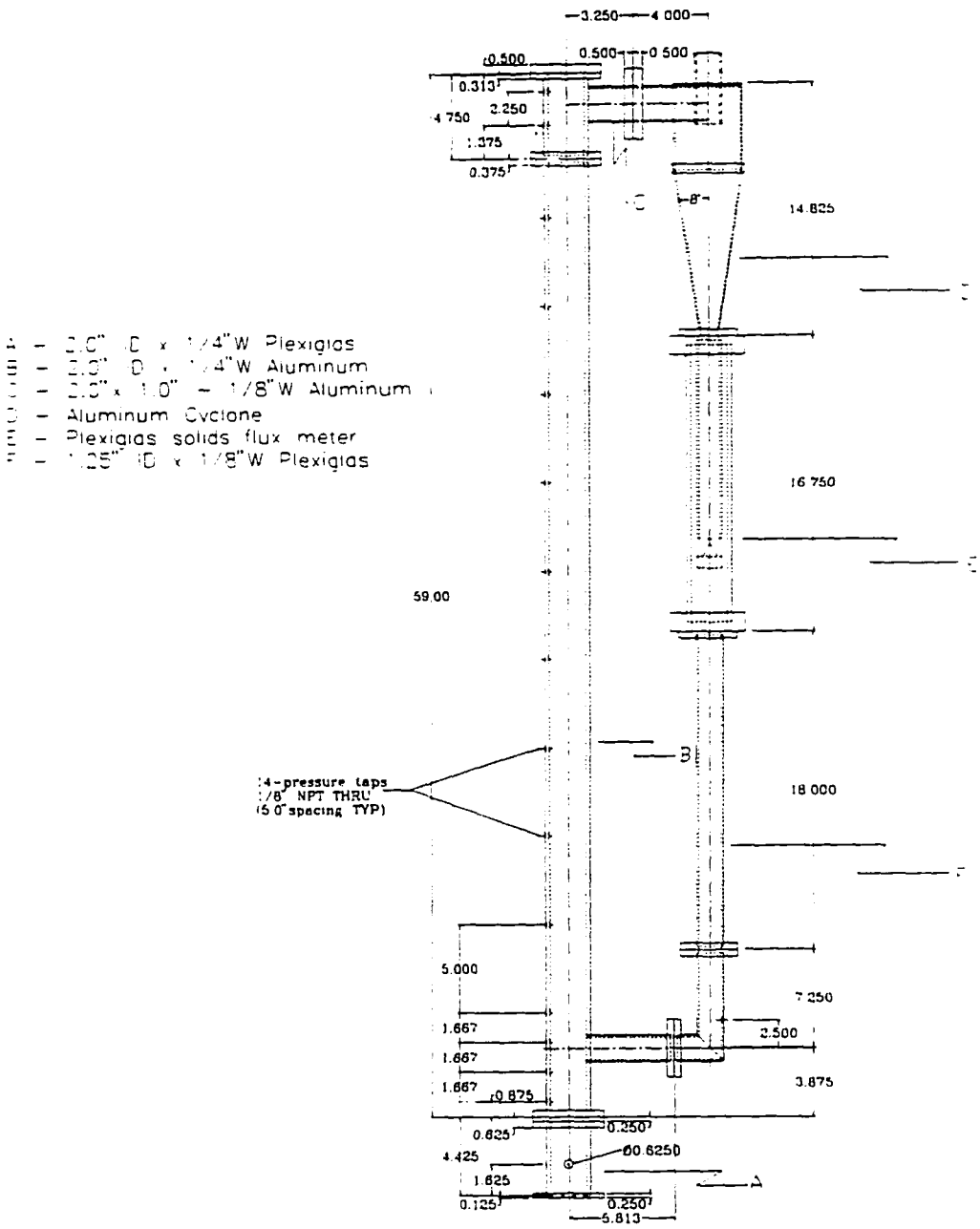

- Dimensions are given for model CFB in inches

(Dimensions for prototype CFB are twice those given above)

Figure 5.1: Cold-flow model CFB

Electrostatic effects

A problem common to many CFB cold models is buildup of electrostatic charge in the bed. This effect cannot be ignored with small glass and plastic beads. Initially, an anti-static powder (trade name Larostat 513) was added to the large CFB when operating with glass beads. As shown in Figure 5.2, the addition of Larostat changed the observed axial voidage profile significantly. The lower CFB became more dense with the addition of Larostat. This result is exactly the opposite of what Louge observed in CFBs with the addition of Larostat [12]. The reason for this inconsistency may be rooted in two significant of problems that were encountered during the use of this anti-static powder. The first problem noticed was that the Larostat had the tendency to absorb any humidity in the laboratory air. This absorption made the Larostat powder sticky and cohesive. Under these conditions particles within the bed would agglomerate as a result of the addition of Larostat, and not fluidize homogeneously.. The Larostat did reduce electrostatic effects in the CFB significantly under dry room conditions, but it would gradually lose its effectiveness as it elutriated from the bed during the course of the experiment. By the end of a single run, electrostatic effects would again be pronounced. To solve the problem of electrostatic effects without the use of Larostat, both of the CFB risers were reconstructed using aluminum rather than Plexiglas. By grounding the aluminum riser, most of the static electricity could be dissipated.

Solids flux measurement

Experimentally, the greatest difficulty encountered was the measurement and control of solids flux. A common method for measuring solids flux is the "time of descent" method [77]. This method assumes that all the particles are moving uniformly down in the standpipe. By timing how long it takes for a particle to travel down a measured height h_p the solids flux G_s can be calculated as follows:

$$G_S = \frac{h_p}{t_p}\frac{A_d}{A_r}\rho_b \qquad (5.1)$$

where A_d is the cross sectional area of the downcomer, A_r is the cross-sectional area of the

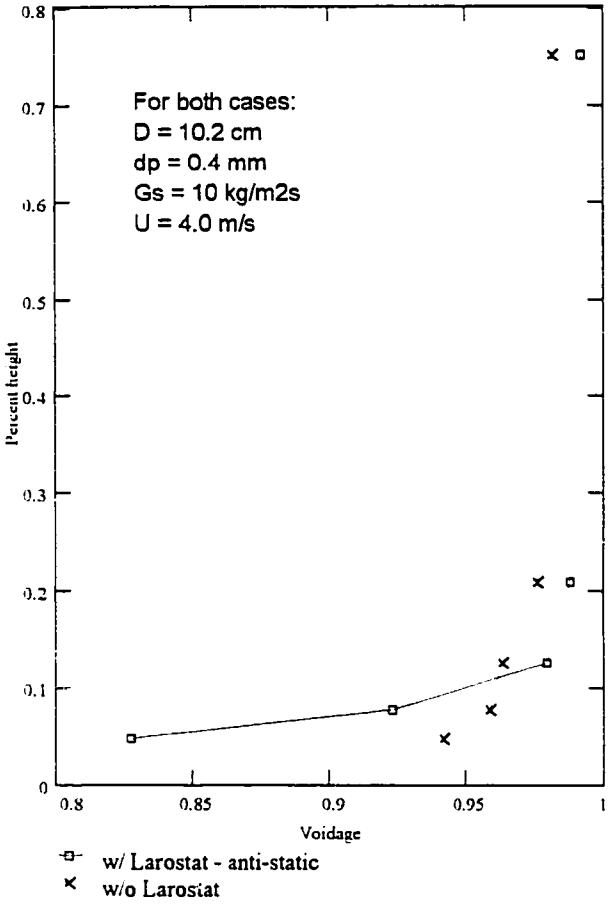

Figure 5.2: The effect of adding anti-static powder to the CFB

riser, ρ_b is the fixed bed density of the particles, and t_p is the time it takes for the particle to descend a height h_p. This method is suitable for properly designed L-valves in which the particles in the downcomer remain unfluidized. If the L-valve aeration is increased so as to approach incipient fluidization in the downcomer, this method will be inaccurate due to non-uniform particle motion and a non-homogeneous bed. The L-valves on both the large and the small bed were initially designed with a large minimum aeration rate [26]. Consequently, the CFBs, as initially constructed, would operate only when the downcomer was at or near minimum fluidization. Even when the L-valve was redesigned to operate in a non-fluidized manner, the measured solids flux was always significantly lower than the solids flux measured using the solids flux meter discussed below. This suggests that the particles near the wall of the downcomer are not moving as fast as those in the center due to frictional or electrostatic effects caused by the wall.

Since the accurate measurement of solids flux is very important for similitude studies, a meter was constructed that, when activated, would capture particles as they exited the cyclone. A schematic of this solids flux meter is shown in Figure 5.3. The time it takes for this meter to fill is recorded and converted to a solids flux in kg/m^2s. The design of this meter involved a trade-off. If the meter was constructed too small, the time at which it filled would be to short for high accuracy measurements. If it was built too large, the particles removed by the meter would significantly reduce the height of the particles in the L-valve. This change in downcomer bed height reduces the solids circulation rate of the system during measurement. Designing a valve to release the particles from the meter after measurement proved to be difficult. In the end, a simple plug suspended from a fine nylon line that extended down through the top of the cyclone worked surprisingly well. The meter measured the solids flux with an overall accuracy of around $\pm$ 10%, which is good considering the variation in the solids flux inherent in bed operation.

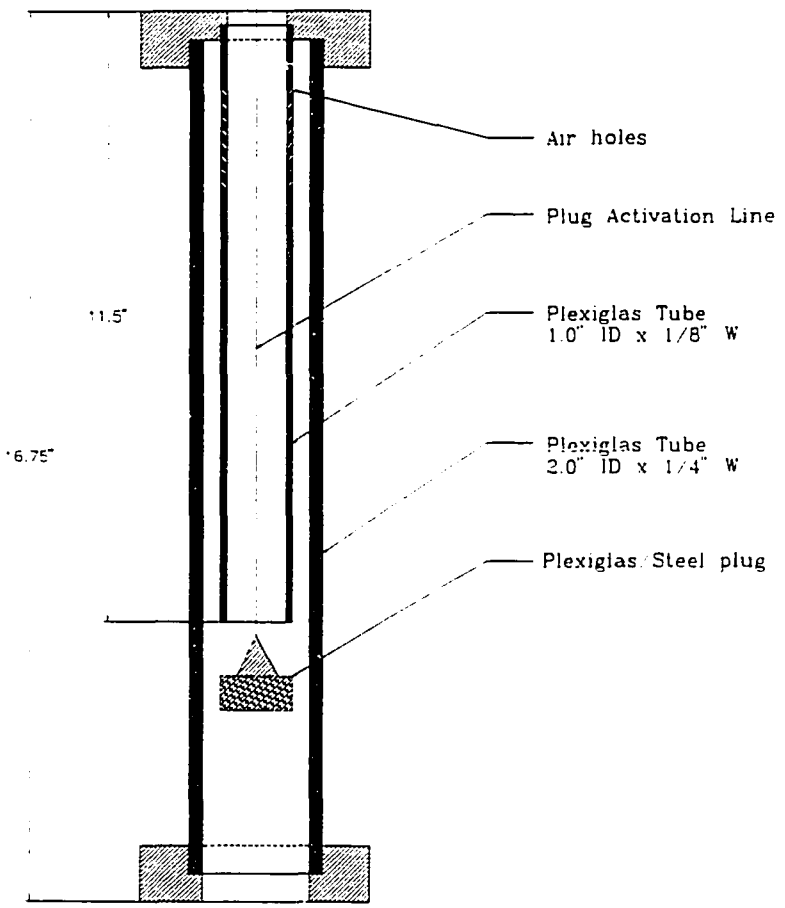

Dimensions given are for the small CFB solids flux meter

Figure 5.3: Solids flux meter

Bubbling Fluidized Bed Models

Two geometrically similar bubbling bed models were also used in this study. Both beds were constructed of Plexiglas tubing with an inside diameter of 10.2 cm and 5.08 cm for the prototype and model respectively. The column height is 64 cm and 32 cm for the large and small beds respectively. Both 36 hole and 72 hole distributor plates were used on the bubbling beds with a 75 μm screen fastened to the plate. This screen not only kept particles from entering the plenum, but also increased the pressure drop across the distributor plate such that even distribution was insured. Pressure taps in the small bed were located at 2.54 cm intervals along the height of the column, between the heights of 3.8 and 8.8 cm. Pressure taps in the large bed were located at 2.54 cm intervals up the column, between the heights of 3.8 and 21.3 cm. The small bed was designed to run at pressures up to 200 kPa gage.

Pressure Measurement

Pressure fluctuations are measured using a Schaevitz P3061-20WD (0-5.0 kPa) and a Schaevitz P3061-20WD (0-2.5 kPa) pressure transducer. The range of the P3061-20WD transducer is more than sufficient to measure the maximum pressure drop across the height of the large CFB with glass beads (2.0-3.8 kPa) and adequate to measure the largest pressure drop across the small bed operating with steel shot at atmospheric pressure (3.0-5.0 kPa). The Schaevitz P3061-10WD is used for smaller differential pressures such as would be measured between two adjacent taps in the CFB models (0.1-0.4 kPa). The transducers require a 12 V (1.2 mA) electrical input from the computer power supply and produce 0-5 V output proportional to the differential pressure. These transducers have a combined static error (non-linearity, hysterisis, and non-repeatability) of ± 0.5% of the full scale deflection. This translates to an accuracy of ± 0.03 kPa, and ± 0.01 kPa for the P3061-20WD, and P3061-10WD respectively. The 12 bit -5 V to +5 V Analog to Digital conversion on the data acquisition board has a resolution of 0.002 V or 0.003 kPa and 0.001 kPa for the P3061-20WD and the P3061-10WD respectively. Even more important for this study is the time response of the transducers which is less than one millisecond. The transducers will not fail

unless the differential pressure measured exceeds 20 kPa. The Schaevitz transducers are constructed to withstand a 1300 kPa line pressure, which is important for our studies in the small pressurized CFB. To keep particles out of the pressure lines, fine screens (<50μm) were welded on to the pressure taps of the small and large CFB.

Data Acquisition System

A MetraByte DAS-8 plug-in data acquisition board is used in a IBM compatible PC. The DAS-8 has a 12 bit A/D with 8 channels that can sample at rates up to 4000 Hz. To observe frequency behavior across the entire bed during experiments, up to eight pressure transducers can be used. A QBasic program was written to initiate the A/D conversion and store the pressure fluctuation data. Figure 5.4 shows the pressure data acquisition system. Dekoron® tubing of varying length was used to connect the transducers to the fluidized bed. Numerous changes in the length, diameter, and configuration of the pressure lines throughout the study had no effect on the pressure fluctuation frequency response. Even complete changes in the data acquisition system (i.e. new data acquisition boards, and numerous different computers) did not change the resulting Bode plots.

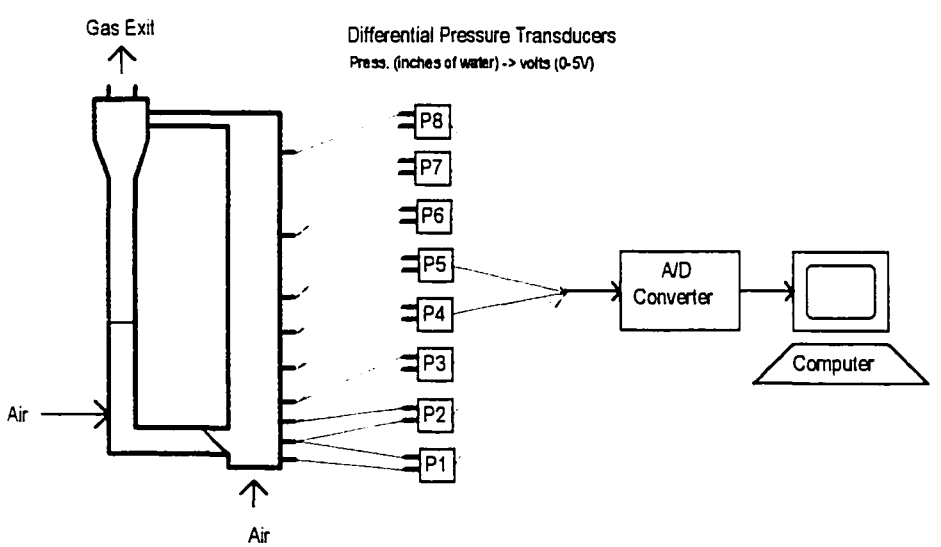

Figure 5.4: CFB pressure data acquisition system

ISU Power Plant CFB Boiler

A number of experiments were completed to determine the nature of industrial scale CFB Boiler pressure fluctuations. These tests were developed to determine whether CFB pressure fluctuations can be used as diagnostic indicators in industrial scale CFB boilers, and also whether these signals can be related to similar pressure fluctuations observed in small-scale cold-model CFBs. Two 170,000 lb/hr steam Pyropower CFB boilers are located on the campus of Iowa State University. ISU's CFB Boiler #1 and CFB Boiler #2 both had two transducers installed along the CFB wall to monitor absolute pressure. All four transducers in the two boilers had an output of 1 to 4 volts. The transducers that measure what was referred to as the bed pressure record static pressure fluctuations immediately above the gas distribution plate. These transducers have a range of 0 to 60 inches of H_20. The transducers in the combustion chamber measure the static pressure fluctuations at an elevation of 60 feet above the distributor plate. These transducers have a range of -3 to 17 inches of H_20. The boilers have a square cross-section of 4.3 x 4.3 meters (14'x14'), and a height from distributor to top of CFB riser of around 20 meters (65 feet). Under standard operating conditions, the boiler operates with 137,000 lb/hr fluidizing air and 74,000 lb/hr secondary air. The bed material (ash, limestone, and coal) consists of particles which predominantly range between 100 and 1000 micrometers in diameter. The pressure measured at the bottom of the bed under these conditions approximately ranges from 15-25 inches of H_20, and the bed temperature is maintained between 1400-1600 °F. The fluctuation data was sampled at 20, 50, 90, 200, 400, and 1000 Hz, with data set sizes ranging from 70,000 to 620,000 data points to insure adequate Bode plot resolution. Using a portable computer with a 12 bit A/D (0-5V) board, the output voltage from the boiler transducers was recorded and stored.

CHAPTER 6. THEORETICAL BACKGROUND

This chapter is organized into three subsections: theoretical description of second order phenomena in fluidized beds; similitude theory for bubbling fluidized beds; and similitude theory for circulating fluidized beds. A principle goal of this research is to examine the characteristics of pressure fluctuations in circulating fluidized beds in order to assess their usefulness as a design tool (e.g. model scale-up) or diagnostic tool (e.g. boiler control) in industrial scale CFB combustors. In order to achieve this objective, it is necessary to understand pressure fluctuations in bubbling fluidized beds prior to studying similar fluctuations in CFBs for a number of reasons. First, the majority of previous research on pressure fluctuations has been conducted in bubbling fluidized beds. This body of published data and proposed theories provides a basis for comparison to our experimental results and subsequent hypotheses. Secondly, there are similarities in the structure of pressure fluctuations in bubbling fluidized beds and circulating fluidized beds. The fluctuations in the lower dense region of the CFB exhibit a similar frequency response profile as those observed in bubbling fluidized beds. Oscillatory second order system dynamics are observed in the pressure fluctuations of all fluidization systems. Finally, fluidized bed similitude relations were first applied to bubbling beds and then extended to CFBs. Before the relations for CFB similitude can be validated using pressure fluctuations, the validity of using fluctuations to verify similitude in bubbling beds must be addressed.

Despite the wealth of published research dealing with bubbling fluidized bed fluctuations, there is still no consensus as to the phenomena that governs pressure fluctuations. The following section will develop two possible models for pressure dynamics in fluidized beds.

Evaluation of the Global Theories of Fluidized Bed Oscillations

It is hypothesized that two global fluidization phenomena are partially responsible for the structure of fluctuations. These two oscillatory phenomena can be generally referred to as

voidage fluctuations and surface waves. When evaluating potential theories that describe fluctuations in bubbling beds, two requirements must be considered. The first requirement is that the theory must be able to account for the second order system behavior observed in fluidized bed systems. The Bode plots of all fluidized bed systems exhibit a final asymptotic slope of -40 dB/decade. Figures 6.1 and 6.2 show examples of simple second order systems. In many cases, a single second order system is not sufficient to describe fluidization hydrodynamics. Experiments suggest that the dynamics of fluidization can be described by a model that assumes multiple second order systems acting concurrently within the fluidized bed system. Second order systems acting in parallel will also yield -40 dB/decade final Bode plot roll off (as shown by example in Figure 6.3). Secondly, the theory must be able to predict the observed dominant frequencies accurately and explain why at low bed heights they appear to be inversely proportional to the square root of bed height. Using a similar approach as Hiby [54], and making some important modifications in his derivation, a theory for voidage fluctuations can be developed that satisfies these two criteria in shallow, low velocity BFBs.

Derivation of a Modified-Hiby Model for Bubbling Fluidized Bed Dynamics

While Hiby's research provides the most plausible theory and rigorous derivation to date, he makes a fundamental error in the assumptions used in his theoretical derivation. By correcting this error, a more accurate relation can be developed to both predict the frequency of voidage fluctuations and make explicit why second order dynamics are observed in the BFB pressure fluctuations. Hiby begins his derivation by considering a single particle suspended in a fluidized bed [54]. If this particle is displaced from its equilibrium position (either upwards or downwards), the forces on the particle are altered in such a way to bring it back to its equilibrium position. As the bed expands from its state of equilibrium, the voidage increases, decreasing the interstitial velocity. This decrease in interstitial velocity reduces the upward acting frictional force resulting from the gas flow on the individual particle. Using h_i to denote the vertical elevation of an individual particle, Newton's second law on a single particle in a fluidized bed system (neglecting damping mechanisms) can be written as:

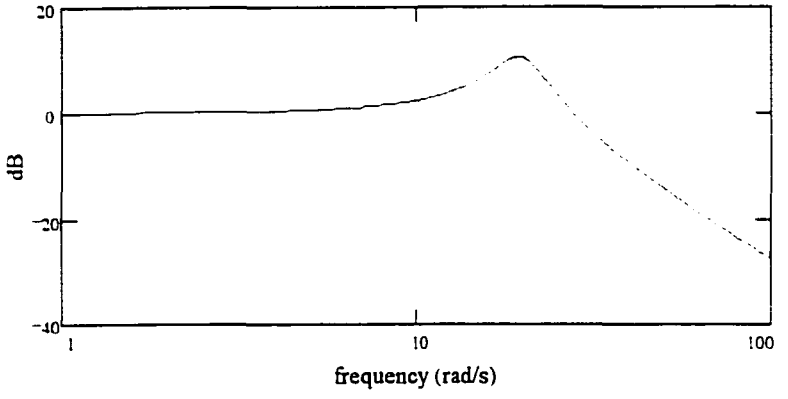

Figure 6.1: Example - simple 2nd order underdamped system Bode plot (ω_n=20 s^{-1}, ς=0.3)

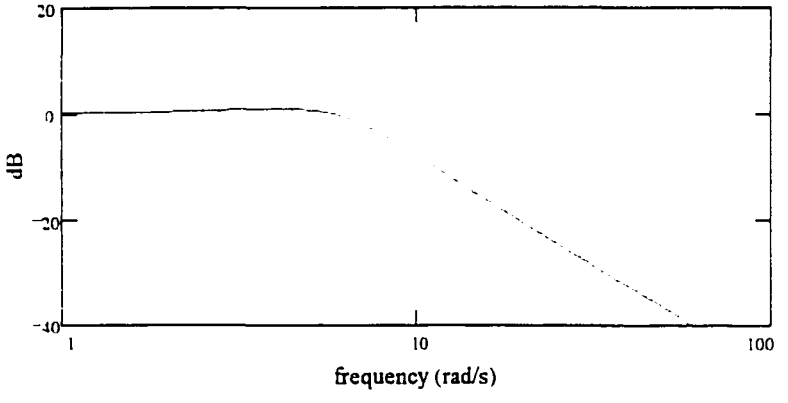

Figure 6.2: Example - simple 2nd order overdamped system Bode plot (ω_n=6 s^{-1}, ς=1.1)

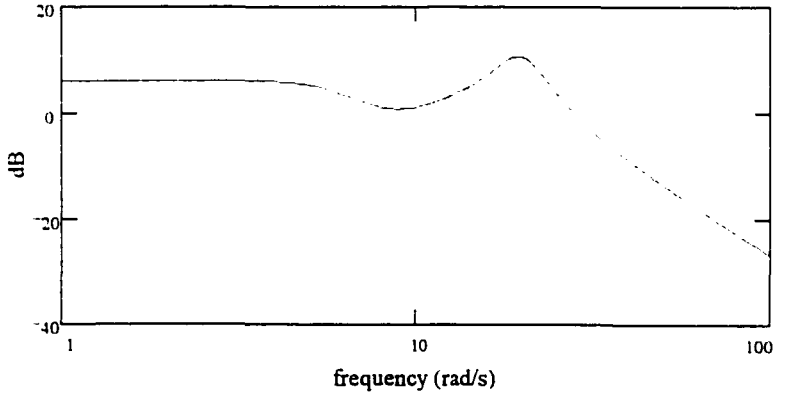

Figure 6.3: Example - Bode plot of the above second order systems acting in parallel

$$K_R \cdot h_i = m_i \cdot \frac{d^2 h_i}{dt^2} \tag{6.1}$$

where K_R is a constant analogous to the spring constant in a spring-mass system. It is the quantitative measure of how the restoring force changes with changes in the particle height. This linear estimate of system behavior can be used for small changes in the elevation of a single particle:

$$K_R = \frac{dF_i}{dh_i} \tag{6.2}$$

To develop an expression for K_R, a force balance on a single particle is required. The force acting on a single particle is the sum of its weight and the frictional force exerted by the gas flow (neglecting buoyancy forces which are typically very small in gas fluidization systems). The average force on an individual particle can be estimated by dividing the total lifting force acting on the bed ($\Delta p \cdot A$) by the total number of particles (N).

$$F_i = -m_i g + \frac{\Delta p A}{N} \tag{6.3}$$

The number of particles in a fluidized bed can be defined as:

$$N = \frac{V_s}{V_p} = \frac{V \cdot (1-\varepsilon)}{\left(\frac{\pi}{6}\right) \cdot d_p^{\,3}} \tag{6.4}$$

Combining 6.3 and 6.4:

$$F = -mg + \frac{\pi \cdot \Delta p \cdot A \cdot d_p^{\,3}}{6 \cdot V \cdot (1-\varepsilon)} \tag{6.5}$$

Substituting A/V = 1/H:

$$F = -mg + \left(\frac{\pi \cdot d_p^{\,3}}{6 \cdot (1-\varepsilon)}\right) \cdot \left(\frac{\Delta p}{H}\right) \tag{6.6}$$

Under fluidization conditions the pressure drop can be estimated using the Ergun equation at minimum fluidization velocity (U_{mf}). Hiby uses superficial velocity U rather than the constant

U_{mf} to estimate the pressure drop in an incipiently fluidized bed. This is Hiby's fundamental error. From the Ergun equation at minimum fluidization:

$$\frac{\Delta p}{H} = 150 \cdot \frac{U_{mf} \cdot \mu}{d_p^2} \cdot \frac{(1-\varepsilon)^2}{\varepsilon^3} + 1.75 \cdot \frac{\rho_g \cdot U_{mf}^2}{d_p} \cdot \frac{(1-\varepsilon)}{\varepsilon^3} \tag{6.7}$$

Therefore:

$$F = -mg + \left(\frac{\pi \cdot d_p^3}{6}\right) \cdot \left(150 \cdot \frac{U_{mf} \cdot \mu}{d_p^2} \cdot \frac{(1-\varepsilon)}{\varepsilon^3} + 1.75 \cdot \frac{\rho_g \cdot U_{mf}^2}{d_p} \cdot \frac{1}{\varepsilon^3}\right) \tag{6.8}$$

The assumption is made that individual particles oscillate such that at every moment all particles show the same relative vertical displacement from their equilibrium position. The bed voidage is only a function of time, and is independent of the height in the bed. The amplitude of an individual particle i is then proportional to its height h_i and,

$$\frac{dh_i}{h_i} = \frac{dH}{H} \tag{6.9}$$

relating ε to the bed height,

$$\varepsilon = \frac{V - V_s}{V} = 1 - \frac{V_s}{A \cdot H} \tag{6.10}$$

solving for H,

$$H = \frac{V_s}{A \cdot (1-\varepsilon)} \tag{6.11}$$

From equation 6.9

$$\frac{dH}{dh_i} = \frac{H}{h_i} \tag{6.12}$$

Differentiating equation 6.10,

$$\frac{d\varepsilon}{dH} = \frac{V_s}{A \cdot H^2} \tag{6.13}$$

Combining equations 6.13, 6.12, and 6.11,

$$\frac{d\varepsilon}{dh_i} = \frac{d\varepsilon}{dH} \cdot \frac{dH}{dh_i} = \frac{V_s}{A \cdot H \cdot h_i} = \frac{1-\varepsilon}{h_i} \tag{6.14}$$

Differentiating equation 6.8,

$$\frac{dF_i}{d\varepsilon} = -\left(\frac{\pi \cdot d_p^{\,3}}{6}\right) \cdot \left(150 \cdot \frac{U_{mf} \cdot \mu}{d_p^{\,2}} \cdot \frac{3-2\cdot\varepsilon}{\varepsilon^4} + 1.75 \cdot \frac{\rho_g \cdot U_{mf}^{\,2}}{d_p} \cdot \frac{3}{\varepsilon^4}\right) \tag{6.15}$$

Combining equations 6.14 and 6.15,

$$\frac{dF_i}{dh_i} = K_R = \left(\frac{\pi \cdot d_p^{\,3}}{6 \cdot h_i}\right) \cdot \left(150 \cdot \frac{U_{mf} \cdot \mu}{d_p^{\,2}} \cdot \frac{(1-\varepsilon)\cdot(3-2\cdot\varepsilon)}{3\cdot\varepsilon^4} + 1.75 \cdot \frac{\rho_g \cdot U_{mf}^{\,2}}{d_p} \cdot \frac{1-\varepsilon}{\varepsilon^4}\right) \tag{6.16}$$

As in a mass-spring system the frequency of oscillation can be predicted by:

$$\omega_i = \sqrt{\frac{K_R}{m_i}} = \sqrt{\left(\frac{3}{\rho_s \cdot h_i}\right)\left(150 \cdot \frac{U_{mf} \cdot \mu}{d_p^{\,2}} \cdot \frac{(1-\varepsilon)(3-2\cdot\varepsilon)}{3\cdot\varepsilon^4} + 1.75 \cdot \frac{\rho_g \cdot U_{mf}^{\,2}}{d_p} \cdot \frac{1-\varepsilon}{\varepsilon^4}\right)} \tag{6.17}$$

Therefore

$$\omega_i = C_1 \cdot h_i^{-0.5} \tag{6.18}$$

For small changes in the equilibrium voidage ($\varepsilon \approx \varepsilon_{mf}$), C_1 is a constant equal to:

$$C_1 = \sqrt{\frac{3}{\rho_s}\left(150 \cdot \frac{U_{mf} \cdot \mu}{d_p^{\,2}} \cdot \frac{(1-\varepsilon_{mf})\cdot(3-2\cdot\varepsilon_{mf})}{3\cdot\varepsilon_{mf}^{\,4}} + 1.75 \cdot \frac{\rho_g \cdot U_{mf}^{\,2}}{d_p} \cdot \frac{1-\varepsilon_{mf}}{\varepsilon_{mf}^{\,4}}\right)} \tag{6.19}$$

This shows that the natural frequency of a particle depends on its height in the bed. The entire bed will tend to oscillate at an overall mean frequency of the particles, as the bed is "pulled into tune". Hiby estimates this mean frequency by summing up a weighted average based on the amplitude of oscillation of each level of particles.

$$\omega_m = \frac{\int_0^H \left(C_1 \cdot h^{-0.5}\right) \cdot h dh}{\int_0^H h dh} = \frac{4}{3} \cdot C_1 \cdot H^{-0.5} \tag{6.20}$$

therefore,

$$\omega_m = \frac{4}{3}\sqrt{\frac{3}{\rho_s \cdot H}\left(150 \cdot \frac{U_{mf} \cdot \mu}{d_p^{\,2}} \cdot \frac{(1-\varepsilon_{mf})\cdot(3-2\cdot\varepsilon_{mf})}{3\cdot\varepsilon_{mf}^{\,4}} + 1.75 \cdot \frac{\rho_g \cdot U_{mf}^{\,2}}{d_p} \cdot \frac{1-\varepsilon_{mf}}{\varepsilon_{mf}^{\,4}}\right)} \tag{6.21}$$

and converting to cycles per second (Hz),

$$v_m = \frac{2}{3 \cdot \pi} \sqrt{\frac{3}{\rho_s \cdot H} \left(150 \cdot \frac{U_{mf} \cdot \mu}{d_p^2} \cdot \frac{\left(1 - \varepsilon_{mf}\right)\left(3 - 2 \cdot \varepsilon_{mf}\right)}{3 \cdot \varepsilon_{mf}^4} + 1.75 \cdot \frac{\rho_g \cdot U_{mf}^2}{d_p} \cdot \frac{1 - \varepsilon_{mf}}{\varepsilon_{mf}^4} \right)} \quad (6.22)$$

For Rep < 20 the first term within the bracket dominates and U_{mf} can be estimated.

$$U_{mf} = \frac{d_p^2 \cdot \rho_s \cdot g}{150 \cdot \mu} \frac{\varepsilon_{mf}^3}{1 - \varepsilon_{mf}} \quad (6.23)$$

For ($\varepsilon = \varepsilon_{mf}$)The natural frequency from equation 6.22 would reduce to:

$$v_m = \frac{2}{3 \cdot \pi} \sqrt{\frac{g}{H} \cdot \left(\frac{\left(3 - 2 \cdot \varepsilon_{mf}\right)}{\varepsilon_{mf}} \right)} \quad (6.24)$$

For Rep > 20 the second term within the bracket dominates and U_{mf} can be estimated.

$$U_{mf} = \sqrt{\frac{d_p \cdot \rho_s \cdot g \cdot \varepsilon_{mf}^3}{1.75 \cdot \rho_g}} \quad (6.25)$$

Again, assuming $\varepsilon_{mf} \approx \varepsilon$, the natural frequency from equation 6.22 would reduce to:

$$v_m = \frac{2}{3 \cdot \pi} \sqrt{\frac{3 \cdot g}{H} \cdot \left(\frac{1 - \varepsilon_{mf}}{\varepsilon_{mf}} \right)} \quad (6.26)$$

Equation 6.26 is identical to the relation that Hiby derives. In bubbling beds, Re_p is significantly less than twenty and equation 6.24 should predict the frequency of oscillation for shallow fluidized beds.

In addition to establishing a modified Hiby relation (equation 6.24) to predict the observed natural frequency of the bed, it is evident from the derivation of this dynamic model that pressure fluctuations will exhibit second order behavior. From Newton's second law on a single particle with u(t) as the white noise forcing function and neglecting damping mechanisms:

$$\frac{dh_i^2(t)}{dt^2} + \frac{K_R}{m} h_i(t) = u(t) \quad (6.27)$$

Knowing that the change in position is proportional to the change in voidage, and the change in voidage proportional to the change in pressure drop:

$$\frac{d\Delta p^2(t)}{dt^2} + \frac{K_R}{m}\Delta p(t) = u(t) \tag{6.28}$$

The modified Hiby relation satisfies the two important criteria for a global dynamic model of shallow fluidized bed systems. It not only predicts the dominant frequency, but also provides an explanation for the second order pressure fluctuation response observed.

Surface Waves in Fluidized Bed Systems

Another second order phenomenon that may be responsible for pressure fluctuations in fluidized beds is surface waves analogous to surface waves observed in water. As proposed by Sun et. al [60], since the hydrodynamics of fluidized bed systems exhibit many of the characteristics of liquid, surface waves are expected in a fluidized bed. Water waves are classified according to the ratio of water depth (H) to wave length (λ) [78]. For $H/\lambda < 1/20$, the waves are termed shallow waves and the frequency is dependent on both the water depth and wave length. For shallow waves, the governing wave equation (presented by Sun [60]) reduces to a simplified relation that can be used to estimate the wave frequency:

$$\omega = \frac{\sqrt{gH}}{\lambda} \tag{6.29}$$

For intermediate depth waves $1/20 > H/\lambda < 1/2$, the wave equation cannot be reduced to a simple expression for wave frequency, and must be estimated as:

$$\omega = \frac{1}{2\cdot\pi}\sqrt{\left[\frac{g}{\lambda\cdot 2\cdot\pi}\cdot\tanh\left(\frac{2\cdot\pi}{\lambda}\cdot H\right)\right]} \tag{6.30}$$

For deep waves ($H/\lambda > 1/2$), the wave equation can be again be simplified and the frequency is only dependent on the wavelength and can be estimated as:

$$\omega = \sqrt{\frac{g}{2\pi\lambda}} \tag{6.31}$$

For surface waves in a cylindrical container the wavelength is determined by the container diameter:

$$D = \frac{n}{2}\lambda \tag{6.32}$$

where n is an integer greater than zero. The fundamental frequency is represented by n = 1, with overtones represented by higher integer values. Assuming that a half-wave is established in the bed ($\lambda/2 = D$) the deep wave frequency in a fluidized bed could be estimated as:

$$\omega = \sqrt{\frac{g}{4\pi D}} \tag{6.33}$$

As will be shown in the following chapter, both the modified-Hiby and a wave phenomena provide insight into the pressure dynamics of both bubbling and circulating beds.

The Use of Pressure Fluctuations to Validate Similitude Parameters

The most extensive research on the subject of similitude in fluidized bed systems has been done by Glicksman [63, 14]. Using both the Buckingham Pi theorem and derivations based on fundamental equations of motion, Glicksman proposes a set of similitude parameters that govern fluidization. Glicksman assumes that if the PSDs or PDFs of pressure fluctuations match between model and prototype, then the fluidized beds are in hydrodynamic similitude. However, he does not distinguish the important characteristics of the PSD that must match in order for two beds to be governed by similar dynamics. Particularly in CFBs, Glicksman's data does not show the important spectral characteristics in the PSD due to inadequate data sampling. Furthermore, Glicksman never questioned whether pressure fluctuations were correlated to the hydrodynamic state of a fluidized bed. After relating Bode plot characteristics to physical phenomena in fluidized beds, this study will reassess whether pressure fluctuations can be used to validate proposed BFB and CFB similitude parameters.

BFB Similitude

The Buckingham Pi theorem will be used to develop the important non-dimensional fluidized bed parameters. Using the frequency of pressure fluctuations as the dependent parameter, all independent variables important for bubbling fluidization can be defined:

$$\omega = f(U, g, D, H, d_p, \rho_s, \rho_g, \mu, \phi)$$

The dimensions are as follows:

$[\omega] = 1/T$	$[U] = L/T$	$[g] = L/T^2$	$[D] = L$
$[H] = L$	$[d_p] = L$	$[\rho_s] = M/L^3$	$[\rho_g] = M/L^3$
$[\mu] = M/LT$	$[\phi] = 1$		

If we choose U, d_p, and ρ_g as the dimensionally independent parameters the remaining variables can be non-dimensionalized based on these variables.

$$g \rightarrow \frac{g \cdot d_p}{U^2} \qquad H \rightarrow \frac{H}{d_p} \qquad D \rightarrow \frac{D}{d_p}$$

$$\rho_s \rightarrow \frac{\rho_s}{\rho_g} \qquad \mu \rightarrow \frac{\mu}{\rho_g \cdot U \cdot d_p} \qquad \omega \rightarrow \omega \cdot \frac{d_p}{U}$$

Recognizing the dimensionless g and μ as the inverse of the Froude number and Reynolds number respectively the full set of dimensionless parameters as Glicksman defines them is:

$$Fr = \frac{U^2}{g \cdot d_p} \qquad \frac{H}{d_p} \qquad \frac{D}{d_p} \qquad \frac{\rho_g}{\rho_s} \qquad \mathrm{Re}_p = \frac{\rho_g \cdot U \cdot d_p}{\mu}$$

Also, it is more convenient to modify the dependent frequency spectrum parameter by multiplying by other dimensionless groupings as shown below.

$$\omega \cdot \frac{d_p}{U} \Rightarrow \omega \cdot \frac{d_p}{U} \times \sqrt{\frac{U^2}{g \cdot d_p}} \times \sqrt{\frac{H}{d_p}} \Rightarrow \omega \cdot \sqrt{\frac{H}{g}}$$

By matching the dimensionless parameters in a 10.2 cm BFB and a 5.1 cm pressurized BFB, the corresponding non-dimensionalized Bode plots can be compared.

Another important dependent variable that should be compared in fluidized bed systems is the pressure drop per unit length. Non-dimensionalizing this dependent variable via the same Buckingham Pi approach used above yields:

$$\frac{\Delta P}{L} = \rho_s \cdot (1-\varepsilon) \cdot g \Rightarrow \rho_s \cdot (1-\varepsilon) \cdot g \cdot \frac{D}{U^2 \cdot \rho_f} = \frac{\rho_s}{\rho_f}(1-\varepsilon) \cdot Fr \Rightarrow (1-\varepsilon)$$

In addition to the Bode plot profiles of pressure fluctuations being similar, the local voidage measured in the fluidized bed should be equal.

CFB Similitude

For CFB hydrodynamics, Glicksman [15] adds an additional independent variable, Gs [kg/m^{2}s], to the list previously described for bubbling fluidized bed systems. Using the Buckingham Pi theorem, the full set of independent dimensionless parameters for circulating fluidized beds is summarized as follows:

$$Fr = \frac{U^2}{g \cdot d_p} \qquad \frac{H}{d_p} \qquad \frac{D}{d_p} \qquad \frac{\rho_g}{\rho_s} \qquad \mathrm{Re}_p = \frac{\rho_g \cdot U \cdot d_p}{\mu} \qquad \frac{Gs}{\rho_s \cdot U}$$

As will be shown in the following chapter, the reactor loading or total mass of particles in the entire CFB system is another independent variable that must be considered in CFB systems that use L-valves. Under identical conditions, changing the reactor loading will significantly change the resulting axial voidage profile. This additional non-dimensional reactor loading variable was matched in this similitude study. The full set of CFB dimensionless parameters used in this study is:

$$Fr = \frac{U^2}{g \cdot d_p} \qquad \frac{H}{d_p} \qquad \frac{D}{d_p} \qquad \frac{\rho_g}{\rho_s} \qquad \mathrm{Re}_p = \frac{\rho_g \cdot U \cdot d_p}{\mu} \qquad \frac{Gs}{\rho_s \cdot U} \qquad \frac{M}{\rho_s \cdot D^3}$$

where M is the total mass of particles within the CFB system.

CHAPTER 7. RESULTS AND DISCUSSION

This section is organized into three subsections: bubbling regime fluctuations; turbulent regime fluctuations; and fast fluidization fluctuations. The first section provides a general description of BFB fluctuations and compares experimental data to the theoretical models that are hypothesized to govern pressure dynamics. Following this discussion, the results of a BFB similitude study are presented and discussed. The principle objective of the turbulent bed section is to provide the link between BFB fluctuations and CFB fluctuations. The similarities between fluctuations in these two different regimes are discussed in this section. The final fast fluidization regime section will follow the same general outline as the BFB section. The nature of fluctuations are discussed, and the results of a similitude study are presented. Most previous studies have focused on only one of these regimes. By addressing the similarities observed in the fluctuations of each regime, this study attempts to provide greater insight into the phenomena governing fluctuations. From this better understanding of pressure dynamics, the analysis of fluctuations can be used as a tool for verifying that similitude has been achieved.

Bubbling Regime Fluctuations

General characteristics

In most cases, fluidized bed systems cannot be described by a single frequency peak in the Bode plots of pressure fluctuations. In addition, these multiple peaks are not always observed as well defined peaks. Typically they are made up of a broad distribution of frequencies. Because of the presence of multiple phenomena and the appearance of broad peaks in the spectrum, accurate quantitative descriptions of the fluctuations can be difficult to develop. However, a number of trends in BFB pressure fluctuations can be observed.

The first important characteristic of BFB pressure fluctuations is that they exhibit the dynamics of a second order system. The Bode plots of all BFB fluctuations show a final asymptotic slope of -40 dB/decade, indicative of second order behavior. The Bode plots do

not suggest that a single second order system is sufficient to describe BFB dynamics. The results suggest that more than one second order system acting concurrently within the bed may be responsible for pressure fluctuations. The final asymptotic slope of -40 dB/decade and the multiple frequency phenomena are shown in the BFB Bode plot in Figure 7.1. There are three predominant peaks that may be observed in BFB systems. These three peaks will be termed α_1, α_2, and α_3 as shown in Figure 7.1. Occasionally, as will be seen in the results of the similitude study, an additional peak (α_0) is observed at a frequency lower than α_1 under high velocity conditions.

Under conditions of low to moderate velocity bubbling fluidization, particle size does not significantly effect the overall dynamic character of the fluctuations. Figures 7.2 - 7.4 show three Bode plots of fluctuations taken from similar beds of 0.2 mm, 0.3 mm, and 0.4 mm glass beads fluidized at $U/U_{mf} = 1.4$. The profiles are identical for these different particle sizes. Any slight variations in the dominant frequency, are likely due to variations in bubble properties or bed voidage. For further verification that particle diameter does not strongly influence the frequency of the system see Figures 7.5 - 7.8.

As shown in Figures 7.5-7.8, for $U/U_{mf} > 1.2$, changes in the superficial velocity do not effect the dominant frequency in the bubbling fluidization regime. At the onset of fluidization, the dominant frequency increases only slightly and then levels off as the superficial velocity is increased for $U/U_{mf} > 1.2$. It should be emphasized that although the superficial velocity does not change the characteristic period of oscillation of the system, it may effect the damping (or relative magnitude) of the observed frequencies in the spectrum.

Bed diameter will also affect the relative magnitude of the frequencies observed in the spectrum, although it will not (in the bubbling regime) affect the position at which the dominant system frequencies are observed. Figures 7.9 and 7.10 show the Bode plots of the 5.1 and 10.2 cm diameter beds respectively. In both beds the particle size, bed height, tap height and spacing, and superficial velocity are identical. It is evident that changes in the bed diameter can significantly effect the appearance of the resulting Bode plot. Despite differences in the relative magnitude of peaks, the dominant frequencies at which the bed

Experimental operating conditions			
Bed diameter	10.16 ± 0.01 cm	Bed height	20.0 ± 0.2 cm
Particle diameter	0.30 ± 0.01 mm	Pressure measurement	differential
Particle density	2600 ± 100 kg/m^3	Pressure tap position	Lower-2.5 cm/Upper-7.6 cm
Gas density (air)	1.20 ± 0.04 kg/m^3	Avg. voidage bwt. taps	0.48 ± 0.06
Superficial velocity	12.7 ± 0.6 cm/s (U/U_{mf} = 1.4)	Experiment number	6-21-1995-14.1

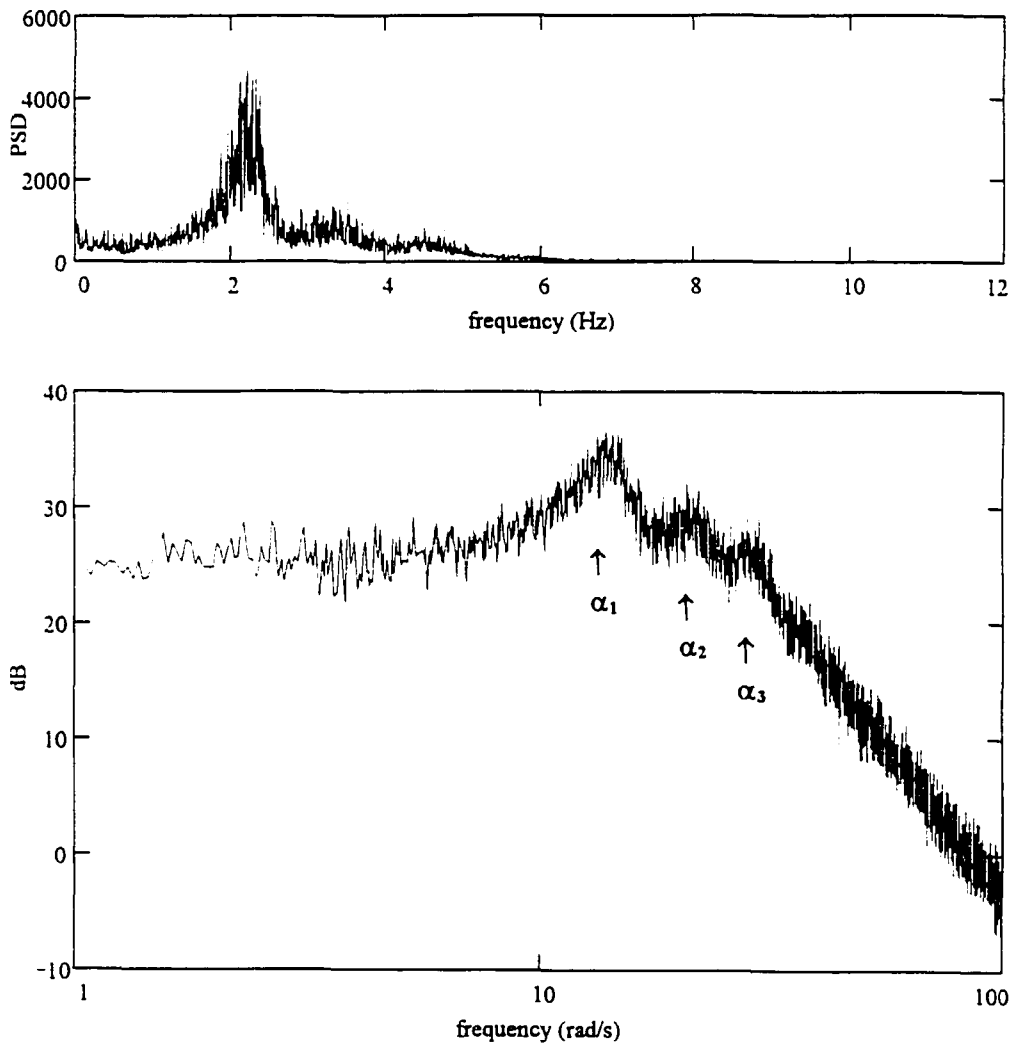

Figure 7.1: PSD and Bode plot of BFB fluctuations

Experimental operating conditions			
Bed diameter	10.16 ± 0.01 cm	Bed height	10.0 ± 0.2 cm
Particle diameter	0.20 ± 0.01 mm	Pressure measurement	differential
Particle density	2600 ± 100 kg/m^3	Pressure tap position	Lower - 2.5 cm/Upper - 7.6 cm
Gas density (air)	1.20 ± 0.04 kg/m^3	Avg. voidage bwt. taps	0.49 ± 0.06
Superficial velocity	5.7 ± 0.6 cm/s (U/U_{mf} = 1.4)	Experiment number	6-30-1995-11.1

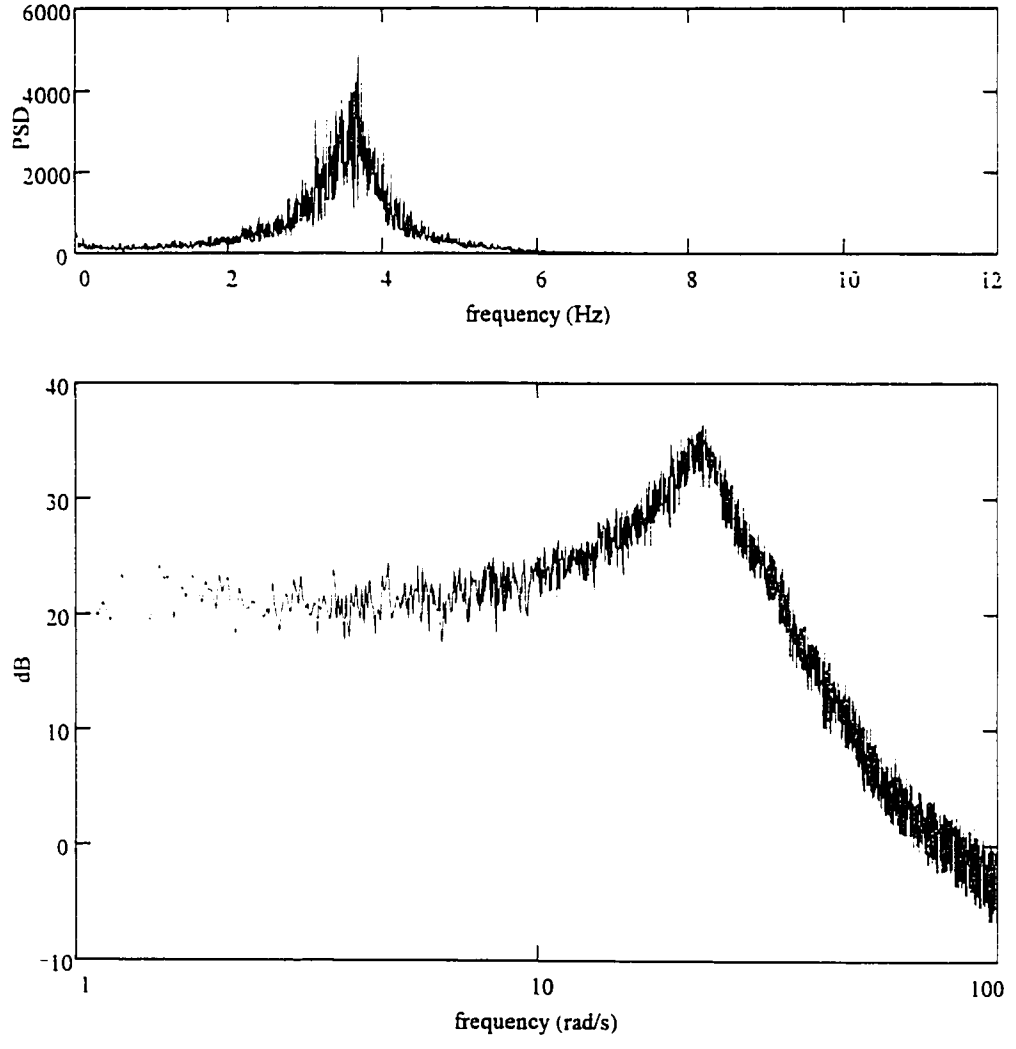

Figure 7.2. PSD and Bode plot of 0.2 mm glass bead BFB fluctuations

Experimental operating conditions			
Bed diameter	10.16 ± 0.01 cm	Bed height	10.0 ± 0.2 cm
Particle diameter	0.30 ± 0.01 mm	Pressure measurement	differential
Particle density	2600 ± 100 kg/m^3	Pressure tap position	Lower - 2.5 cm/Upper - 7.6 cm
Gas density (air)	1.20 ± 0.04 kg/m^3	Avg. voidage bwt. taps	0.49 ± 0.06
Superficial velocity	12.7 ± 0.6 cm/s (U/U_{mf} = 1.4)	Experiment number	6-22-1995-16.4

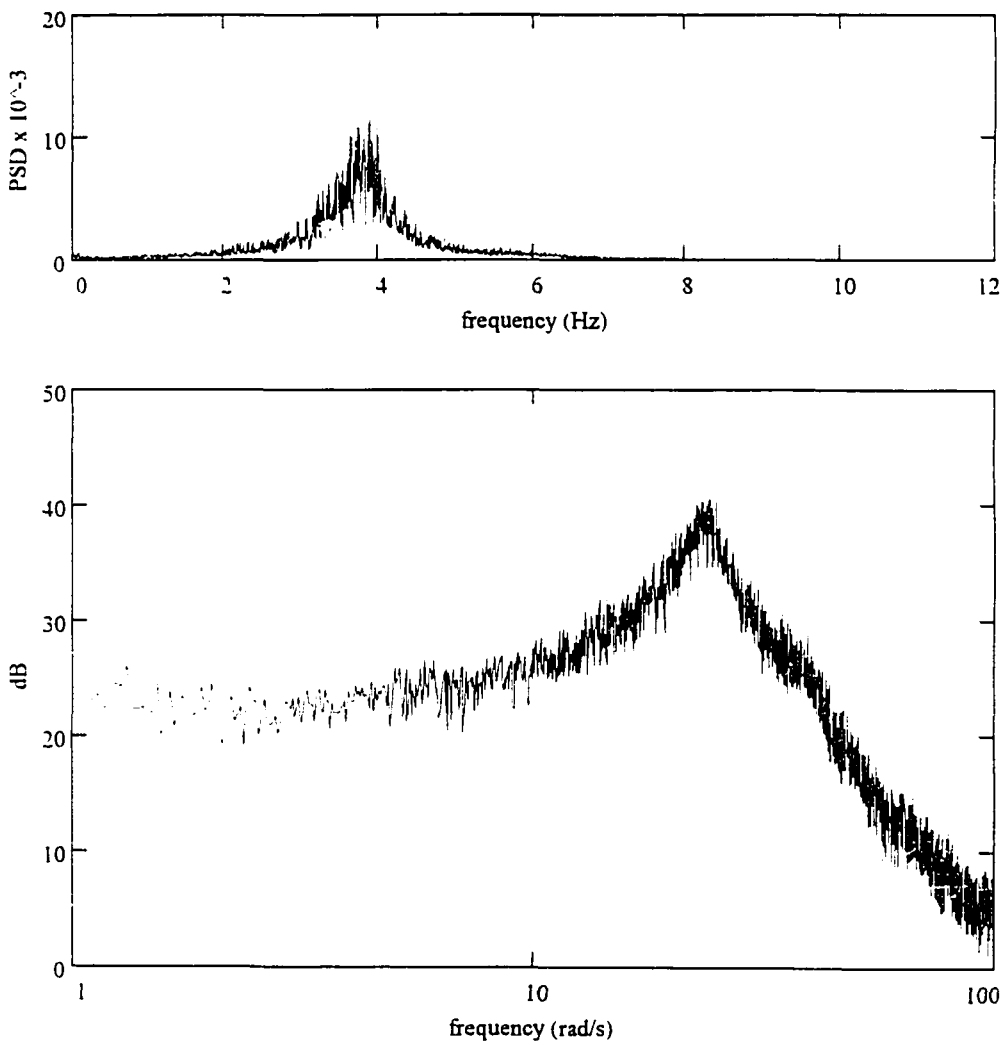

Figure 7.3: PSD and Bode plot of 0.3 mm glass bead BFB fluctuations

Experimental operating conditions			
Bed diameter	10.16 ± 0.01 cm	Bed height	10.0 ± 0.2 cm
Particle diameter	0.40 ± 0.01 mm	Pressure measurement	differential
Particle density	2600 ± 100 kg/m^3	Pressure tap position	Lower - 2.5 cm/Upper - 7.6 cm
Gas density (air)	1.20 ± 0.04 kg/m^3	Avg. voidage bwt. taps	0.50 ± 0.06
Superficial velocity	19.6 ± 0.6 cm/s (U/U_{mf} = 1.4)	Experiment number	7-3-1995-8.4

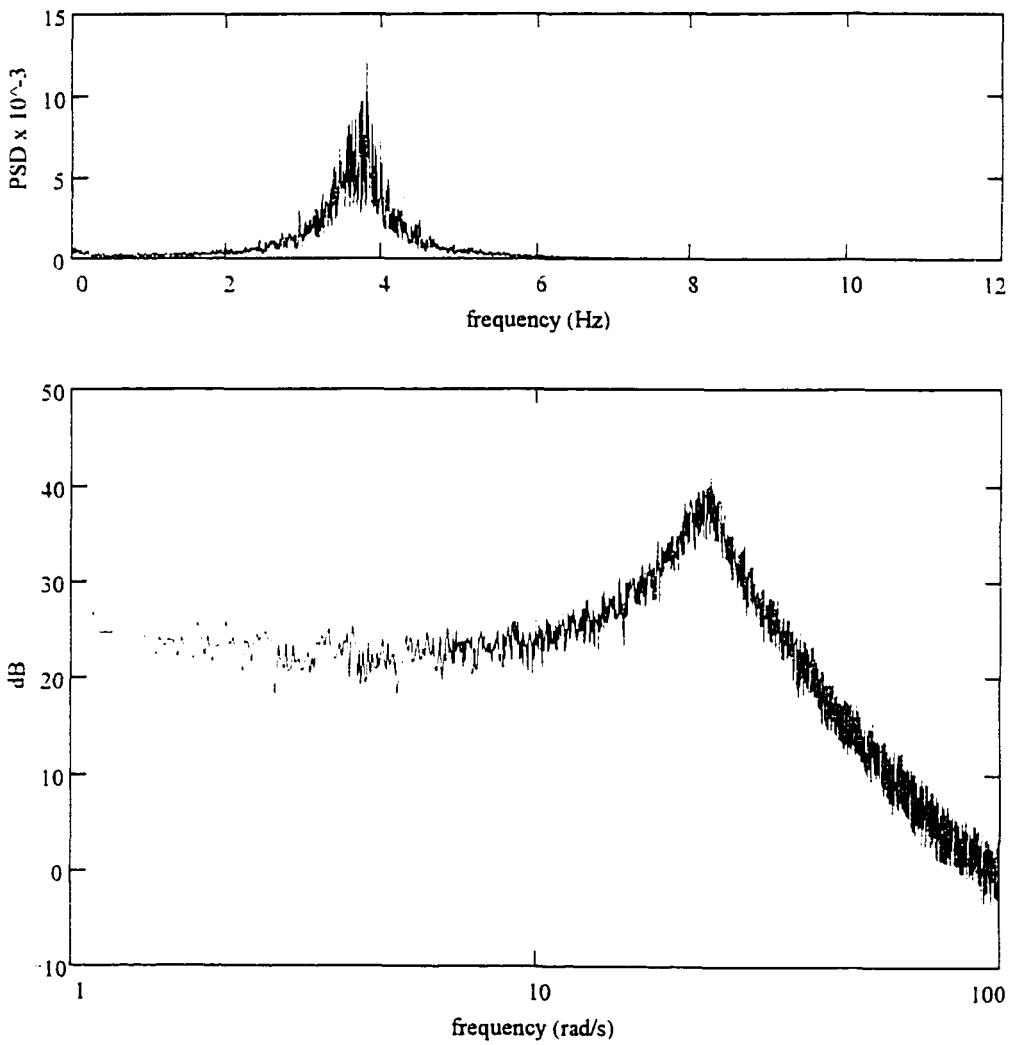

Figure 7.4: PSD and Bode plot of 0.4 mm glass bead BFB fluctuation

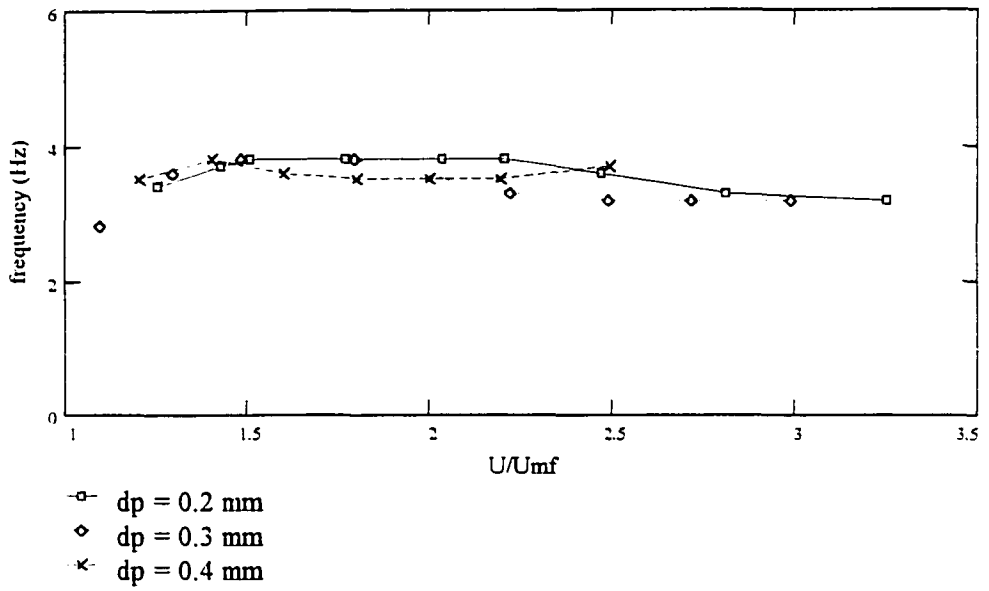

Figure 7.5: Fluctuation frequency versus U/Umf for 10.0 cm bed height

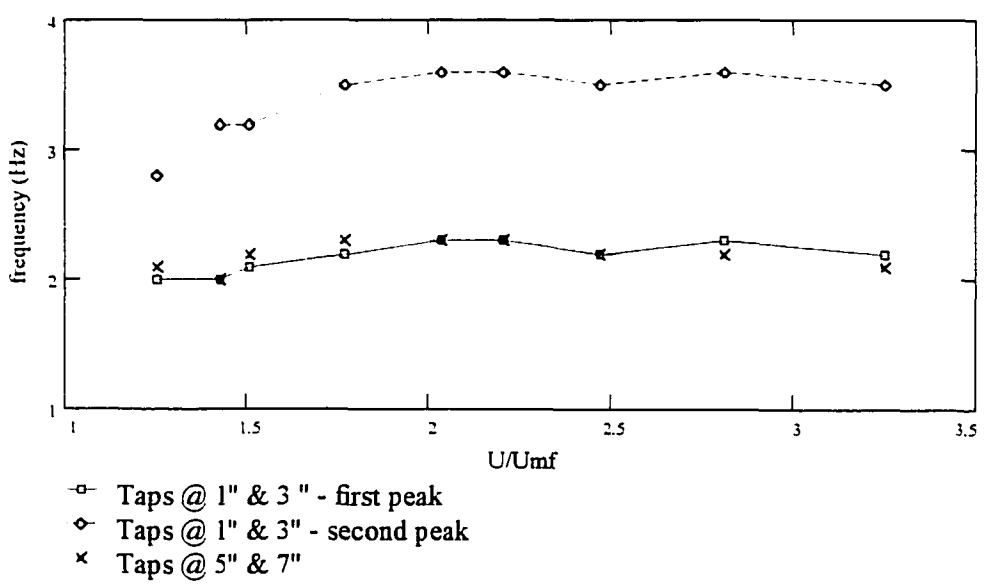

Figure 7.6: Fluctuation frequency versus U/Umf for 20 cm bed height and dp = 0.2 mm

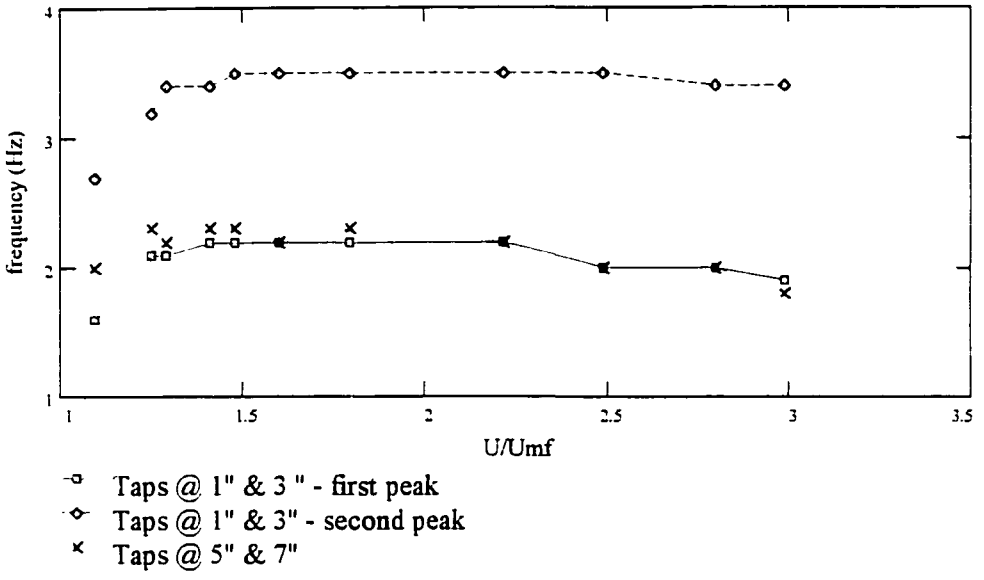

Figure 7.7: Fluctuation frequency versus U/Umf for 20 cm bed height and dp = 0.3 mm

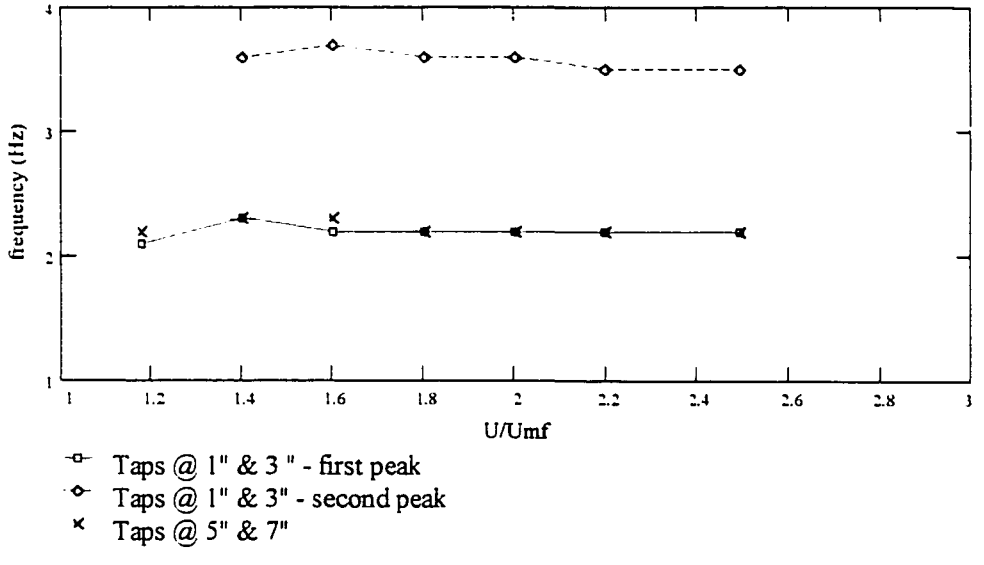

Figure 7.8: Fluctuation frequency versus U/Umf for 20 cm bed height and dp = 0.4 mm

Experimental operating conditions			
Bed diameter	5.08 ± 0.01 cm	Bed height	12.0 ± 0.2 cm
Particle diameter	0.20 ± 0.01 mm	Pressure measurement	differential
Particle density	2600 ± 100 kg/m^3	Pressure tap position	Lower - 3.8 cm/Upper - 6.4 cm
Gas density (air)	1.20 ± 0.04 kg/m^3	Avg. voidage bwt. taps	0.48 ± 0.06
Superficial velocity	5.6 ± 0.6 cm/s (U/U_{mf} = 1.4)	Experiment number	11-21-1995-11.8

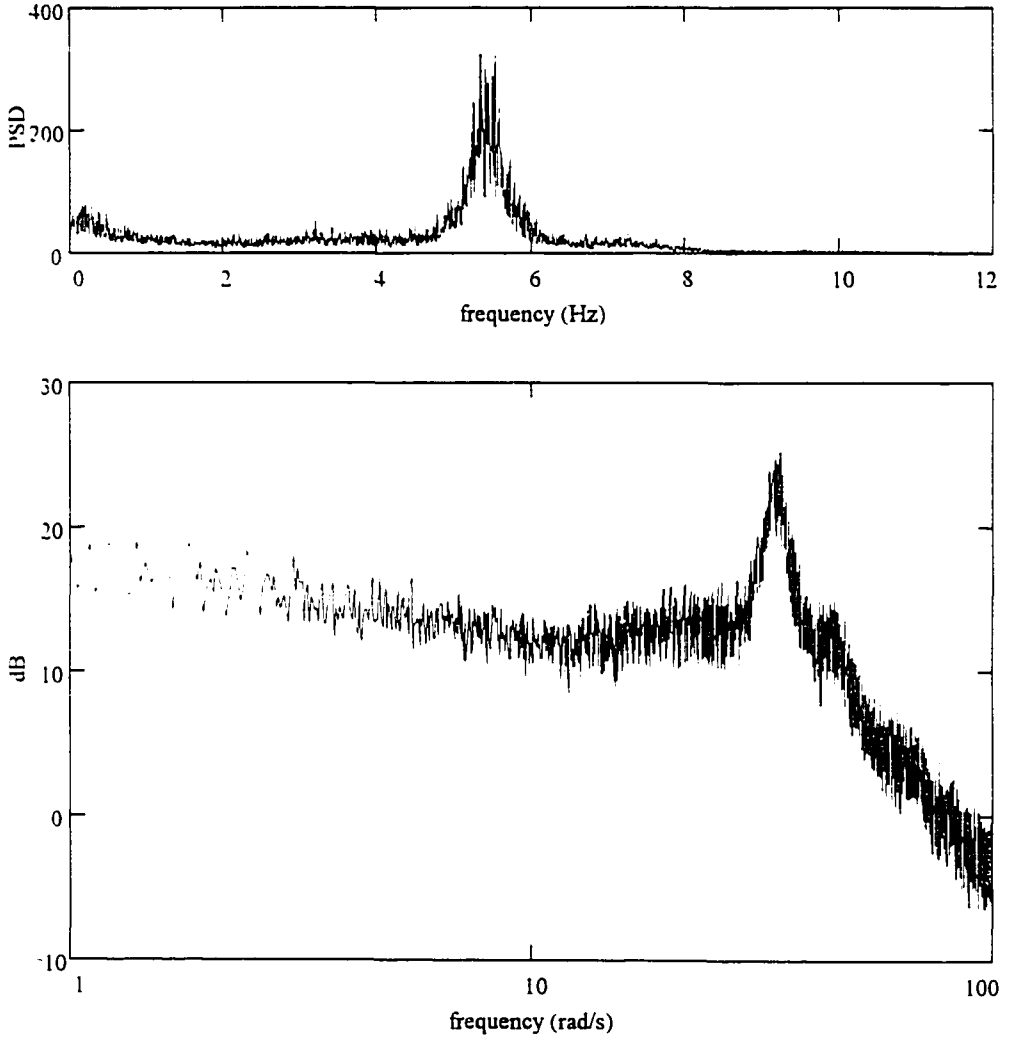

Figure 7.9: PSD and Bode plot of BFB fluctuations in 5.1 cm diameter bed

Experimental operating conditions			
Bed diameter	10.16 ± 0.01 cm	Bed height	12.0 ± 0.2 cm
Particle diameter	0.20 ± 0.01 mm	Pressure measurement	differential
Particle density	2600 ± 100 kg/m^3	Pressure tap position	Lower - 3.8 cm/Upper - 6.4 cm
Gas density (air)	1.20 ± 0.04 kg/m^3	Avg. voidage bwt. taps	0.48 ± 0.06
Superficial velocity	5.6 ± 0.6 cm/s ($U/U_{mf} = 1.4$)	Experiment number	11-21-1995-11.8

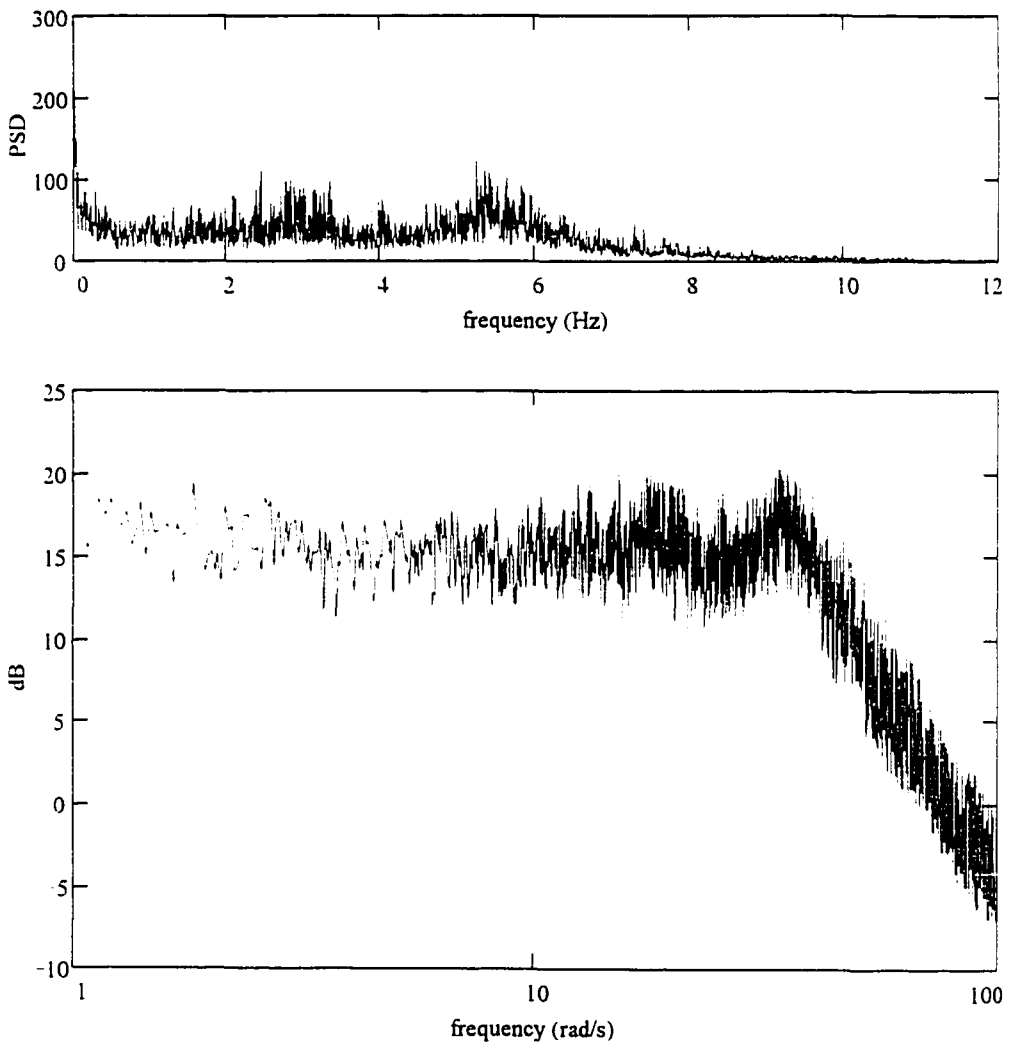

Figure 7.10: PSD and Bode plot of BFB fluctuations in 10.2 cm diameter bed

oscillates do not change. In both figures, dominant frequencies appear at 3.1 and 5.5 Hz, although the higher (5.5 Hz) frequency dominates as the bed diameter decreases.

Experiments suggest that global phenomena govern pressure fluctuations in bubbling fluidized beds. In previous work, static pressure measurements in a BFB were simultaneously recorded from the center of the bed and at the bed wall. The Bode plot profiles of the fluctuations at these two locations were identical. If the passage of local bubbles was solely responsible for pressure fluctuations, the hydrodynamics at the center of the bed would produce a different fluctuation structure, since the majority of bubbles rise to the surface through the center of the bed. Further evidence of the global nature of pressure fluctuations was obtained from an experiment in which two different distributor plates were tested under identical operating conditions. The two distributor plates had the same flow area, but one had 72 holes while the other had only 36 holes. Since bubbles form at the distributor plate holes, the 72 hole plate would produce more bubbles than the 36 hole plate. As is shown in Figures 7.11 - 7.12, the Bode plots of the pressure fluctuations from the two different distributor plate cases are identical, suggesting that random bubble passage in the vicinity of the region of pressure measurement is not a sufficient explanation for the observed fluctuations.

Discussion of α_1-frequency phenomena

It is hypothesized in this study that the modified-Hiby relation for fluidization can be used to predict oscillatory behavior in non-homogeneous systems. The derivation of this model neglects any bubble phenomena and uses assumptions valid only for homogeneous (non-bubbling) systems. Because of these assumptions in the model development, previous studies [54,55,60] have only compared this model to incipiently fluidized bed data. Our results suggest that this relation not only governs incipiently fluidized beds, but is also the mechanism that dictates bubble production in bubbling fluidized beds. Using $\varepsilon_{mf} = 0.48$ at U/Umf = 1.4, Figure 7.13 compares the BFB α_1-frequency to previous models and to the modified Hiby model proposed in this study. For bed heights less than 10 cm it is evident that the modified-Hiby relation best predicts the observed frequency. In shallow beds, the

Experimental operating conditions			
Bed diameter	10.16 ± 0.01 cm	Bed height	10.0 ± 0.2 cm
Particle diameter	0.40 ± 0.01 mm	Pressure measurement	differential
Particle density	2600 ± 100 kg/m^3	Pressure tap position	Lower - 2.5 cm/Upper - 7.6 cm
Gas density (air)	1.20 ± 0.04 kg/m^3	Avg. voidage bwt. taps	0.50 ± 0.06
Superficial velocity	19.6 ± 0.6 cm/s (U/U_{mf} = 1.4)	Experiment number	7-7-1995-11.6

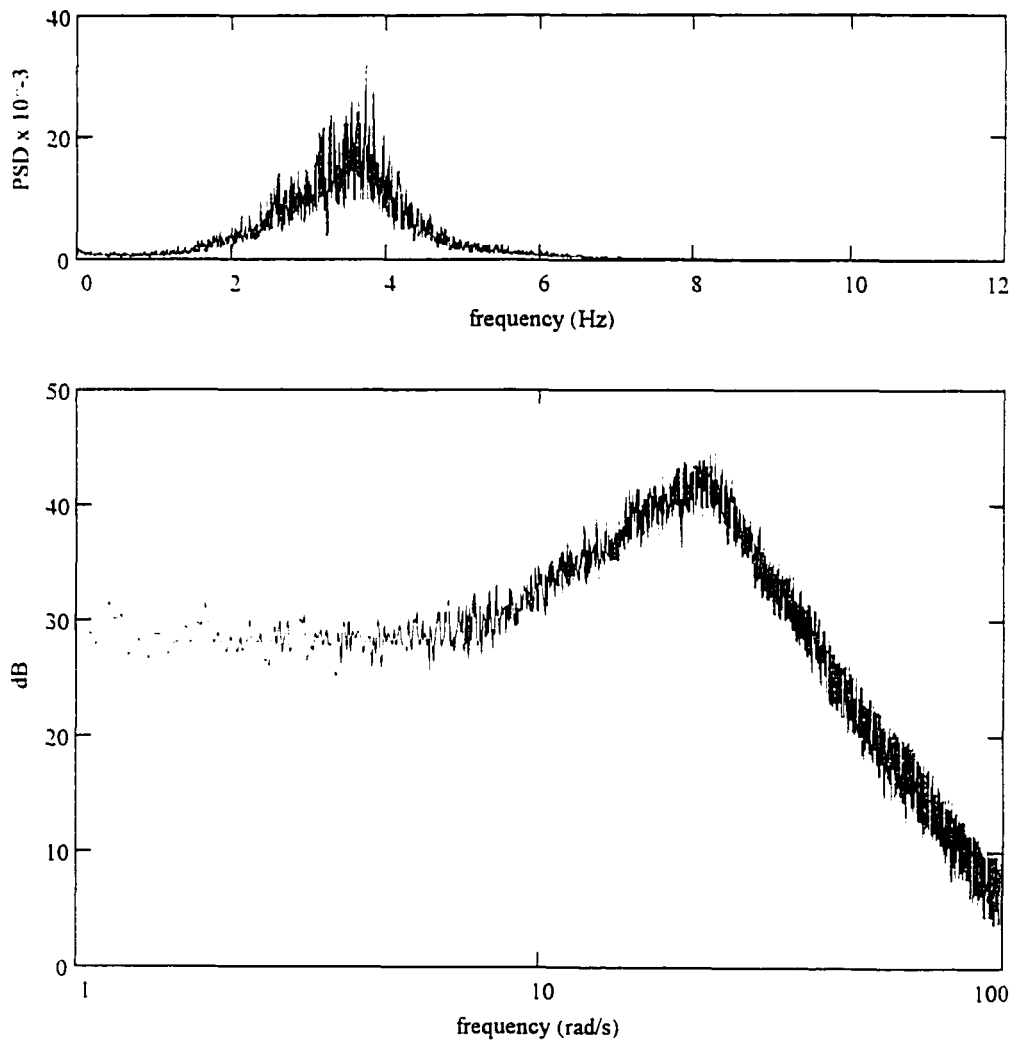

Figure 7.11 PSD and Bode plot of BFB fluctuations with 36 hole distributor

Experimental operating conditions			
Bed diameter	10.16 ± 0.01 cm	Bed height	10.0 ± 0.2 cm
Particle diameter	0.40 ± 0.01 mm	Pressure measurement	differential
Particle density	2600 ± 100 kg/m^3	Pressure tap position	Lower - 2.5 cm/Upper - 7.6 cm
Gas density (air)	1.20 ± 0.04 kg/m^3	Avg. voidage bwt. taps	0.50 ± 0.06
Superficial velocity	19.6 ± 0.6 cm/s ($U/U_{mf} = 1.4$)	Experiment number	7-3-1995-8.4

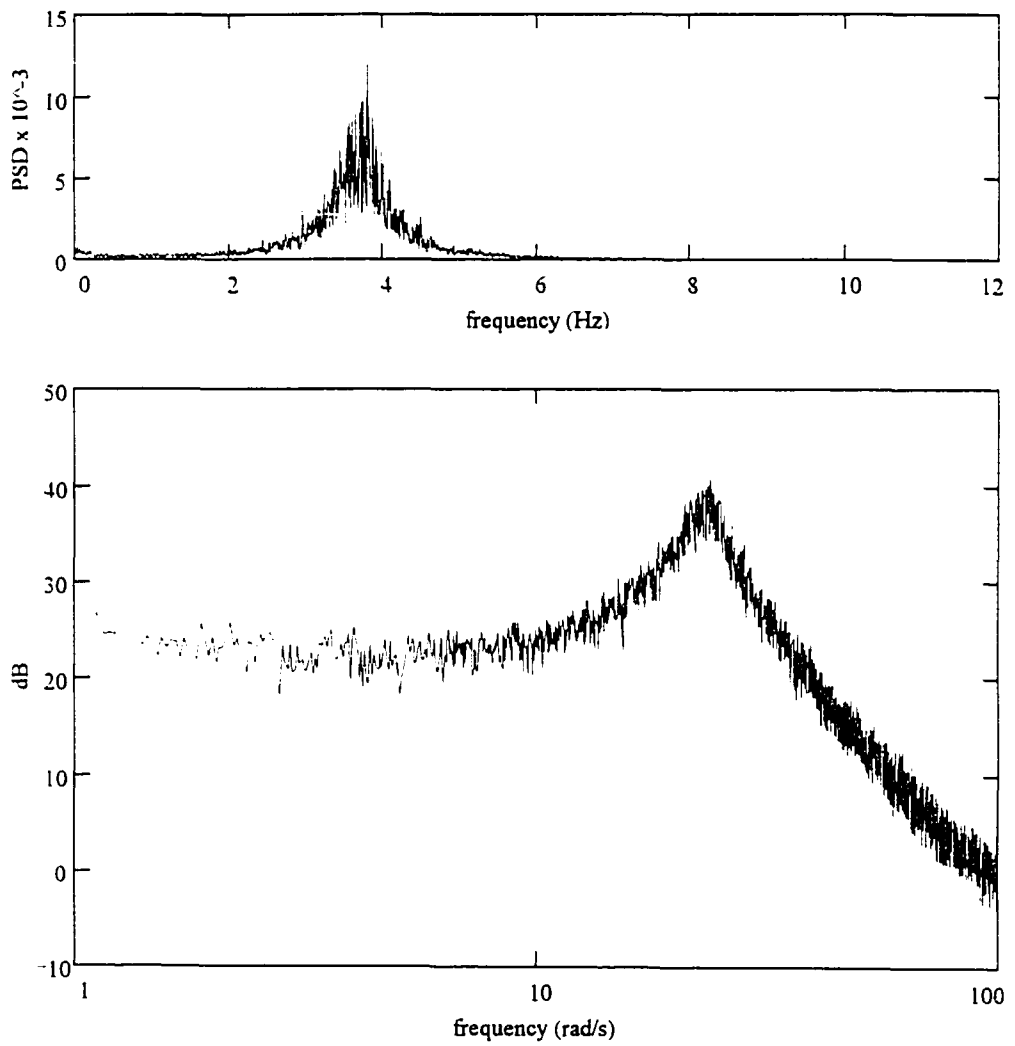

Figure 7.12: PSD and Bode plot of BFB fluctuations with 72 hole distributor plate

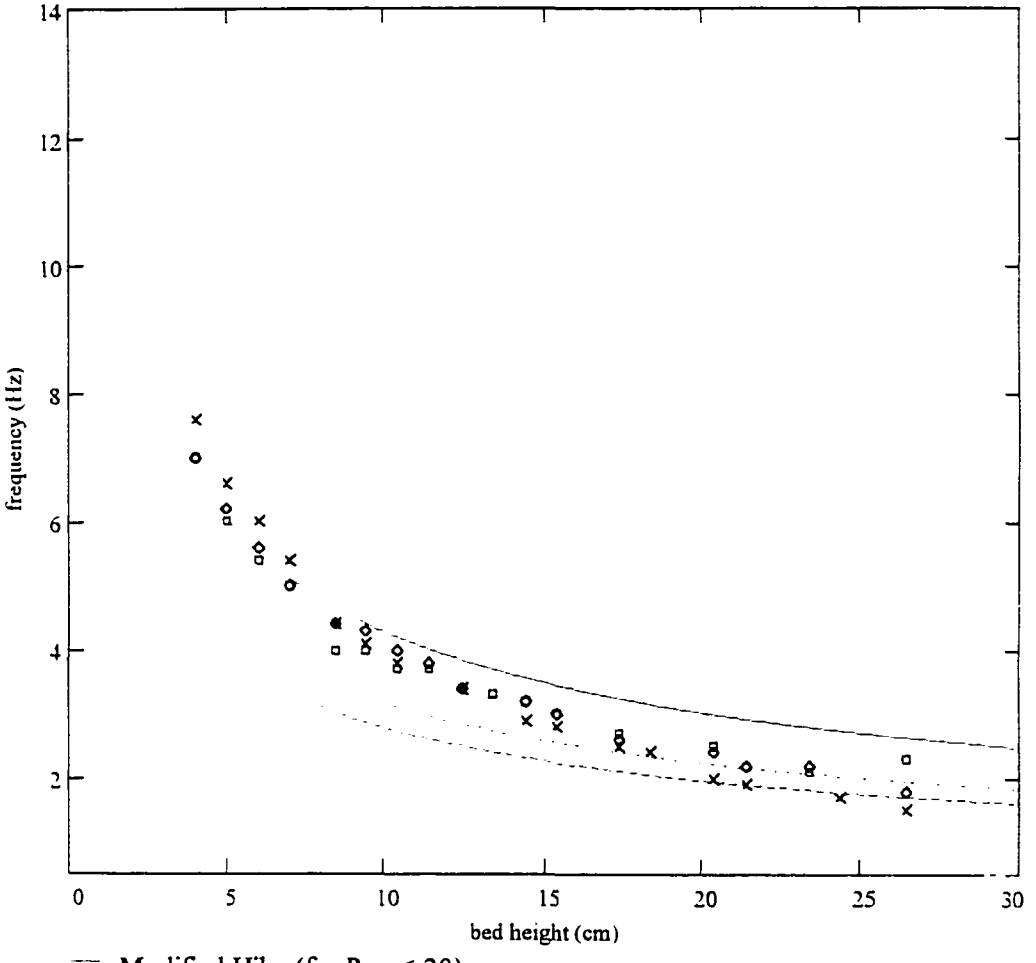

Figure 7.13: Comparison of proposed models to experimental data (D = 10.1 cm)
α_1-frequency vs. bed height

frequency is inversely proportional to $\sqrt{H}$, as is shown in the log-log plot of frequency versus bed height (see Figure 7.14). This good correlation is expected at low bed heights, since the bed height under fluidization is nearly equal to the fixed bed height (i.e. bed expansion is minimal). Effects of bubble coalescence are also minimized as bed height decreases. The bubbles produced in shallow beds remain relatively small. Under such conditions, the fluidized bed operates in a near homogeneous manner and the bed will continue to be dominated by voidage fluctuation phenomena. These voidage fluctuations facilitate the periodic production of bubbles in layers. It is the passage of these bubble layers (governed by voidage fluctuations) that results in the observed pressure fluctuations.

The deviation of experimental data from theory in deep beds may be due to the fact that as bed height increases, the amount of bed expansion from the fixed bed height also increases. The frequency data in Figures 7.13 and 7.14 is plotted versus the fixed bed height. The increased bed height would lower the observed frequency from the predicted value. Bubble coalescence also increases as the bed height increases. Under increased bubble coalescence, the bed can no longer be consider a quasi-homogeneous system (an assumption necessary for the modified Hiby relation). Increased coalescence interferes with the voidage fluctuations, augmenting this dominant frequency to a lower frequency (as observed in Figures 7.13 and 7.14). More research must be done to show how bed expansion and bubble coalescence affect the voidage fluctuations in bubbling fluidized beds.

Discussion of α_2-frequency phenomena

In Figure 7.15 the α_2-frequency is plotted versus the bed height for the 10.2 cm diameter BFB at U/Umf = 1.4 for three particle sizes. It is hypothesized that this frequency is the result of the BFB surface eruptions. As expected, this frequency decreases with increasing bed height, since bubble coalescence results in fewer (but larger) bubbles erupting at the surface. The magnitude of these surface fluctuations increases as the bubble size at the surface increases. For very shallow beds, the α_2-frequency does not appear in the spectrum

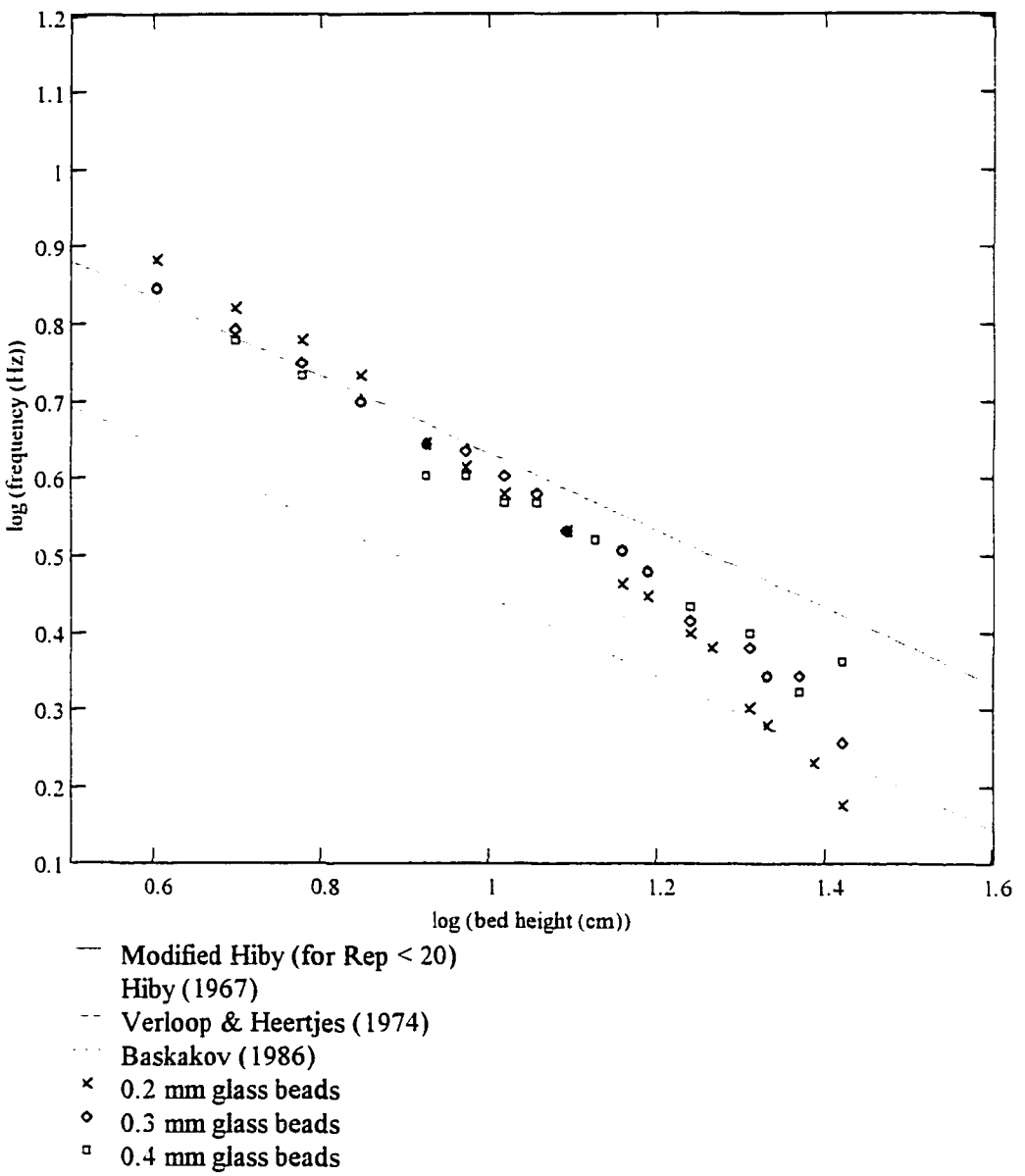

Figure 7.14: log-log comparison of proposed models to experimental data (D = 10.1 cm) log(α_1-frequency) vs. log(bed height)

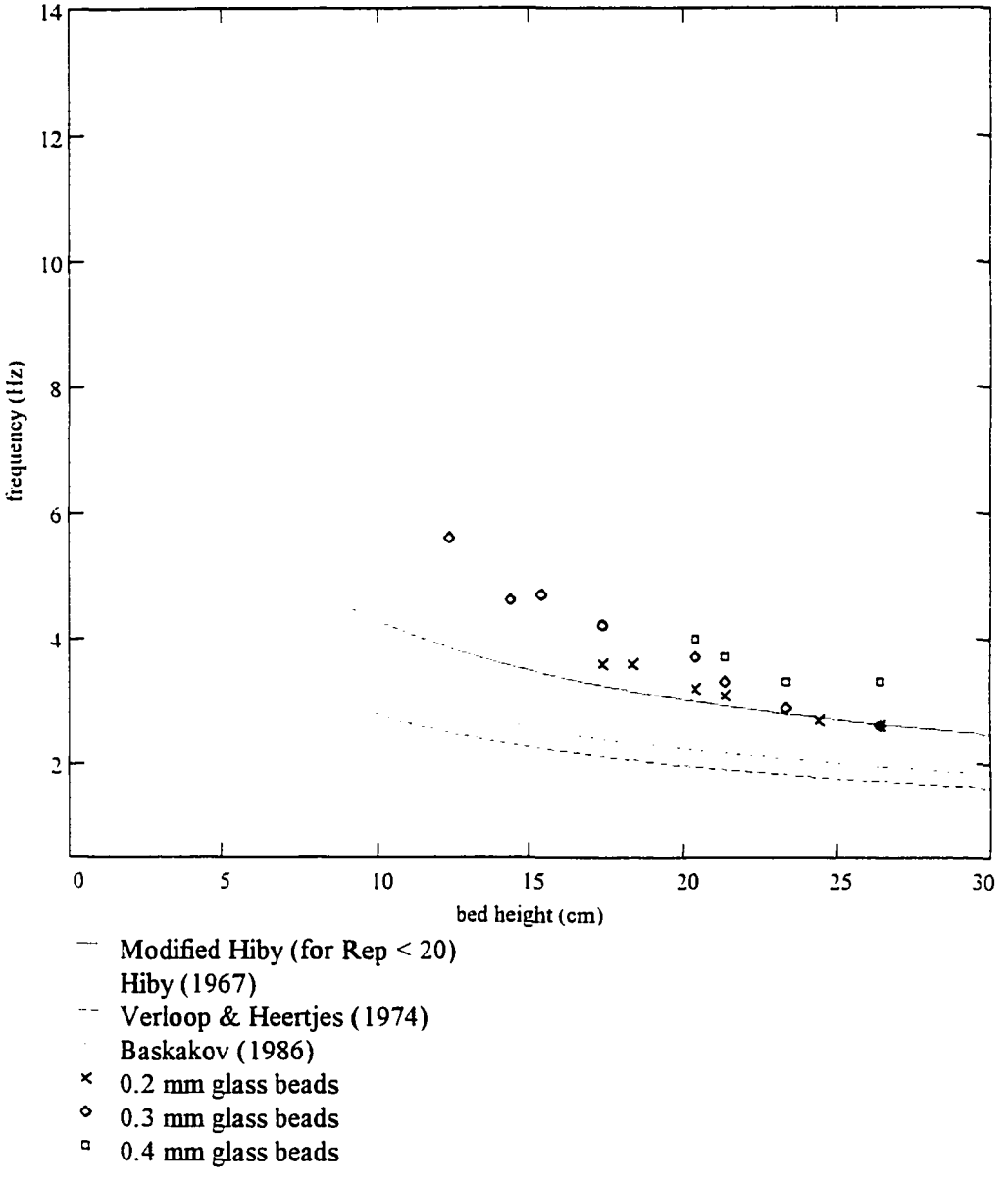

Figure 7.15: Comparison of proposed models to experimental data (D = 10.1 cm)
α_2-frequency vs. bed height

since the magnitude of the small bubble eruptions is not large enough to be measured throughout the bed.

Discussion of α_3 & α_0 -frequency phenomena

As shown previously in Figure 7.1, a third low magnitude frequency (α_3) occasionally appears in the spectrum of deep bed fluctuations. This peak always appears at a frequency twice that of the α_1-frequency, suggesting that α_3 is a harmonic of this fundamental frequency. The α_0-frequency phenomenon that only rarely appears under conditions of high superficial velocity at 0.4-0.5 Hz in the prototype bed, and 0.6-0.7 Hz in the model bed is also observed in turbulent and fast fluidization. This phenomenon will be discussed in more detail in the turbulent bed section.

Summary of BFB phenomena

In summary, it is hypothesized that bubbling bed pressure fluctuations are governed by voidage waves interacting simultaneously with bubble eruption/coalescence effects. The various characteristics observed in BFB fluctuations suggest that:

- For shallow beds and beds operated at or near incipient fluidization, the natural bed frequency (α_1-frequency) dominates the pressure fluctuations, dictating the bubble production frequency (in layers). Bubble coalescence is not significantly present at shallow bed heights to affect the observed frequency.
- As the bed gets deeper, increased bed expansion and increased bubble coalescence may explain the deviation of experimental data from the frequency predicted for voidage waves.
- The α_2-frequency represents surface eruptions which become more dominant as the bubble size at the surface increases. The frequency of eruptions decreases with increasing BFB height as fewer bubbles erupt at the surface due to bubble coalescence.

Although more research must be conducted to definitively support these hypotheses, this study provides a qualitative description of what the Bode plots of BFB fluctuations

exhibit under a variety of conditions. From this better understanding of pressure fluctuations in bubbling fluidized beds, it is possible to reassess the use of pressure fluctuation analysis as a tool to verify the validity of proposed similitude parameters.

Validation of BFB similitude parameters

Table 7.1 summarizes the results from a similitude study on the prototype and model bubbling fluidized beds over a broad range of operating conditions. The table indicates which experiments resulted in similar Bode plot profiles in the prototype and model. For hydrodynamics to be considered similar, the voidage must be equal in the two beds. Also, the dimensionless frequency and damping of the observed peaks in the fluctuation spectrum must match. The damping coefficients and system frequencies were quantitatively estimated by fitting multiple second order systems (acting in parallel) to the BFB Bode plots, as was done in previous work [76]. Table 7.1 rates the degree of similarity between the important dependent parameters in the prototype and model BFB under similitude. The rating for each observed frequency (α_1, α_2, α_0) includes both a comparison of the damping and a comparison of the dimensionless frequency. The table includes the complete set of independent dimensionless parameters used in each run. The percent height at which the pressure measurement is taken is also given (see Appendix A for a detailed summary of these experiments). In general, matching dimensionless parameters in two BFBs results in similar pressure dynamics. The average voidage matches well in both beds under all conditions.

The only exception is that under conditions of relatively high superficial velocity, when pressure fluctuations are measured in the upper regions of the bed, the peaks that result from surface phenomena (α_2 & α_0) do not always show similar damping or dimensionless frequency. Evidently, the nature of bubble coalescence in the model and prototype differ as the surface eruptions begins to dominate the spectrum. Visual observation of the bubbling bed surfaces confirm the differences. The surface of the small bed is noticeably lifted by large single bubble eruptions, while the prototype surface exhibits multiple bubble eruptions across a more stationary surface.

Table 7.1. Summary of BFB similitude study

Exp. #	U/U_{mf}	Re_p	Fr	ρ_s/ρ_g	H/D	D/d_p	% H	ε	α_1	α_2	α_0
1	1.1	4.1	5.9	2.2	1.06	254	100	N/A	**	**	-
2	1.1	4.0	5.9	2.2	1.06	254	100	N/A	**	**	-
3	1.4	5.4	10	2.2	1.06	254	100	N/A	**	**	-
4a	1.1	4.2	5.9	2.2	1.48	254	68	**	**	-	-
4b	1.1	4.2	5.9	2.2	1.48	254	100	**	*	**	-
5a	1.4	5.3	10	2.2	1.48	254	68	*	**	*	-
5b	1.4	5.3	10	2.2	1.48	254	100	N/A	*	*	-
6a	1.8	6.9	16	2.2	1.48	254	68	**	**	-	-
6b	1.8	6.9	16	2.2	1.48	254	100	N/A	*	**	-
7a	1.1	4.2	5.9	2.2	1.97	254	25	**	**	**	-
7b	1.1	4.2	5.9	2.2	1.97	254	50	**	**	*	-
8a	1.4	5.3	10	2.2	1.97	254	25	**	**	**	-
8b	1.4	5.3	10	2.2	1.97	254	50	**	**	-	-
9a	1.8	6.9	16	2.2	1.97	254	25	**	**	-	-
9b	1.8	6.9	16	2.2	1.97	254	50	**	**	-	-
10	1.1	2.0	3.3	2.2	1.06	339	100	N/A	*	**	-
11	1.4	2.6	5.5	2.2	1.06	339	100	N/A	**	**	-
12	1.8	3.3	9	2.2	1.06	339	100	N/A	*	*	-
13	2.2	4.0	13	2.2	1.06	339	100	N/A	*	no	-
14a	1.1	2.0	3.3	2.2	1.48	339	68	**	**	*	-
14b	1.1	2.0	3.3	2.2	1.48	339	100	N/A	*	*	-
15a	1.4	2.6	5.6	2.2	1.48	339	68	**	**	*	-
15b	1.4	2.6	5.6	2.2	1.48	339	100	N/A	*	*	-
16a	1.8	3.3	9	2.2	1.48	339	68	**	**	*	-
16b	1.8	3.3	9	2.2	1.48	339	100	N/A	no	*	no

Rating system:

** Dependent parameter identical in prototype and model
* Dependent parameter is approximately the same in prototype and model
no Dependent parameter does not match in prototype and model

(Table 7.1 continued)

Exp. #	U/U_{mf}	Re_p	Fr	ρ_s/ρ_g	H/D	D/d_p	% H	ε	α_1	α_2	α_0
17a	2.2	4.0	13	2.2	1.48	339	68	**	*	**	*
17b	2.2	4.0	13	2.2	1.48	339	100	N/A	no	*	no
18a	1.1	2.0	3.3	2.2	1.97	339	25	*	**	**	-
18b	1.1	2.0	3.3	2.2	1.97	339	50	**	*	**	-
19a	1.4	2.6	5.5	2.2	1.97	339	25	**	**	**	-
19b	1.4	2.6	5.5	2.2	1.97	339	50	**	*	**	-
20a	1.8	3.3	9	2.2	1.97	339	25	**	**	**	-
20b	1.8	3.3	9	2.2	1.97	339	50	**	*	**	-
21a	2.2	4.0	13	2.2	1.97	339	25	**	**	no	no
21b	2.2	4.0	13	2.2	1.97	339	50	**	*	*	no
22a	1.1	0.6	1.0	2.2	1.48	508	68	**	*	no	-
22b	1.1	0.6	1.0	2.2	1.48	508	100	N/A	no	*	-
23a	1.4	0.7	1.6	2.2	1.48	508	68	**	*	*	-
23b	1.4	0.7	1.6	2.2	1.48	508	100	N/A	*	no	-
24a	1.8	1.0	2.7	2.2	1.48	508	68	**	*	no	-
24b	1.8	1.0	2.7	2.2	1.48	508	100	N/A	*	no	-
25a	1.1	0.6	1.0	2.2	1.97	508	25	**	**	-	-
25b	1.1	0.6	1.0	2.2	1.97	508	50	**	**	-	-
26a	1.4	0.7	1.6	2.2	1.97	508	25	**	**	*	-
26b	1.4	0.7	1.6	2.2	1.97	508	50	**	**	*	-
27a	1.8	0.6	2.7	2.2	1.97	508	25	*	**	*	-
27b	1.8	0.6	2.7	2.2	1.97	508	50	**	**	no	-

Transition Regime Fluctuations

Pressure fluctuations in the transition regime provide an important link between the nature of fluctuations in bubbling and circulating beds. Depending on the diameter of the bed, this regime can be described as a slugging or turbulent bed. The Bode plots throughout this regime continue to represent the output of multiple second order systems (i.e. a -40 dB/decade asymptotic slope). As previously shown, the α_1-frequency observed in BFB pressure fluctuations stays relatively constant as the superficial velocity increases. This holds true in the transition regime even as the bed approaches the fast fluidization regime (U/Umf > 20.0 for the prototype BFB). This is shown in Figure 7.16 which plots the observed frequencies versus U/U_{mf} for the transition regime. The α_2-frequency phenomena observed in bubbling fluidized beds is also observed in the transition regime. This surface eruption frequency approaches the α_1-frequency as the superficial velocity increases. At high velocities near fast fluidization, these two frequencies become nearly impossible to differentiate.

An interesting result observed in Figure 7.16, is that the α_0-frequency, that is nearly non-existent in BFBs, begins to appear in the spectrum of transition regime beds at a frequency of 0.9 Hz in the prototype. This frequency (although significantly damped) is seen first in the pressure fluctuations recorded immediately above the bed surface as the bed moves from bubbling to fast fluidization (see Appendix B for the complete presentation of transition regime Bode plots). At U/Umf > 18 this frequency is observed in the bed fluctuation measurements as well. This suggests that the α_0-frequency phenomena is not solely a characteristic of fast fluidization. As the superficial velocity increases in the transition regime, a well defined bed surface is no longer observed. While some bubbles are still observed propagating through the system, the predominant motion of the bed is the sloshing motion at the surface. This sloshing motion increases in magnitude until, near the fast fluidization regime, some particles are projected 1-3 m above the original surface of the bed. Visually it is easy to relate such a motion to the wave behavior of a liquid.

According to surface wave theory, deep beds should exhibit a wave frequency inversely proportional to the $\sqrt{D}$. For the prototype BFB, the predicted frequency for

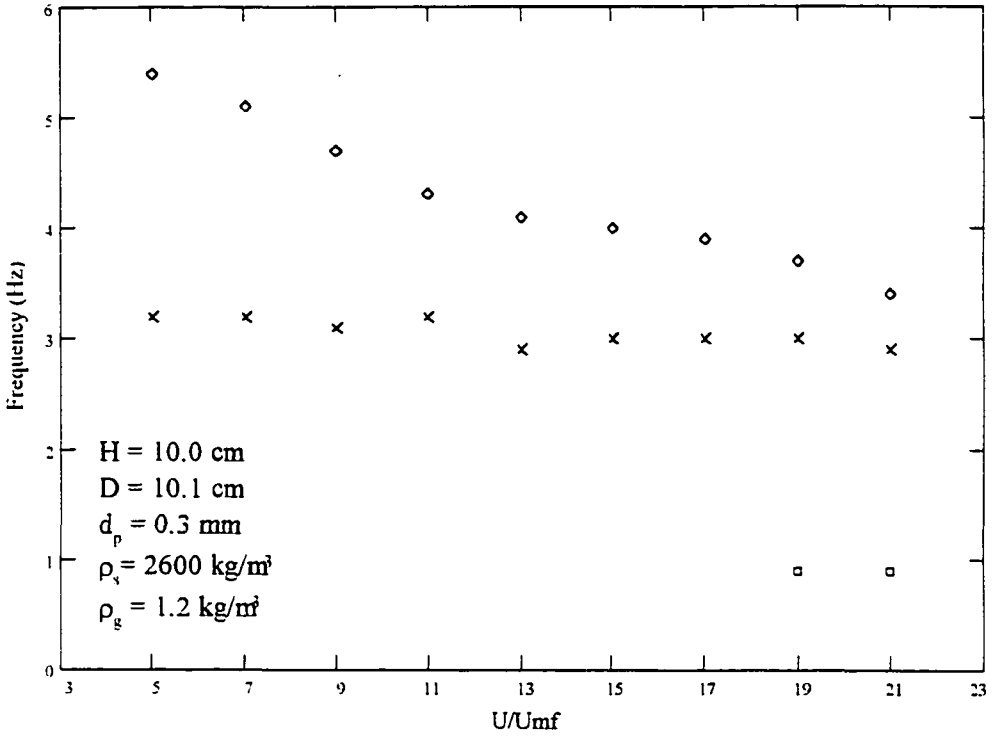

Figure 7.16: Dominant frequencies observed in turbulent bed pressure fluctuations (measured at 50% bed height)

surface waves is 0.45 Hz for the fundamental, and 0.9 Hz for the first harmonic. For the model BFB, the predicted frequency is 0.65 Hz for the fundamental, and 1.3 Hz for the first harmonic. These values correspond closely to the α_0-frequency measured in fluidized systems approaching the fast fluidization regime for both the model and the prototype.

In summary, the α_1-frequency (voidage fluctuation phenomena) and α_2-frequency are observed throughout the transition from turbulent to fast fluidization. The α_0-frequency and corresponding harmonics can be observed near the onset of fast fluidization. This frequency phenomena suggests the presence of a wave phenomena analogous to deep water waves.

Fast Fluidization Fluctuations

General characteristics

Two predominant phenomena are observed in the frequency spectrum of fast fluidization systems. Figures 7.17-7.19 show typical CFB Bode plots under different operating conditions. Under relatively dilute conditions (and in the upper regions of the bed) the α_0-frequency phenomena appears along with its first harmonic in the spectrum (see Figure 7.17). In the transition from dilute to dense conditions, the Bode plot of fluctuations appears highly damped as shown in Figure 7.18 (i.e. no distinct peaks are observed in the pressure dynamics). Under the dense conditions shown in Figure 7.19, the α_1-frequency is evident in the Bode plot. This α_1-frequency phenomena is most dominant when fluctuations are measured at low elevations in the bed (5-10 % bed height). The CFB Bode plots under all conditions exhibit a final asymptotic slope of -40 dB/decade.

Before examining the two predominant phenomena observed in fast fluidization, preliminary experiments were conducted to verify that fluctuations did not originate from local disturbances that occur only along the wall near the pressure tap. A probe was mounted down from the riser top-plate to measure static pressure fluctuations at the center of the riser cross-section. Simultaneously, the static pressure fluctuations at the wall were recorded at this same elevation. The Bode plots of the pressure fluctuations, at the wall and in the center

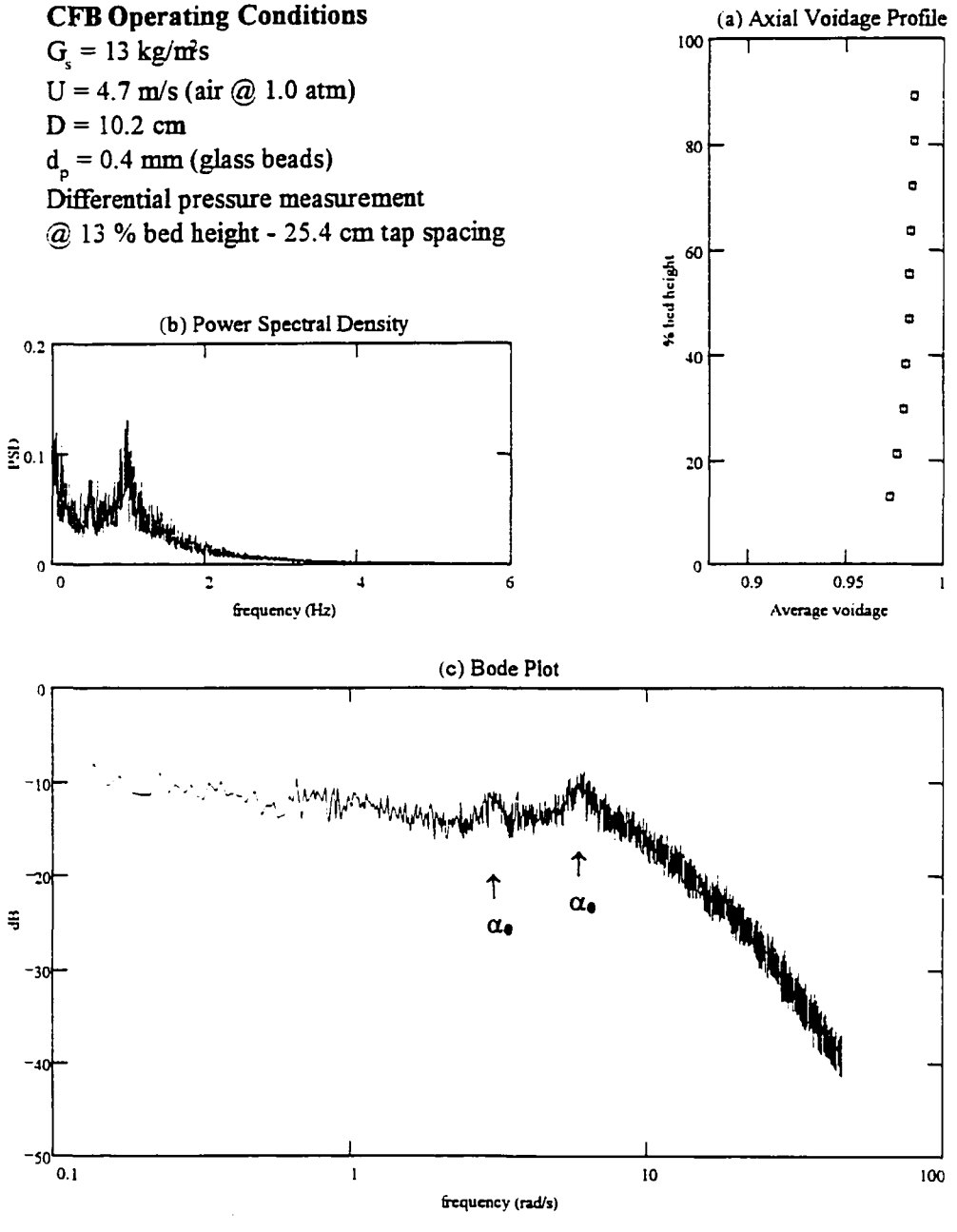

Figure 7.17: Dilute CFB operating conditions - a) axial voidage profile, b) PSD, c) Bode plot

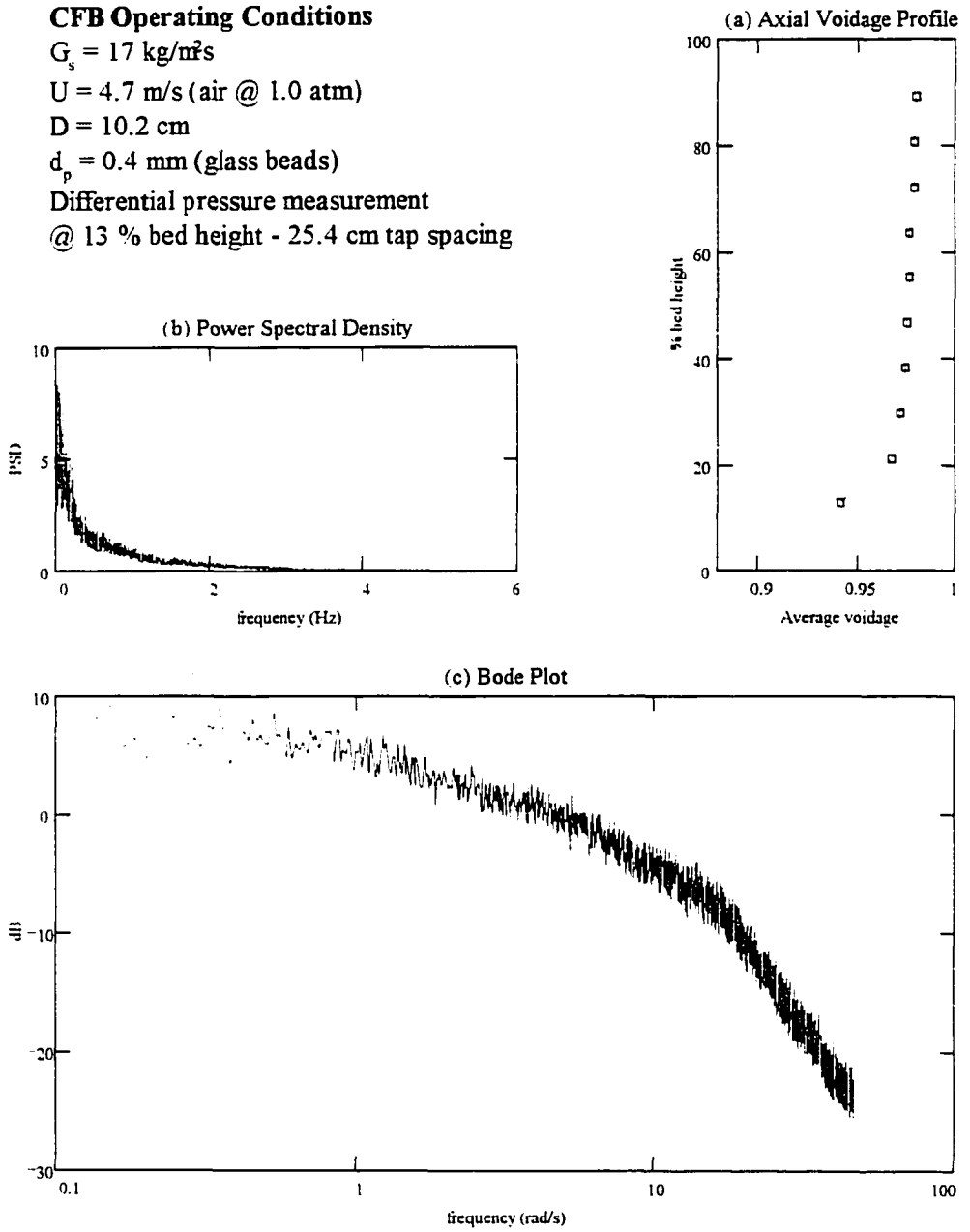

Figure 7.18: Damped CFB operating conditions - a) axial voidage, b) PSD, c) Bode plot

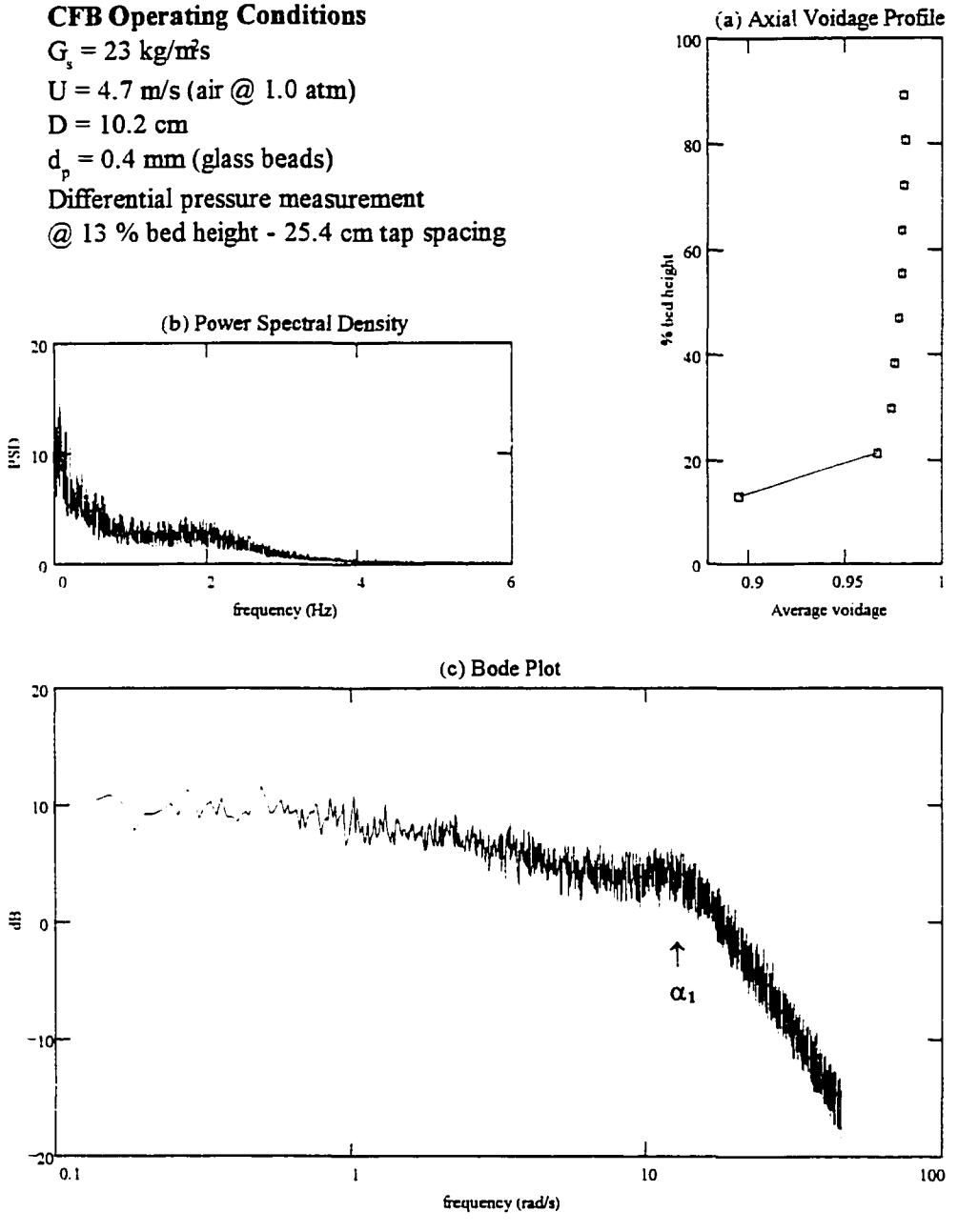

Figure 7.19: Dense CFB operating conditions - a) axial voidage profile, b) PSD, c) Bode plot

of the bed two feet down from the top plate of the riser, are shown in Figures 8.20a and 8.20b. The frequency response profiles are identical in each case suggesting that pressure fluctuations are a global phenomena, and not simply the result of local changes in the solids concentration along the wall. If the pressure fluctuations were solely the result of local behavior, distinctly different pressure fluctuation behavior would be expected from the upward moving dilute core, and the dense downward flowing annulus.

Discussion of α_1-frequency phenomena in CFBs

Pressure fluctuations in bubbling and turbulent beds provide insight as to the origin of the α_1-frequency in circulating fluidized beds. By observing pressure fluctuations throughout the transition from bubbling to turbulent to fast fluidization, it is evident that the α_1-frequency is present in all three regimes. This α_1-frequency originates from the lower dense regions of the CFB. It appears only when a lower dense bed has been established (i.e. the axial voidage profile shows decreasing voidage at low bed heights). It is also most dominantly sensed at the lower elevations of the CFB. Figure 7.21 shows how the α_1-frequency is manifest in the CFB Bode plots of fluctuations measured at different elevations. Secondly, in addition to the observation of this phenomena throughout bubbling, turbulent, and fast fluidization regimes, the frequency of this phenomena can be predicted from the modified-Hiby model proposed for bubbling fluidized beds. The height of the lower dense bed can be estimated from the axial voidage profiles to be between 10-20 cm (in the 10.2 diameter CFB model). The theory for voidage oscillations under turbulent conditions predicts that this frequency should appear between 2-3 Hz. All Bode plots of lower dense bed pressure fluctuations confirm this (see Figures 7.19, 7.21 and Appendix C).

As expected, this α_1-frequency also exhibits an inverse square root dependence on dense bed height. When the two CFB models are operated such that similar axial voidage profiles are attained, the lower dense bed height in the large CFB will be twice the height of the small CFB dense bed. Consequently, the lower dense bed frequency in the model CFB appears at a frequency that is 1.4 (or $2^{1/2}$) times the frequency that is observed in the

a) 80 % bed height, Gs = 19 ± 3 kg/m s^2, U = 3.0 ± 0.3 m/s, D = 10.2 cm, d_p = 0.2 mm

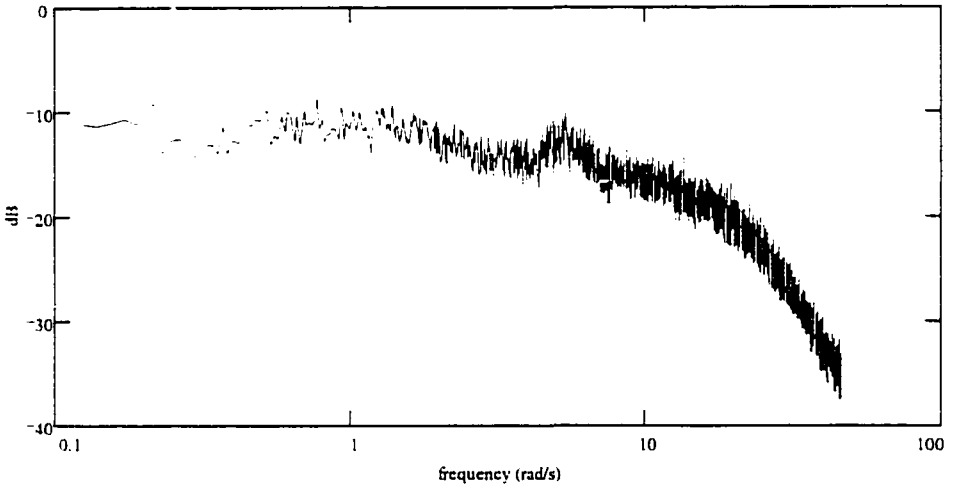

b) 80 % bed height, Gs = 19 ± 3 kg/m s^2, U = 3.0 ± 0.3 m/s, D = 10.2 cm, d_p = 0.2 mm

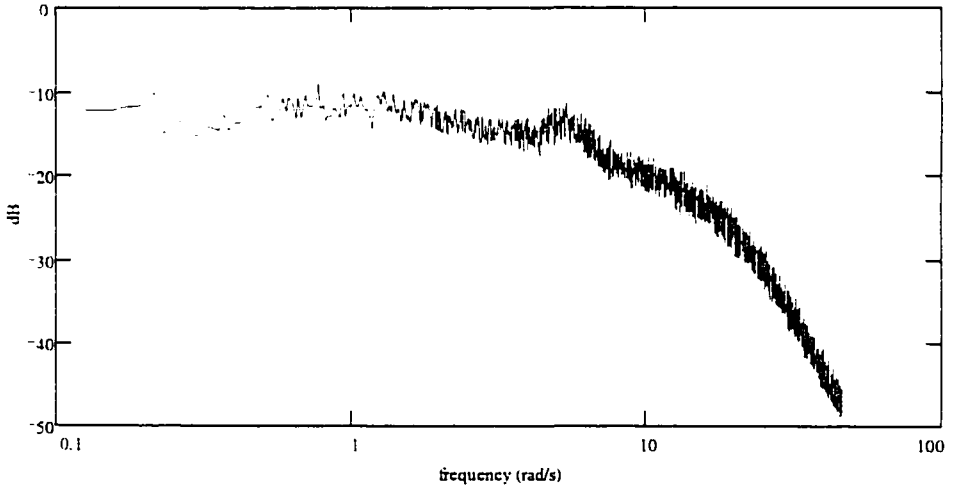

Figure 7.20: Bode plot of static pressure fluctuations at a) center of bed, and b) bed wall

CFB Operating conditions:

U = 4.1 ± 0.2 m/s (air @ 1.0 atm)
G_s = 18 ± 4 kg/m^{2}s
D = 10.2 cm
d_p = 0.3 mm (glass beads)

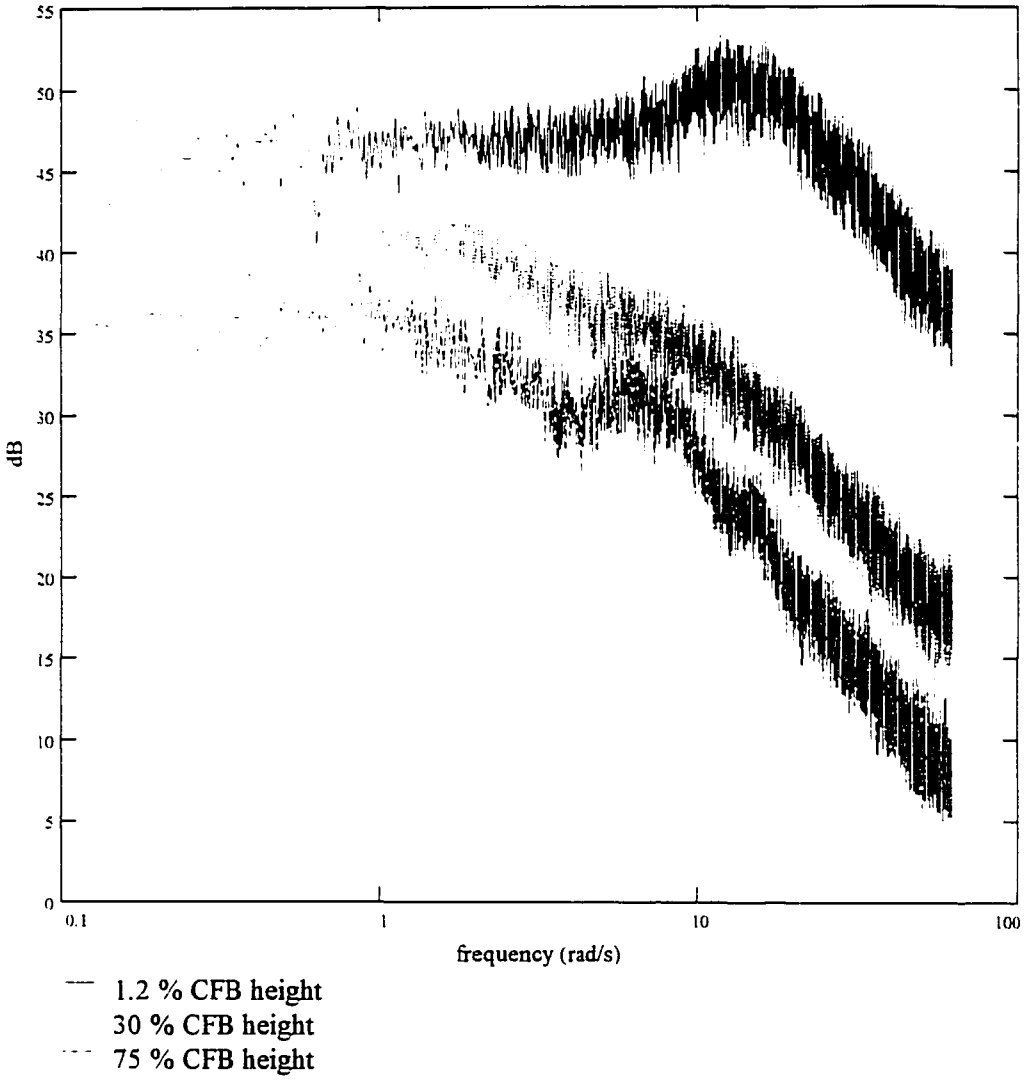

Figure 7.21: Appearance of dense phase phenomena at various bed elevations

prototype CFB. This is shown conclusively in the results of the similitude study that follow. This result suggests that pressure fluctuation measurements at one location could be used as an indicator of the height of the lower dense region in a CFB

Discussion of α_0-frequency phenomena in CFBs

The α_0-frequency phenomenon was previously hypothesized to be governed by an acoustical wave phenomena similar to that observed in an organ pipe [74]. Two tests have shown that this is not a correct hypothesis. First, if this α_0-phenomenon was the result of an acoustical wave in the riser, varying the length of the riser would vary the observed frequency. Two extensions were used to modify the small CFB such that it could be operated at 1.5 and 2 times the original bed height. The bed was fluidized with air at atmospheric pressure and 0.2 mm steel shot as the bed material. The PSDs presented in Figure 7.22 show that the α_0-frequency observed in CFB pressure fluctuations does not change significantly with changes in the CFB height. Secondly, as seen in the transition regime, the α_0-frequency begins to appear in the high velocity turbulent regime prior to fast fluidization. This suggests that α_0-frequency results from a phenomena associated with the behavior of particles leaving and returning to the dense bed surface, rather than a phenomena associated with the structural CFB height.

Visual observations in circulating fluidized beds and turbulent beds (as they approach fast fluidization) show clusters of solids leaving the dense bed surface at approximately 1 Hz, which corresponds to the α_0-frequency observed in the Bode plots. Similar to the transition regime, this frequency of sloshing/cluster propagation at the lower dense region of the CFB is also hypothesized to be governed by a surface wave phenomena.

This α_0-frequency is independent of superficial velocity, solids flux, particle density and gas density, although these operating variables will also affect the observed magnitude (or damping) of this phenomena. Particle diameter has only a small effect on the observed frequency. The α_0-frequency will increase slightly with increasing particle diameter. The bed diameter has the greatest effect on the frequency observed in this dilute phase. It appears that this frequency is inversely proportional to the square root of the bed diameter. All these

a) 2 x standard bed height (48" extension) - ($G_s = 34 \pm 4$ kg/m s^2, $U = 5.5 \pm 0.4$ m/s)

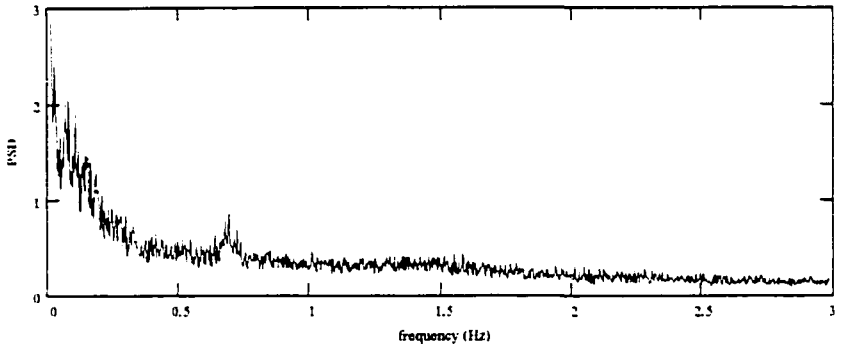

b) 1.5 x standard bed height (24" extension) - ($G_s = 49 \pm 5$ kg/m s^2, $U = 6.2 \pm 0.4$ m/s)

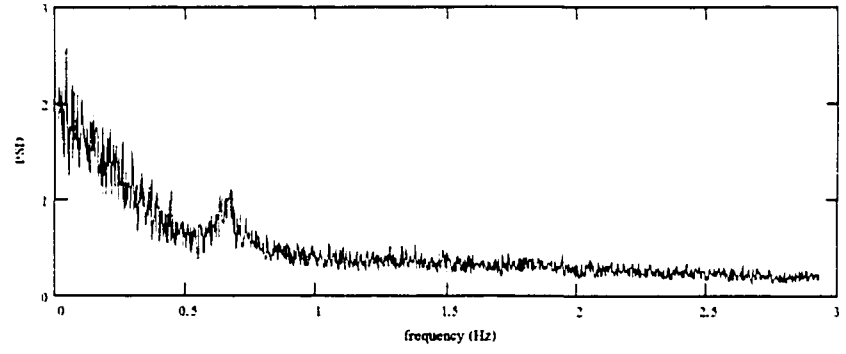

c) standard bed height (no extension) - ($G_s = 38 \pm 7$ kg/m s^2, $U = 5.6 \pm 0.4$ m/s)

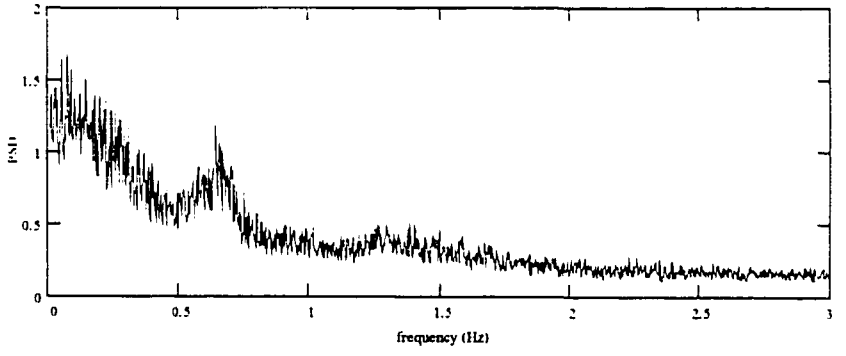

Figure 7.22: Effect of bed height on the dilute phase frequency a) 2 x H, b) 1.5 x H, c) H

observed characteristics further support the hypothesis that the α_0-frequency is governed by a deep wave phenomena.

Discussion of the initial cornering frequency in CFBs

Another observation that can be made from both the results of previous studies [76, 79], and the results presented in Appendix C is that there appears to be an initial break frequency (α_5) at around 0.15 Hz in the CFB Bode plots. This initial roll-off is predominantly observed at high elevations in the bed and whenever the dilute phase phenomena is observed. The damping or location of this frequency does not change significantly with changes in operating conditions. This initial roll-off may be the result of a very slow component in the dynamics (on the order of 5 to 7 seconds), or it may be the result of the interaction of multiple phenomena within the CFB. Further study is needed to develop an explanation of the origin of this Bode plot characteristic.

Summary of CFB pressure fluctuations

CFB pressure fluctuations are indicative of CFB hydrodynamics in two ways. First, the α_1-frequency that is observed in the lower regions of the CFB under conditions of high solids loading is the result of lower dense bed voidage oscillations as observed in bubbling and turbulent beds also. Our results suggest that a surface wave phenomena (α_0) inversely proportional to the square root of the bed diameter is also be observed in CFB pressure fluctuations under most conditions. Knowing how pressure fluctuations reflect CFB hydrodynamics, it is possible to use the analysis of pressure fluctuations to validate proposed similitude parameters.

Investigation of CFB similitude parameters

Prior to testing the similitude parameters proposed by Glicksman, it was discovered that the total mass of solids loaded into the CFB (M) must also be used as an additional independent parameter for CFBs with L-valve solids re-circulation systems. While holding all

other dimensionless parameters the same, the hydrodynamics of the bed can be altered measurably by changes in the reactor loading (see Figure 7.23). For this reason the addition of a dimensionless reactor loading term has been added to the set of similitude parameters matched in this study, as was proposed in Chapter 6.

The results of the CFB similitude study are summarized in Table 7.2. In Table 7.2 the degree of similarity between the hydrodynamics in the model and prototype CFB is presented. The Bode plots from this study are shown in Appendix C. Under these proposed conditions of similitude, a number of characteristics can be noted. The Bode plot profiles in the upper bed (75% bed height) match relatively well in the model and prototype CFB under most conditions. This occurs even when the axial voidage profiles do not match well. This is to be expected from the present understanding of the α_0-frequency phenomenon, which dominates in the upper CFB elevations. The α_0-frequency is primarily a function of bed diameter and is not expected to vary with changing operating conditions. The α_0 (dimensionless) frequency will match in two CFBs as long as the bed diameters are scaled properly. Consequently, it cannot be assumed in similitude studies that pressure fluctuations in the upper regions can by themselves verify similitude relations. Upper bed fluctuations must be used in conjunction with lower bed fluctuations and axial voidage profiles before any valid conclusions regarding CFB similitude can be made.

In contrast to upper CFB Bode plots, the lower dense bed fluctuations and axial voidage profiles are rarely similar in prototype and model under Glicksman's conditions of similitude. The α_1-frequency in the prototype and model CFB rarely exhibit similar dimensionless frequency and damping. The pressurized model shows a significantly higher voidage in the lower bed than the prototype. This distinct difference was overlooked in the small model results published by Glicksman [11]. He minimizes this dramatic difference by plotting the voidage axis on a logarithmic scale. Louge [80] also observed similar behavior in the axial voidage profiles of pressurized CFB models, and attributes it to the shorter acceleration region in the pressurized models. Only under dilute operating conditions were approximately similar hydrodynamics occasionally observed.

CFB Operating conditions:

U = 2.8 ± 0.2 m/s (air @ 28 psig)
G_s = 30 ± 4 kg/m^{2}s
D = 5.1 cm
d_p = 0.15 mm (steel shot)

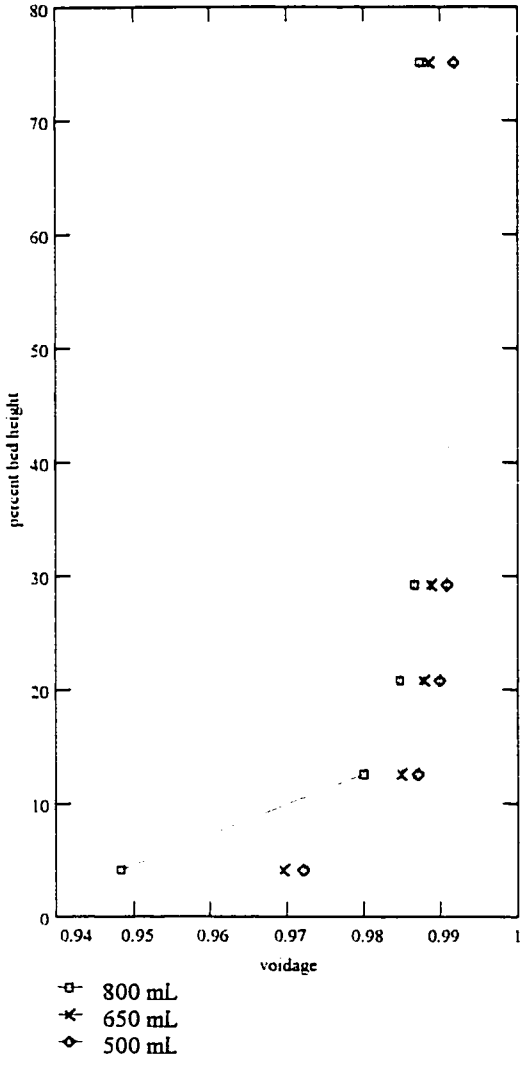

Figure 7.23: CFB axial voidage profiles at different reactor loadings

Table 7.2. Summary of CFB similitude tests using Glicksmans parameters

Dependent parameters compared: AVP - axial voidage profiles
5 % - Bode plots from 5 % total bed height
21 % - Bode plots from 21 % total bed height
75 % - Bode plots from 75 % total bed height

#	H/dp ($x10^{-1}$)	D/dp ($x10^{-2}$)	ρ_f/ρ_s ($x10^{-4}$)	Re_p	Fr ($x10^{-3}$)	$G_s/\rho_s U$ ($x10^{-3}$)	$M/\rho_s D^3$	AVP	5 %	21 %	75 %
1	1.5	5.1	4.7	40	4.6	1.3	2.1	*	no	*	**
2	1.5	5.1	4.7	40	4.6	1.9	2.1	*	no	no	*
3	1.5	5.1	4.7	47	6.3	1.7	2.1	no	no	*	*
4	1.5	5.1	4.7	47	6.3	2.1	2.1	no	no	no	**
5	1.5	5.1	4.7	47	6.3	2.8	2.7	*	no	*	**
6	1.5	5.1	4.7	54	8.2	1.9	2.1	no	*	*	*
7	1.5	5.1	4.7	54	8.2	2.4	2.7	*	no	no	*
8	1.1	3.4	4.7	71	4.2	1.1	2.1	no	no	no	*
9	1.1	3.4	4.7	71	4.2	1.7	2.1	NP	NP	NP	NP
10	1.1	3.4	4.7	81	5.4	1.4	2.1	no	no	no	*
11	1.1	3.4	4.7	81	5.4	1.9	2.7	no	no	no	*
12	1.1	3.4	4.7	81	5.4	2.4	2.1	NP	NP	NP	NP
13	1.1	3.4	4.7	110	11	1.4	2.1	no	no	*	**
14	1.1	3.4	4.7	110	11	1.7	2.7	no	no	*	**
15	0.8	2.5	4.7	108	4.1	1.0	2.1	no	no	no	**
16	0.8	2.5	4.7	108	4.1	1.4	2.1	NP	NP	NP	NP
17	0.8	2.5	4.7	126	5.6	1.2	2.1	no	no	**	**
18	0.8	2.5	4.7	126	5.6	1.6	2.7	*	no	*	**
19	0.8	2.5	4.7	148	7.7	1.4	2.1	no	*	*	**
20	0.8	2.5	4.7	148	7.7	1.7	2.7	no	no	*	**

Rating system:

** Bode plots match well in both models
* Not all Bode plot characteristics are similar in prototype and model
no Bode plots are not similar in prototype and model
NP Experiment *not possible* since chosen similitude parameters resulted in choking conditions in the protoype

It is also important to observe that the matching of Glicksman's similitude parameters does not guarantee that choking conditions in one bed will yield choking conditions in the other. There are three experiments in the model (shown in Table 7.2) that could not be duplicated in the prototype due to conditions of complete choking under the prescribed similitude parameters.

It is hypothesized from these experiments that solids flux is not an appropriate independent variable for the establishing of similitude. Representing a measure of the rate of particles leaving the riser, it is not fundamentally an indicator of the total amount of solids suspended in the riser, which is more important for similitude studies.

An alternative to dimensionless solids flux is suggested by these results. Dimensionless solids loading in the riser was substituted for dimensionless solids flux in the experiments illustrated in Figures 7.24-7.33. This was done by maintaining the appropriate level of solids (L_v) in the CFB downcomer. The full set of dimensionless similitude parameters used in this approach is:

$$Fr = \frac{U^2}{g \cdot d_p} \qquad \frac{H}{d_p} \qquad \frac{D}{d_p} \qquad \frac{\rho_g}{\rho_s} \qquad \mathrm{Re}_p = \frac{\rho_g \cdot U \cdot d_p}{\mu} \qquad \frac{M}{\rho_s \cdot D^3} \qquad \frac{L_v}{D}$$

The pressure fluctuation Bode plots and the axial voidage profiles match very well when this full set of parameters is matched. In spite of these hydrodynamic similarities, there is one obvious difference between the conditions in the two cases. The dimensionless solids flux (now used as a dependent parameter) is over 50% greater in the model than the prototype. It was hypothesized that this may be the result of differences in the elasticity of the solids in the riser; changing the dynamics of particle/particle or particle/bed collisions.

Since the predominant collisions in the riser that take place between the particles and the riser top-plate, differences between the steel shot/aluminum top-plate (model) collisions and the glass bead/Plexiglas top-plate (prototype) collisions were investigated. By measuring the rebound height of steel and glass beads the coefficients of restitution were estimated:

$$e = \sqrt{\frac{h_r}{H_d}} \qquad 7.1$$

Table 7.3. Operating conditions for similitude experiments (Figs. 7.24-7.28) Using riser loading as the independent solids parameter

SMALL CFB

L_v	23 ± 1 inches
Reactor loading	750 ± 25 mL
Superficial velocity	2.9 ± 0.1 m/s
Solids flux	30 ± 4 kg/m^{2}s
Rep	85 ± 12
Fr	5700 ± 800
$G_s/\rho_s U$	0.0014 ± 0.0002
H/d_p	10200 ± 1400
D/d_p	340 ± 50
ρ_g/ρ_s	2150 ± 30
$M/\rho_s D^3$	3.15 ± 0.08

LARGE CFB

L_v	45 ± 2 inches
Reactor loading	6000 ± 200 mL
Superficial velocity	4.1 ± 0.1 m/s
Solids flux	10 ± 2 kg/m^{2}s
Rep	84 ± 5
Fr	5800 ± 500
$G_s/\rho_s U$	0.0009 ± 0.0002
H/d_p	10200 ± 300
D/d_p	340 ± 10
ρ_g/ρ_s	2150 ± 70
$M/\rho_s D^3$	3.15 ± 0.05

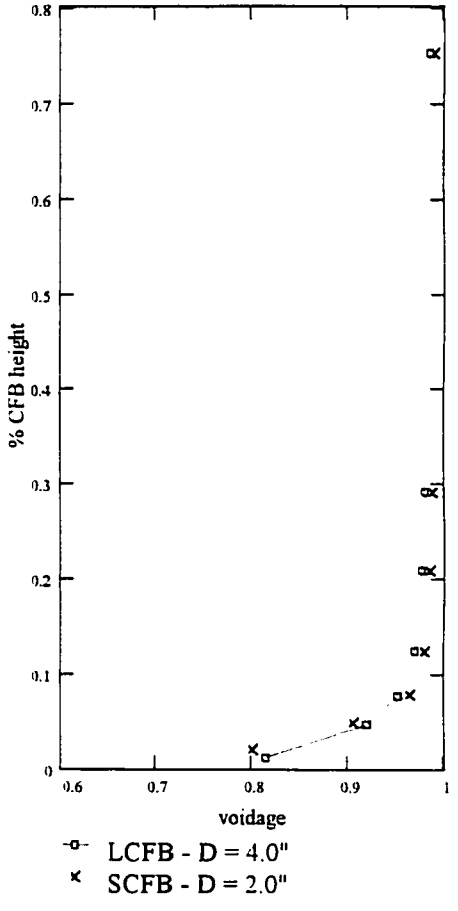

Figure 7.24: CFB axial voidage profiles (Using revised similitude parameters)

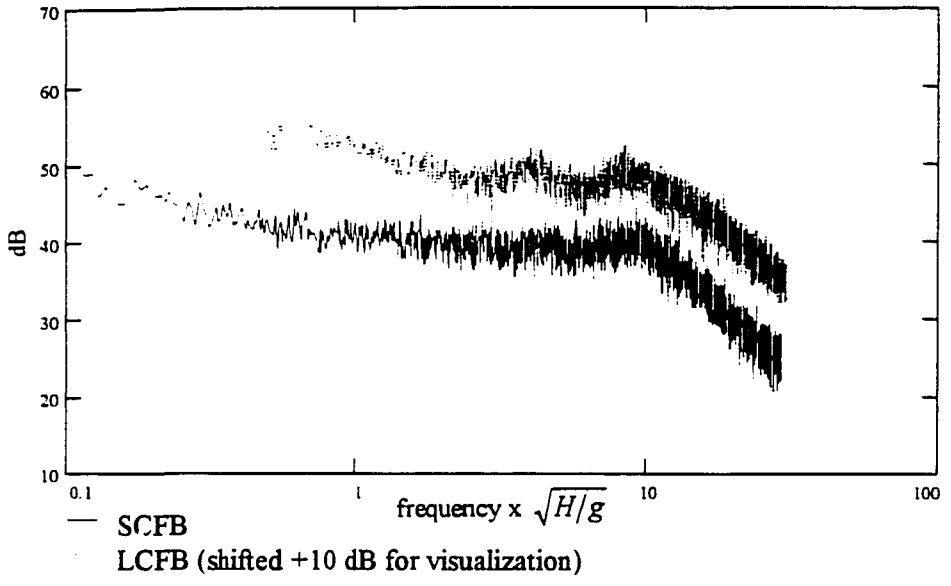

Figure 7.25: Bode plots of CFB under similitude conditions (1-2 % bed height) Using revised similitude parameters

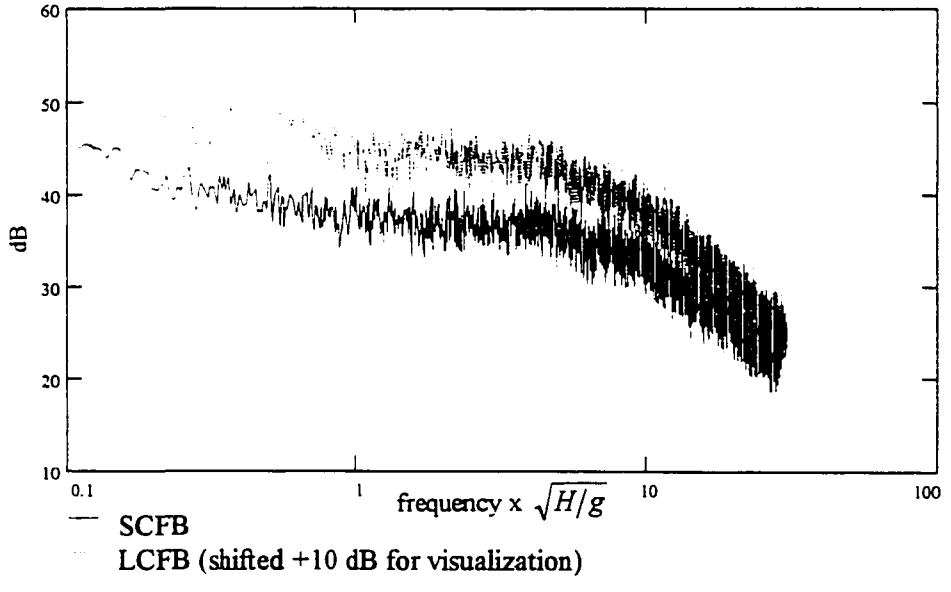

Figure 7.26: Bode plots of CFB under similitude conditions (5 % bed height) Using revised similitude parameters

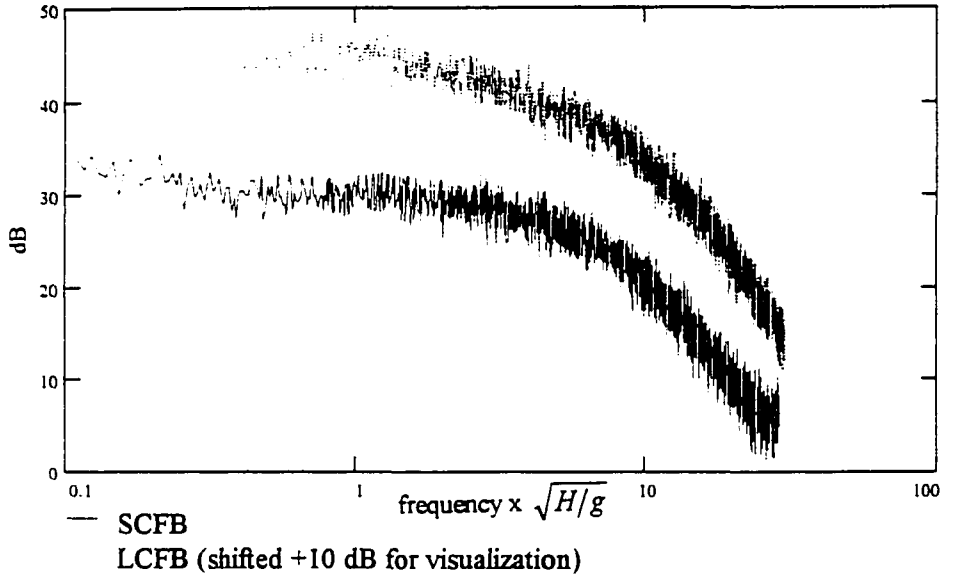

Figure 7.27: Bode plots of CFB under similitude conditions (13 % bed height) Using revised similitude parameters

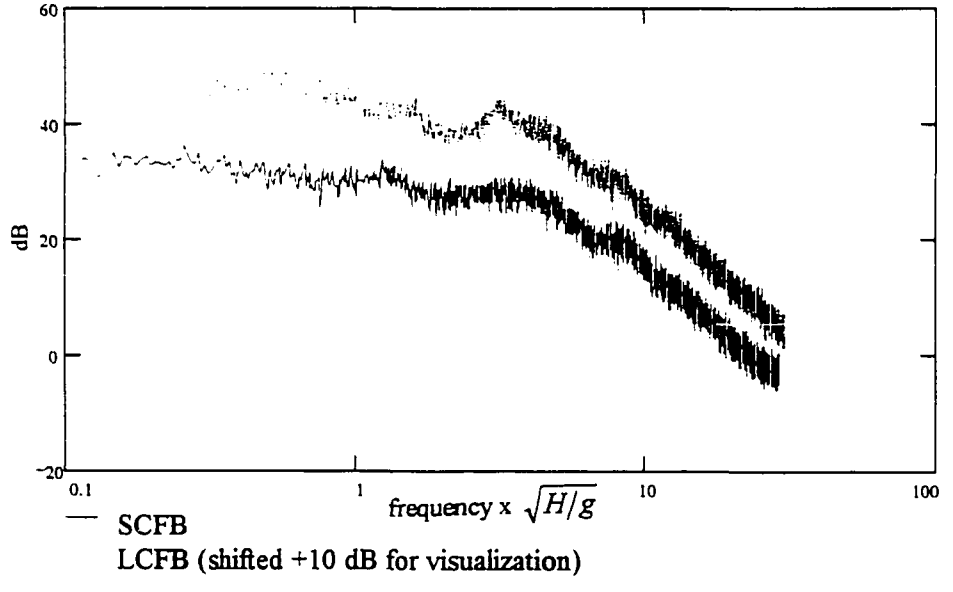

Figure 7.28: Bode plots of CFB under similitude conditions (75 % bed height) Using revised similitude parameters

Table 7.4. Operating conditions for similitude experiments (Figs. 7.29-7.33) Using riser loading as the independent solids parameter

SMALL CFB

L_v	16 ± 2 inches
Reactor loading	750 ± 25 mL
Superficial velocity	3.2 ± 0.1 m/s
Solids flux	35 ± 2 kg/m^{2}s
Rep	95 ± 13
Fr	7000 ± 1000
$G_s/\rho_s U$	0.0014 ± 0.0002
H/d_p	10200 ± 1400
D/d_p	340 ± 50
ρ_g/ρ_s	2150 ± 30
$M/\rho_s D^3$	3.15 ± 0.08

LARGE CFB

L_v	32 ± 1 inches
Reactor loading	6000 ± 200 mL
Superficial velocity	4.5 ± 0.1 m/s
Solids flux	13 ± 5 kg/m^{2}s
Rep	92 ± 5
Fr	7000 ± 500
$G_s/\rho_s U$	0.0010 ± 0.0004
H/d_p	10200 ± 300
D/d_p	340 ± 10
ρ_g/ρ_s	2150 ± 70
$M/\rho_s D^3$	3.15 ± 0.05

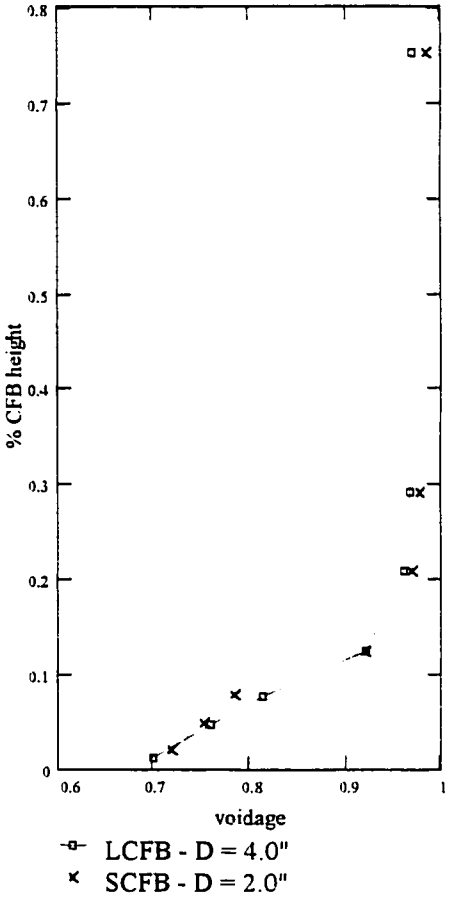

Figure 7.29: CFB axial voidage profiles (Using revised similitude parameters)

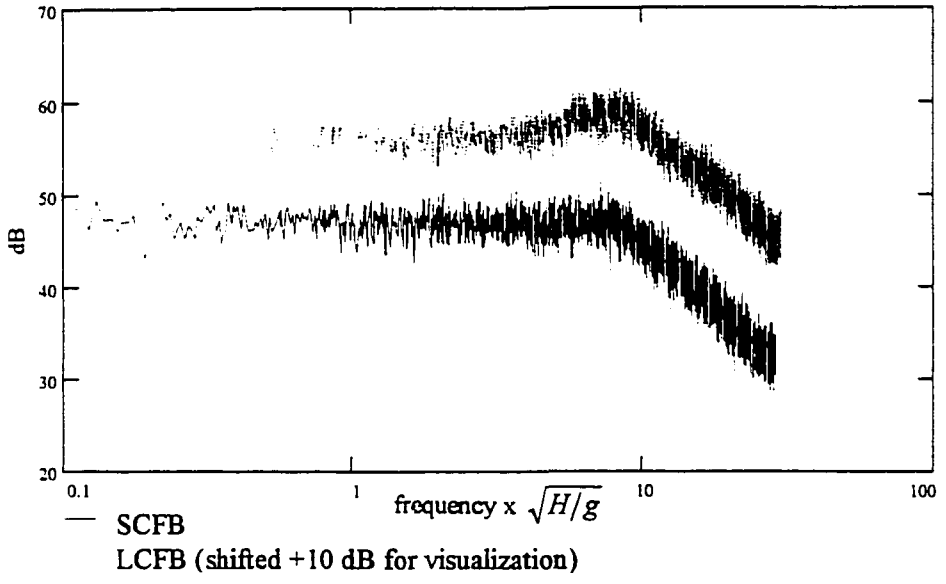

Figure 7.30: Bode plots of CFB under similitude conditions (1-2 % bed height) Using revised similitude parameters

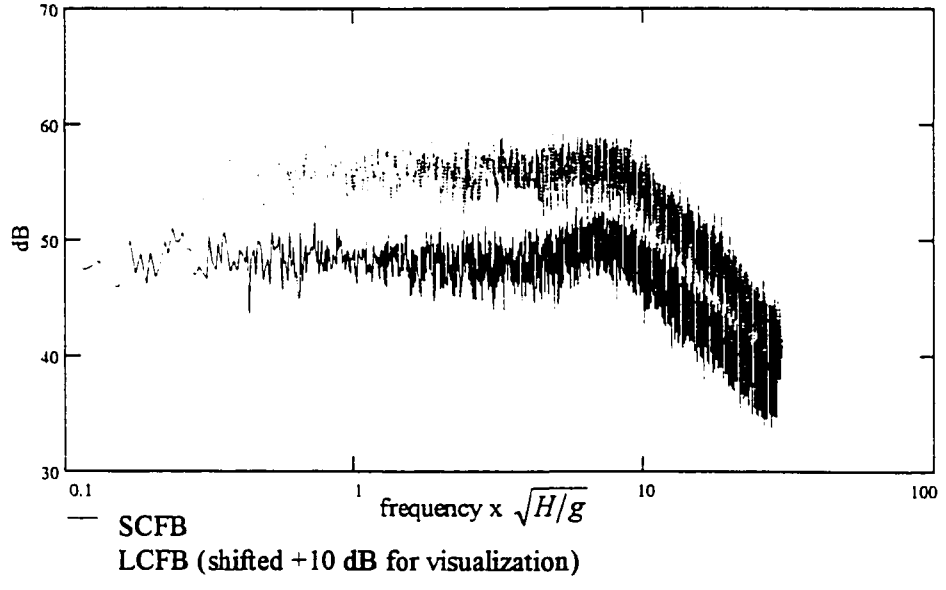

Figure 7.31: Bode plots of CFB under similitude conditions (5 % bed height) Using revised similitude parameters

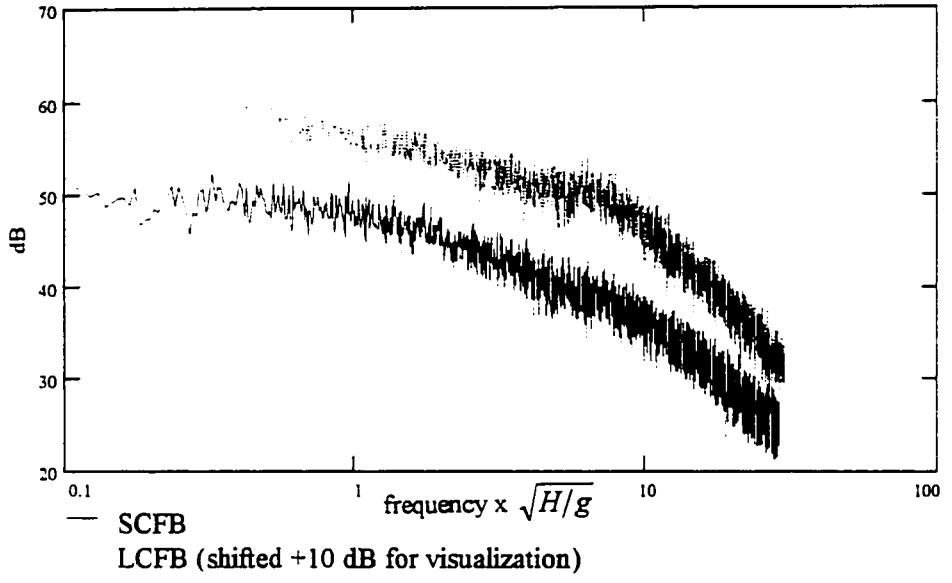

Figure 7.32: Bode plots of CFB under similitude conditions (13 % bed height) Using revised similitude parameters

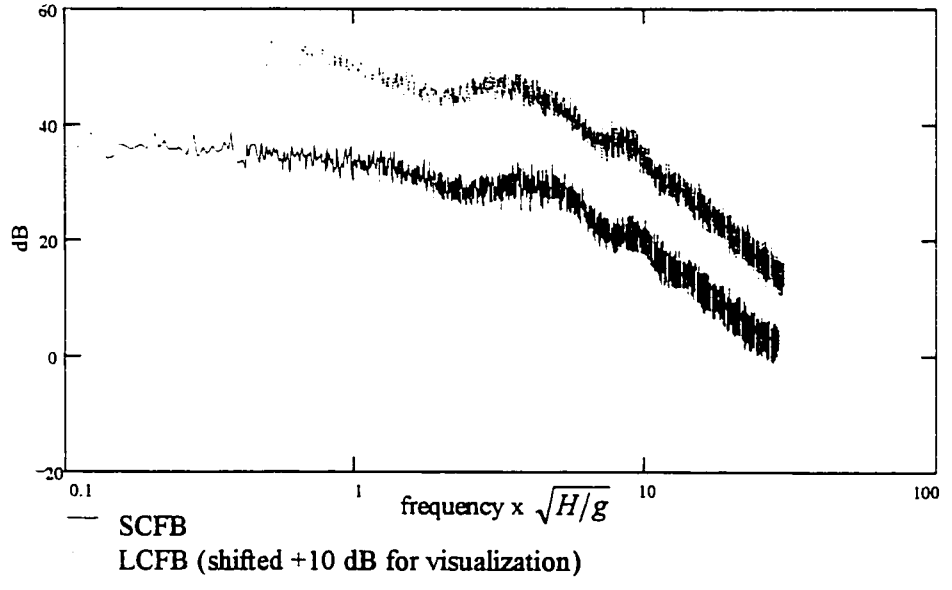

Figure 7.33: Bode plots of CFB under similitude conditions (75 % bed height) Using revised similitude parameters

where H_d is the drop height and h_r is the rebound height. The resulting coefficient of restitution of glass/Plexiglas collision is over 50% higher than the coefficient of restitution of steel/aluminum collision. This being the case, the glass particles in the large CFB model are more likely to rebound off the top-plate and back down into the riser, rather than exiting the riser to the cyclone. As a result, the external recycle rate of steel shot will be much higher, yielding a higher solids flux in the model reactor. The axial voidage profiles in Figures 7.24 and 7.29 support this hypothesis by showing a slightly denser upper region in the prototype.

To definitively support this hypothesis that the top-plate collision strongly affects the measured solids flux, 26" and 13" extensions were added to the large and small CFBs respectively. These extensions allowed particles to progress beyond the riser exit, and change direction, without contacting the riser top-plate. The results of this experiment presented in Figures 7.34 - 7.38 confirms that the coefficient of restitution of particle/bed collisions is an important consideration in similitude studies. In this experiment, the dimensionless solids flux matches exactly in both beds, in addition to pressure fluctuations and axial voidage profiles. Complete hydrodynamic similitude was achieved in this test.

A number of conclusions can be drawn from this CFB similitude study. First, spectral analysis of pressure fluctuations, if properly applied, can be used to verify that similitude has been achieved. To do this, not only must the Bode plot characteristics important for hydrodynamics be identified, but the pressure fluctuation structure at all elevations of the CFB must be similar. The set of similitude parameters defined by Glicksman is not sufficient to establish hydrodynamic similitude. The overall reactor loading must also be considered in L-valve systems. The solids flux as typically measured in the downcomer does not contain information on the solids hold-up in the riser, or the amount of solids that progress downwards in the annulus rather than exit the riser. It is better to use the total mass contained in the riser (using a measurement such as L_v) as the important "solids" parameter for the establishment of similitude, rather than the solids flux. This measurement of L_v can be made more accurately, monitored continuously, and is a much simpler measurement to perform in most CFB systems. Even with this new set of dimensionless parameters, the differences in the

Table 7.5. Operating conditions for similitude experiments (Figs. 7.29-7.33) Using dead-space extensions

SMALL CFB

L_v	23 ± 1 inches
Reactor loading	750 ± 25 mL
Superficial velocity	2.9 ± 0.1 m/s
Solids flux	22 ± 3 kg/m^{2}s
Rep	85 ± 12
Fr	5700 ± 800
$G_v/\rho_s U$	0.0010 ± 0.0001
H/d_p	10200 ± 1400
D/d_p	340 ± 50
ρ_g/ρ_s	2150 ± 30
$M/\rho_s D^3$	3.15 ± 0.08

LARGE CFB

L_v	46 ± 2 inches
Reactor loading	6000 ± 200 mL
Superficial velocity	4.1 ± 0.1 m/s
Solids flux	11 ± 2 kg/m^{2}s
Rep	84 ± 5
Fr	5800 ± 500
$G_v/\rho_s U$	0.0010 ± 0.0002
H/d_p	10200 ± 300
D/d_p	340 ± 10
ρ_g/ρ_s	2150 ± 70
$M/\rho_s D^3$	3.15 ± 0.05

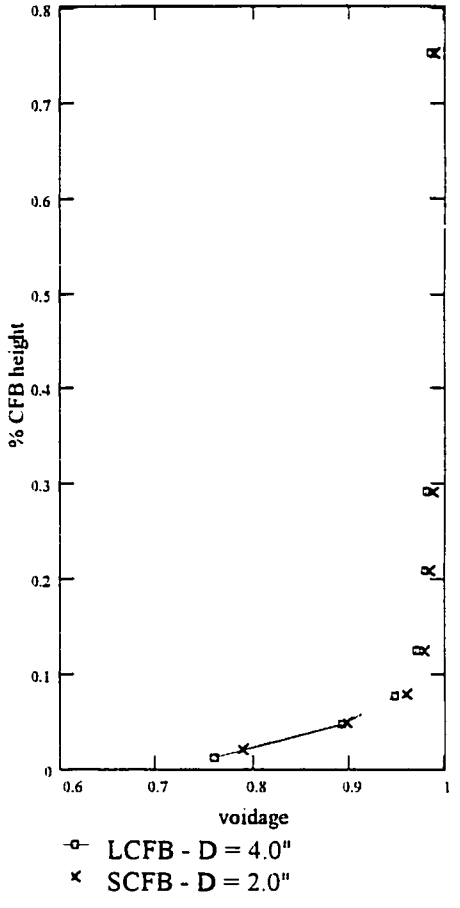

Figure 7.34: CFB axial voidage profiles (Using dead-space extensions)

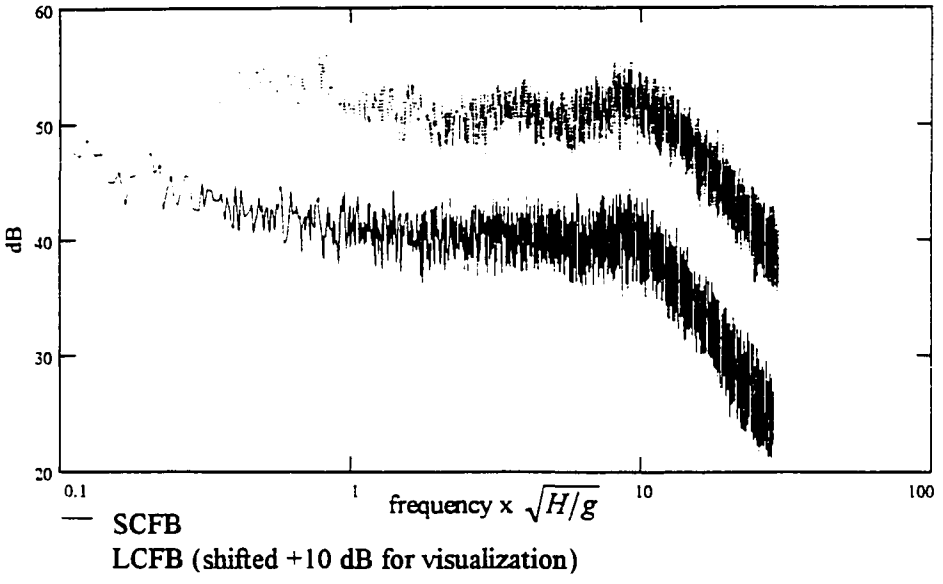

Figure 7.35: Bode plots of CFB under similitude conditions (1-2 % bed height) Using dead-space extensions

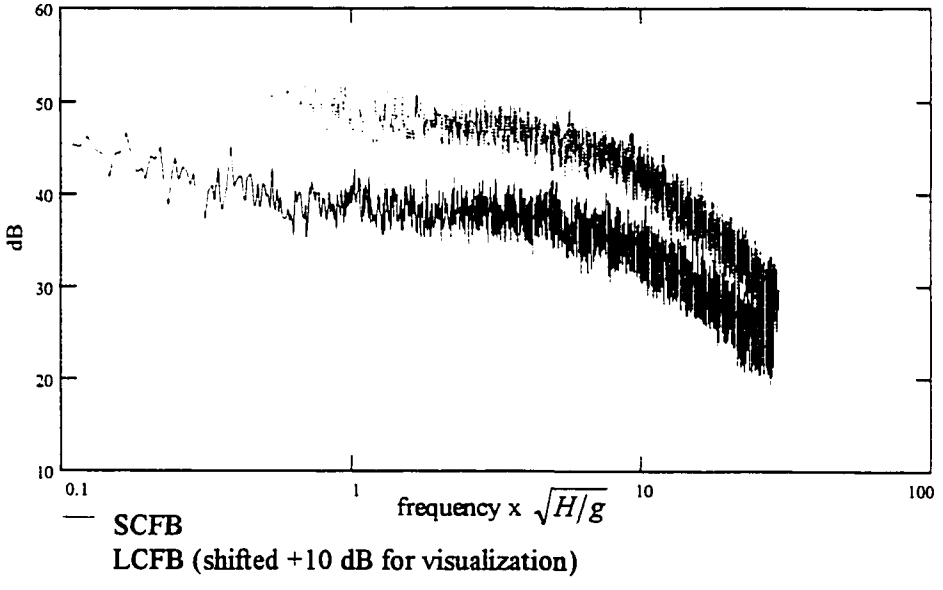

Figure 7.36: Bode plots of CFB under similitude conditions (5 % bed height) Using dead-space extensions

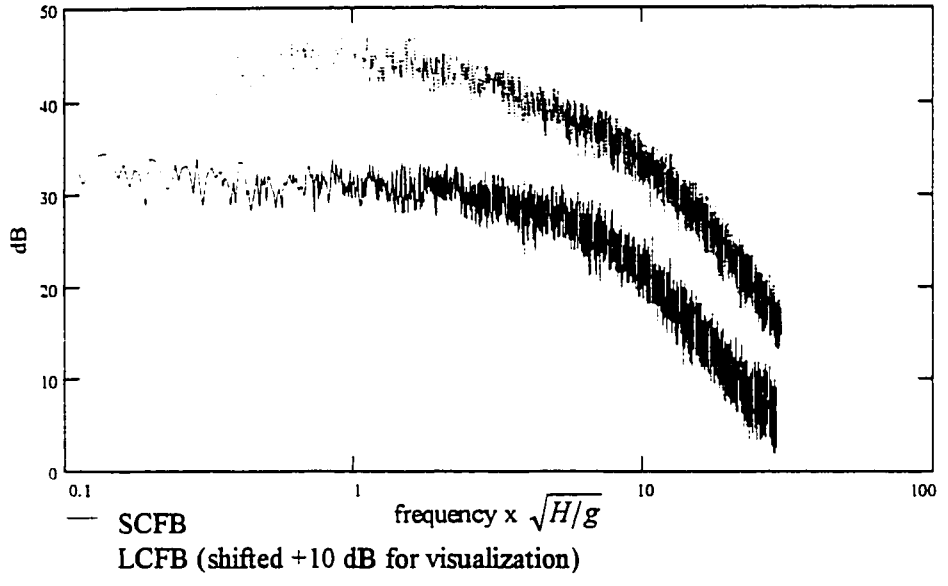

Figure 7.37: Bode plots of CFB under similitude conditions (13 % bed height) Using dead-space extensions

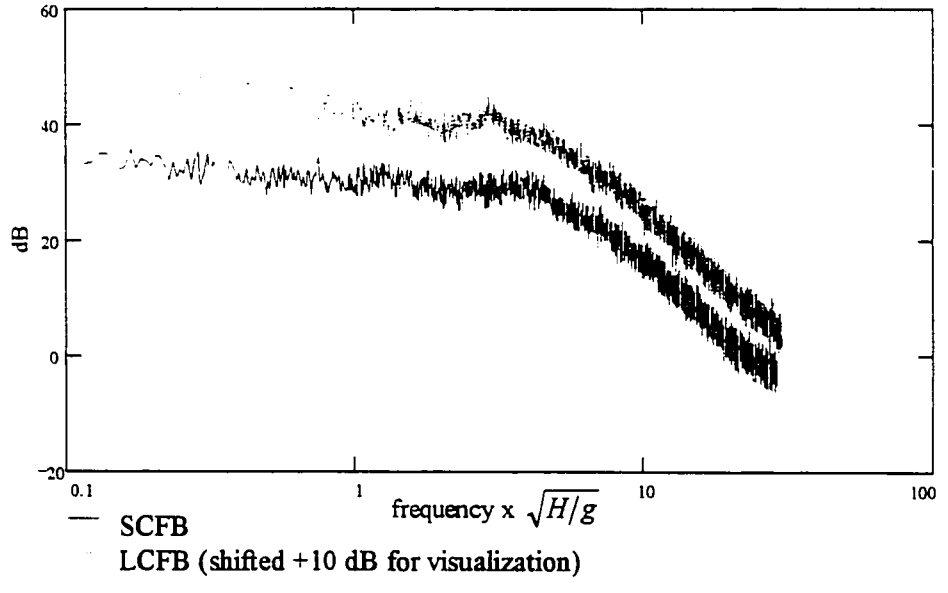

Figure 7.38: Bode plots of CFB under similitude conditions (75 % bed height) Using dead-space extensions

coefficient of restitution of particle/bed collisions may make a significant difference in the CFB hydrodynamics. The effects of particle collisions with the riser top-plate must be considered in similitude studies.

Pressure Fluctuations in Industrial Scale CFB Boilers

The final phase of this study was to determine if the analysis of pressure fluctuations in industrial scale CFB boilers could provide similar information about fluidized bed operation as was observed in the laboratory scale models.

Discussion of low elevation CFB boiler fluctuations

Although there is some variation in the structure of the lower bed fluctuations, as seen in time domain plots of Figures 7.39 and 7.40, they always exhibit a signal similar to a 0.25 - 0.3 Hz square wave. It is evident that the lower bed signal has a dominant period, on the order of a cycle every 3 to 4 seconds. This dominant frequency at 0.25 - 0.3 Hz is very pronounced in the power spectral density of these signals shown in Figures 7.41 and 7.42. Examining the Bode plot of the bed pressure fluctuations in Figure 7.41b, the low frequency region of the Bode plot seemingly exhibits a system behavior that rolls-off at around -40 dB/decade (or greater). This does not lead to the definitive conclusion that the boiler fluctuations are governed by second order phenomena. The Bode plots are difficult to interpret due to the presence of strong harmonics as illustrated in the full spectrum of Bode plots (see Figure 7.41c).

These strong harmonics can be explained by recognizing that the fluctuations in the time domain exhibit a square wave behavior. Subsequent harmonics observed in the PSD appear at odd multiples of the fundamental frequency (see Figure 7.42). These harmonics are what is expected as the Fourier transform estimates a square wave with multiple sinusoids at odd multiples of the fundamental frequency. Before the conclusion can be made that the pressure fluctuations are indicative of CFB boiler hydrodynamics, the nature of the dominant 0.25 - 0.3 Hz phenomena must be examined further.

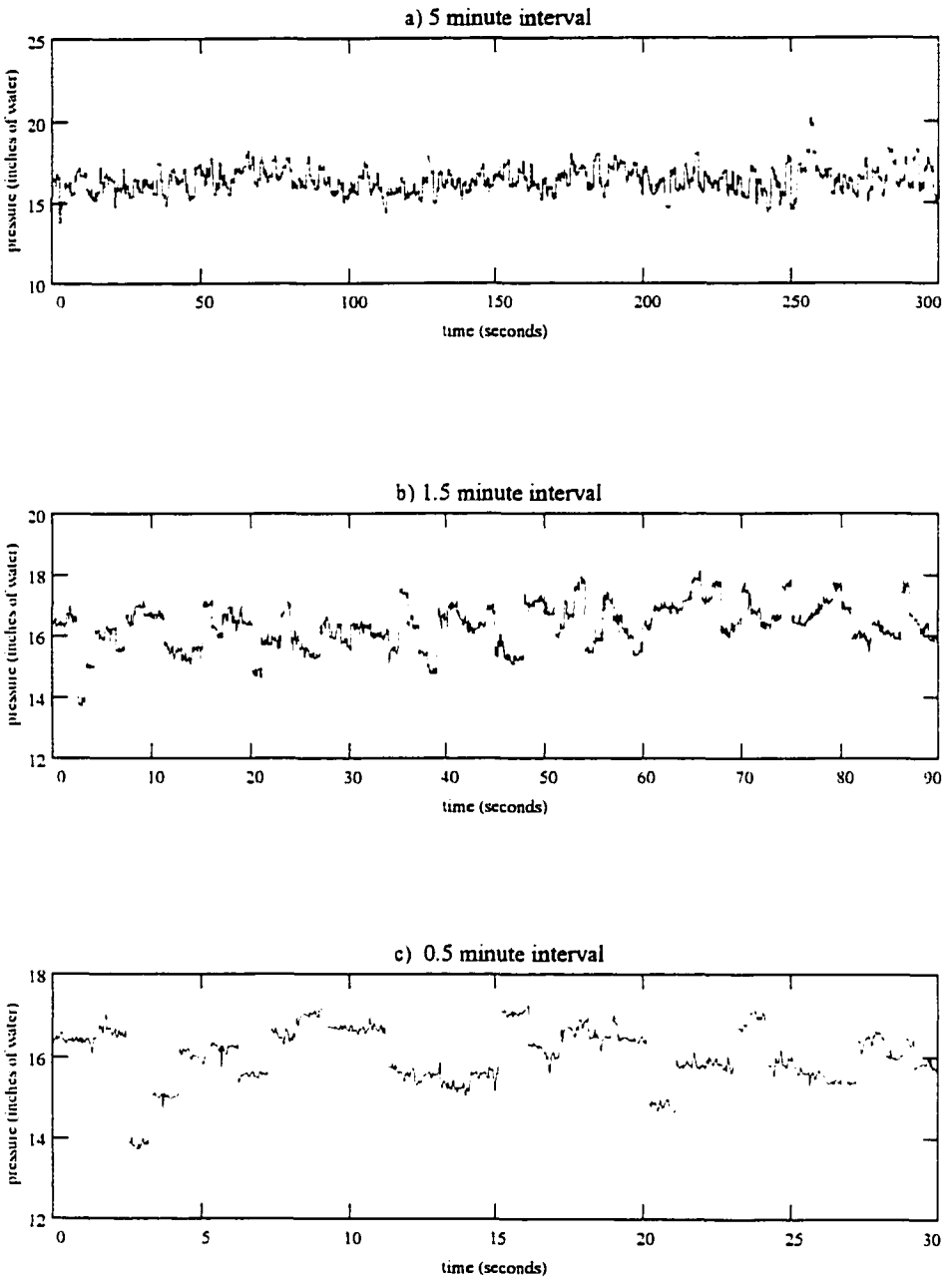

Figure 7.39: ISU CFB boiler lower bed pressure fluctuations (peak load - morning)

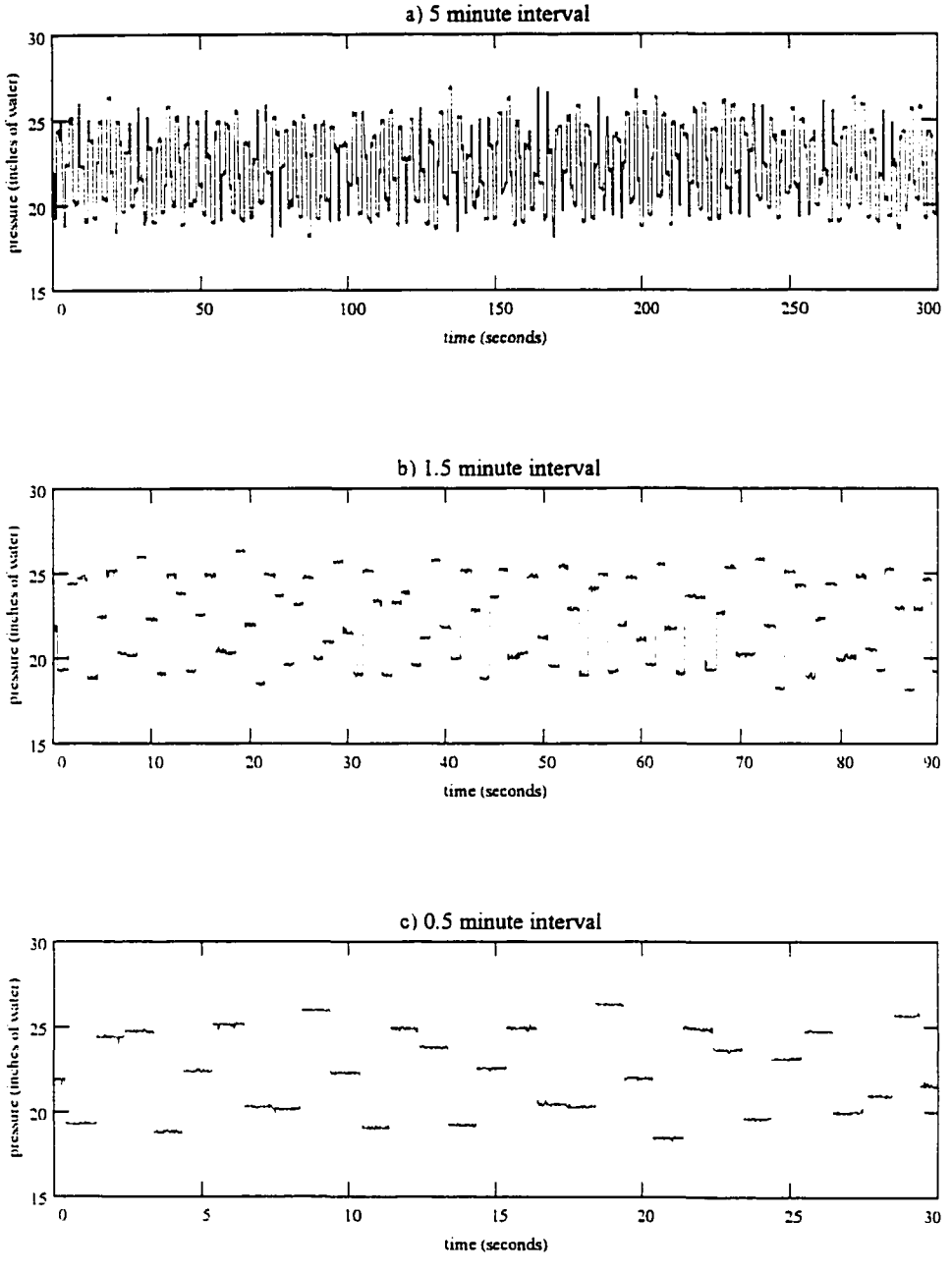

Figure 7.40: ISU CFB boiler lower bed pressure fluctuations (afternoon load)

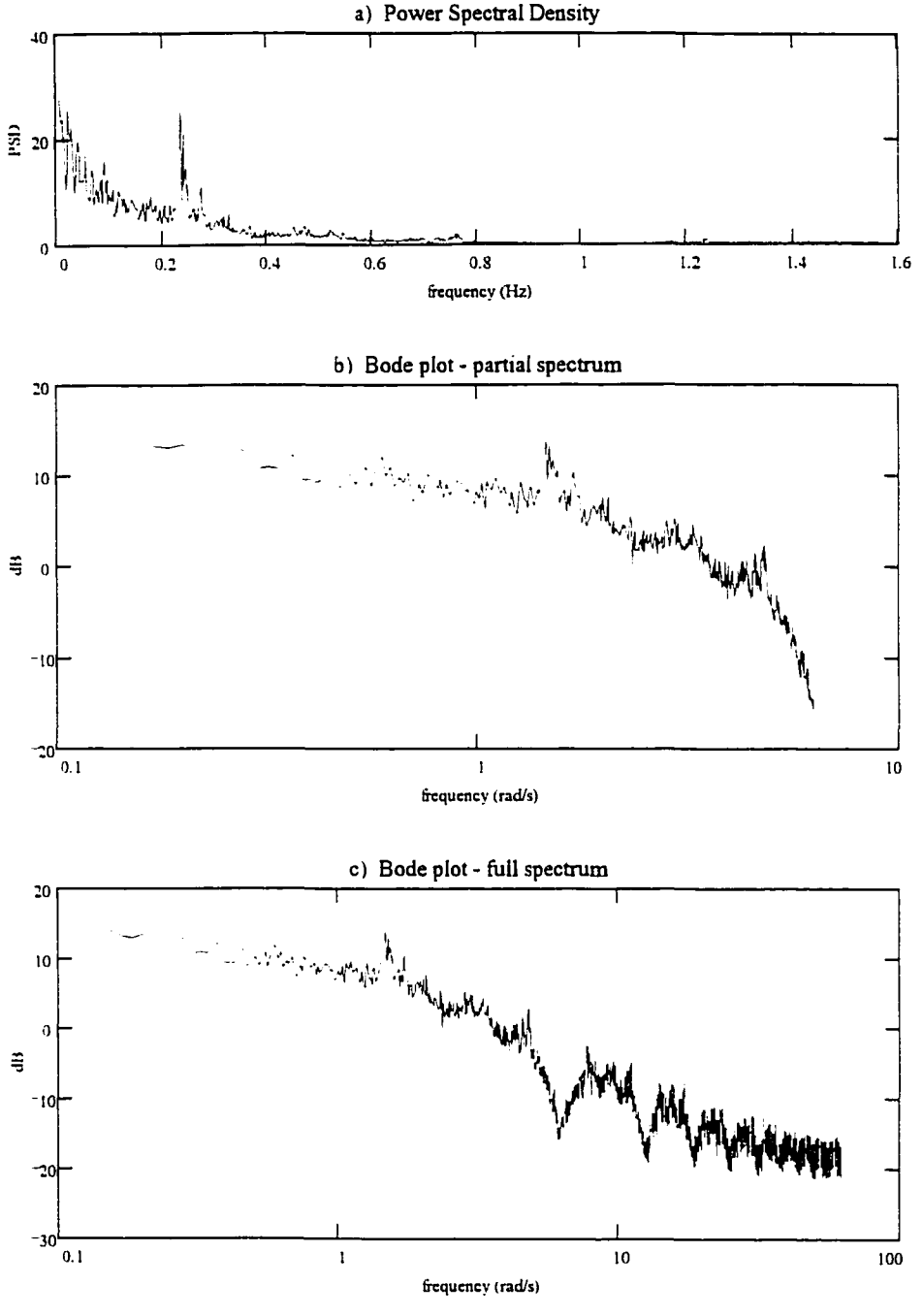

Figure 7.41: Peak load CFB boiler fluctuations a) PSD b) partial b) full Bode

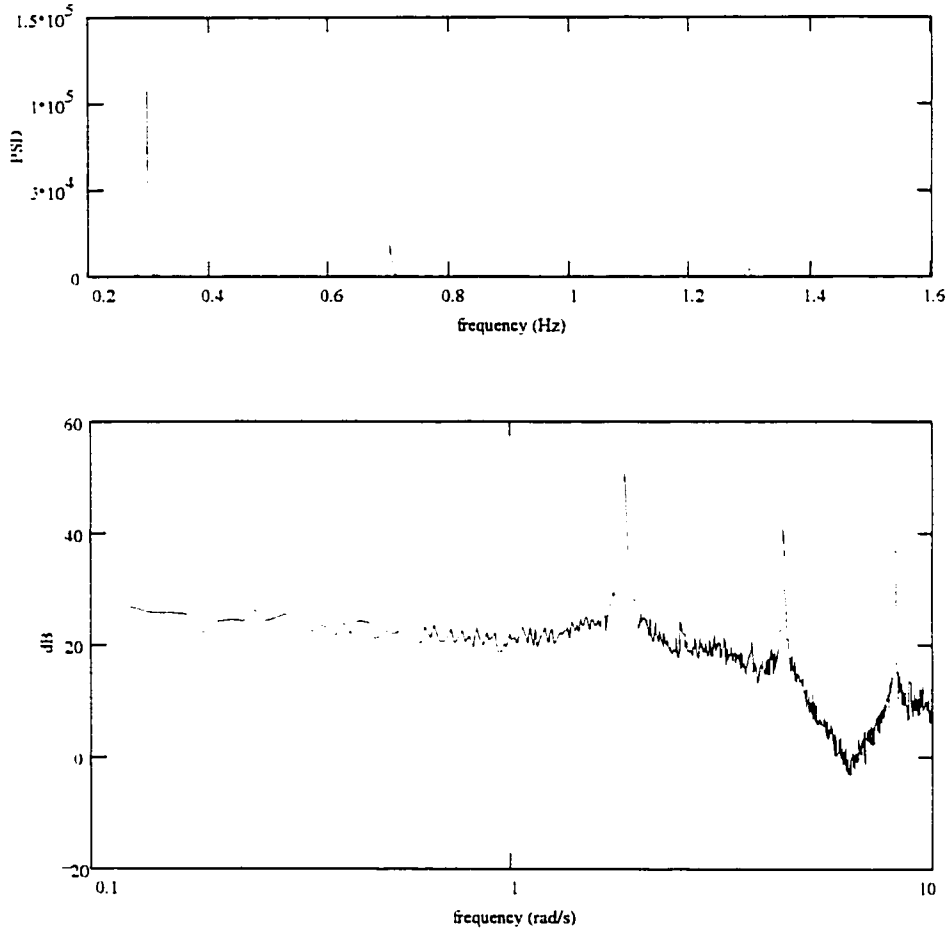

Figure 7.42: Bode plot & PSD of CFB boiler lower bed fluctuations (afternoon load)

Experiments were conducted to better understand the nature of the 0.25-0.3 Hz dominant frequency measured at the bottom of the boiler. First, an analog anti-aliasing filter was used while recording data to insure that the dominant frequency observed in the spectrum was not simply the result of a frequency phenomena higher that the sampling frequency (e.g. 60 Hz line frequency) being manifest in the low frequency spectrum. A 3rd-order Butterworth filter was designed and constructed with a 16 Hz (100 rad/s) cut-off frequency. Figure 7.43 compares the Bode plot of filter data to that of the unfiltered data. Although it is also evident that the filtered data begins to attenuate the signal slightly as the spectrum approaches 100 rad/s, as expected, there is no significant difference in the plots. It can be concluded from this result that the 0.25-0.3 Hz phenomena is not the result of aliasing. Data recorded at sampling frequencies of up to 1000 Hz confirms this conclusion, since no dominant frequency phenomena between 0-500 Hz (other than the 0.25 - 0.3 Hz phenomena) is observed in the spectrum.

It was hypothesized that this dominant frequency was not the result of the CFB hydrodynamics but of a standard periodic operation of the CFB Boiler. It was believed that oscillations in the limestone or coal feed systems were the origin of the square wave signal. If this was the case, any dynamics resulting from fluidization fluctuations would be hidden within the dynamics of boiler operation. By analyzing only the part of the signal that resides between subsequent 0.25-0.3 Hz oscillations, this hypothesis was tested. The Bode plots that resulted from this analysis did not show any dynamic behavior that could be attributed to CFB hydrodynamics. The resulting plots were typical of the Bode plots of a white noise signal, containing no important dynamic information. It is assumed that all observed dynamics contained in the spectrum are related to the 0.25-0.3 Hz oscillation.

The most likely explanation for this periodic behavior is the coal feed system. Coal is fed into the boiler at two locations; via the loop seal and directly into the bed on a cleated conveyor belt. Due to the spacing of the cleats and the typical speed of the conveyor, a cleat reaches the entrance of the boiler every 3 to 4 seconds. Assuming that the coal will have a tendency to pile up near the cleat, the rate at which coal enters the boiler will not be

a) CFB Boiler pressure fluctuation Bode plot (filtered)

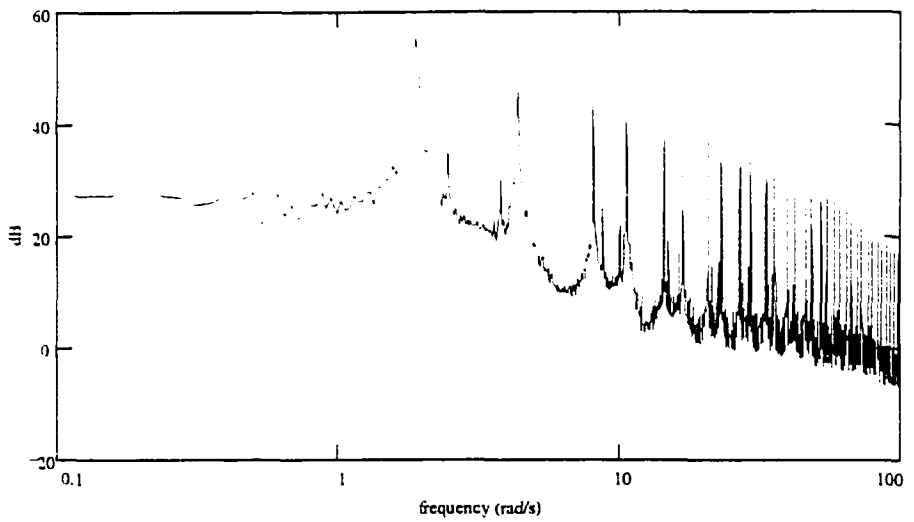

b) CFB Boiler pressure fluctuation Bode plot (unfiltered)

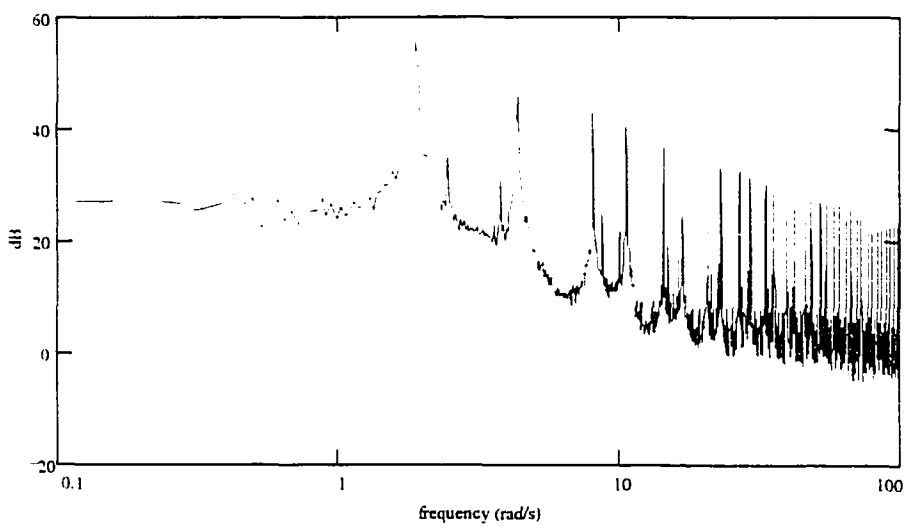

Figure 7.43: Bode plot of CFB boiler fluctuations a) w/ anti-aliasing filter b) unfiltered

continuous. Rather, the feeder will input a batch of coal every 3 to 4 seconds.

By observing boiler fluctuations under high and low loading conditions, this hypothesis is supported. Figure 7.40 shows bed fluctuations measured mid-afternoon while Figure 7.39 represents the fluctuations measure during peak operation 8:00-9:00 a.m. During this period of high load, the fluctuations appear less dominated by the "square wave" coal feed fluctuations. This is expected since an increased circulation rate increases the solids suspended in the bed and decreases the observed effect of the coal feed directly into the CFB. The more dilute the operation of the CFB is, the more evident the periodic coal feed will be in the frequency spectrum.

Discussion of upper CFB boiler fluctuations

The combustion chamber pressure fluctuations differ from the lower bed fluctuations because the periodic nature of the coal feed no longer is sensed as strongly at the top of the bed (see Figure 7.44). At this elevation, the periodic batches of coal entering the combustor have been more evenly dispersed in the upward moving gas flow. The Bode plot of the combustion chamber pressure fluctuations shown in Figure 7.45 does seem to exhibit an initial roll-off of around -40 dB/decade. This characteristic frequency occurring at around 0.4-0.5 rad/s (0.06 - 0.08 Hz) may be a highly damped α_0-frequency phenomena similar to that observed in the CFB models.

The equivalent diameter of the CFB boilers is 4.85 meters. This is 47.5 times greater than the 10.2 cm diameter CFB model. If the α_0-frequency phenomena was observed in the CFB boiler, it would appear at a frequency inversely proportional to the square root of the diameter. Observing a frequency at around 0.5 Hz in the 10.2 cm CFB model (absolute pressure fluctuations), the predicted α_0-frequency for the boiler would be 0.07 Hz, as is observed. It is difficult to asses how much of an effect the periodic coal feed has on the combustion chamber fluctuations, therefore this hypothesis that a dilute phase phenomena similar to that observed in the models is acting in the CFB boilers cannot be definitively supported. Additionally, this combustion chamber pressure is a controlled pressure. Exhaust

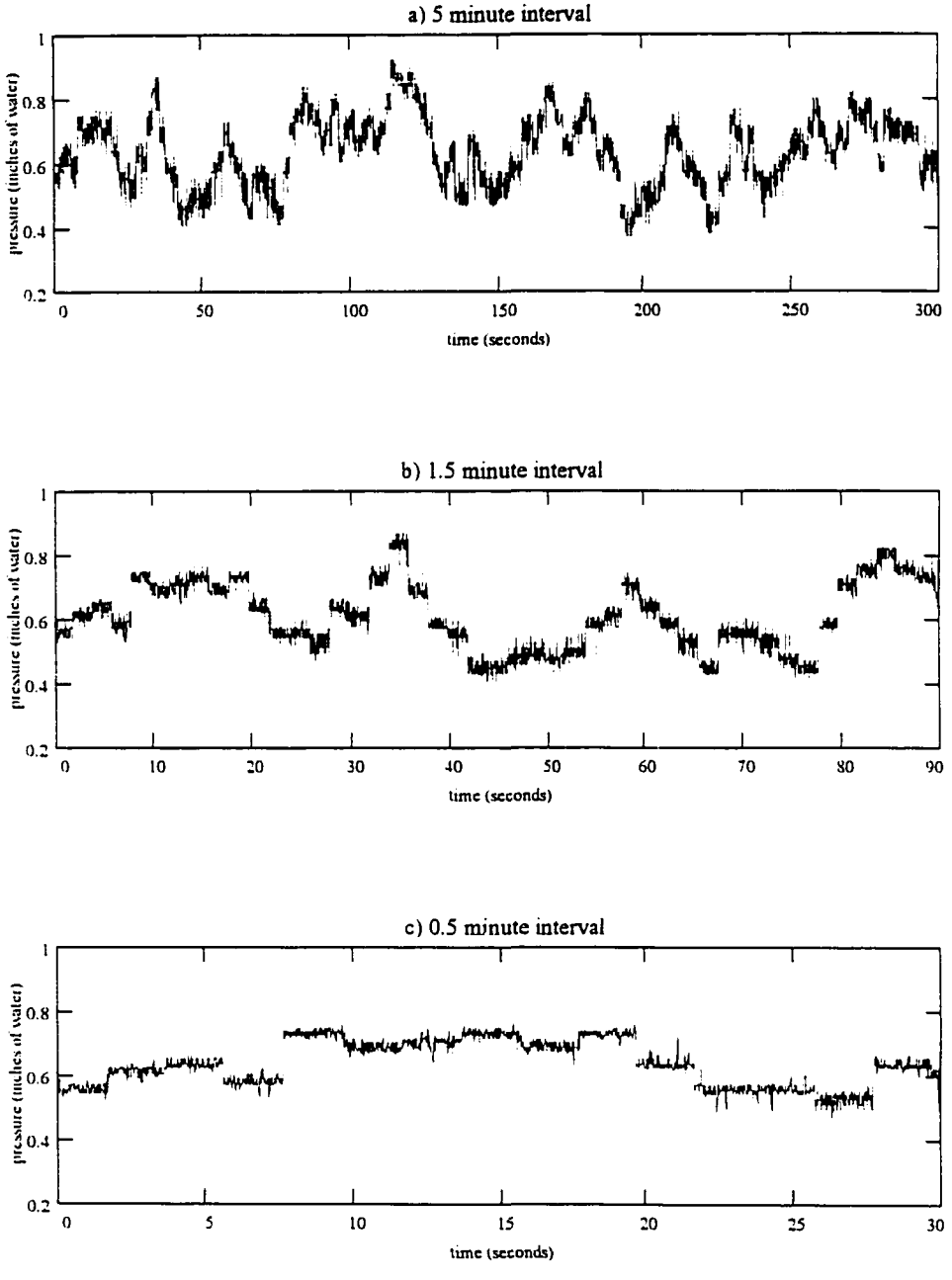

Figure 7.44: ISU CFB boiler combustion chamber pressure fluctuations

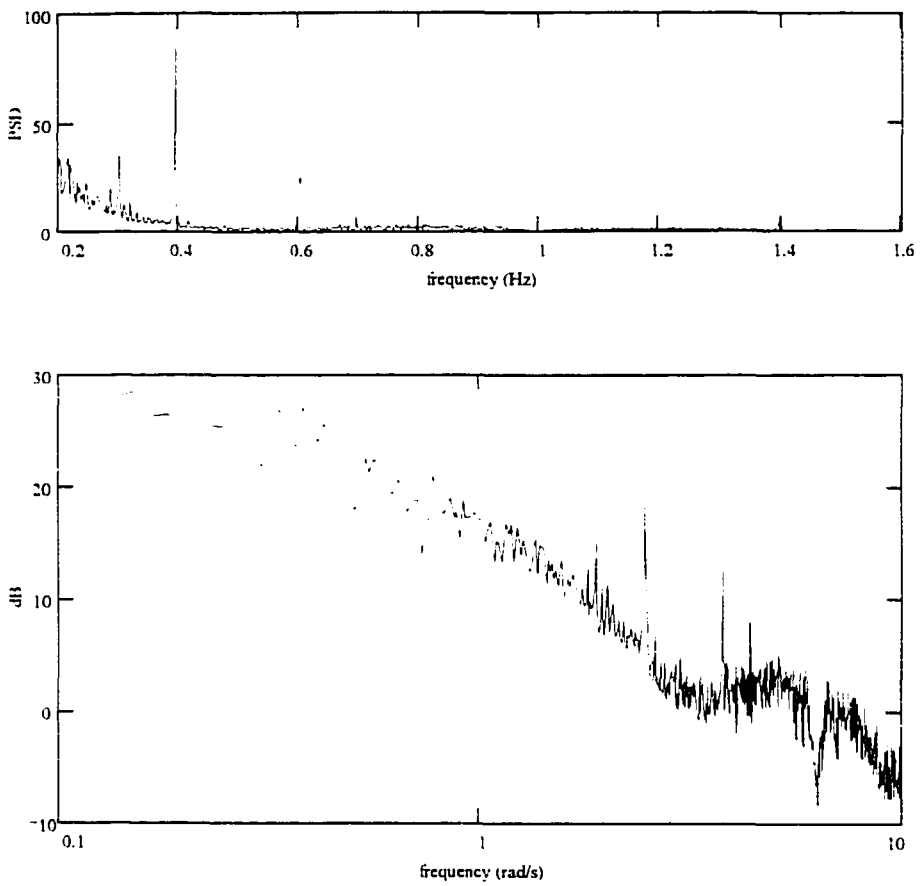

Figure 7.45: Bode plot & PSD of CFB boiler combustion chamber pressure fluctuations

fans are used to keep this pressure at acceptable levels. More must be known regarding the control system dynamics before any definitive conclusions can be drawn regarding the relation of pressure fluctuations to fluidization hydrodynamics in industrial scale CFB boilers.

CHAPTER 8. CONCLUSIONS

This study has shown that pressure fluctuations can be used as a diagnostic and design tool for fluidized beds if an appropriate method of analysis is applied. Adequate data sampling and averaging is necessary to achieve a valid system description. The numerous pressure fluctuation phenomena in fluidized bed systems are identified using a system identification approach. Using this approach, the differences and similarities between the pressure dynamics of bubbling, turbulent, and fast fluidization are compared. This comparison results in a better understanding of the hydrodynamics in each of these regimes. As a diagnostic tool, the analysis of pressure fluctuations in CFBs can be used to estimate the solids hold-up in the riser, and the height of the lower dense bed. The ISU CFB boiler pressure fluctuations do not exhibit the dynamics seen in the CFB models. The boiler fluctuations are dominated by the effects of the coal feed system and other dynamics associated with boiler control.

As a tool for fluidized bed design and scale-up, the spectral analysis of pressure fluctuations can be used as a dependent parameter in similitude studies. Pressure fluctuations in bubbling fluidized beds validate the similitude parameters previously derived by Glicksman. However, circulating fluidized bed similitude results show that matching Glicksman's parameters in two circulating beds does not guarantee that similar hydrodynamics have been established in the model and prototype. Using a revised set of similitude parameters that replaces the dimensionless solids flux with a dimensionless riser loading, the hydrodynamics in the model and prototype come closer to achieving similarity. Even with these revised similitude parameters, the results suggest that the coefficient of restitution of particle/top-plate collisions will significantly alter CFB hydrodynamics.

REFERENCES

[1] Noble, D. F. Forces of Production: A Social History of Industrial Automation; Oxford University Press: New York, 1984.

[2] Pacey A. The Maze of Ingenuity: Ideas and Idealism in the Development of Technology, 2nd Ed.; MIT Press: Cambridge, 1992.

[3] Perrin N. Giving up the Gun; David R. Godine Publishing: Boston, 1979.

[4] Monsma, S. V., C. Christians, E. R. Dykema, A. Leegwater, E. Schuurman, L. Van Poolen. Responsible Technology: A Christian Perspective; William B. Eerdmans Publishing Company: Grand Rapids, 1986.

[5] Postman N. Amusing Ourselves to Death; Penguin Books: New York, 1985.

[6] Marcus, A., and H. P. Segal. Technology in America: A Brief History; Harcourt Brace Jovanovich: San Diego, 1989.

[7] Nye, D. E Electrifying America: Social Meanings of a New Technology; MIT press: Cambridge, 1990.

[8] Corn, J. J. The Winged Gospel: America's Romance with Aviation, 1900-1950; Oxford University Press: New York, 1983.

[9] Headrick, D. R. The Tools of Empire: Technology and European Imperialism in the Nineteenth Century; Oxford University Press: New York, 1981.

[10] Glicksman L.R., M.T. Nicastro. "Experimental verification of scaling relationships for fluidized bed." *Chem. Eng. Science* 1984, 39(9), 1381-1391.

[11] Glicksman, L.R., D. Westphalen, C. Bereton, and J. Grace. "Verification of the scaling laws for circulating fluidized beds." In *Circulating Fluidized Bed Technology III*. P. Basu, M. Hasatan, and M. Horio, Eds.; Pergamon Press: Oxford, 1991; 199-124.

[12] Louge M, and H. Chang. "Fluid dynamic similarity of circulating fluidized beds" *Powder Technology* 1992, 70, 259-270.

[13] Gidaspow, D., I.K. Gamwo, and A. Miller. "Predictive models of circulating fluidized bed combustors" *Technical Progress Report (U.S. Dept. of Energy)*, April 1992.

[14] Glicksman L.R., M.R. Hyre, and P.A. Farrell. "Dynamic similarity in fluidization." *Int. J. Multiphase Flow* 1994, 20, 331-386.

[15] Glicksman L.R., M.R. Hyre, and K. Woloshun. "Scale models of circulating fluidized bed combustors: simplification of scaling laws and the scaling of convective heat tranfer." *Report # DOE/MC/25049-3372*, USDOE, Washington D.C., 1993.

[16] Daw, C.S., W.F. Lawkins, D.J. Downing, and N.E. Clapp, Jr. "Chaotic characteristics of a complex gas-solids flow." *Physical Review* A 1989, 41(2), 1179.

[17] Tam, S.W., and M. Darine. "A study of fluidized-bed dynamical behavior: a chaos perspective." In *Applied Chaos*; J.H. Kim, and J. Stringer, Eds.; John Wiley & Sons: New York, 1992; 381.

[18] Van der Stapper, M.L.M., J.C. Schouten, and C.M. Van den Breek. "Application of deterministic chaos analysis to pressure fluctuation measurements in a .96 m^2 CFB riser." To be published in *Circulating Fluidized Bed Technology IV* (1993 Conference Proceedings).

[19] Boulillard, J.X. and A. Miller. "Experimental investigations of chaotic hydrodynamic attractors in circulating fluidized beds." To be published in *Circulating Fluidized Bed Technology IV* (1993 Conference Proceedings).

[20] Daw C. S., and J. S. Halow. "Evaluation and control of fluidization quality through chaotic time series analysis of pressure drop measurements." In *Fluid-Particle Processes, AIChE Symposium Series*. A.W. Weimer, Ed.; AIChE: New York, 1993.

[21] Van der Stappen M.L.M., J.C. Schouten, and C.M. van den Bleek. "Application of deterministic chaos theory in understanding the fluid dynamic behavior of gas-solids fluidization." In *Fluid-Particle Processes, AIChE Symposium Series*. A.W. Weimer, Ed.; AIChE: New York, 1993.

[22] Lynn, P.A. An Introduction to the Analysis and Processing of Signals, 3rd ed.; Macmillan Press: Hong Kong, 1989.

[23] Komo, J.J. Random Signal Analysis in Engineering Systems; Academic Press Inc.: Orlando, 1987.

[24] Kunni D. and O. Levenspiel. Fluidization Engineering; Butterworth-Heinemann: Boston, 1991.

[25] Geldart, D. "Characterizatior of fluidized powders." In *Gas Fluidization Technology;* D. Geldart, Ed; John Wiley & Sons: Chichester, 1980; 1-52.

[26] Basu, P. and S.A. Fraser. Circulating Fluidized Bed Boilers; Butterworth-Heinemann: Boston, 1991.

[27] Dry, R.J. and R.D. La Nauze. "Combustion in fluidized beds." *Chemical Engng. Progress* July 1990; 31-47.

[28] Furusawa T. and T. Shimizu. "Analysis of circulating fluidized bed combustion technology and scope for future development." In *Circulating Fluidized Bed Technology II*; P. Basu and J.F. Large, Eds.; Pergamon Press: Oxford, 1988; 51-62.

[29] Davison, J.E., P.J.I. Cross, and J.M. Topper. "Application of CFBC to power generation in the UK." In *Circulating Fluidized Bed III*; P. Basu, M. Hasatani, and M. Horio, Eds.; Pergamon Press: Oxford, 1991; 445-450.

[30] Yerushalmi, J. "High velocity fluidized beds." In *Gas Fluidization Technology*; D. Geldart, Ed; John Wiley & Sons: Chichester, 1980; 155-196.

[31] Takeuchi, H., T. Hirama, T. Chiba, J. Biswas, and L.S. Leung. "A quantitative definition and flow regime diagram for fast fluidization." *Powder Technology* 1986, 47, 195-199.

[32] Reddy-Karri, S.B. and T. Knowlton. "A practical definition of the fast fluidization regime." In *Circulating Fluidized Bed Technology III*; P. Basu, M. Hasatani, and M. Horio, Eds.; Pergamon Press: Oxford, 1991; 67-72.

[33] Kwank M., L. Jinghai, and T. Yuanki. "Axial voidage profiles of fast fluidized beds in different operating regions." In *Circulating Fluidized Bed Technology II*; P. Basu and J.F. Large, Eds.; Pergamon Press: Oxford, 1988; 193-203.

[34] Werther J. "Fluid mechanics of large scale CFB units." To be published in *Circulating Fluidized Bed Technology IV* (1993 Conference Proceedings).

[35] Bader R., J. Findlay, and T.M. Knowlton. "Gas/solids flow patterns in a 30.5 cm. diameter circulating fluidized bed." In *Circulating Fluidized Bed Technology II*; P. Basu and J.F. Large, Eds.; Pergamon Press: Oxford, 1988; 123-137.

[36] Rhodes, M.J., P. Laussmann, F. Villain, and D. Geldart. "Measurement of radial and axial solids flux variations in the riser of a circulating fluidized bed." In *Circulating Fluidized Bed Technology II*; P. Basu and J.F. Large, Eds.; Pergamon Press: Oxford, 1988; 155-164.

[37] Van Breugel, J.W., J. J. M. Stein, and R. J. Vries. "Isokinetic sampling in a dense gas-solid stream." *Proc. Inst. Mechanical Engineers* 1970, 184, 18-23.

[38] Weinstein, H., M. Shao and M. Schnitzlein. "Radial variations in solid density in high velocity fluidization." In *Circulating Fluidized Bed Technology*; ed. P. Basu: Pergamon Press: Toronto, 1986; 201-206.

[39] Weinstein, H. and L. Chen. "The radial pressure gradient in a circulating fluidized bed riser." To be published in *Circulating Fluidized Bed Technology IV* (1993 Conference Proceedings).

[40] Morse, R.D. and C.O. Ballou. "The uniformity of fluidization- its measurement and use." *Chem. Eng. Prog.* 1951, 47(4), 199-204.

[41] Gerald, C.F. A response to work of R.D. Morse regarding measurement of fluidization uniformity. *Chem. Eng. Prog.* 1951, 47(9), 483-484.

[42] Shuster, W.W. and P. Kisliak. "The measurement of fluidization quality." *Chem. Eng. Prog.* 1952, 48(9), 455-458.

[43] Davidson, J.F. and D. Harrison. Fluidized Particles; Cambridge University Press: Cambridge, 1963.

[44] Rueter, H. "On the nature of bubbles in gas and liquid fluidized beds." In *Fluid Particle Technology: Chem. Eng. Prog. Symposium Series*; B.S. Lee, Ed.; *AIChE J.* 1966, 62(62), 92-99.

[45] Tamarin, A.I. "The origin of self-excited oscillations in fluidized beds." *International Chemical Engineering* 1964, 4(1), 50-54.

[46] Winter, O. "Density and pressure fluctuations in gas fluidized beds." *AIChE J.* 1968, 14(3), 426-433.

[47] Kang, W.K., J.P. Sutherland and G.L. Osberg. "Pressure fluctuations in a fluidized bed with and without screen cylindrical packings." *Ind. Eng. Chem. Fundamentals* 1967, 6(4), 499-504.

[48] Lirag, R.C. Jr., and H. Littman. "Statistical study of the pressure fluctuations in a fluidized bed." *Fluidization: AIChE Symposium Series*, H. Littman and R. Pfeffer, Eds. *AIChE J.* 1971, 67(116), 11-22.

[49] Sitnai, O. "Utilization of the pressure differential records from gas fluidized beds with internals for bubble parameters determination." *Chem. Eng. Science* 1982, 37(7), 1059-1066.

[50] Fan, L.T., T.C. Ho, and W.P. Walawender. "Measurements of the rise velocities of bubbles, slugs, and pressure waves in a gas-solid fluidized bed using pressure fluctuation signals." *AIChE J.* 1983, 29(1), 33-39.

[51] Fan, L.T., T.C. Ho, S. Hiraoka, and W.P. Walawender. "Pressure fluctuations in a fluidized bed." *AIChE J.* 1981, 27(3), 388-396.

[52] Dhodapkar S.V., and G.E. Klinzing. "Pressure fluctuation analysis for a fluidized bed." In *Fluid-Particle Processes, AIChE Symposium Series*. A.W. Weimer, Ed.: AIChE: New York, 1993.

[53] Kage H., N. Iwasaki, and Y. Matsuno. "Frequency analysis of pressure fluctuations in plenum as a diagnostic method for fluidized beds." In *Fluid-Particle Processes, AIChE Symposium Series*. A.W. Weimer, Ed.; AIChE: New York, 1993.

[54] Hiby, J.W. "Periodic phenomena connected with gas-solid fluidization." In *Proceedings of the International Symposium on Fluidization, Eindhoven*; Netherlands University Press: Amsterdam, 1967; 99.

[55] Verloop, J. and P.M. Heertjes. "Periodic pressure fluctuations in fluidized beds." *Chem. Eng. Science* 1974, 29, 1035-1042.

[56] Roy, R., J.F. Davidson, and V.G. Tuponogov. "The velocity of sound in fluidized beds." *Chem. Eng. Sci.* 1990, 45(11), 3233-3245.

[57] Davidson, J.F. In *Triparte Chemical Engineering Conference Symposium on Fluidization, Montreal*; Institution of Chemical Engineers: London, 1968; 3.

[58] Wong, H.W. and M.H. Baird. "Fluidisation in pulsed gas flow." *Chem. Engng. J.* 1971, 2, 104-113.

[59] Sun, J., M.M. Chen, and B.T. Chao. "On the fluctuation motions due to surface waves in gas fluidized beds." In *Proceedings of the First World Conference on Experimental Heat Transfer, Fluid Mechanics and Thermodynamics, Dubrovnik.* R.K. Shah, E.N. Ganic, and K.T. Yang, Eds.;Elsevier: New York, 1988; 1310.

[60] Baskakov, A.P., V.G. Tuponogov, and N.F. Filippovsky. "A study of pressure fluctuations in a bubbling fluidised bed." *Powder Technology* 1986, 45, 113-117.

[61] Kehoe, P.W.K., and J.F. Davidson. "Pressure fluctuations in slugging fluidized beds." *AIChE Symposium Series* 1973, 69(128), 34-40.

[62] Baeyens, J., and D. Geldart. "An investigation into slugging fluidised beds." *Chem. Engng. Sci.* 1974, 29, 255-265.

[63] Glicksman, L.R. "Scaling relationships for fluidized beds." *Chem. Eng. Science* 1984, 30(9), 1373-1379.

[64] Fitzgerald, T., D. Bushnell, S. Crane, and Yeong-Cheng Shieh. "Testing of cold scaled bed modeling for fluidized bed combustors." *Powder Technology* 1984, 38, 107-120.

[65] De Felice, R., S. Rapagna, and P.U. Foscolo. "Dynamic similarity rules: validity check for bubbling and slugging fluidized beds." *Powder Technology* 1992, 71, 281-287.

[66] De Felice, R., S. Rapagna, P.U. Foscolo, and L.G. Gibilaro. "Cold modeling studies of fluidised bed reactors." *Chem. Eng. Science* 1992, 47(9-11), 2233-2238.

[67] Schnitzlein, M.G. and H. Weinstein. "Flow characterization in high-velocity fluidized beds using pressure fluctuations." *Chem. Eng. Science* 1988, 43(10), 2605-2614.

[68] Glicksman, L.R., M. Hyre, and K. Woloshun. "Simplified scaling relationships for fluidized beds." *Powder Technology* 1993, 77, 177-199.

[69] Glicksman, L.R., P.A. Farrell, and M.R. Hyre. "Verification of a simplified set of hydrodynamic scaling relationships for pressurized fluidized bed combustors." *in Fluidization andFluid-Particle Systems* AIChE, Miami, 1995.

[70] Glicksman, L.R., D. Westphalen, K. Woloshun, T. Ebert, K. Roth, and M. Lints. "Experimental scale models of circulating fluidized bed combustors." *Fluidized Bed Combustion, ASME* 1991; 1169-1174.

[71] Plasynski, S.I., G.E. Klinzing, and M.P. Mathur. "Pressure fluctuations investigation for high pressure vertical pneumatic transport." To be published in *Circulating Fluidized Bed Technology IV* (1993 Conference Proceedings).

[72] Nowak, W., H. Matsuda, K.K. Win, and M. Hasatani. "Diagnosis of multi-solid fluidized beds by power spectrum analysis of pressure fluctuations." To be published in *Circulating Fluidized Bed Technology IV* (1993 Conference Proceedings).

[73] Jenkins, G.M. and D.G. Watts. Spectral Analysis and its Applications; Holden Day: San Francisco, 1968.

[74] Dorf, R.C. Modern Control Systems, 6th Edition; Addison-Wesley: Reading, 1992.

[75] Smith, C.A. and A.B. Corripio. Principles and Practice of Automatic Process Control; John Wiley & Sons: New York, 1985.

[76] Brue, E. "Process model identification of circulating fluidized bed hydrodynamics." M.S. Thesis, Iowa State University, 1994.

[77] Burkell, J.J., J.R. Grace, J. Zhao, and C.J. Lim. "Measurement of solids circulation rates in circulating fluidized beds." In *Circulating Fluidized Bed Technology II*; P. Basu and J.F. Large, Eds.; Pergamon Press: Oxford, 1988; 501-507.

[78] Rahman, M.. Water Waves: Relating Modern Theory to Advanced Engineering Applications; Claredon Press: Oxford, 1995.

[79] Brue, E., Moore, J., and R. C. Brown. "Wave phenomena in fluidized beds." In the proceedings of *First International Particle Technology Forum*, AIChE, Denver 1994.

[80] Martin-Letellier, S., and M. Y. Louge. "The role of gas density in circulating fluidized bed risers." *In Fluidization and Fluid-Particle Systems*, AIChE, Miami, 1995.

APPENDIX A

BFB SIMILITUDE STUDY RESULTS

Table A.1. Similitude tests for dp =0.4 mm and H = 10 cm prototype conditions

Exp. #	U/U_{mf}	Re_p	Fr	$\rho_s/\rho_g x10^{-3}$	H/D	D/d_p	% H	ε (avg.)	ω_{n1}	ω_{n2}	ζ_1	ζ_2
1	1.1	4.0 ± 0.3	5.8 ± 0.7	2.2 ± 0.1	1.06 ± 0.02	254 ± 6	100	N/A	2.5	3.7	0.2	0.3
	1.1	4.2 ± 0.3	6.0 ± 0.6	2.2 ± 0.1	1.06 ± 0.04	254 ± 13	100	N/A	2.5	3.7	0.3	0.3
2	1.1	4.0 ± 0.3	5.8 ± 0.7	2.2 ± 0.1	1.06 ± 0.02	254 ± 6	100	N/A	2.5	3.6	0.3	0.4
	1.1	4.2 ± 0.3	6.0 ± 0.6	2.2 ± 0.1	1.06 ± 0.04	254 ± 13	100	N/A	2.4	3.7	0.3	0.3
3	1.4	5.3 ± 0.4	10 ± 1	2.2 ± 0.1	1.06 ± 0.02	254 ± 6	100	N/A	2.7	3.8	0.3	0.4
	1.4	5.4 ± 0.4	10 ± 1	2.2 ± 0.1	1.06 ± 0.04	254 ± 13	100	N/A	2.6	3.7	0.3	0.4

white - parameters for prototype BFB
grey - parameters for model BFB

ω - frequency of peak in BFB Bode plot
ζ - damping coefficient of peak in BFB Bode plot

Table A.2. Similitude tests for dp =0.4 mm and H = 15 cm prototype conditions

Exp. #	U/U_{mf}	Re_p	Fr	$\rho_s/\rho_g x10^{-3}$	H/D	D/d_p	% H	ε (avg.)	ω_{n1}	ω_{n2}	ζ_1	ζ_2
4a	1.1	4.1 ± 0.3	5.8 ± 0.7	2.2 ± 0.1	1.48 ± 0.02	254 ± 6	68	0.46 ± 0.03	2.4	-	0.3	-
	1.1	4.3 ± 0.3	6.1 ± 0.6	2.2 ± 0.1	1.48 ± 0.04	254 ± 13	68	0.47 ± 0.04	2.3	-	0.4	-
4b	1.1	4.1 ± 0.3	5.8 ± 0.7	2.2 ± 0.1	1.48 ± 0.02	254 ± 6	100	N/A	2.3	4.7	0.3	0.7
	1.1	4.3 ± 0.3	6.1 ± 0.6	2.2 ± 0.1	1.48 ± 0.04	254 ± 13	100	N/A	2.4	4.7	0.6	0.7
5a	1.4	5.3 ± 0.4	10 ± 1	2.2 ± 0.1	1.48 ± 0.02	254 ± 6	68	0.47 ± 0.03	2.5	3.5	0.2	0.3
	1.4	5.4 ± 0.4	10 ± 1	2.2 ± 0.1	1.48 ± 0.04	254 ± 13	68	0.50 ± 0.04	2.3	3.6	0.2	0.5
5b	1.4	5.3 ± 0.4	10 ± 1	2.2 ± 0.1	1.48 ± 0.02	254 ± 6	100	N/A	2.4	3.8	0.4	0.5
	1.4	5.4 ± 0.4	10 ± 1	2.2 ± 0.1	1.48 ± 0.04	254 ± 13	100	N/A	2.0	4.1	0.6	0.6
6a	1.8	6.7 ± 0.4	16 ± 1	2.2 ± 0.1	1.48 ± 0.02	254 ± 6	68	0.49 ± 0.03	2.5	-	0.2	-
	1.8	7.0 ± 0.4	15 ± 2	2.2 ± 0.1	1.48 ± 0.04	254 ± 13	68	0.50 ± 0.04	2.5	-	0.3	-
6b	1.8	6.7 ± 0.4	16 ± 1	2.2 ± 0.1	1.48 ± 0.02	254 ± 6	100	N/A	2.5	3.8	0.4	0.5
	1.8	7.0 ± 0.4	15 ± 2	2.2 ± 0.1	1.48 ± 0.04	254 ± 13	100	N/A	2.1	3.8	0.5	0.6

Table A.3. Similitude tests for dp =0.4 mm and H = 20 cm prototype conditions

Exp. #	U/U_{mf}	Re_p	Fr	$\rho_s/\rho_g x10^{-3}$	H/D	D/d_p	% H	ε (avg.)	ω_{n1}	ω_{n2}	ζ_1	ζ_2
7a	1.1	4.1 ± 0.3	5.8 ± 0.7	2.2 ± 0.1	1.97 ± 0.02	254 ± 6	25	0.44 ± 0.03	2.3	4.1	0.3	1.0
	1.1	4.3 ± 0.3	6.1 ± 0.6	2.2 ± 0.1	1.97 ± 0.04	254 ± 13	25	0.46 ± 0.04	2.5	4.1	0.3	0.9
7b	1.1	4.1 ± 0.3	5.8 ± 0.7	2.2 ± 0.1	1.97 ± 0.02	254 ± 6	50	0.46 ± 0.03	2.3	3.8	0.3	0.9
	1.1	4.3 ± 0.3	6.1 ± 0.6	2.2 ± 0.1	1.97 ± 0.04	254 ± 13	50	0.46 ± 0.04	2.5	4.4	0.4	0.9
8a	1.4	5.3 ± 0.4	10 ± 1	2.2 ± 0.1	1.97 ± 0.02	254 ± 6	25	0.45 ± 0.03	2.4	4.1	0.3	1.0
	1.4	5.4 ± 0.4	10 ± 1	2.2 ± 0.1	1.97 ± 0.04	254 ± 13	25	0.47 ± 0.04	2.4	4.1	0.2	1.0
8b	1.4	5.3 ± 0.4	10 ± 1	2.2 ± 0.1	1.97 ± 0.02	254 ± 6	50	0.48 ± 0.03	2.5	-	0.3	-
	1.4	5.4 ± 0.4	10 ± 1	2.2 ± 0.1	1.97 ± 0.04	254 ± 13	50	0.47 ± 0.04	2.3	-	0.4	-
9a	1.8	6.7 ± 0.4	16 ± 1	2.2 ± 0.1	1.97 ± 0.02	254 ± 6	25	0.46 ± 0.03	2.4	-	0.3	-
	1.8	7.0 ± 0.4	16 ± 1	2.2 ± 0.1	1.97 ± 0.04	254 ± 13	25	0.48 ± 0.04	2.4	-	0.3	-
9b	1.8	6.7 ± 0.4	16 ± 1	2.2 ± 0.1	1.97 ± 0.02	254 ± 6	50	0.50 ± 0.03	2.4	-	0.3	-
	1.8	7.0 ± 0.4	16 ± 1	2.2 ± 0.1	1.97 ± 0.04	254 ± 13	50	0.49 ± 0.04	2.4	-	0.4	-

Table A.4. Similitude tests for dp =0.3 mm and H = 10 cm prototype conditions

Exp. #	U/U_{mf}	Re_p	Fr	$\rho_s/\rho_g x10^{-3}$	H/D	D/d_p	% H	ε (avg.)	ω_{n1}	ω_{n2}	ζ_1	ζ_2
10	1.1	2.0 ± 0.2	3.3 ± 0.5	2.2 ± 0.1	1.06 ± 0.02	339 ± 11	100	N/A	2.6	3.8	0.2	0.3
	1.1	2.1 ± 0.2	3.3 ± 0.5	2.2 ± 0.1	1.06 ± 0.04	339 ± 22	100	N/A	2.8	4.1	0.5	0.3
11	1.4	2.6 ± 0.2	5.6 ± 0.7	2.2 ± 0.1	1.06 ± 0.02	339 ± 11	100	N/A	2.7	4.1	0.3	0.4
	1.4	2.6 ± 0.2	5.4 ± 0.7	2.2 ± 0.1	1.06 ± 0.04	339 ± 22	100	N/A	2.8	4.1	0.4	0.4
12	1.8	3.3 ± 0.2	9 ± 1	2.2 ± 0.1	1.06 ± 0.02	339 ± 11	100	N/A	2.2	3.1	0.5	0.3
	1.8	3.4 ± 0.3	9 ± 1	2.2 ± 0.1	1.06 ± 0.04	339 ± 22	100	N/A	1.9	3.5	0.5	0.6
13	2.2	4.0 ± 0.3	13 ± 1	2.2 ± 0.1	1.06 ± 0.02	339 ± 11	100	N/A	1.8	3.1	0.4	0.2
	2.2	4.1 ± 0.23	13 ± 1	2.2 ± 0.1	1.06 ± 0.04	339 ± 22	100	N/A	2.0	3.3	0.5	0.5

Table A.5. Similitude tests for dp =0.3 mm and H = 15 cm prototype conditions

Exp. #	U/U_{mf}	Re_p	Fr	$\rho_s/\rho_g x10^{-3}$	H/D	D/d_p	% H	ε (avg.)	ω_{n1}	ω_{n2}	ζ_1	ζ_2
14a	1.1	2.0 ± 0.2	3.3 ± 0.5	2.2 ± 0.1	1.48 ± 0.02	339 ± 11	68	0.45 ± 0.03	2.3	3.1	0.3	0.9
	1.1	2.1 ± 0.2	3.3 ± 0.5	2.2 ± 0.1	1.48 ± 0.04	339 ± 22	68	0.46 ± 0.04	2.3	3.8	0.4	0.8
14b	1.1	2.0 ± 0.2	3.3 ± 0.5	2.2 ± 0.1	1.48 ± 0.02	339 ± 11	100	N/A	2.4	4.1	0.3	0.8
	1.1	2.1 ± 0.2	3.3 ± 0.5	2.2 ± 0.1	1.48 ± 0.04	339 ± 22	100	N/A	2.6	4.1	0.4	0.4
15a	1.4	2.6 ± 0.2	5.6 ± 0.5	2.2 ± 0.1	1.48 ± 0.02	339 ± 11	68	0.46 ± 0.03	2.5	3.5	0.3	0.7
	1.4	2.6 ± 0.2	5.4 ± 0.5	2.2 ± 0.1	1.48 ± 0.04	339 ± 22	68	0.47 ± 0.04	2.5	3.8	0.4	0.6
15b	1.4	2.6 ± 0.2	5.6 ± 0.5	2.2 ± 0.1	1.48 ± 0.02	339 ± 11	100	N/A	2.5	4.1	0.4	0.7
	1.4	2.6 ± 0.2	5.4 ± 0.5	2.2 ± 0.1	1.48 ± 0.04	339 ± 22	100	N/A	2.7	4.1	0.5	0.3
16a	1.8	3.3 ± 0.2	9 ± 1	2.2 ± 0.1	1.48 ± 0.02	339 ± 11	68	0.47 ± 0.03	2.8	4.1	0.3	0.7
	1.8	3.4 ± 0.2	9 ± 1	2.2 ± 0.1	1.48 ± 0.04	339 ± 22	68	0.47 ± 0.04	2.8	3.8	0.5	0.6
16b	1.8	3.3 ± 0.2	9 ± 1	2.2 ± 0.1	1.48 ± 0.02	339 ± 11	100	N/A	2.5	4.0	0.6	0.6
	1.8	3.4 ± 0.2	9 ± 1	2.2 ± 0.1	1.48 ± 0.04	339 ± 22	100	N/A *(third peak)*	- *0.2*	4.1	- *1.2*	0.8
17a	2.2	4.0 ± 0.3	13 ± 1	2.2 ± 0.1	1.48 ± 0.02	339 ± 11	68	0.48 ± 0.03	2.8	4.1	0.2	0.7
	2.2	4.1 ± 0.3	13 ± 1	2.2 ± 0.1	1.48 ± 0.04	339 ± 22	68	0.49 ± 0.04 *(third peak)*	2.8 *1.3*	4.1	0.5 *0.8*	0.7
17b	2.2	4.0 ± 0.3	13 ± 1	2.2 ± 0.1	1.48 ± 0.02	339 ± 11	100	N/A *(third peak)*	2.8 *1.8*	4.1	0.4 *0.7*	0.7
	2.2	4.1 ± 0.3	13 ± 1	2.2 ± 0.1	1.48 ± 0.04	339 ± 22	100	N/A *(third peak)*	2.2 *1.1*	3.8	0.7 *0.9*	0.7

Table A.6. Similitude tests for dp =0.3 mm and H = 20 cm prototype conditions

Exp. #	U/U_{mf}	Re_p	Fr	$\rho_s/\rho_g x10^{-3}$	H/D	D/d_p	% H	ε (avg.)	ω_{n1}	ω_{n2}	ζ_1	ζ_2
18a	1.1	2.0 ± 0.2	3.3 ± 0.5	2.2 ± 0.1	1.97 ± 0.02	339 ± 11	25	0.44 ± 0.03	2.4	4.1	0.3	1.0
	1.1	2.1 ± 0.2	3.3 ± 0.5	2.2 ± 0.1	1.97 ± 0.04	339 ± 22	25	0.47 ± 0.04	2.4	4.1	0.3	1.0
18b	1.1	2.0 ± 0.2	3.3 ± 0.5	2.2 ± 0.1	1.97 ± 0.02	339 ± 11	50	0.45 ± 0.03	2.4	3.8	0.3	1.0
	1.1	2.1 ± 0.2	3.3 ± 0.5	2.2 ± 0.1	1.97 ± 0.04	339 ± 22	50	0.44 ± 0.04	2.4	4.1	0.7	1.1
19a	1.4	2.6 ± 0.2	5.6 ± 0.7	2.2 ± 0.1	1.97 ± 0.02	339 ± 11	25	0.45 ± 0.03	2.4	3.5	0.3	1.0
	1.4	2.6 ± 0.2	5.4 ± 0.7	2.2 ± 0.1	1.97 ± 0.04	339 ± 22	25	0.46 ± 0.04	2.5	3.5	0.3	1.0
19b	1.4	2.6 ± 0.2	5.6 ± 0.7	2.2 ± 0.1	1.97 ± 0.02	339 ± 11	50	0.47 ± 0.03	2.4	3.5	0.3	0.5
	1.4	2.6 ± 0.2	5.4 ± 0.7	2.2 ± 0.1	1.97 ± 0.04	339 ± 22	50	0.46 ± 0.04	2.4	3.5	0.5	0.6
20a	1.8	3.3 ± 0.2	9 ± 1	2.2 ± 0.1	1.97 ± 0.02	339 ± 11	25	0.46 ± 0.03	2.4	3.1	0.3	0.8
	1.8	3.4 ± 0.2	9 ± 1	2.2 ± 0.1	1.97 ± 0.04	339 ± 22	25	0.46 ± 0.04	2.5	3.1	0.3	0.8
20b	1.8	3.3 ± 0.2	9 ± 1	2.2 ± 0.1	1.97 ± 0.02	339 ± 11	50	0.49 ± 0.03	2.4	3.3	0.3	0.5
	1.8	3.4 ± 0.2	9 ± 1	2.2 ± 0.1	1.97 ± 0.04	339 ± 22	50	0.47 ± 0.04	2.4	3.5	0.5	0.6
21a	2.2	4.0 ± 0.3	13 ± 1	2.2 ± 0.1	1.97 ± 0.02	339 ± 11	25	0.46 ± 0.03	2.5	3.5	0.2	0.7
	2.2	4.1 ± 0.3	13 ± 1	2.2 ± 0.1	1.97 ± 0.04	339 ± 22	25	0.47 ± 0.04 *(third peak)*	2.5 *1.8*	3.1	0.2 *0.7*	0.3
21b	2.2	4.0 ± 0.3	13 ± 1	2.2 ± 0.1	1.97 ± 0.02	339 ± 11	50	0.51 ± 0.03	2.5	3.5	0.2	0.7
	2.2	4.1 ± 0.3	13 ± 1	2.2 ± 0.1	1.97 ± 0.04	339 ± 22	50	0.49 ± 0.04 *(third peak)*	2.5 *1.6*	3.1	0.5 *0.7*	0.6

Table A.8. Similitude tests for dp =0.2 mm and H = 20 cm prototype conditions

Exp. #	U/U_{mf}	Re_p	Fr	$\rho_s/\rho_g x10^{-3}$	H/D	D/d_p	% H	ε (avg.)	ω_{n1}	ω_{n2}	ζ_1	ζ_2
25a	1.1	0.6 ± 0.1	1.0 ± 0.3	2.2 ± 0.1	1.97 ± 0.02	508 ± 25	25	0.45± 0.03	2.2	-	0.6	-
	1.1	0.6 ± 0.1	1.0 ± 0.3	2.2 ± 0.1	1.97 ± 0.04	508 ± 50	25	0.45 ± 0.04	2.2	-	0.6	-
25b	1.1	0.6 ± 0.1	1.0 ± 0.3	2.2 ± 0.1	1.97 ± 0.02	508 ± 25	50	0.44± 0.03	2.2	-	0.8	-
	1.1	0.6 ± 0.1	1.0 ± 0.3	2.2 ± 0.1	1.97 ± 0.04	508 ± 50	50	0.43± 0.04	2.2	-	1.2	-
26a	1.4	0.7 ± 0.1	1.6 ± 0.4	2.2 ± 0.1	1.97 ± 0.02	508 ± 25	25	0.45± 0.03	2.3	-	0.4	-
	1.4	0.8 ± 0.1	1.6 ± 0.4	2.2 ± 0.1	1.97 ± 0.04	508 ± 50	25	0.47 ± 0.03	2.3	3.8	0.4	0.9
26b	1.4	0.7 ± 0.1	1.6 ± 0.4	2.2 ± 0.1	1.97 ± 0.02	508 ± 25	50	0.46± 0.03	2.3	-	0.4	-
	1.4	0.8 ± 0.1	1.6 ± 0.4	2.2 ± 0.1	1.97 ± 0.04	508 ± 50	50	0.45± 0.04	2.3	3.8	0.6	0.8
27a	1.8	0.6 ± 0.1	2.7 ± 0.5	2.2 ± 0.1	1.97 ± 0.02	508 ± 25	25	0.45± 0.03	2.4	-	0.5	-
	1.8	0.6 ± 0.1	2.6 ± 0.5	2.2 ± 0.1	1.97 ± 0.04	508 ± 50	25	0.48 ± 0.03	2.3	3.8	0.4	0.9
27b	1.8	0.6 ± 0.1	2.7 ± 0.5	2.2 ± 0.1	1.97 ± 0.02	508 ± 25	50	0.47± 0.03	2.5	-	0.5	-
	1.8	0.6 ± 0.1	2.6 ± 0.5	2.2 ± 0.1	1.97 ± 0.04	508 ± 50	50	0.45± 0.04	2.3	4.1	0.5	0.7

Table A.7. Similitude tests for dp =0.2 mm and H = 15 cm prototype conditions

Exp. #	U/U_{mf}	Re_p	Fr	$\rho_s/\rho_g x10^{-3}$	H/D	D/d_p	% H	ε (avg.)	ω_{n1}	ω_{n2}	ζ_1	ζ_2
22a	1.1	0.6 ± 0.1	1.0 ± 0.3	2.2 ± 0.1	1.48 ± 0.02	508 ± 25	68	0.46 ± 0.03	2.1	-	0.4	-
	1.1	0.6 ± 0.1	1.0 ± 0.3	2.2 ± 0.1	1.48 ± 0.04	508 ± 50	68	0.44 ± 0.04	2.0	3.5	0.7	0.7
22b	1.1	0.6 ± 0.1	1.0 ± 0.3	2.2 ± 0.1	1.48 ± 0.02	508 ± 25	100	N/A	2.2	3.1	0.4	0.8
	1.1	0.6 ± 0.1	1.0 ± 0.3	2.2 ± 0.1	1.48 ± 0.04	508 ± 50	100	N/A	2.2	3.5	1.0	0.5
23a	1.4	0.7 ± 0.1	1.6 ± 0.4	2.2 ± 0.1	1.48 ± 0.02	508 ± 25	68	0.47 ± 0.03	2.4	-	0.3	-
	1.4	0.8 ± 0.1	1.6 ± 0.4	2.2 ± 0.1	1.48 ± 0.04	508 ± 50	68	0.45 ± 0.04	2.4	3.5	0.5	0.7
23b	1.4	0.7 ± 0.1	1.6 ± 0.4	2.2 ± 0.1	1.48 ± 0.02	508 ± 25	100	N/A	2.4	3.5	0.3	0.5
	1.4	0.8 ± 0.1	1.6 ± 0.4	2.2 ± 0.1	1.48 ± 0.04	508 ± 50	100	N/A	2.7	4.3	0.5	0.3
24a	1.8	1.0 ± 0.1	2.7 ± 0.5	2.2 ± 0.1	1.48 ± 0.02	508 ± 25	68	0.47 ± 0.03	2.5	-	0.3	-
	1.8	1.0 ± 0.1	2.6 ± 0.5	2.2 ± 0.1	1.48 ± 0.04	508 ± 50	68	0.47 ± 0.03	2.4	4.4	0.7	0.8
24b	1.8	1.0 ± 0.1	2.7 ± 0.5	2.2 ± 0.1	1.48 ± 0.02	508 ± 25	100	N/A	2.4	5.0	0.4	0.8
	1.8	1.0 ± 0.1	2.6 ± 0.5	2.2 ± 0.1	1.48 ± 0.04	508 ± 50	100	N/A	2.6	4.4	0.6	0.4

APPENDIX B

TRANSITION REGIME BODE PLOTS

Experimental operating conditions			
Bed diameter	10.16 ± 0.01 cm	Bed height	10.0 ± 0.2 cm
Particle diameter	0.30 ± 0.01 mm	Pressure measurement	differential
Particle density	2600 ± 100 kg/m^3	Pressure tap position	Lower - 2.5 cm/Upper - 7.6 cm
Gas density (air)	1.20 ± 0.04 kg/m^3	Avg. voidage bwt. taps	0.50 ± 0.1
Superficial velocity	0.45 ± 0.05 m/s (U/U_{mf}=5.0)	Experiment number	12-29-1995-10.1

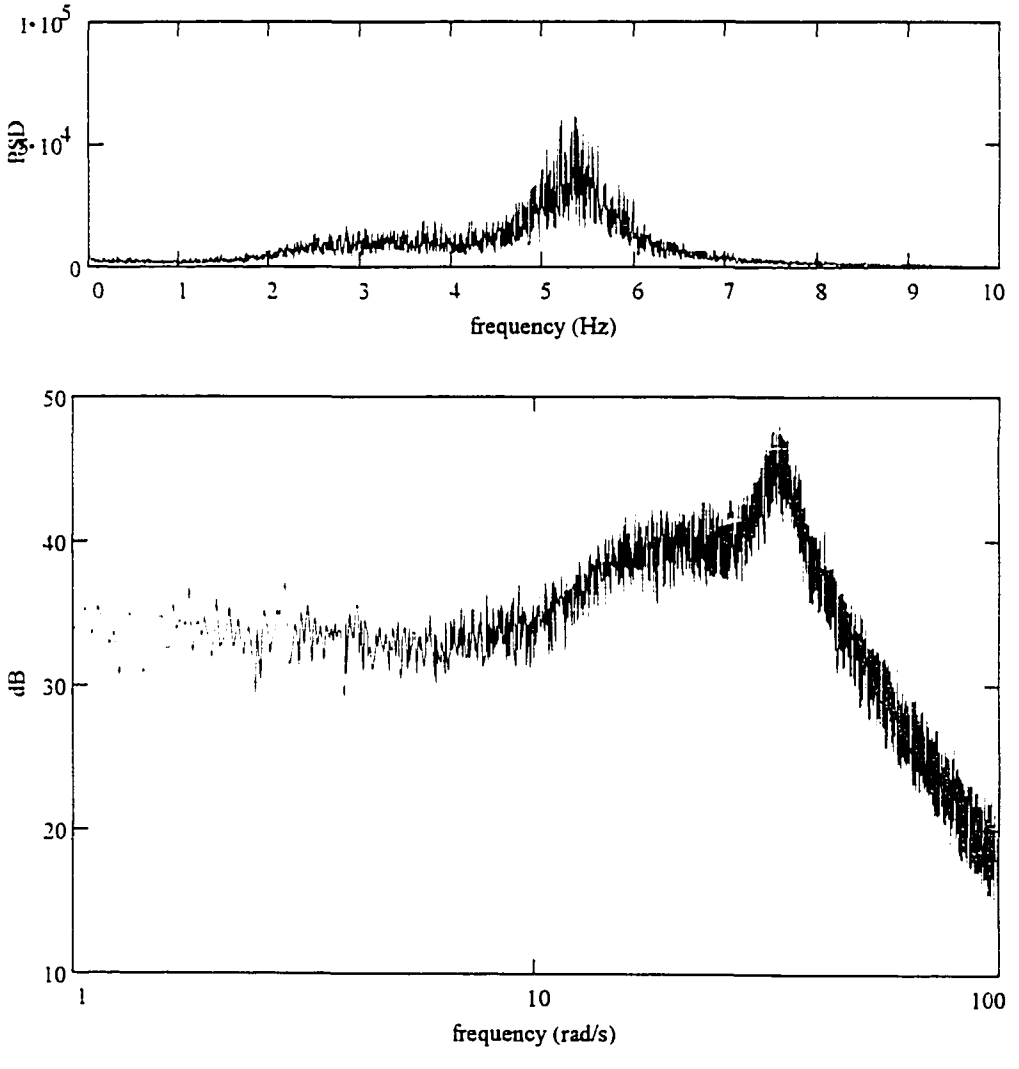

Figure B.1: PSD and Bode plot of bubbling/turbulent bed pressure fluctuations

Experimental operating conditions			
Bed diameter	10.16 ± 0.01 cm	Bed height	10.0 ± 0.2 cm
Particle diameter	0.30 ± 0.01 mm	Pressure measurement	absolute
Particle density	2600 ± 100 kg/m^3	Pressure tap position	22.8 cm
Gas density (air)	1.20 ± 0.04 kg/m^3	Avg. voidage bwt. taps	N/A
Superficial velocity	0.45 ± 0.05 m/s (U/U_{mf}=5.0)	Experiment number	12-29-1995-10.1

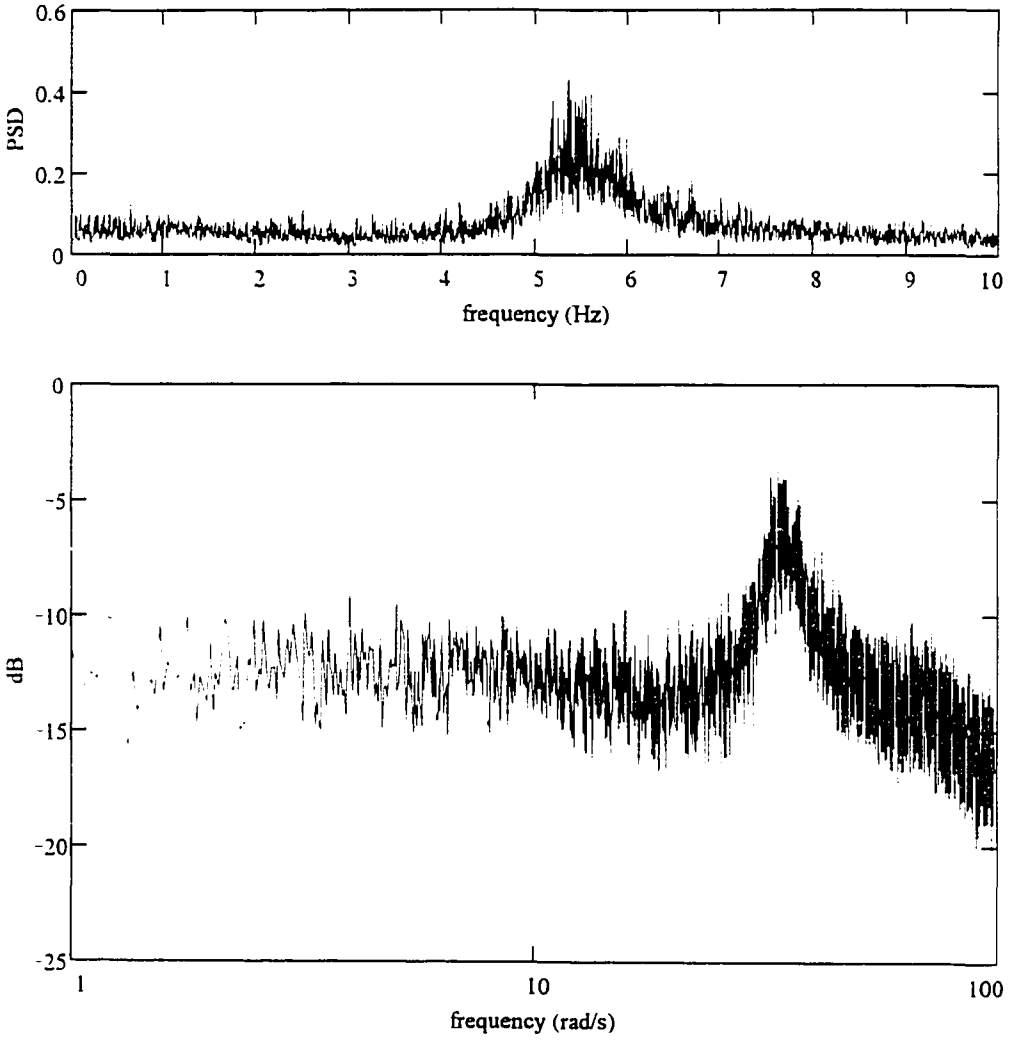

Figure B.2: PSD and Bode plot of bubbling/turbulent bed pressure fluctuations

Experimental operating conditions			
Bed diameter	10.16 ± 0.01 cm	Bed height	10.0 ± 0.2 cm
Particle diameter	0.30 ± 0.01 mm	Pressure measurement	differential
Particle density	2600 ± 100 kg/m^3	Pressure tap position	Lower - 2.5 cm/Upper - 7.6 cm
Gas density (air)	1.20 ± 0.04 kg/m^3	Avg. voidage bwt. taps	0.52 ± 0.1
Superficial velocity	0.63 ± 0.05 m/s (U/U_{mf}=7.0)	Experiment number	12-29-1995-10.8

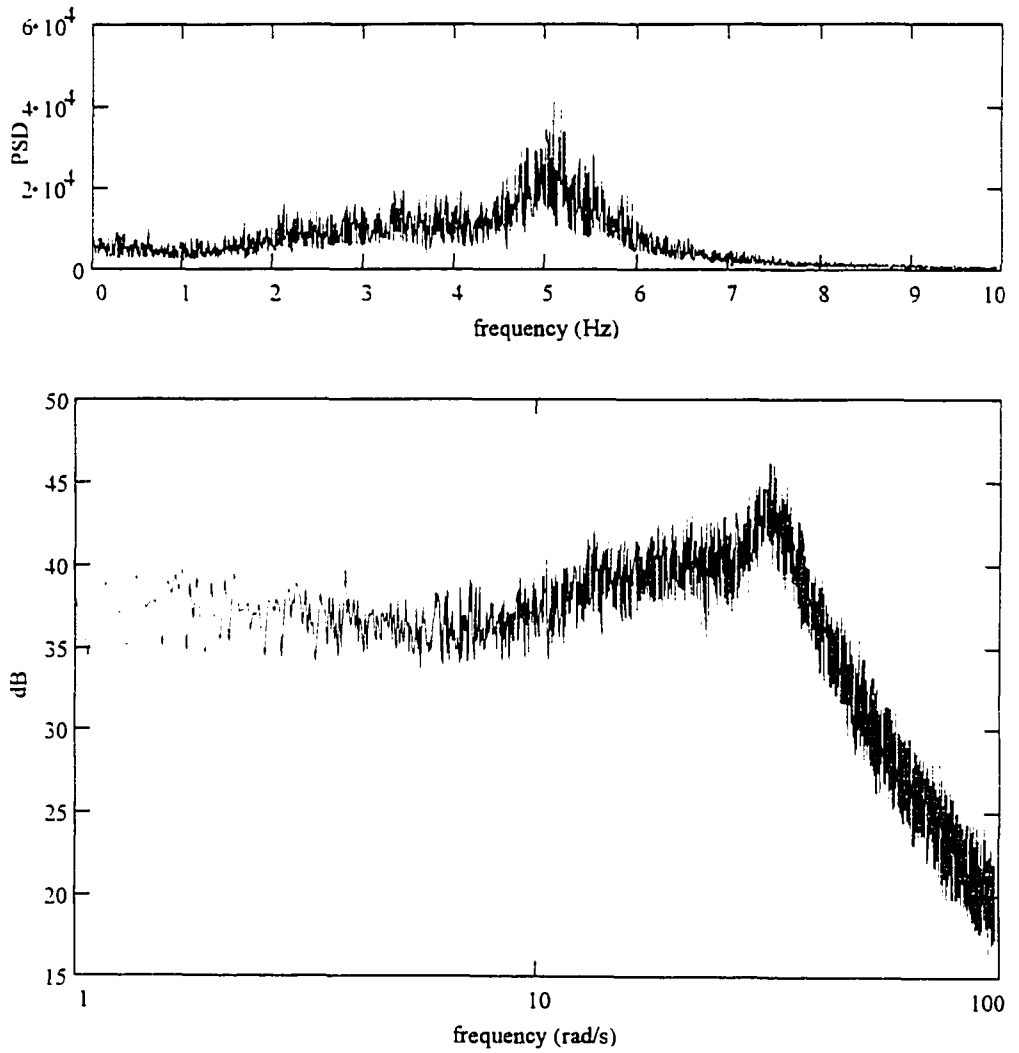

Figure B.3: PSD and Bode plot of bubbling/turbulent bed pressure fluctuations

Experimental operating conditions			
Bed diameter	10.16 ± 0.01 cm	Bed height	10.0 ± 0.2 cm
Particle diameter	0.30 ± 0.01 mm	Pressure measurement	absolute
Particle density	2600 ± 100 kg/m^3	Pressure tap position	22.8 cm
Gas density (air)	1.20 ± 0.04 kg/m^3	Avg. voidage bwt. taps	N/A
Superficial velocity	0.63 ± 0.05 m/s (U/U_{mf}≈7.0)	Experiment number	12-29-1995-10.8

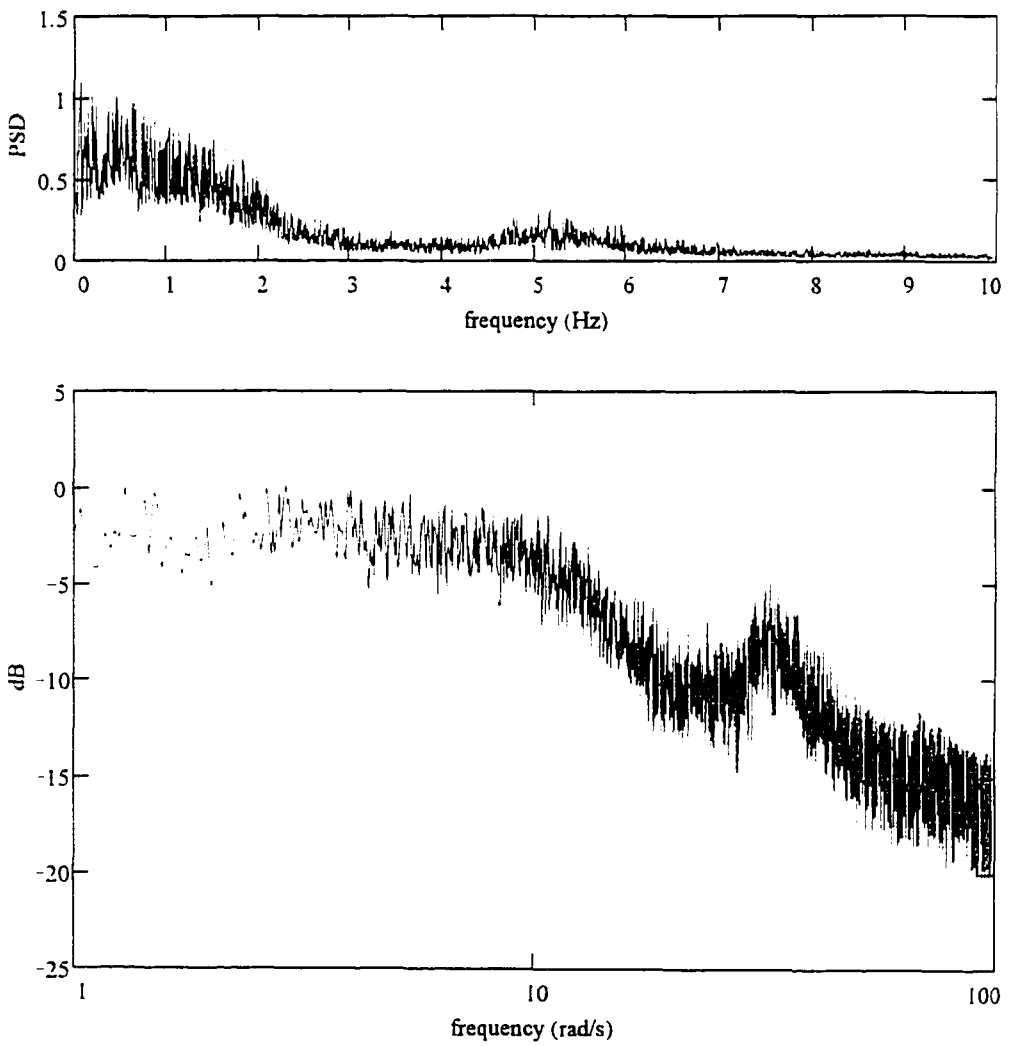

Figure B.4: PSD and Bode plot of bubbling/turbulent bed pressure fluctuations

Experimental operating conditions			
Bed diameter	10.16 ± 0.01 cm	Bed height	10.0 ± 0.2 cm
Particle diameter	0.30 ± 0.01 mm	Pressure measurement	differential
Particle density	2600 ± 100 kg/m^3	Pressure tap position	Lower - 2.5 cm/Upper - 7.6 cm
Gas density (air)	1.20 ± 0.04 kg/m^3	Avg. voidage bwt. taps	0.54 ± 0.1
Superficial velocity	0.81 ± 0.05 m/s (U/U_{mf}=9.0)	Experiment number	12-29-1995-11.4

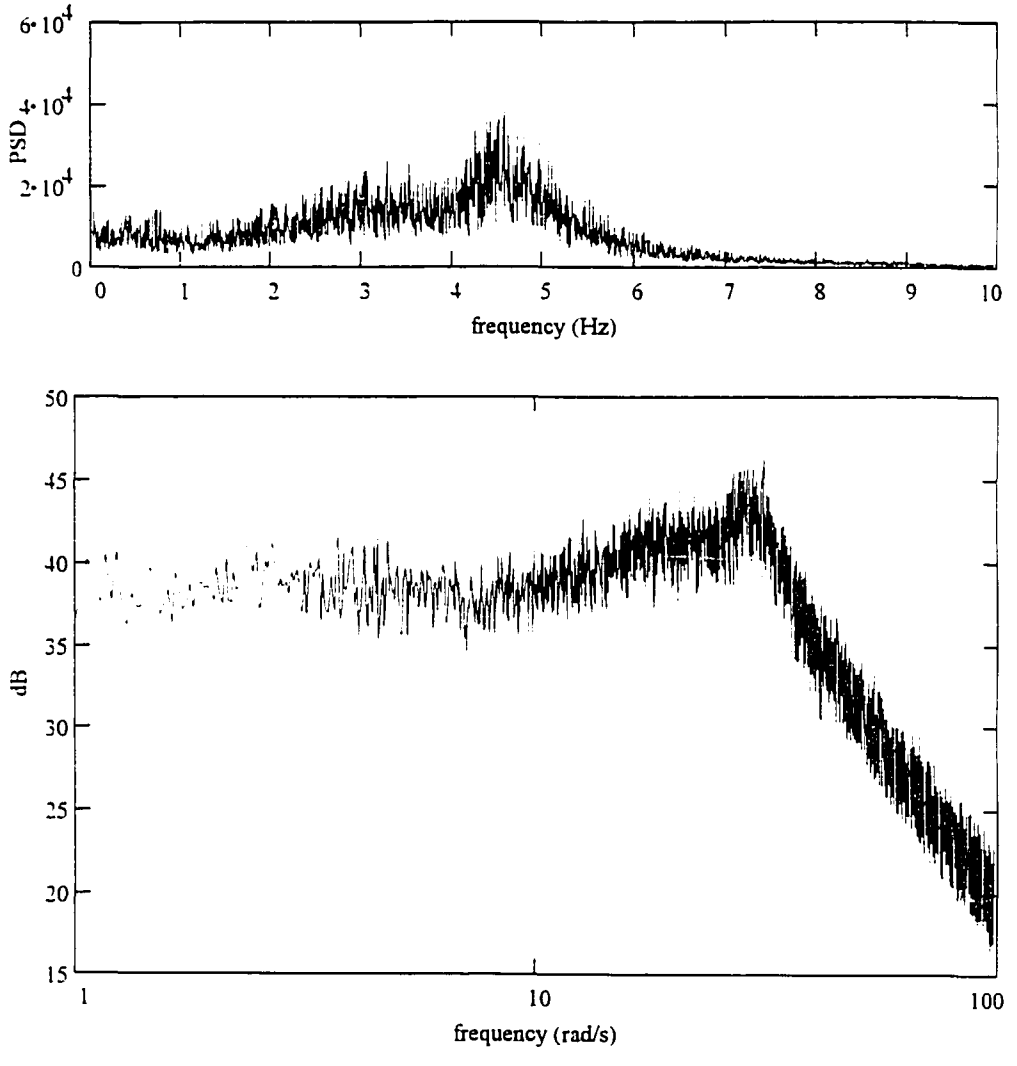

Figure B.5: PSD and Bode plot of bubbling/turbulent bed pressure fluctuations

Experimental operating conditions			
Bed diameter	10.16 ± 0.01 cm	Bed height	10.0 ± 0.2 cm
Particle diameter	0.30 ± 0.01 mm	Pressure measurement	absolute
Particle density	2600 ± 100 kg/m^3	Pressure tap position	22.8 cm
Gas density (air)	1.20 ± 0.04 kg/m^3	Avg. voidage bwt. taps	N/A
Superficial velocity	0.81 ± 0.05 m/s (U/U_{mf}=9.0)	Experiment number	12-29-1995-11.4

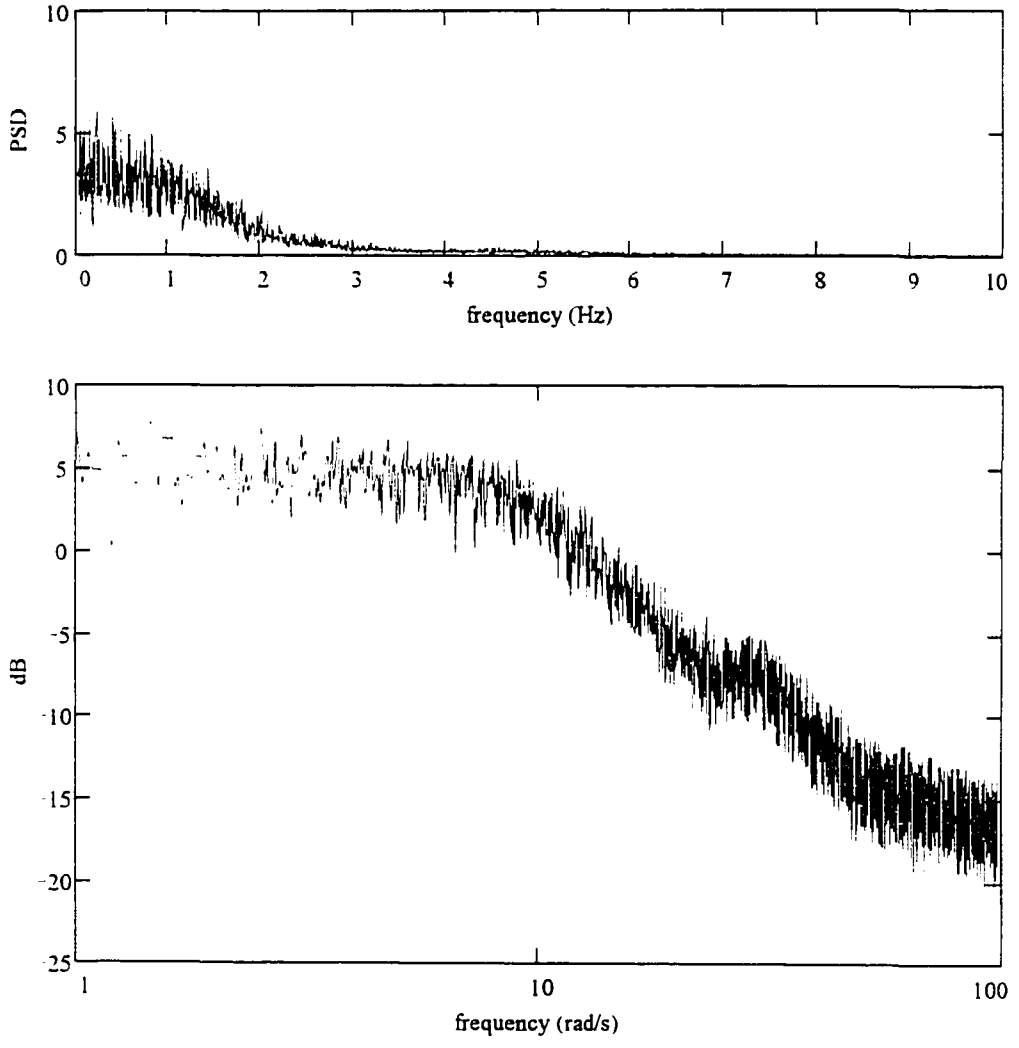

Figure B.6: PSD and Bode plot of bubbling/turbulent bed pressure fluctuations

Experimental operating conditions			
Bed diameter	10.16 ± 0.01 cm	Bed height	10.0 ± 0.2 cm
Particle diameter	0.30 ± 0.01 mm	Pressure measurement	differential
Particle density	2600 ± 100 kg/m^3	Pressure tap position	Lower - 2.5 cm/Upper - 7.6 cm
Gas density (air)	1.20 ± 0.04 kg/m^3	Avg. voidage bwt. taps	0.56 ± 0.1
Superficial velocity	0.99 ± 0.05 m/s (U/U_{mf}=11.0)	Experiment number	12-29-1995-12

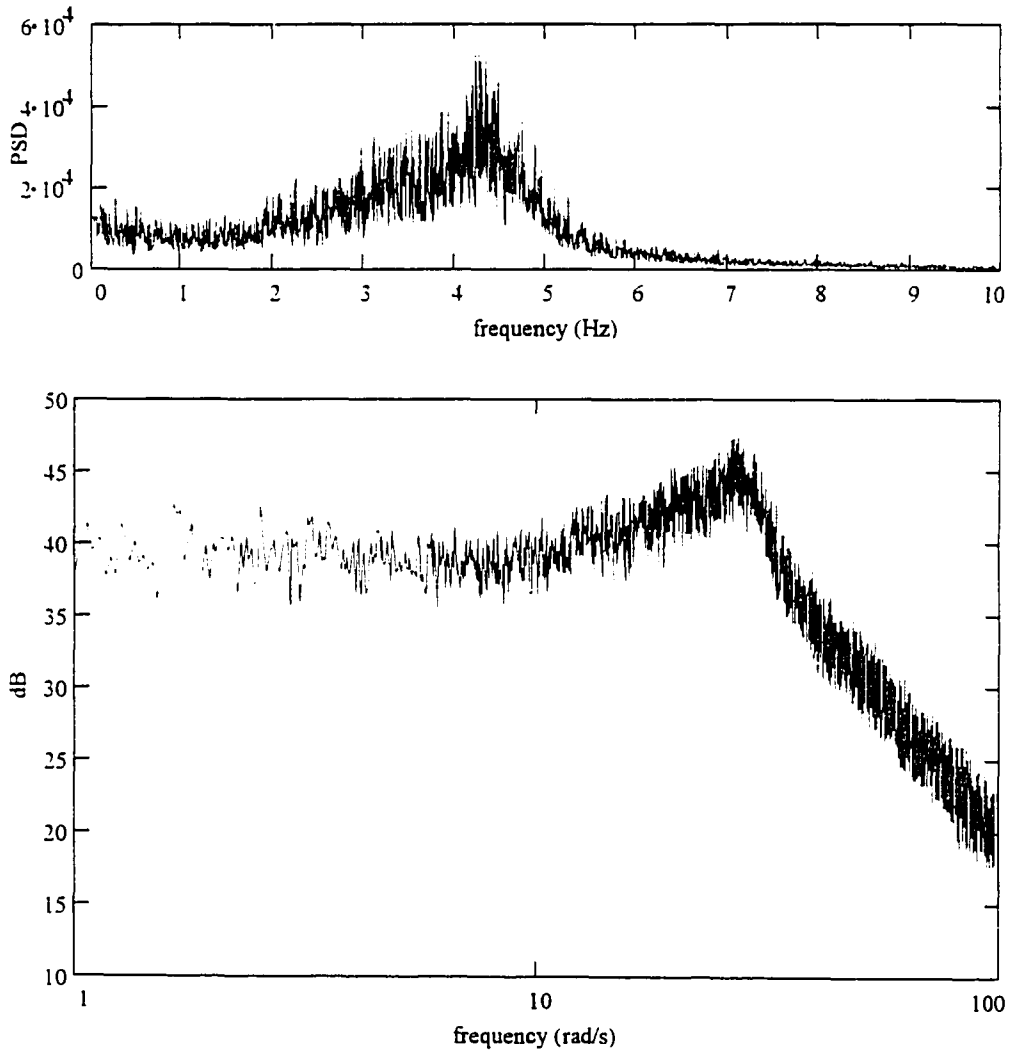

Figure B.7: PSD and Bode plot of bubbling/turbulent bed pressure fluctuations

Experimental operating conditions			
Bed diameter	10.16 ± 0.01 cm	Bed height	10.0 ± 0.2 cm
Particle diameter	0.30 ± 0.01 mm	Pressure measurement	absolute
Particle density	2600 ± 100 kg/m^3	Pressure tap position	22.8 cm
Gas density (air)	1.20 ± 0.04 kg/m^3	Avg. voidage bwt. taps	N/A
Superficial velocity	0.99 ± 0.05 m/s (U/U_{mf}=11.0)	Experiment number	12-29-1995-12

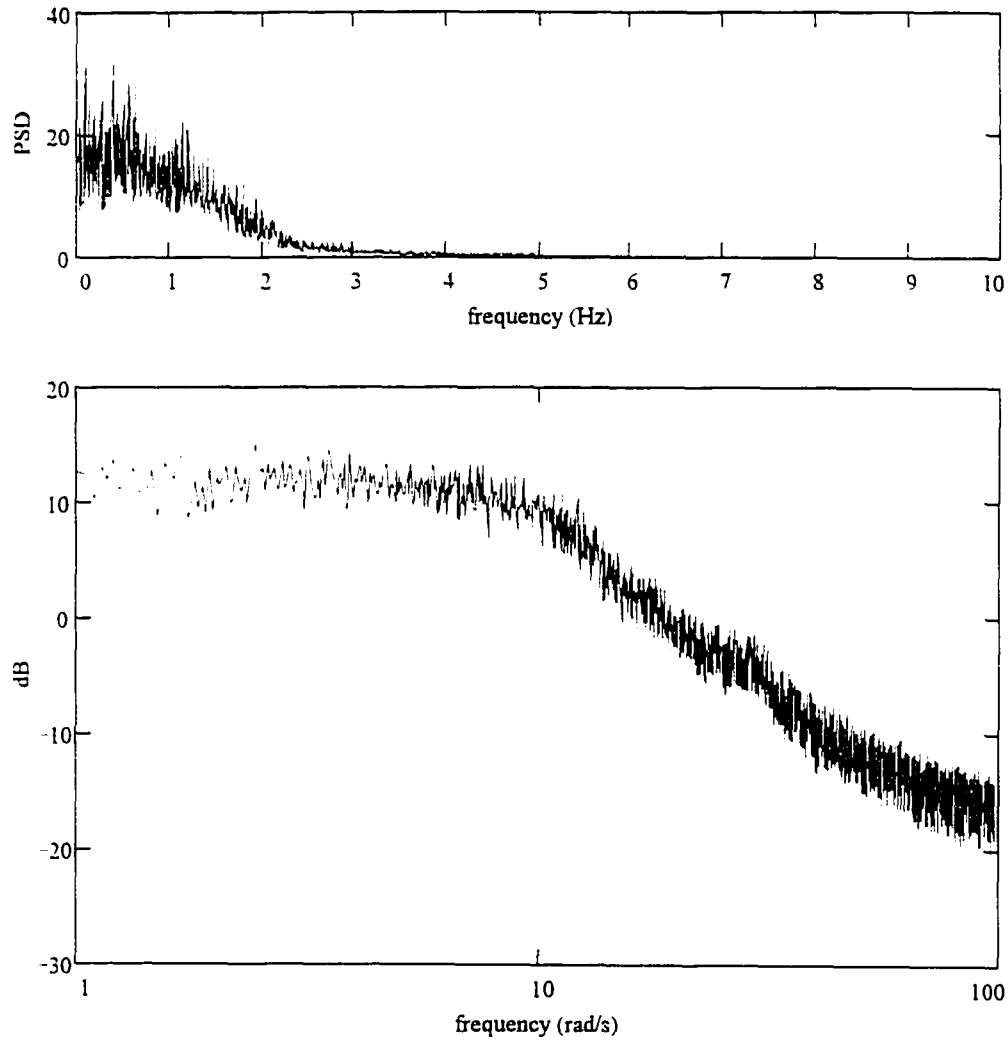

Figure B.8: PSD and Bode plot of bubbling/turbulent bed pressure fluctuations

Experimental operating conditions			
Bed diameter	10.16 ± 0.01 cm	Bed height	10.0 ± 0.2 cm
Particle diameter	0.30 ± 0.01 mm	Pressure measurement	differential
Particle density	2600 ± 100 kg/m^3	Pressure tap position	Lower - 2.5 cm/Upper - 7.6 cm
Gas density (air)	1.20 ± 0.04 kg/m^3	Avg. voidage bwt. taps	0.57 ± 0.1
Superficial velocity	1.17 ± 0.05 m/s (U/U_{mf}=13.0)	Experiment number	12-29-1995-12.6

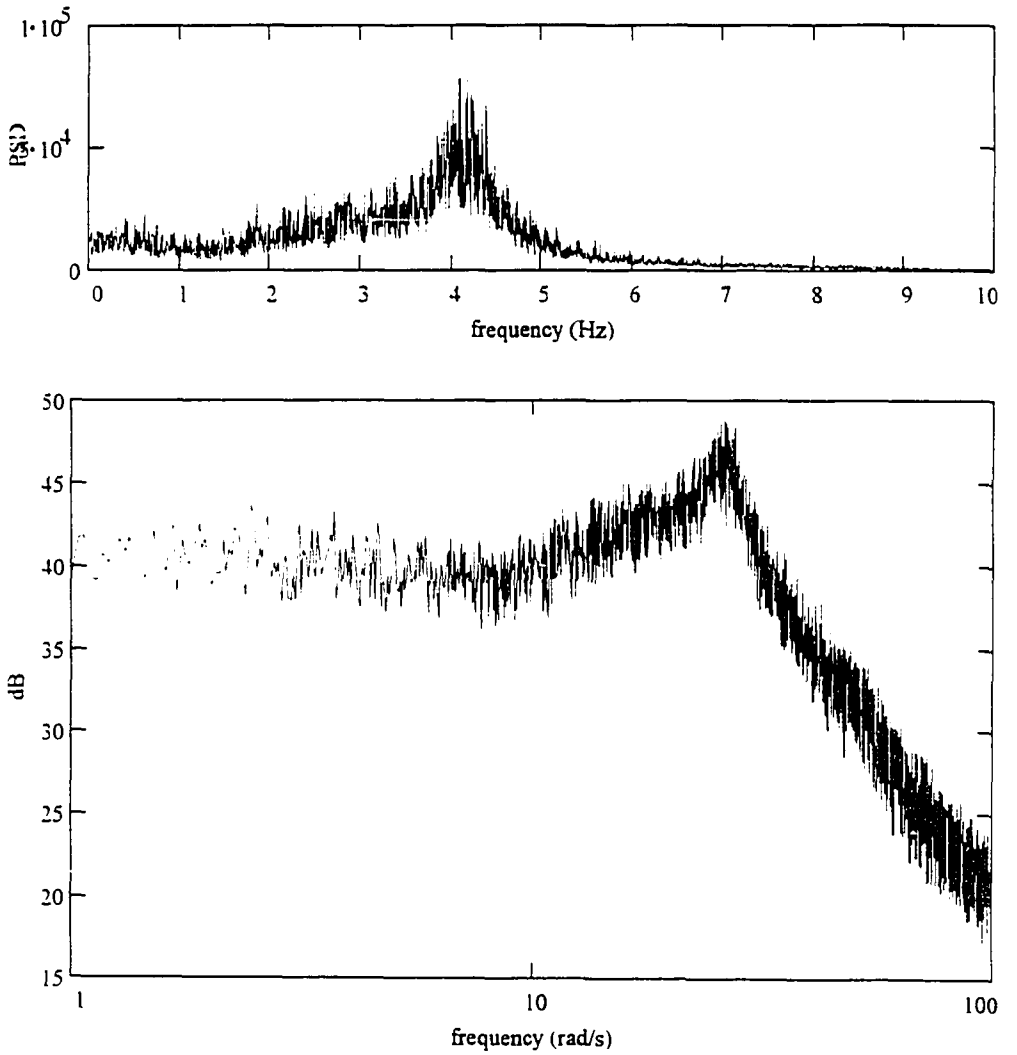

Figure B.9: PSD and Bode plot of bubbling/turbulent bed pressure fluctuations

Experimental operating conditions			
Bed diameter	10.16 ± 0.01 cm	Bed height	10.0 ± 0.2 cm
Particle diameter	0.30 ± 0.01 mm	Pressure measurement	absolute
Particle density	2600 ± 100 kg/m^3	Pressure tap position	22.8 cm
Gas density (air)	1.20 ± 0.04 kg/m^3	Avg. voidage bwt. taps	N/A
Superficial velocity	1.17 ± 0.05 m/s (U/U_{mf}=13.0)	Experiment number	12-29-1995-12.6

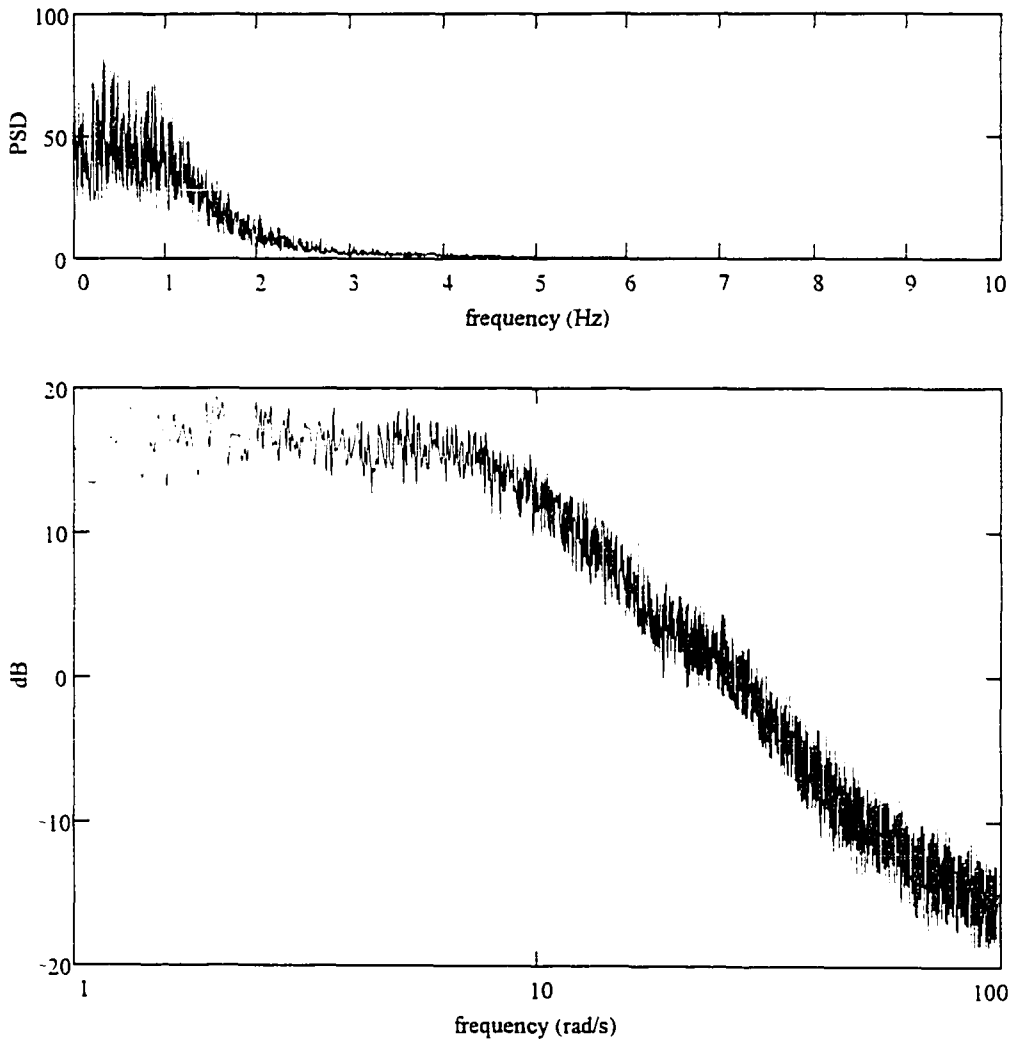

Figure B.10: PSD and Bode plot of bubbling/turbulent bed pressure fluctuations

Experimental operating conditions			
Bed diameter	10.16 ± 0.01 cm	Bed height	10.0 ± 0.2 cm
Particle diameter	0.30 ± 0.01 mm	Pressure measurement	differential
Particle density	2600 ± 100 kg/m^3	Pressure tap position	Lower - 2.5 cm/Upper - 7.6 cm
Gas density (air)	1.20 ± 0.04 kg/m^3	Avg. voidage bwt. taps	0.59 ± 0.1
Superficial velocity	1.35 ± 0.05 m/s (U/U_{mf}=15.0)	Experiment number	12-29-1995-13.1

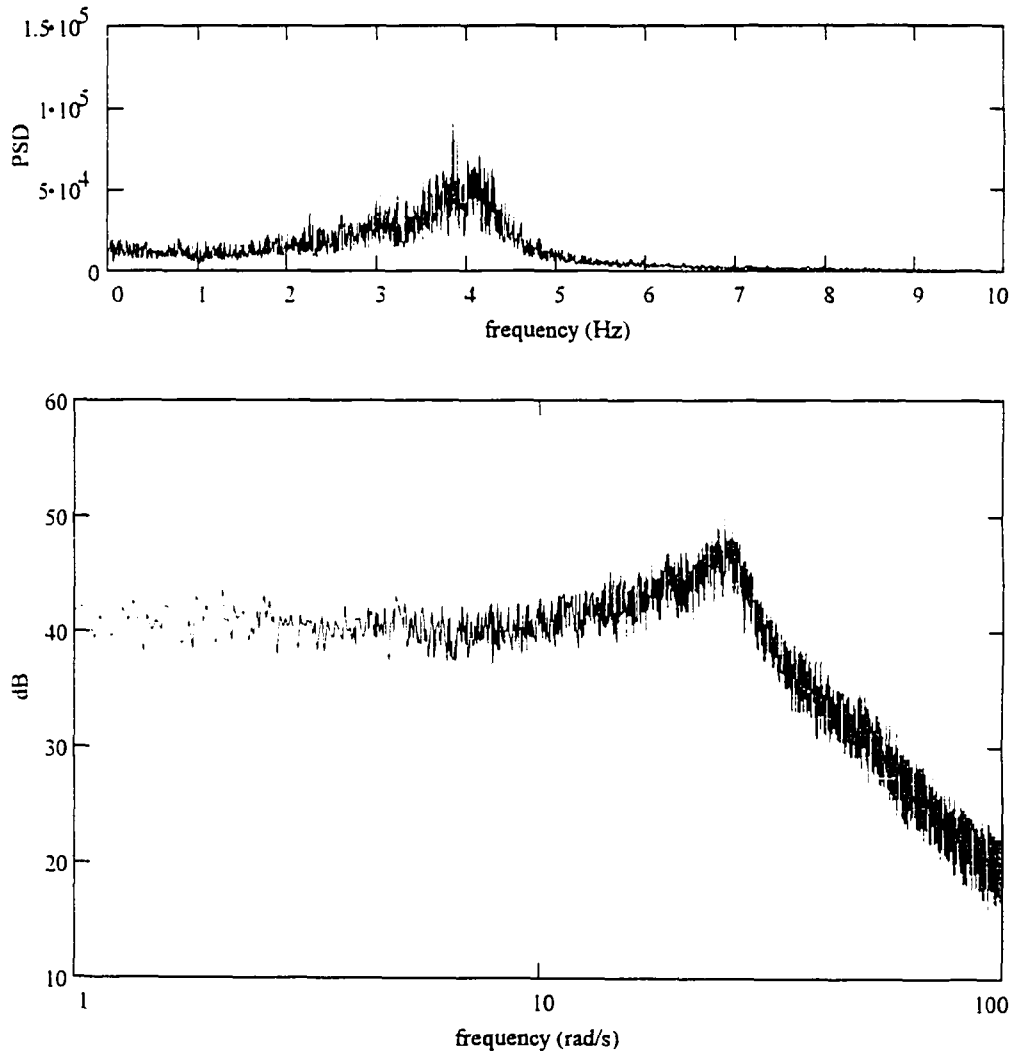

Figure B.11: PSD and Bode plot of bubbling/turbulent bed pressure fluctuations

Experimental operating conditions			
Bed diameter	10.16 ± 0.01 cm	Bed height	10.0 ± 0.2 cm
Particle diameter	0.30 ± 0.01 mm	Pressure measurement	absolute
Particle density	2600 ± 100 kg/m^3	Pressure tap position	22.8 cm
Gas density (air)	1.20 ± 0.04 kg/m^3	Avg. voidage bwt. taps	N/A
Superficial velocity	1.35 ± 0.05 m/s (U/U_{mf}=15.0)	Experiment number	12-29-1995-13.1

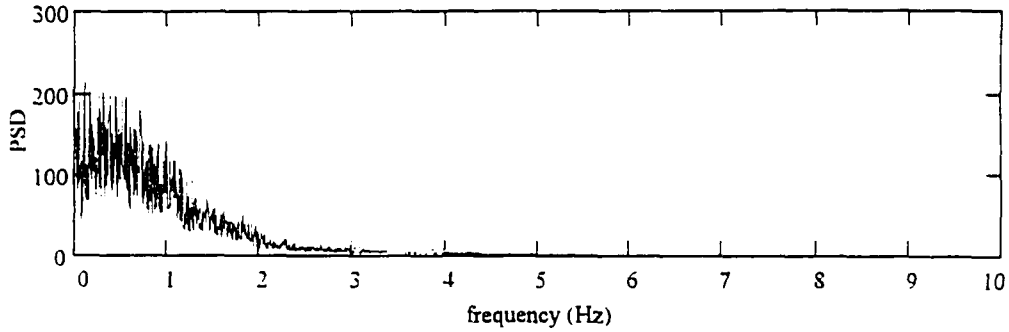

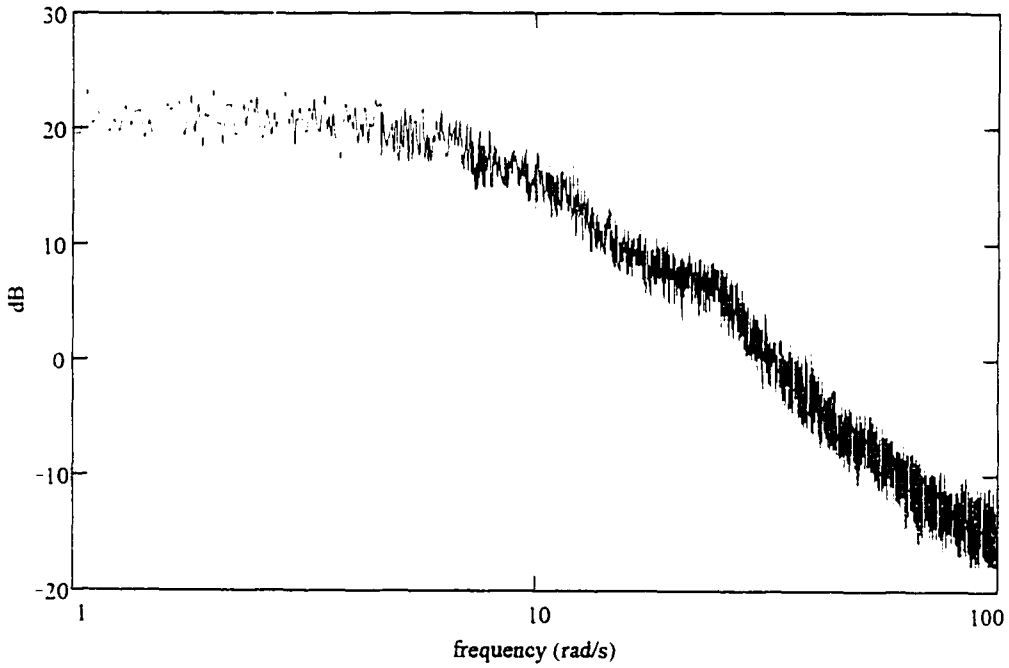

Figure B.12: PSD and Bode plot of bubbling/turbulent bed pressure fluctuations

Experimental operating conditions			
Bed diameter	10.16 ± 0.01 cm	Bed height	10.0 ± 0.2 cm
Particle diameter	0.30 ± 0.01 mm	Pressure measurement	differential
Particle density	2600 ± 100 kg/m^3	Pressure tap position	Lower - 2.5 cm/Upper - 7.6 cm
Gas density (air)	1.20 ± 0.04 kg/m^3	Avg. voidage bwt. taps	0.60 ± 0.1
Superficial velocity	1.53 ± 0.05 m/s (U/U_{mf}=17.0)	Experiment number	12-29-1995-13.8

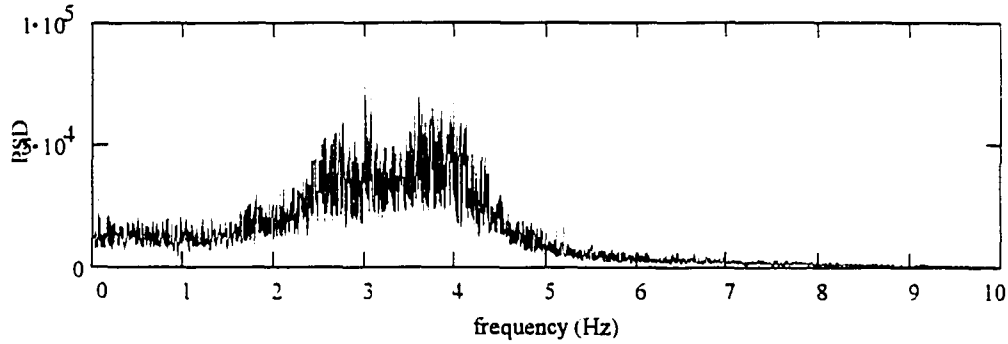

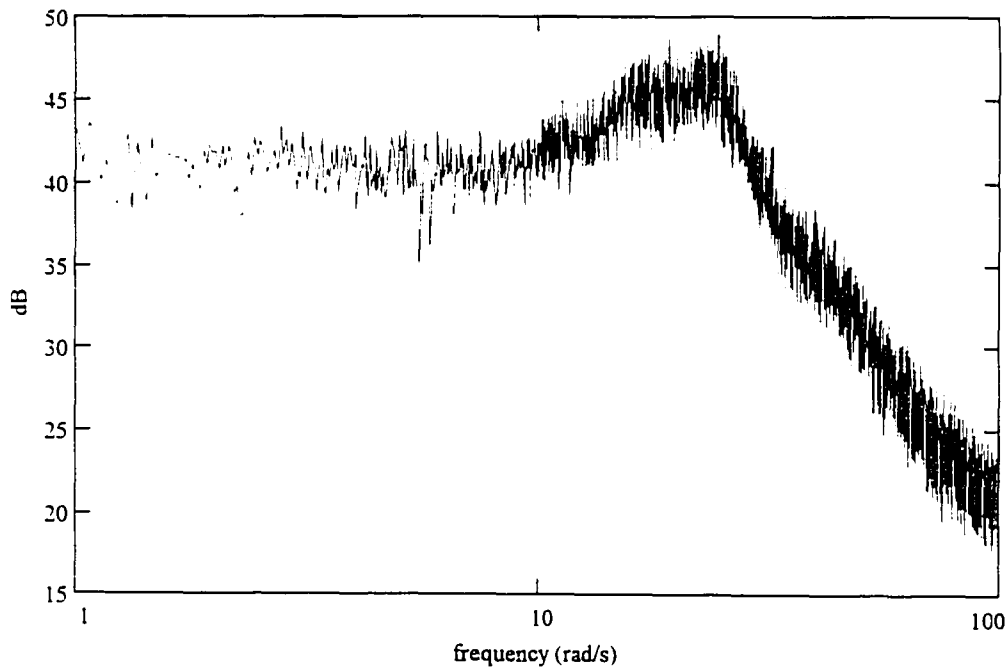

Figure B.13: PSD and Bode plot of bubbling/turbulent bed pressure fluctuations

Experimental operating conditions			
Bed diameter	10.16 ± 0.01 cm	Bed height	10.0 ± 0.2 cm
Particle diameter	0.30 ± 0.01 mm	Pressure measurement	absolute
Particle density	2600 ± 100 kg/m^3	Pressure tap position	22.8 cm
Gas density (air)	1.20 ± 0.04 kg/m^3	Avg. voidage bwt. taps	N/A
Superficial velocity	1.53 ± 0.05 m/s (U/U_{mf}=17.0)	Experiment number	12-29-1995-13.8

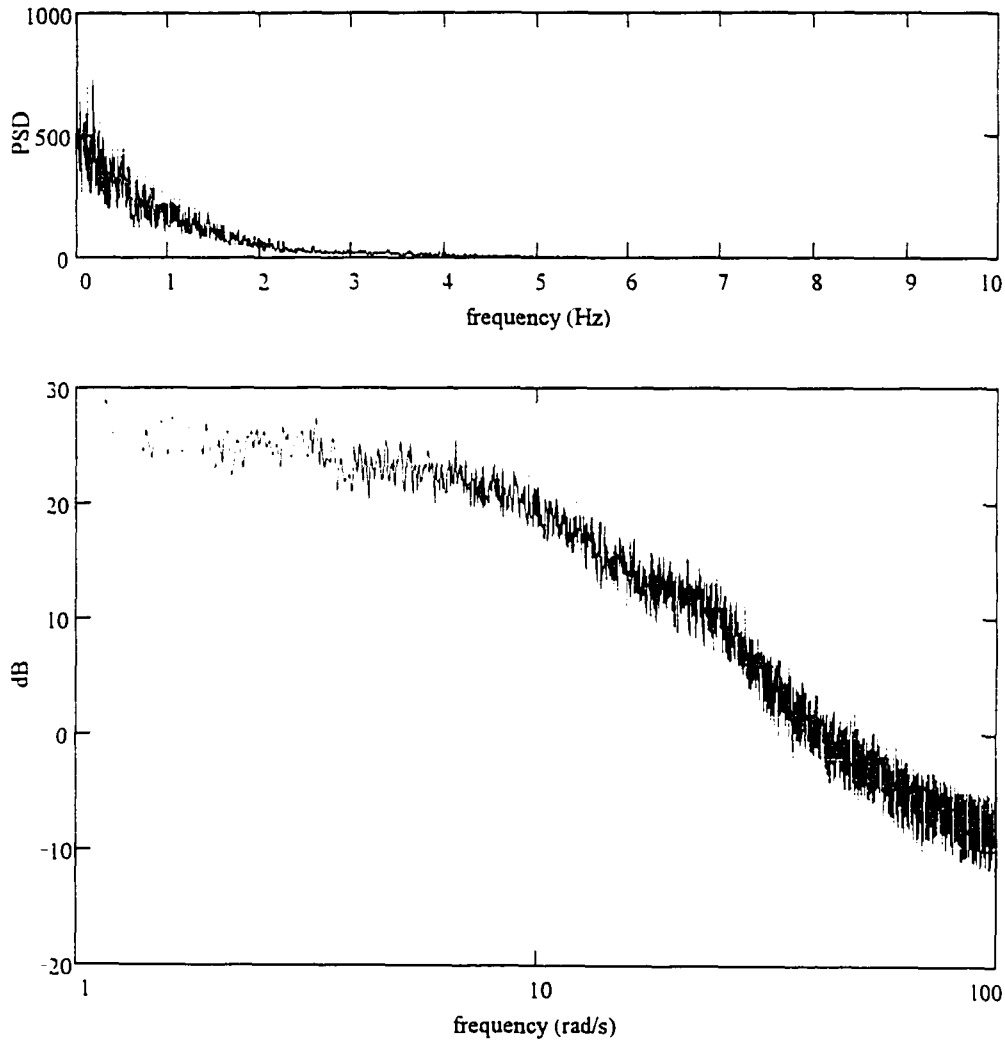

Figure B.14: PSD and Bode plot of bubbling/turbulent bed pressure fluctuations

Experimental operating conditions			
Bed diameter	10.16 ± 0.01 cm	Bed height	10.0 ± 0.2 cm
Particle diameter	0.30 ± 0.01 mm	Pressure measurement	differential
Particle density	2600 ± 100 kg/m^3	Pressure tap position	Lower - 2.5 cm/Upper - 7.6 cm
Gas density (air)	1.20 ± 0.04 kg/m^3	Avg. voidage bwt. taps	0.62 ± 0.1
Superficial velocity	1.71 ± 0.05 m/s (U/U_{mf}=19.0)	Experiment number	12-29-1995-14.4

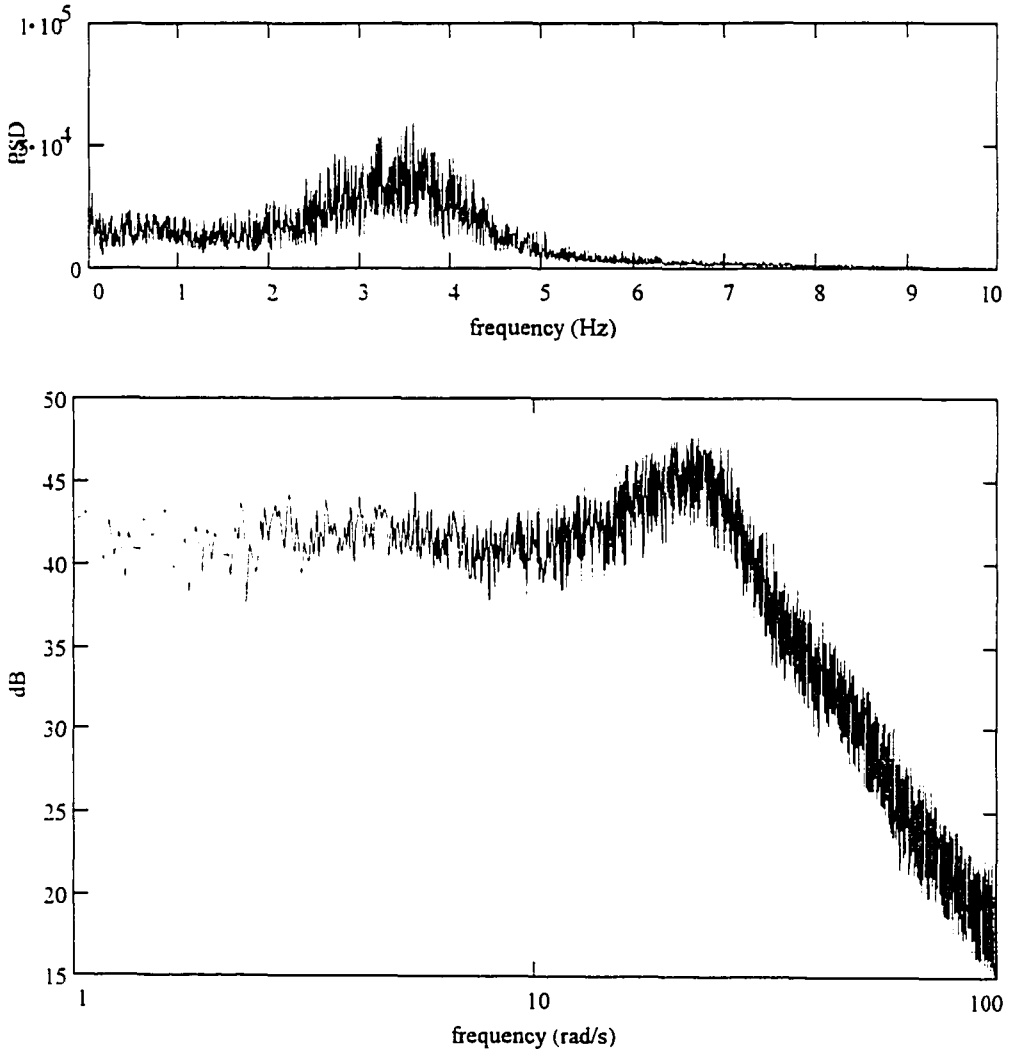

Figure B.15: PSD and Bode plot of bubbling/turbulent bed pressure fluctuations

Experimental operating conditions			
Bed diameter	10.16 ± 0.01 cm	Bed height	10.0 ± 0.2 cm
Particle diameter	0.30 ± 0.01 mm	Pressure measurement	absolute
Particle density	2600 ± 100 kg/m^3	Pressure tap position	22.8 cm
Gas density (air)	1.20 ± 0.04 kg/m^3	Avg. voidage bwt. taps	N/A
Superficial velocity	1.71 ± 0.05 m/s (U/U_{mf}=19.0)	Experiment number	12-29-1995-14.4

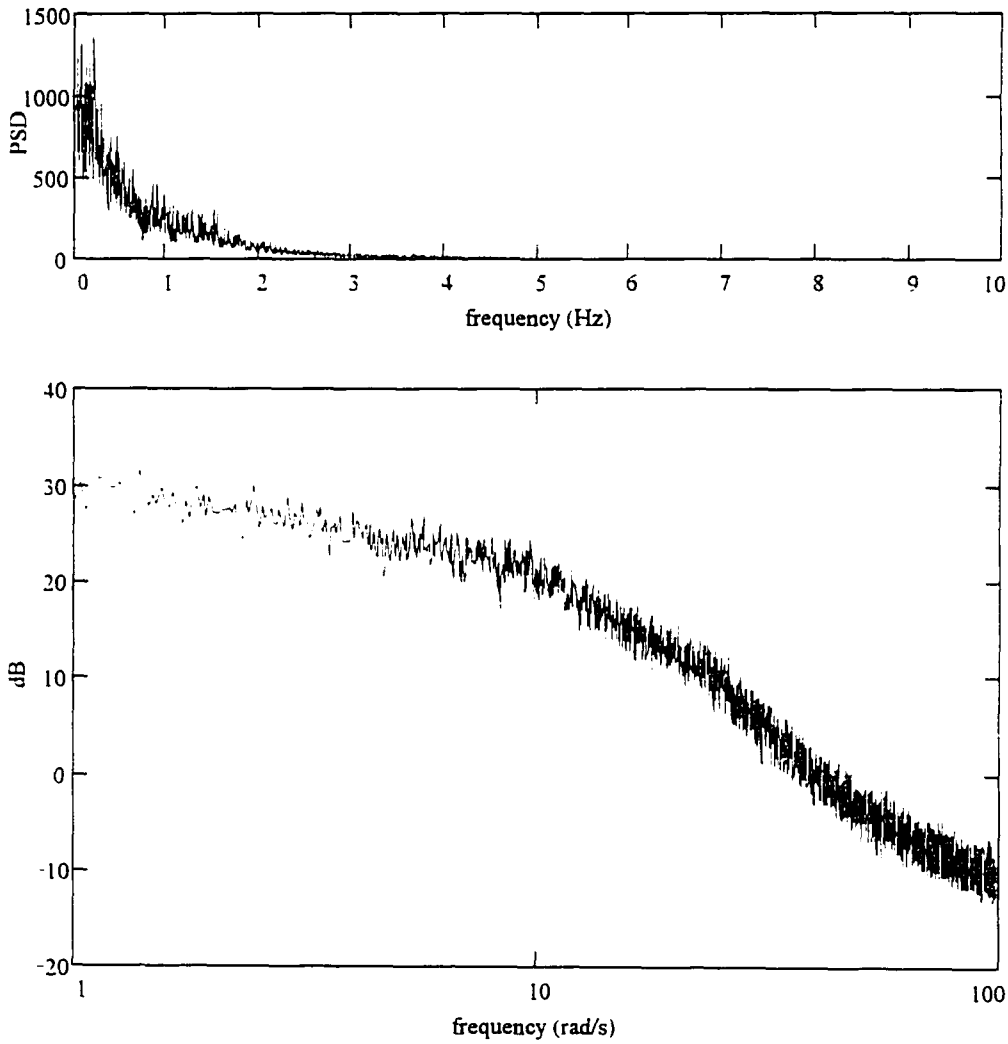

Figure B.16: PSD and Bode plot of bubbling/turbulent bed pressure fluctuations

Experimental operating conditions			
Bed diameter	10.16 ± 0.01 cm	Bed height	10.0 ± 0.2 cm
Particle diameter	0.30 ± 0.01 mm	Pressure measurement	differential
Particle density	2600 ± 100 kg/m^3	Pressure tap position	Lower - 2.5 cm/Upper - 7.6 cm
Gas density (air)	1.20 ± 0.04 kg/m^3	Avg. voidage bwt. taps	0.62 ± 0.1
Superficial velocity	1.89 ± 0.05 m/s (U/U_{mf}=21.0)	Experiment number	12-29-1995-14.9

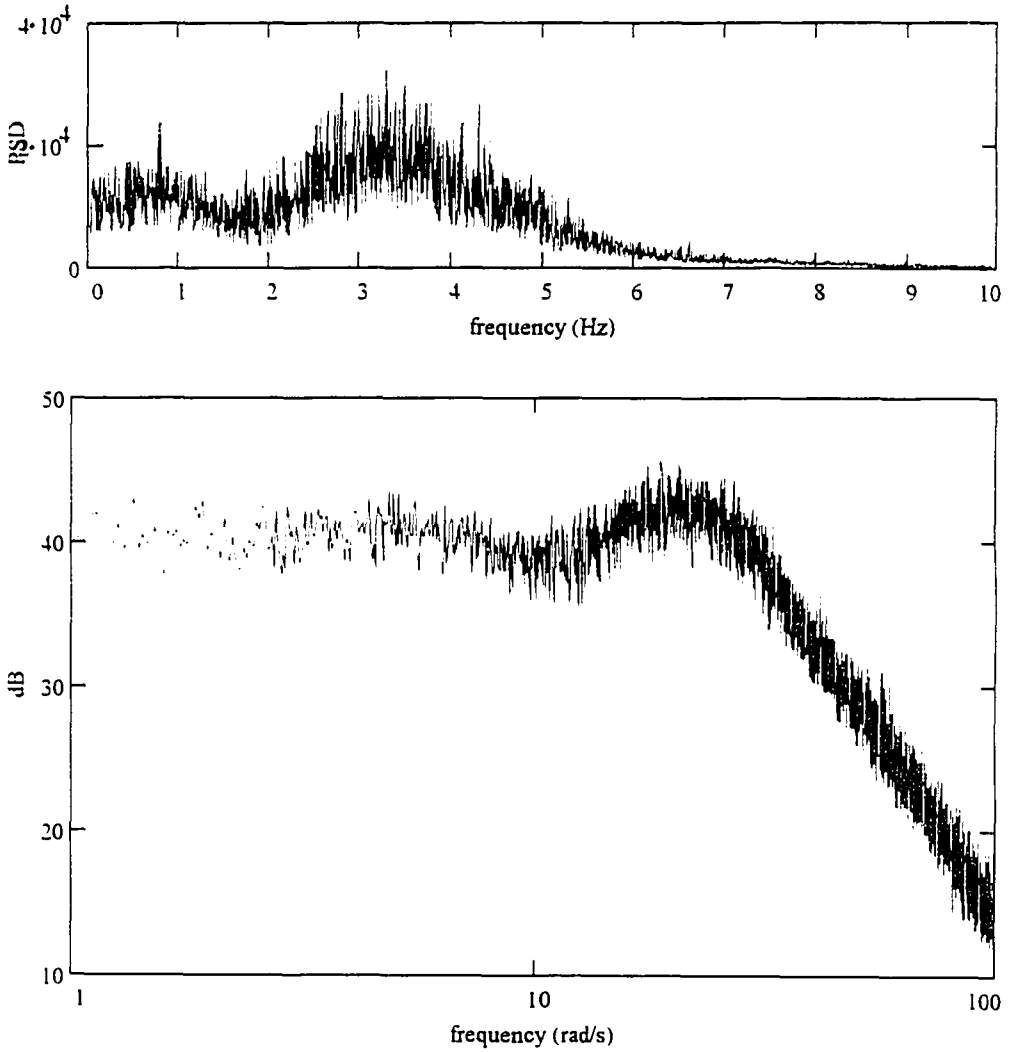

Figure B.17: PSD and Bode plot of bubbling/turbulent bed pressure fluctuations

Experimental operating conditions			
Bed diameter	10.16 ± 0.01 cm	Bed height	10.0 ± 0.2 cm
Particle diameter	0.30 ± 0.01 mm	Pressure measurement	absolute
Particle density	2600 ± 100 kg/m^3	Pressure tap position	22.8 cm
Gas density (air)	1.20 ± 0.04 kg/m^3	Avg. voidage bwt. taps	N/A
Superficial velocity	1.89 ± 0.05 m/s (U/U_{mf}=21.0)	Experiment number	12-29-1995-14.9

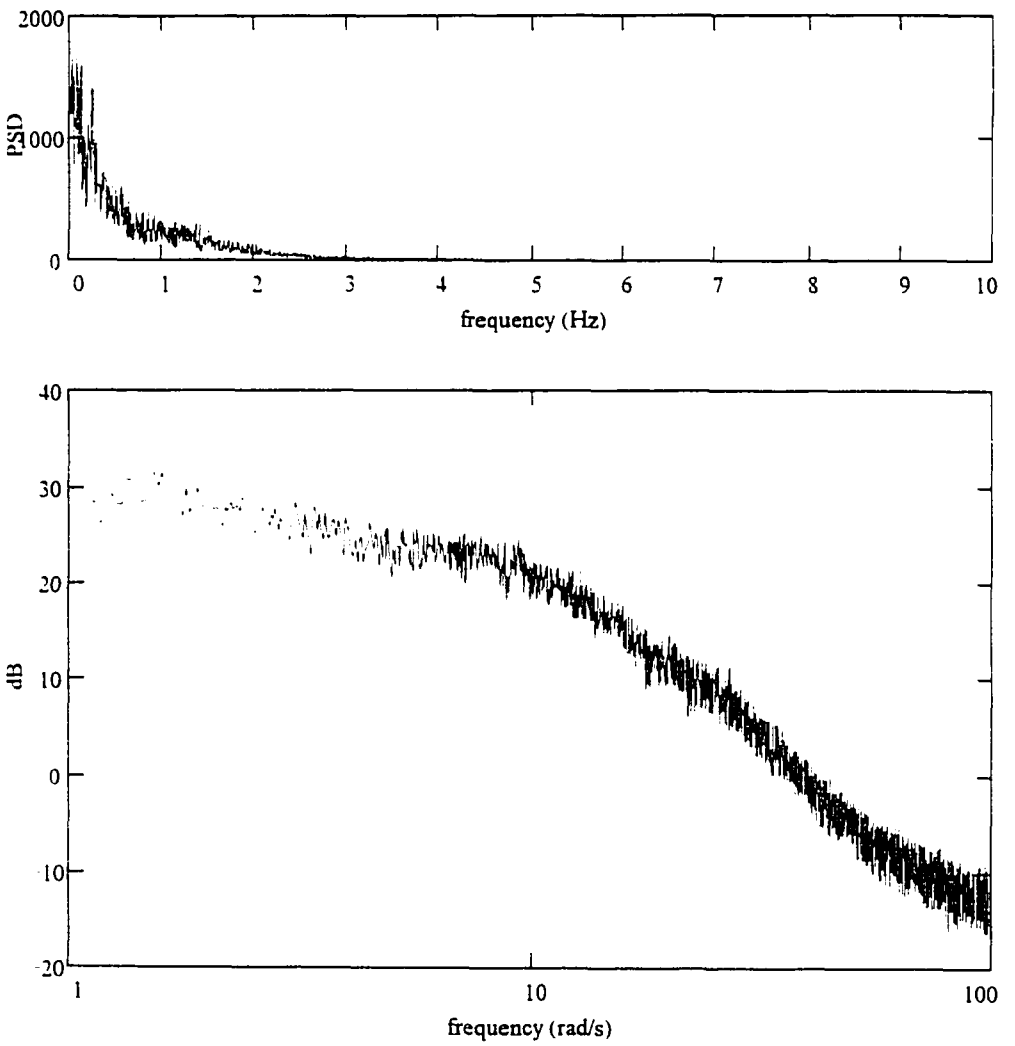

Figure B.18: PSD and Bode plot of bubbling/turbulent bed pressure fluctuations

APPENDIX C

CFB SIMILITUDE STUDY RESULTS

CFB Similitude Experiments - Ethan Brue - ISU - 1995

Dimensionless parameters

(1) denotes LCFB
(2) denotes SCFB

	(+/- Uncertainty)
Fr1 = 4575	UFr1 = 400
Fr2 = 4578	UFr2 = 941
Rep1 = 40	URep1 = 3
Rep2 = 41	URep2 = 8
Gstar1 = 0.0013	UGstar1 = 0.0003
Gstar2 = 0.0013	UGstar2 = 0.0003
Mstar1 = 2.10	UMstar1 = 0.05
Mstar2 = 2.10	UMstar2 = 0.08
ρratio1 = 2147	Uρratio1 = 73
ρratio2 = 2160	Uρratio2 = 25
Hdp1 = 15240	UHdp1 = 762
Hdp2 = 15240	UHdp2 = 3048
Ddp1 = 508	UDdp1 = 25
Ddp2 = 508	UDdp2 = 102

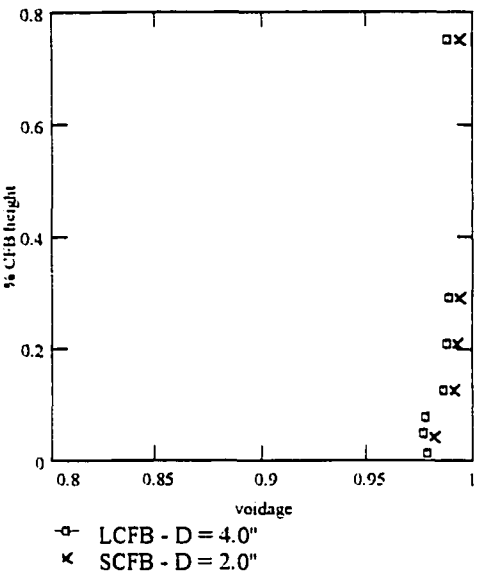

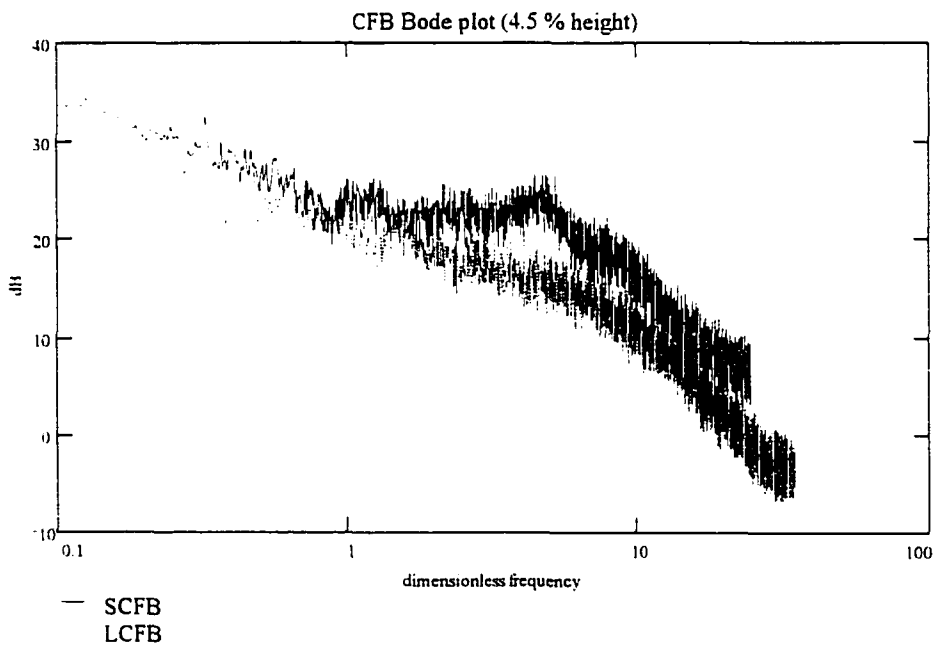

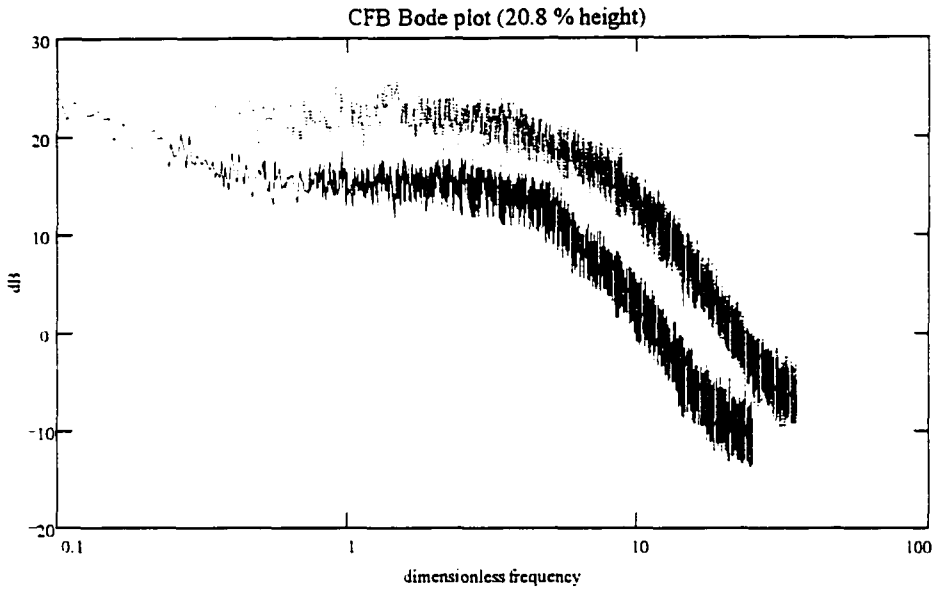
CFB Bode plot (20.8 % height)
30
20
10
0
-10
-20
dB
0.1
1
10
100
dimensionless frequency
SCFB
LCFB

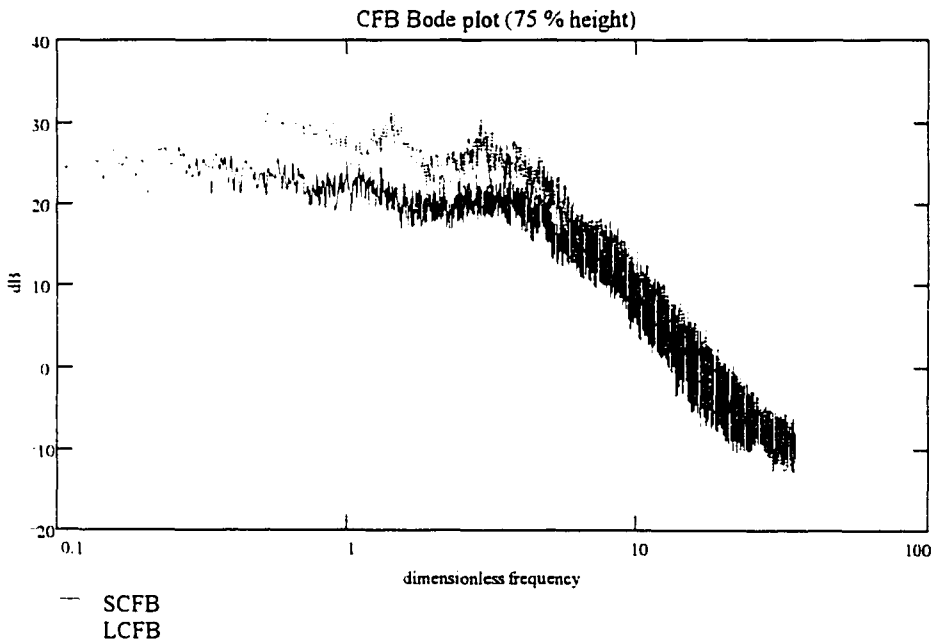
CFB Bode plot (75 % height)
40
30
20
10
0
-10
-20
dB
0.1
1
10
100
dimensionless frequency
SCFB
LCFB

CFB Similitude Experiments - Ethan Brue - ISU - 1995

Dimensionless parameters

(1) denotes LCFB
(2) denotes SCFB

	(+/- Uncertainty)
Fr1 = 4575	UFr1 = 400
Fr2 = 4578	UFr2 = 941
Rep1 = 40	URep1 = 3
Rep2 = 41	URep2 = 8
Gstar1 = 0.0017	UGstar1 = 0.0003
Gstar2 = 0.0019	UGstar2 = 0.0001
Mstar1 = 2.10	UMstar1 = 0.05
Mstar2 = 2.10	UMstar2 = 0.08
ρratio1 = 2147	Uρratio1 = 73
ρratio2 = 2160	Uρratio2 = 25
Hdp1 = 15240	UHdp1 = 762
Hdp2 = 15240	UHdp2 = 3048
Ddp1 = 508	UDdp1 = 25
Ddp2 = 508	UDdp2 = 102

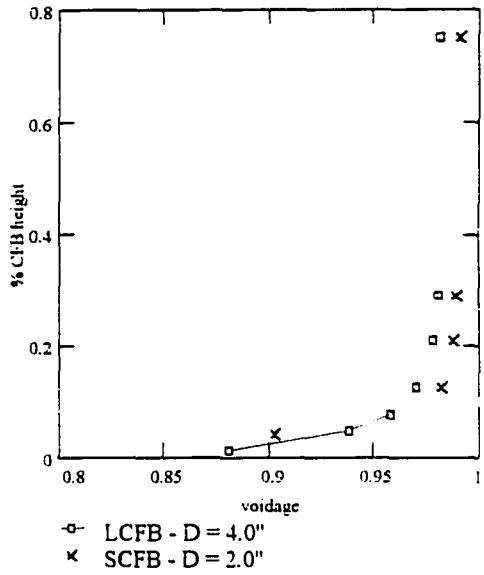

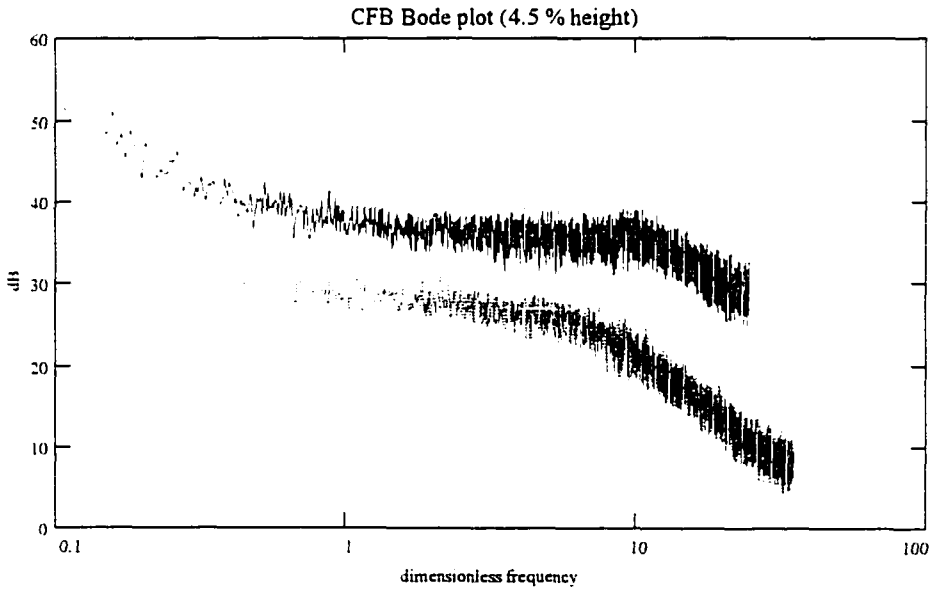

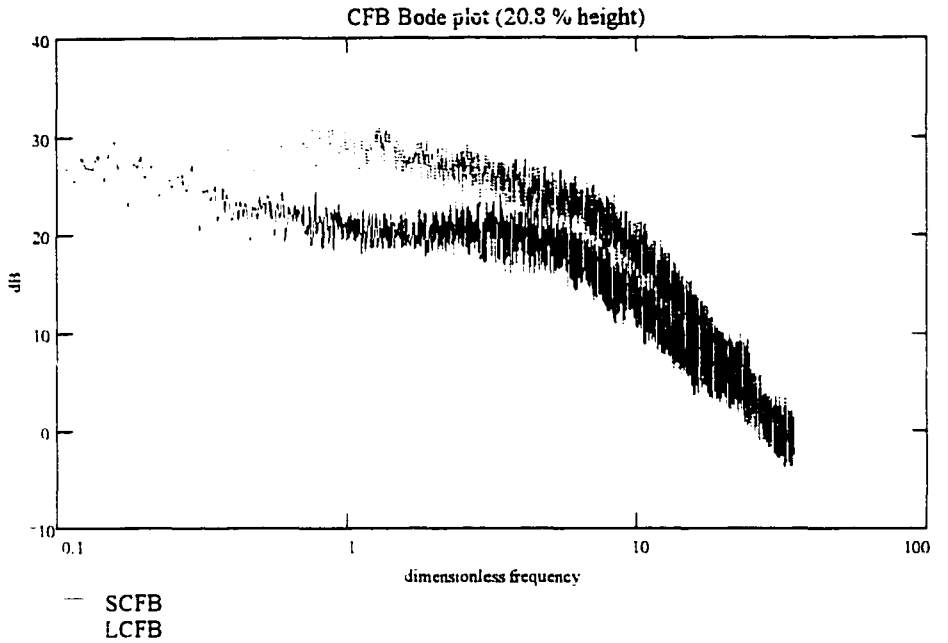
CFB Bode plot (20.8 % height)
40
30
20
10
0
-10
dB
0.1
1
10
100
dimensionless frequency
SCFB
LCFB

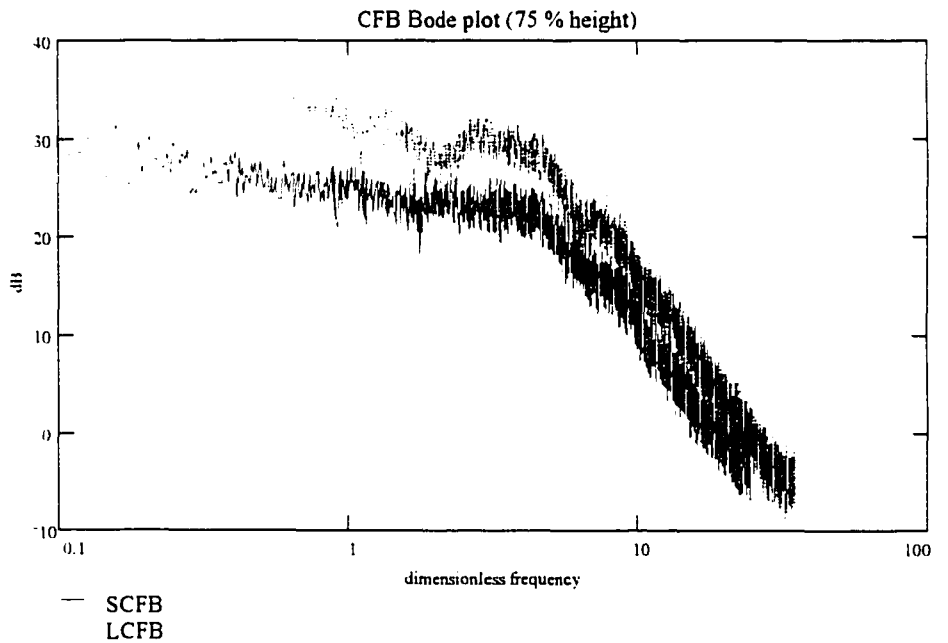
CFB Bode plot (75 % height)
40
30
20
10
0
-10
dB
0.1
1
10
100
dimensionless frequency
SCFB
LCFB

CFB Similitude Experiments - Ethan Brue - ISU - 1995

Dimensionless parameters

(1) denotes LCFB
(2) denotes SCFB

	(+/- Uncertainty)
Fr1 = 6230	UFr1 = 541
Fr2 = 6356	UFr2 = 1299
Rep1 = 47	URep1 = 3
Rep2 = 49	URep2 = 10
Gstar1 = 0.0016	UGstar1 = 0.0002
Gstar2 = 0.0018	UGstar2 = 0.0002
Mstar1 = 2.10	UMstar1 = 0.05
Mstar2 = 2.10	UMstar2 = 0.08
ρratio1 = 2147	Uρratio1 = 73
ρratio2 = 2160	Uρratio2 = 25
Hdp1 = 15240	UHdp1 = 762
Hdp2 = 15240	UHdp2 = 3048
Ddp1 = 508	UDdp1 = 25
Ddp2 = 508	UDdp2 = 102

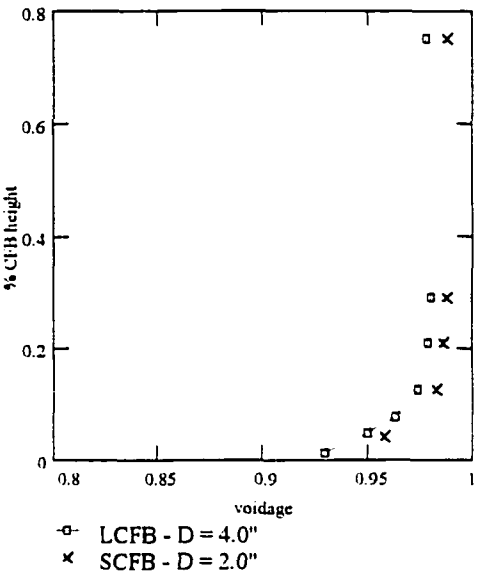

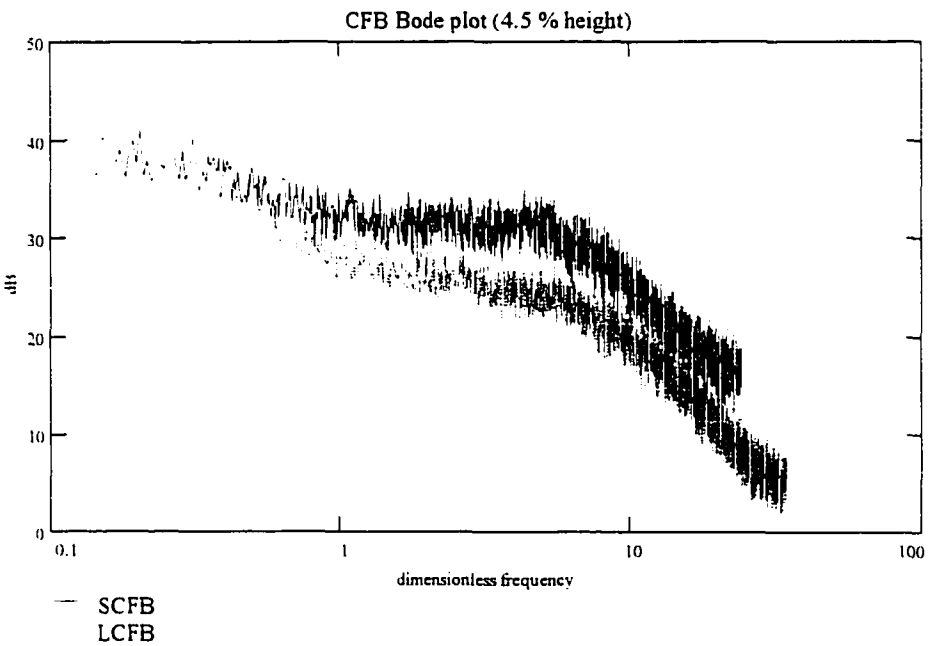

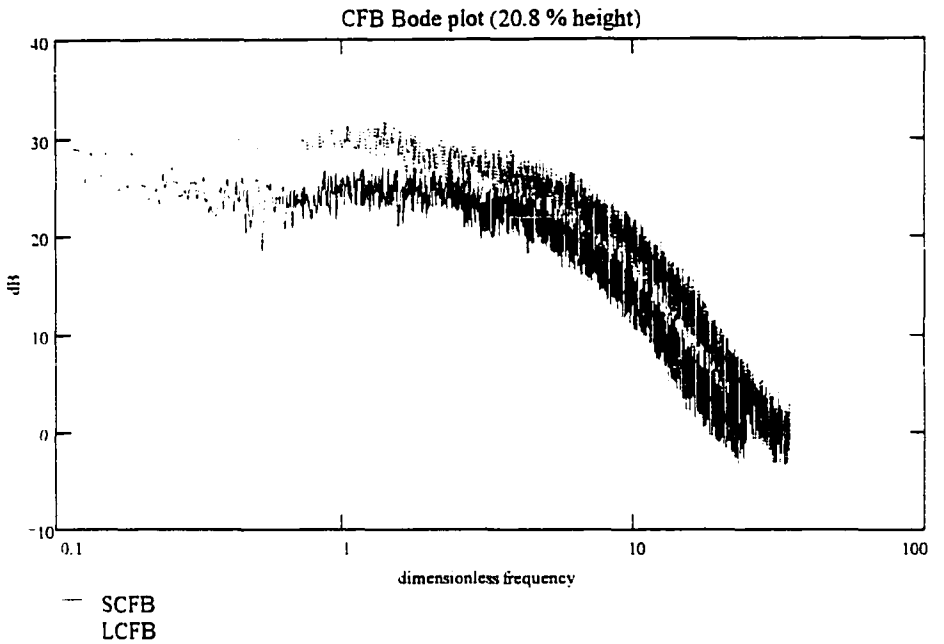
CFB Bode plot (20.8 % height)
40
30
20
10
0
-10
dB
0.1
1
10
100
dimensionless frequency
SCFB
LCFB

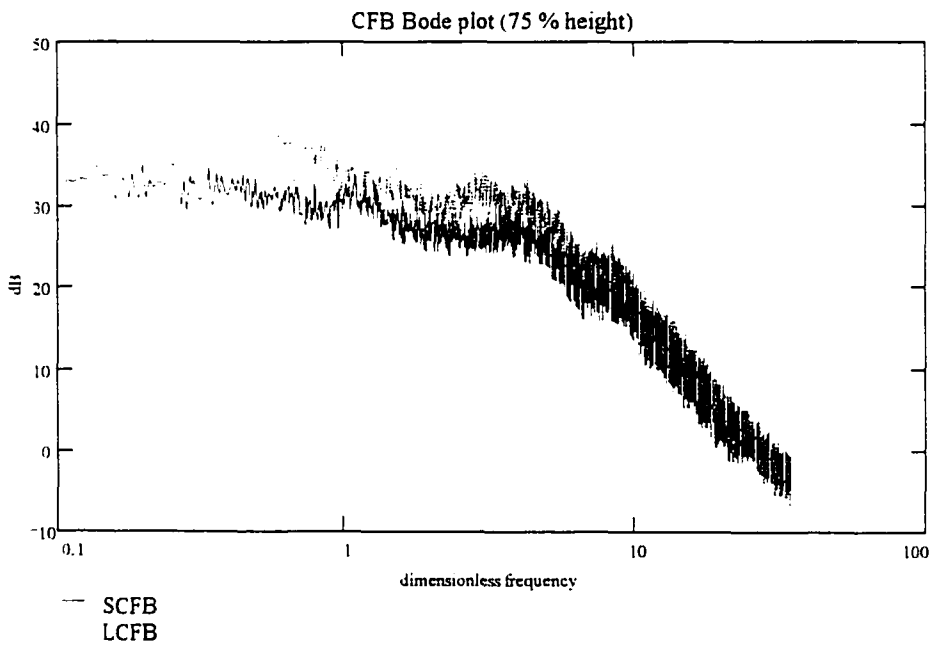
CFB Bode plot (75 % height)
50
40
30
20
10
0
-10
dB
0.1
1
10
100
dimensionless frequency
SCFB
LCFB

CFB Similitude Experiments - Ethan Brue - ISU - 1995

Dimensionless parameters

(1) denotes LCFB
(2) denotes SCFB

	(+/- Uncertainty)
Fr1 = 6230	UFr1 = 541
Fr2 = 6356	UFr2 = 1299
Rep1 = 47	URep1 = 3
Rep2 = 49	URep2 = 10
Gstar1 = 0.0021	UGstar1 = 0.0004
Gstar2 = 0.0023	UGstar2 = 0.0002
Mstar1 = 2.10	UMstar1 = 0.05
Mstar2 = 2.10	UMstar2 = 0.08
ρratio1 = 2147	Upratio1 = 73
ρratio2 = 2160	Upratio2 = 25
Hdp1 = 15240	UHdp1 = 762
Hdp2 = 15240	UHdp2 = 3048
Ddp1 = 508	UDdp1 = 25
Ddp2 = 508	UDdp2 = 102

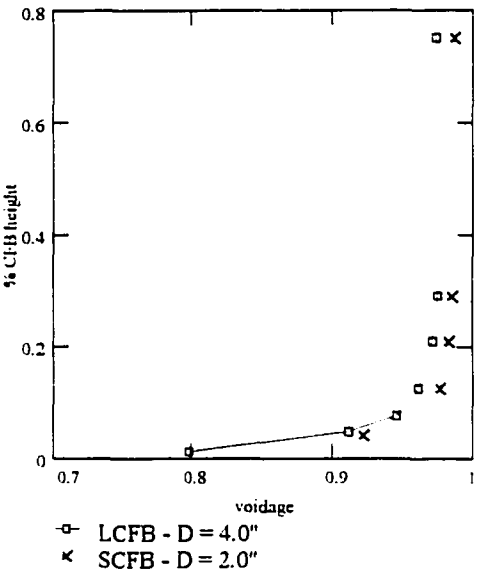

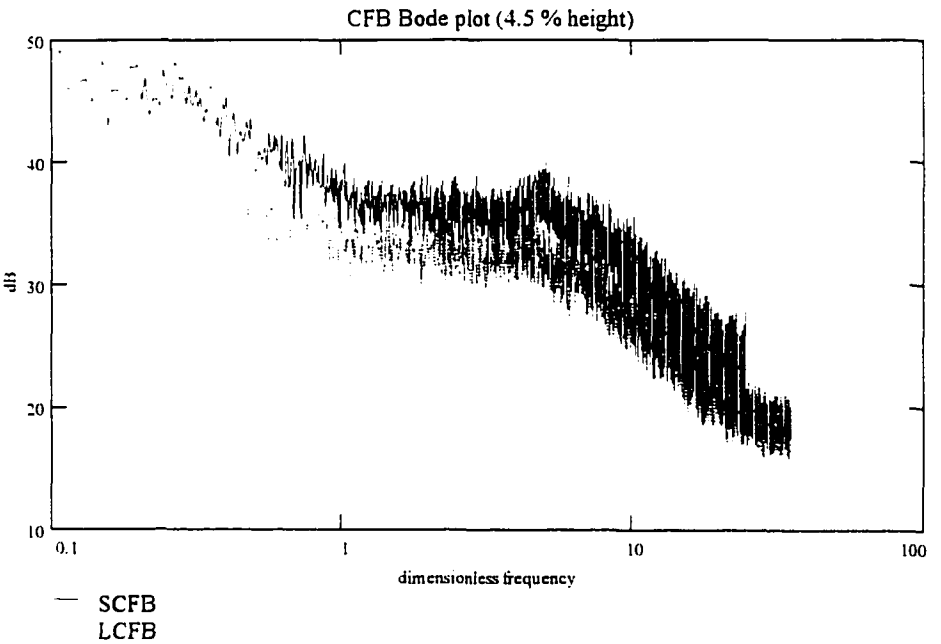

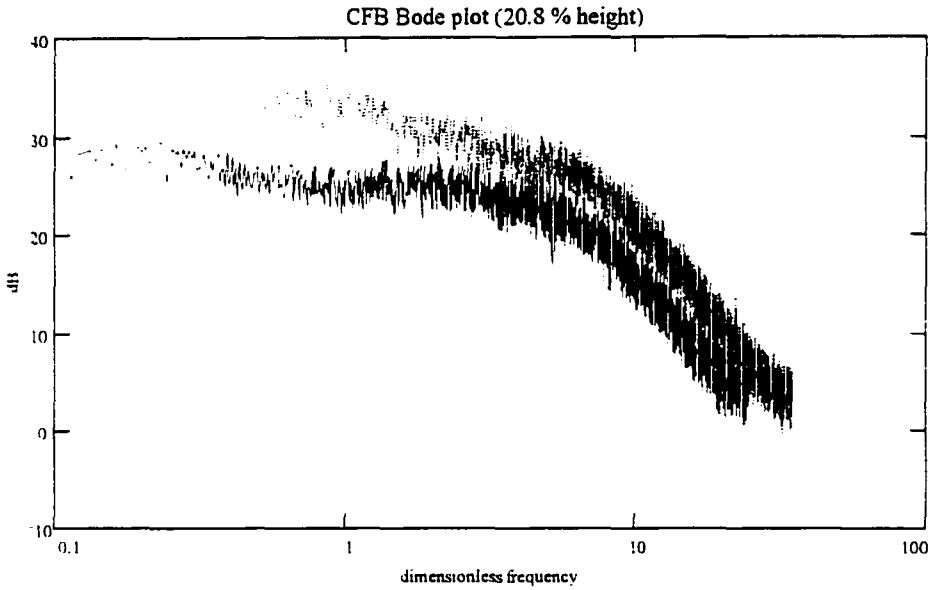
CFB Bode plot (20.8 % height)
40
30
20
10
0
-10
dB
0.1
1
10
100
dimensionless frequency
SCFB
LCFB

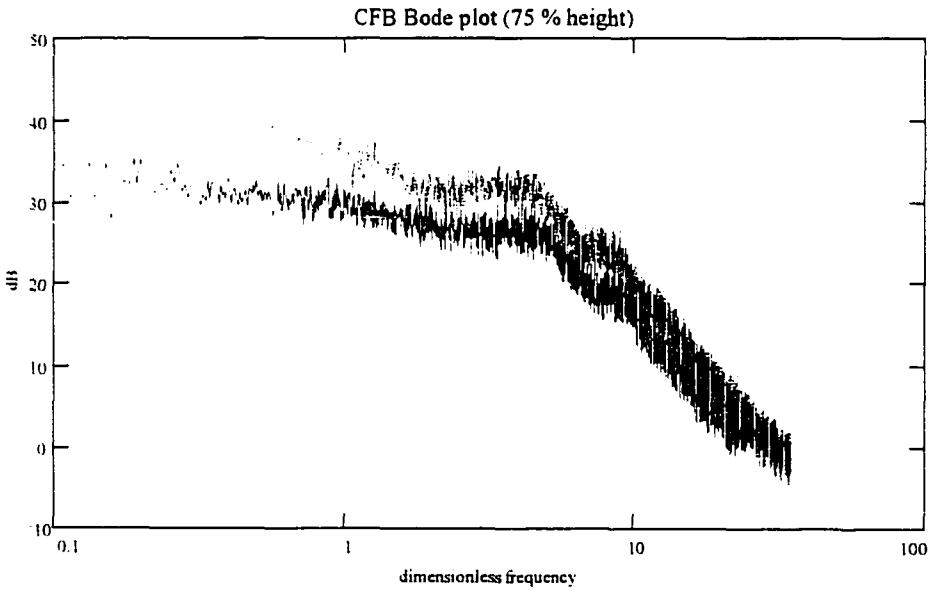
CFB Bode plot (75 % height)
50
40
30
20
10
0
-10
dB
0.1
1
10
100
dimensionless frequency
SCFB
LCFB

CFB Similitude Experiments - Ethan Brue - ISU - 1995

Dimensionless parameters

(1) denotes LCFB
(2) denotes SCFB

	(+/- Uncertainty)
Fr1 = 6230	UFr1 = 541
Fr2 = 6356	UFr2 = 1299
Rep1 = 47	URep1 = 3
Rep2 = 49	URep2 = 10
Gstar1 = 0.0019	UGstar1 = 0.0005
Gstar2 = 0.0021	UGstar2 = 0.0003
Mstar1 = 2.73	UMstar1 = 0.05
Mstar2 = 2.73	UMstar2 = 0.08
pratio1 = 2147	Upratio1 = 73
pratio2 = 2160	Upratio2 = 25
Hdp1 = 15240	UHdp1 = 762
Hdp2 = 15240	UHdp2 = 3048
Ddp1 = 508	UDdp1 = 25
Ddp2 = 508	UDdp2 = 102

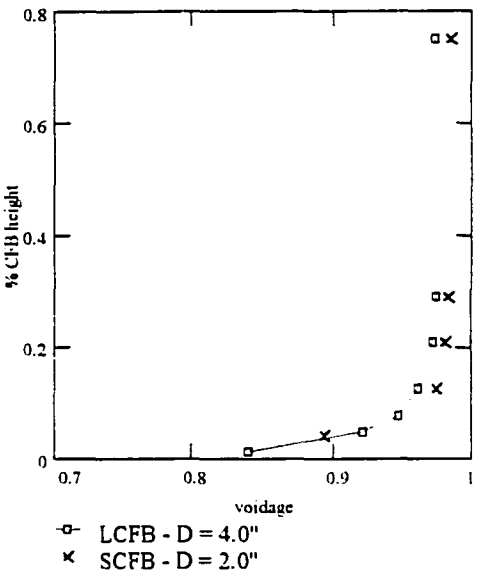

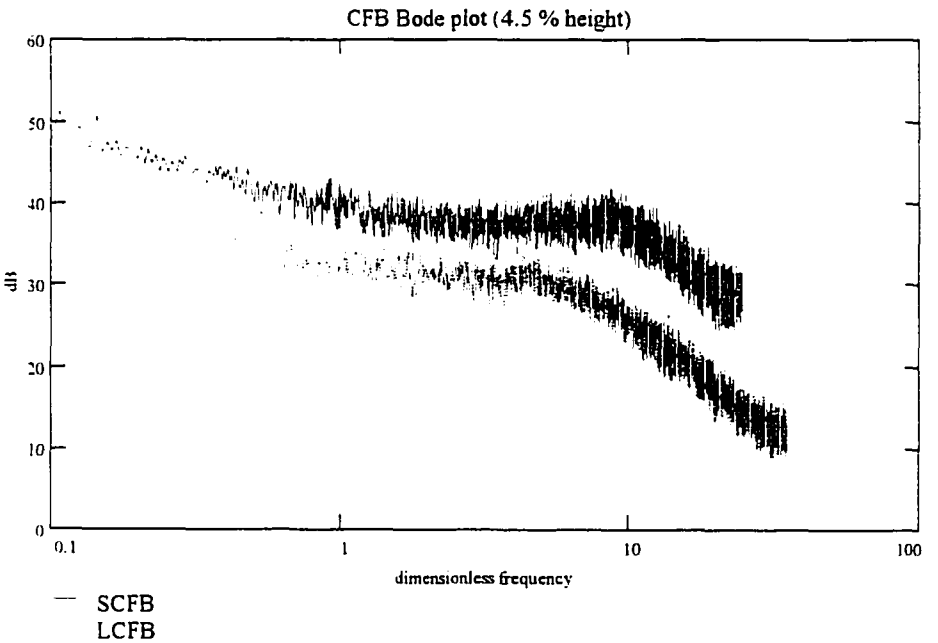

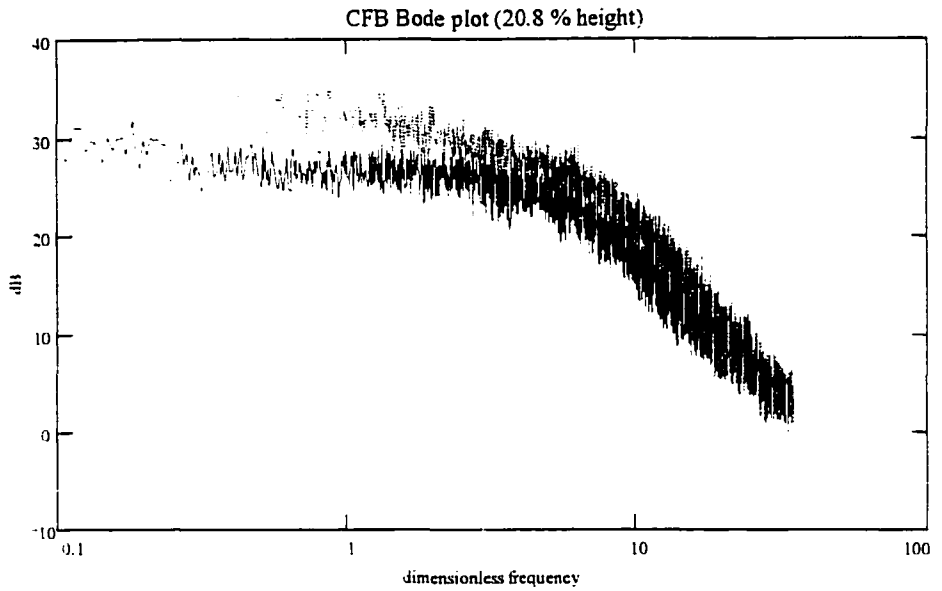
CFB Bode plot (20.8 % height)
40
30
20
10
0
-10
dB
0.1
1
10
100
dimensionless frequency
SCFB
LCFB

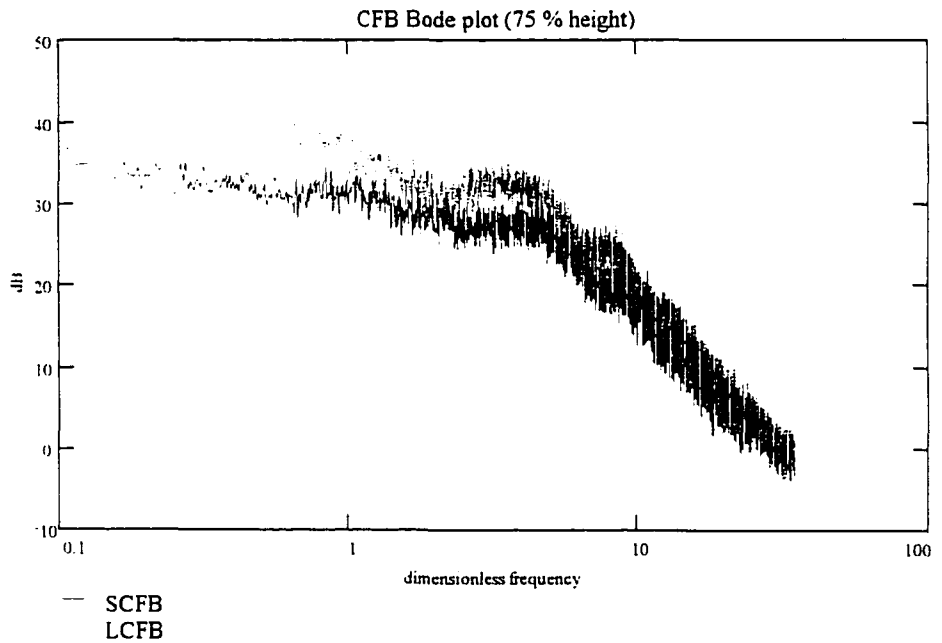
CFB Bode plot (75 % height)
50
40
30
20
10
0
-10
dB
0.1
1
10
100
dimensionless frequency
SCFB
LCFB

CFB Similitude Experiments - Ethan Brue - ISU - 1995

Dimensionless parameters

(1) denotes LCFB
(2) denotes SCFB

	(+/- Uncertainty)
Fr1 = 8143	UFr1 = 703
Fr2 = 8060	UFr2 = 1643
Rep1 = 54	URep1 = 4
Rep2 = 55	URep2 = 11
Gstar1 = 0.0019	UGstar1 = 0.0003
Gstar2 = 0.0021	UGstar2 = 0.0001
Mstar1 = 2.10	UMstar1 = 0.05
Mstar2 = 2.10	UMstar2 = 0.08
ρratio1 = 2147	Upratio1 = 73
ρratio2 = 2160	Upratio2 = 25
Hdp1 = 15240	UHdp1 = 762
Hdp2 = 15240	UHdp2 = 3048
Ddp1 = 508	UDdp1 = 25
Ddp2 = 508	UDdp2 = 102

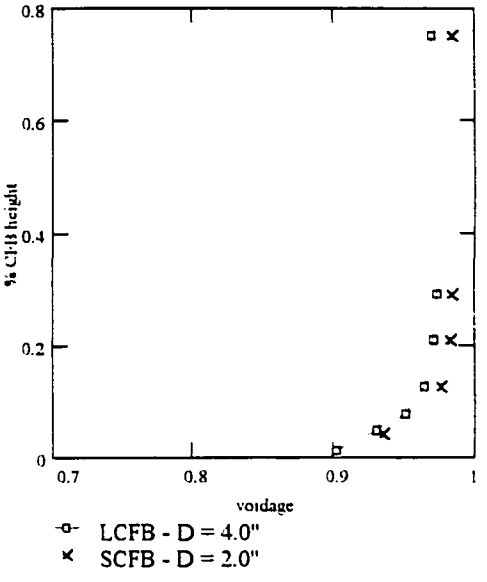

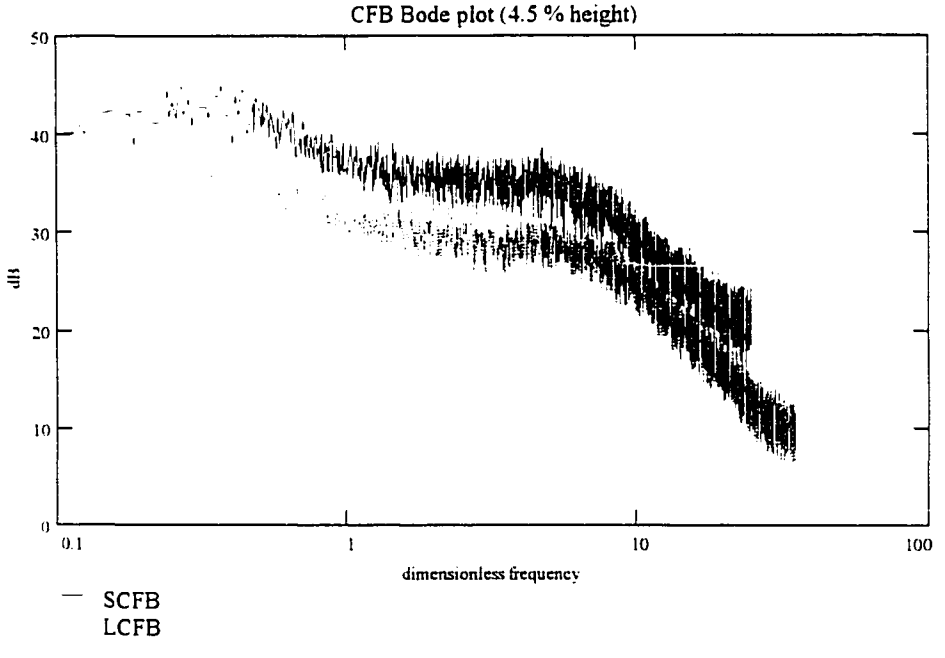

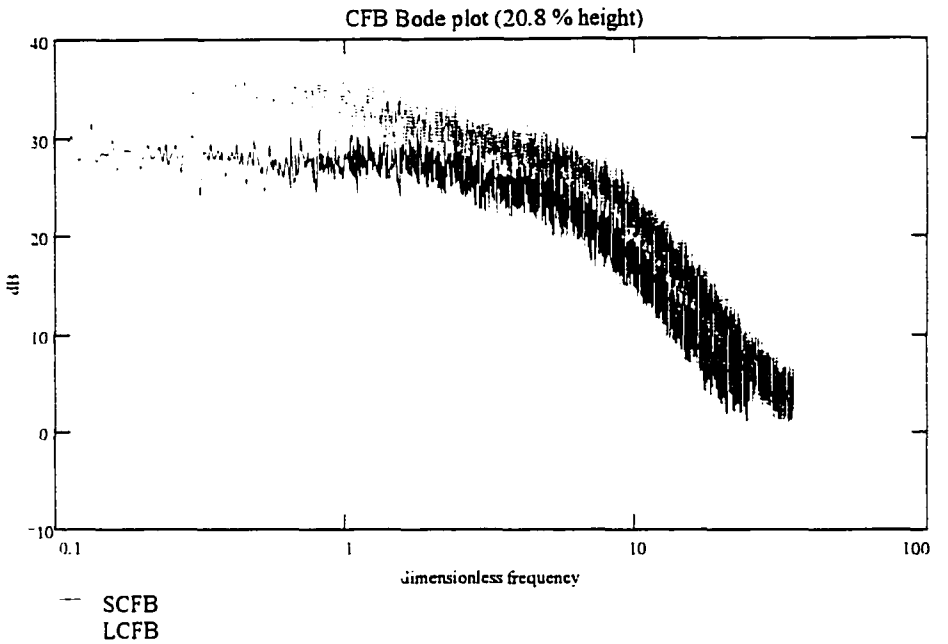
CFB Bode plot (20.8 % height)
40
30
20
10
0
-10
dB
0.1
1
10
100
dimensionless frequency
SCFB
LCFB

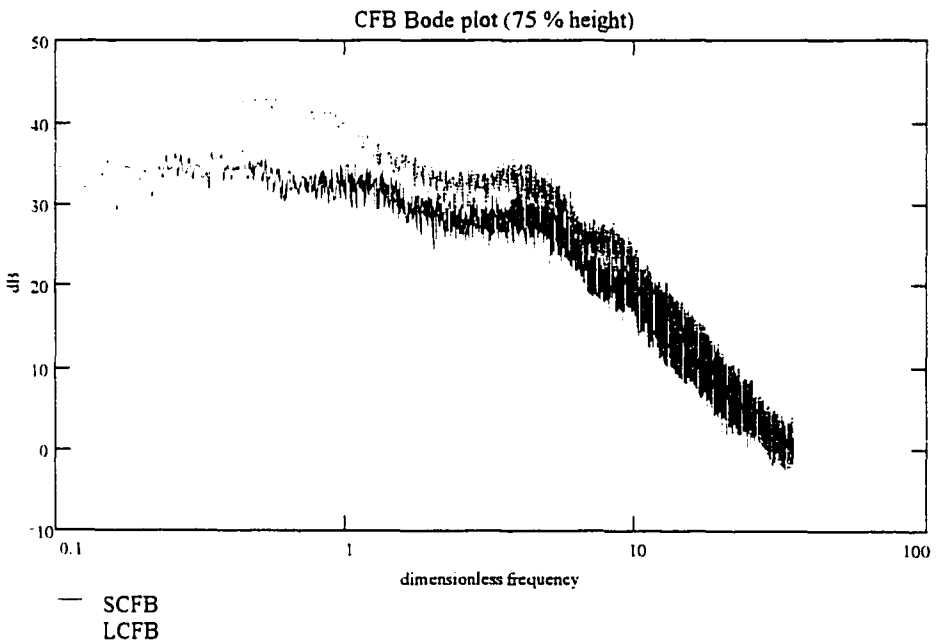
CFB Bode plot (75 % height)
50
40
30
20
10
0
-10
dB
0.1
1
10
100
dimensionless frequency
SCFB
LCFB

CFB Similitude Experiments - Ethan Brue - ISU - 1995

Dimensionless parameters

(1) denotes LCFB
(2) denotes SCFB

	(+/- Uncertainty)
Fr1 = 8160	UFr1 = 705
Fr2 = 8060	UFr2 = 1643
Rep1 = 54	URep1 = 4
Rep2 = 55	URep2 = 11
Gstar1 = 0.0023	UGstar1 = 0.0001
Gstar2 = 0.0025	UGstar2 = 0.0003
Mstar1 = 2.73	UMstar1 = 0.05
Mstar2 = 2.73	UMstar2 = 0.08
ρratio1 = 2147	Uρratio1 = 73
ρratio2 = 2160	Uρratio2 = 25
Hdp1 = 15240	UHdp1 = 762
Hdp2 = 15240	UHdp2 = 3048
Ddp1 = 508	UDdp1 = 25
Ddp2 = 508	UDdp2 = 102

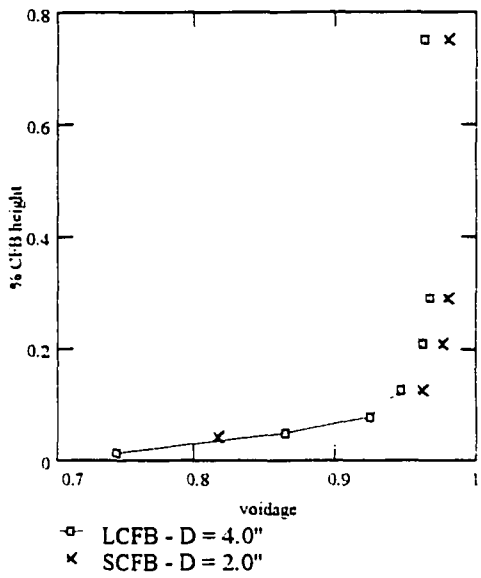

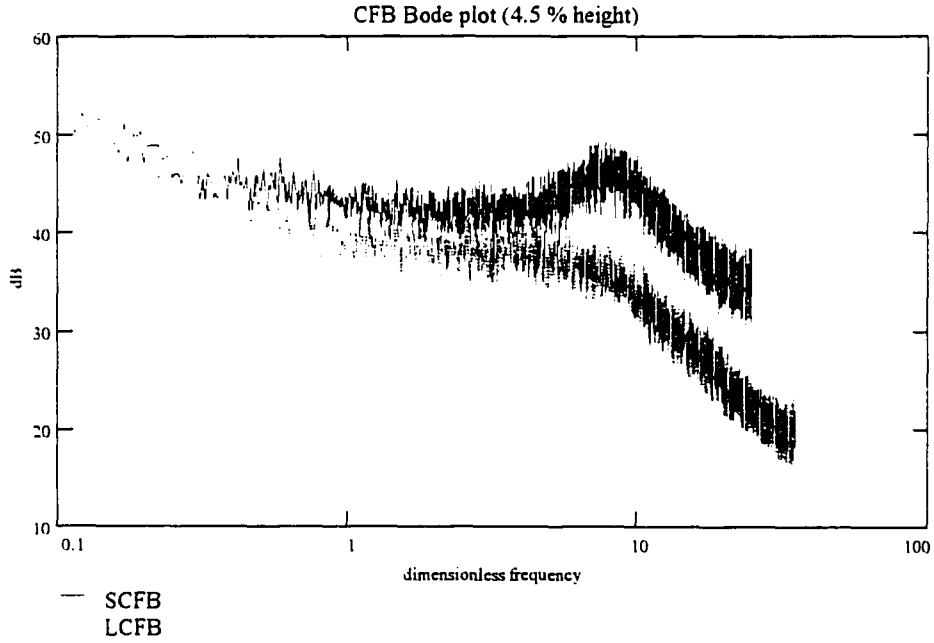

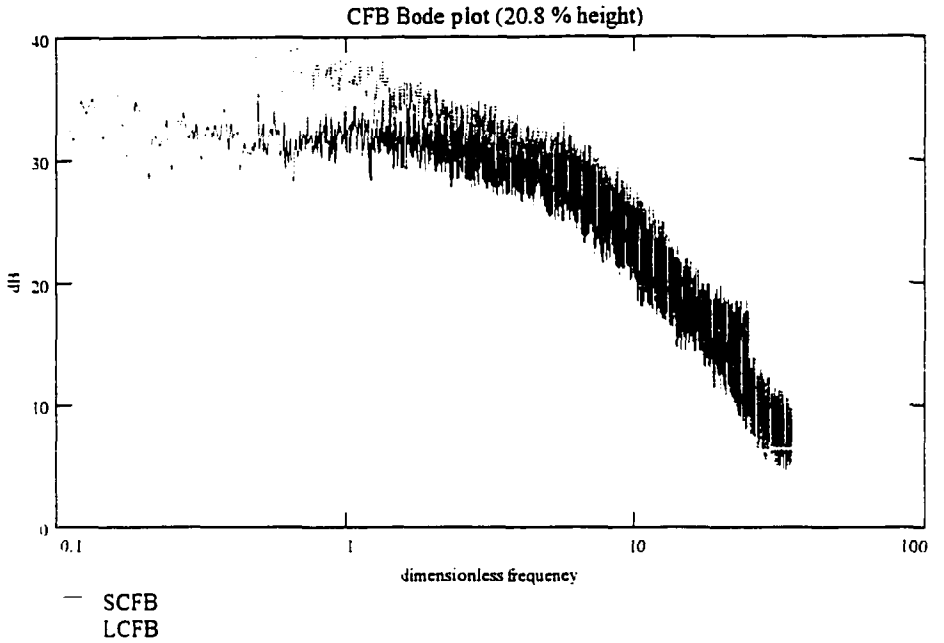
CFB Bode plot (20.8 % height)
40
30
20
10
0
dB
0.1
1
10
100
dimensionless frequency
SCFB
LCFB

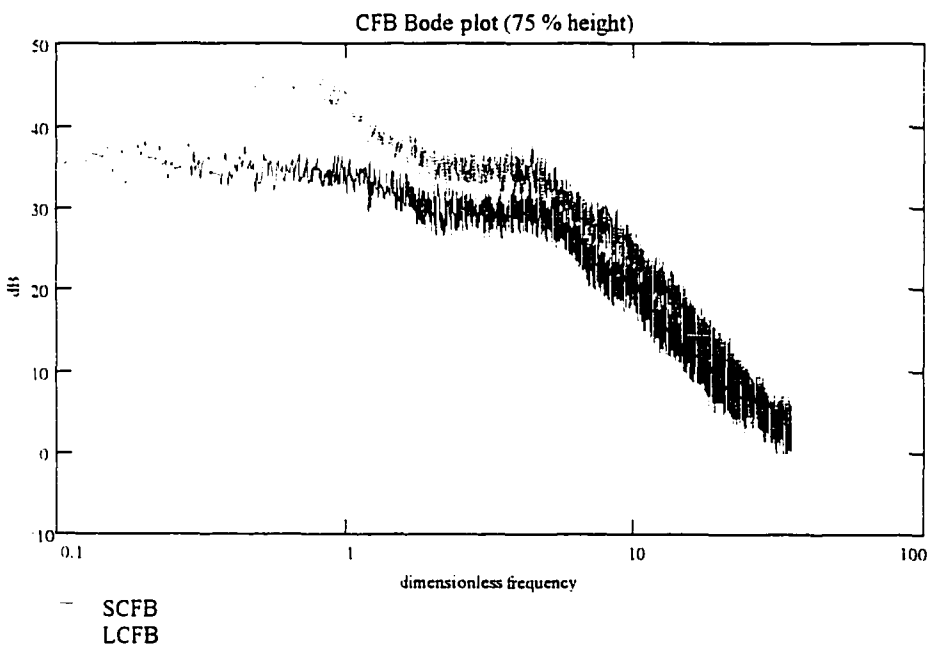
CFB Bode plot (75 % height)
50
40
30
20
10
0
-10
dB
0.1
1
10
100
dimensionless frequency
SCFB
LCFB

CFB Similitude Experiments - Ethan Brue - ISU - 1995

Dimensionless parameters

(1) denotes LCFB
(2) denotes SCFB

	(+/- Uncertainty)
Fr1 = 4098	UFr1 = 321
Fr2 = 4084	UFr2 = 571
Rep1 = 70	URep1 = 4
Rep2 = 72	URep2 = 10
Gstar1 = 0.0011	UGstar1 = 0.0003
Gstar2 = 0.0011	UGstar2 = 0.0001
Mstar1 = 2.10	UMstar1 = 0.05
Mstar2 = 2.10	UMstar2 = 0.08
ρratio1 = 2147	Upratio1 = 73
ρratio2 = 2160	Upratio2 = 25
Hdp1 = 10160	UHdp1 = 339
Hdp2 = 10160	UHdp2 = 1355
Ddp1 = 339	UDdp1 = 11
Ddp2 = 339	UDdp2 = 45

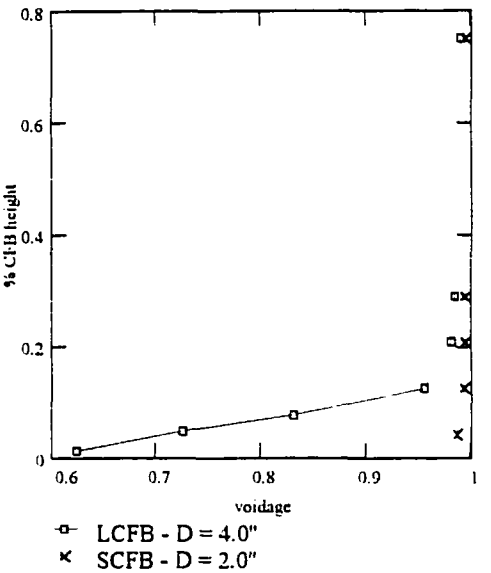

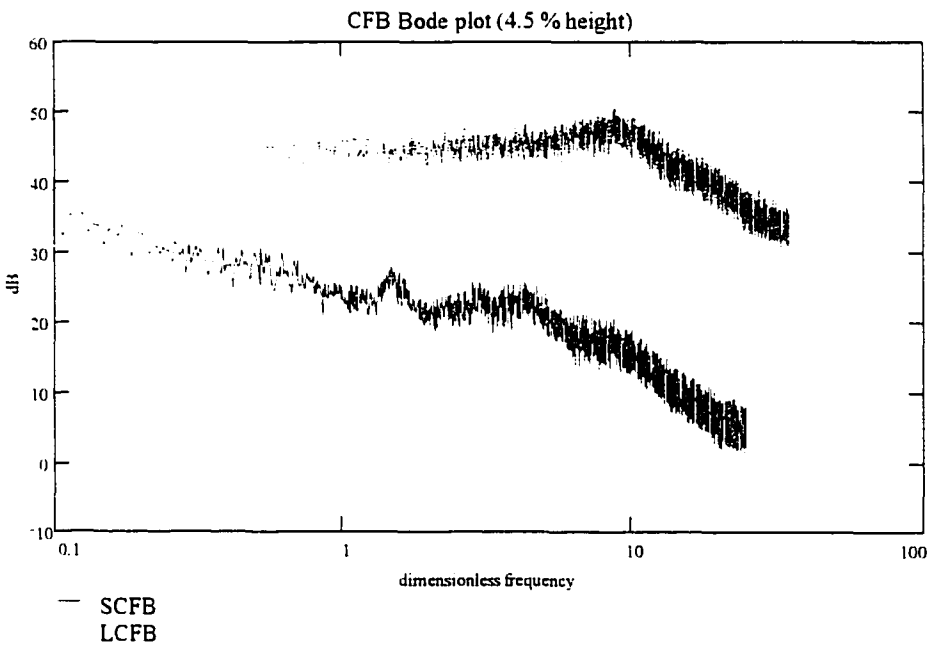

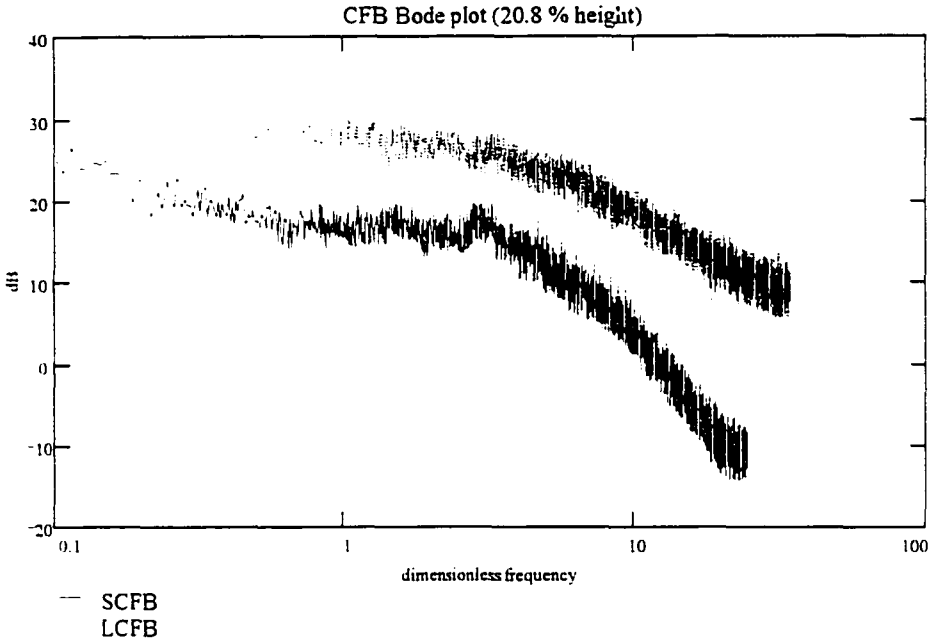
CFB Bode plot (20.8 % height)
40
30
20
10
0
-10
-20
dB
0.1
1
10
100
dimensionless frequency
SCFB
LCFB

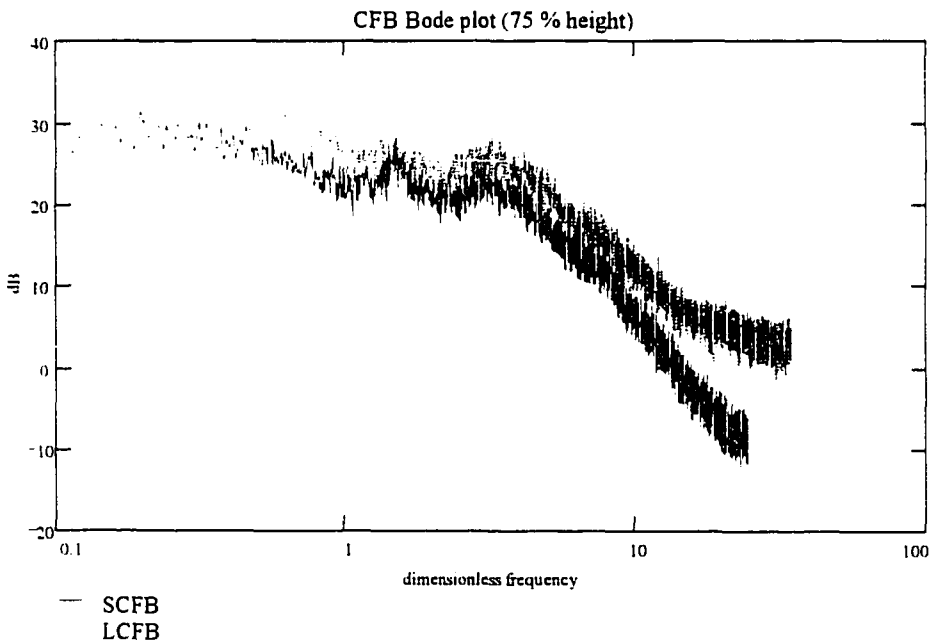
CFB Bode plot (75 % height)
40
30
20
10
0
-10
-20
dB
0.1
1
10
100
dimensionless frequency
SCFB
LCFB

CFB Similitude Experiments - Ethan Brue - ISU - 1995

Dimensionless parameters

(1) denotes LCFB
(2) denotes SCFB

	(+/- Uncertainty)
Fr1 = 5493	UFr1 = 428
Fr2 = 5454	UFr2 = 758
Rep1 = 81	URep1 = 5
Rep2 = 83	URep2 = 11
Gstar1 = 0.0012	UGstar1 = 0.0002
Gstar2 = 0.0014	UGstar2 = 0.0002
Mstar1 = 2.10	UMstar1 = 0.05
Mstar2 = 2.10	UMstar2 = 0.08
ρratio1 = 2147	Upratio1 = 73
ρratio2 = 2160	Upratio2 = 25
Hdp1 = 10160	UHdp1 = 339
Hdp2 = 10160	UHdp2 = 1355
Ddp1 = 339	UDdp1 = 11
Ddp2 = 339	UDdp2 = 45

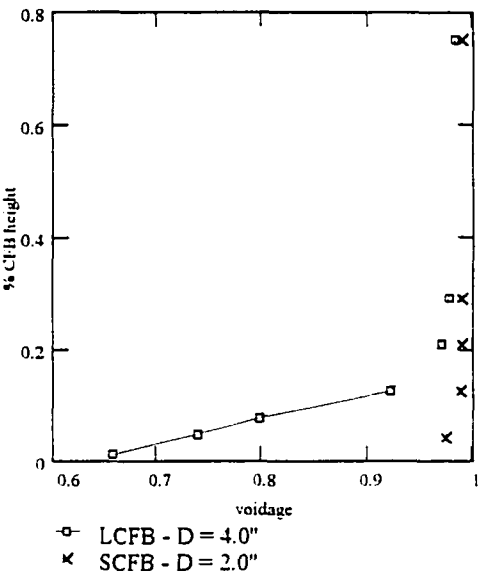

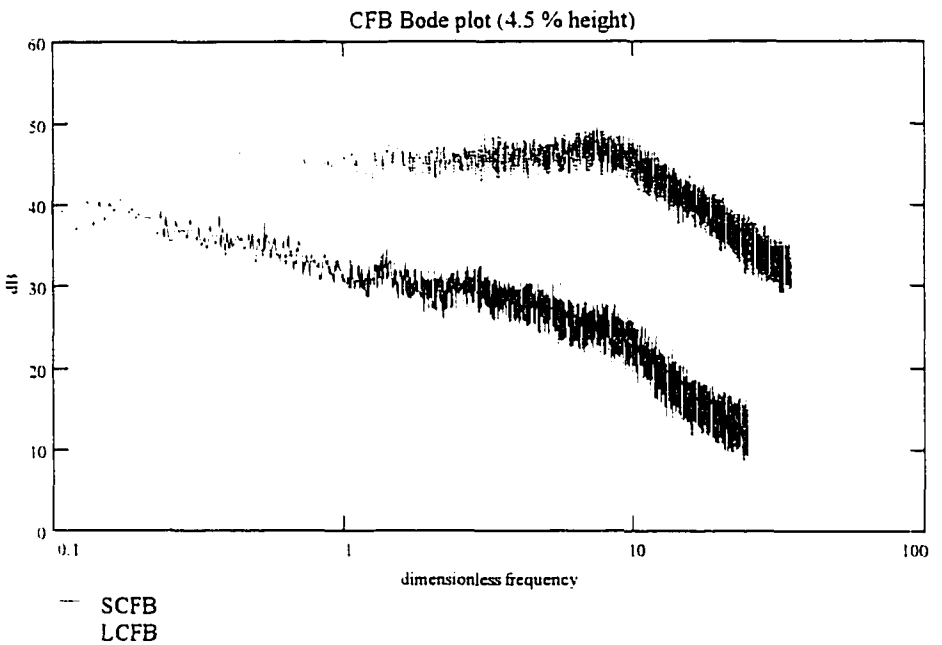

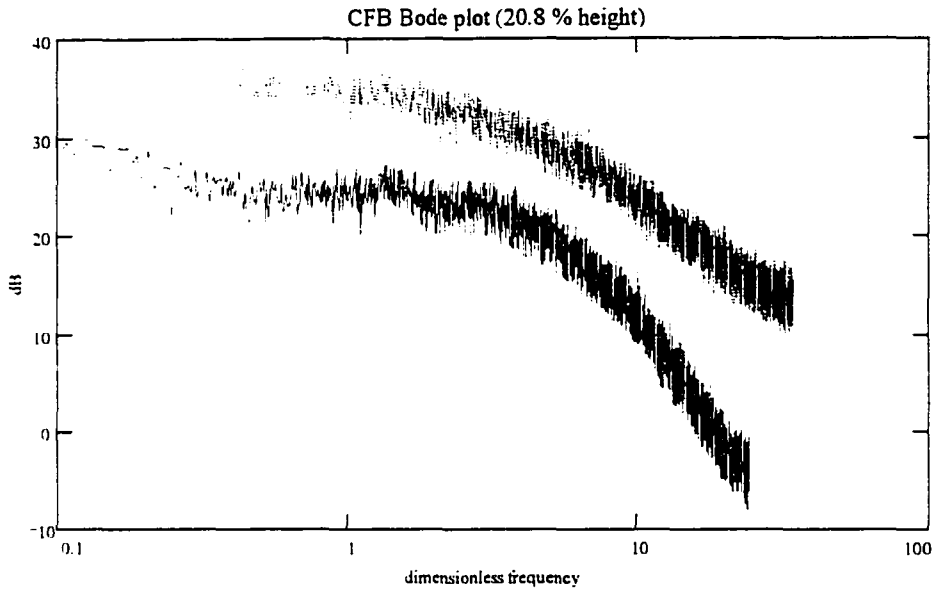
CFB Bode plot (20.8 % height)
40
30
20
10
0
-10
dB
0.1
1
10
100
dimensionless frequency
SCFB
LCFB

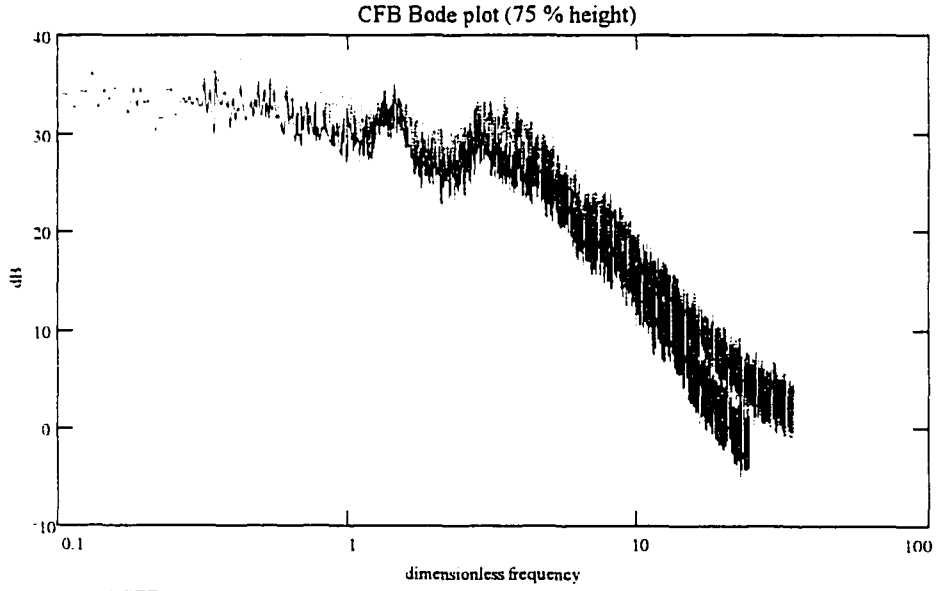
CFB Bode plot (75 % height)
40
30
20
10
0
-10
dB
0.1
1
10
100
dimensionless frequency
SCFB
LCFB

CFB Similitude Experiments - Ethan Brue - ISU - 1995

Dimensionless parameters

(1) denotes LCFB
(2) denotes SCFB

	(+/- Uncertainty)
Fr1 = 5581	UFr1 = 435
Fr2 = 5057	UFr2 = 704
Rep1 = 82	URep1 = 5
Rep2 = 80	URep2 = 11
Gstar1 = 0.0017	UGstar1 = 0.0003
Gstar2 = 0.0019	UGstar2 = 0.0002
Mstar1 = 2.73	UMstar1 = 0.05
Mstar2 = 2.73	UMstar2 = 0.08
ρratio1 = 2147	Upratio1 = 73
ρratio2 = 2160	Upratio2 = 25
Hdp1 = 10160	UHdp1 = 339
Hdp2 = 10160	UHdp2 = 1355
Ddp1 = 339	UDdp1 = 11
Ddp2 = 339	UDdp2 = 45

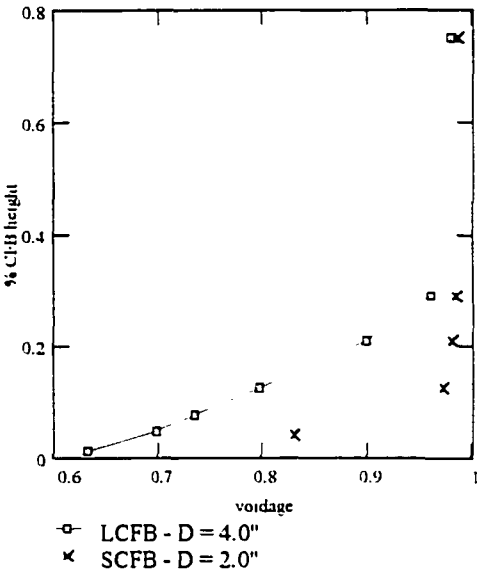

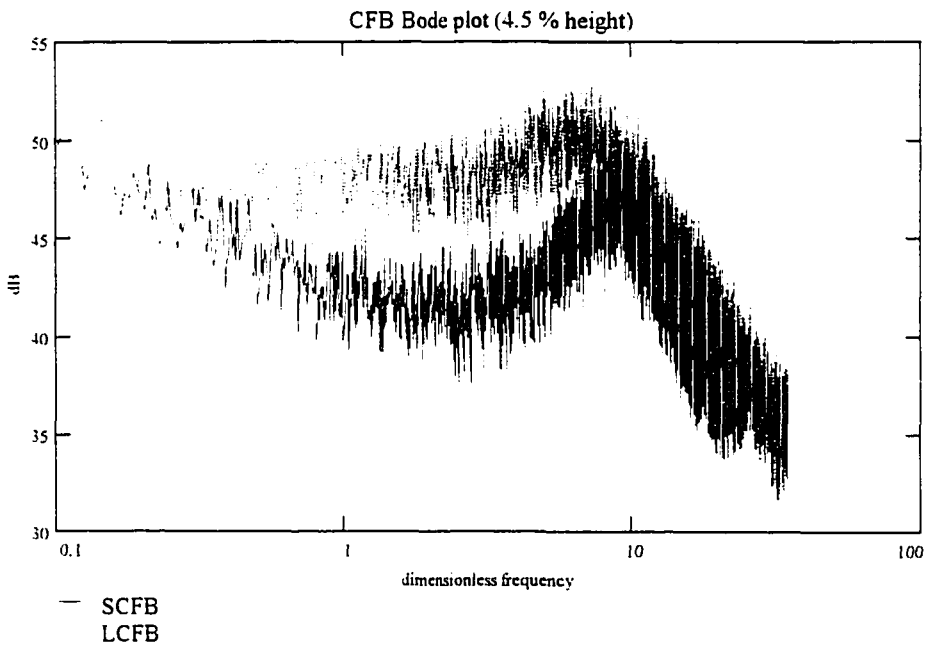

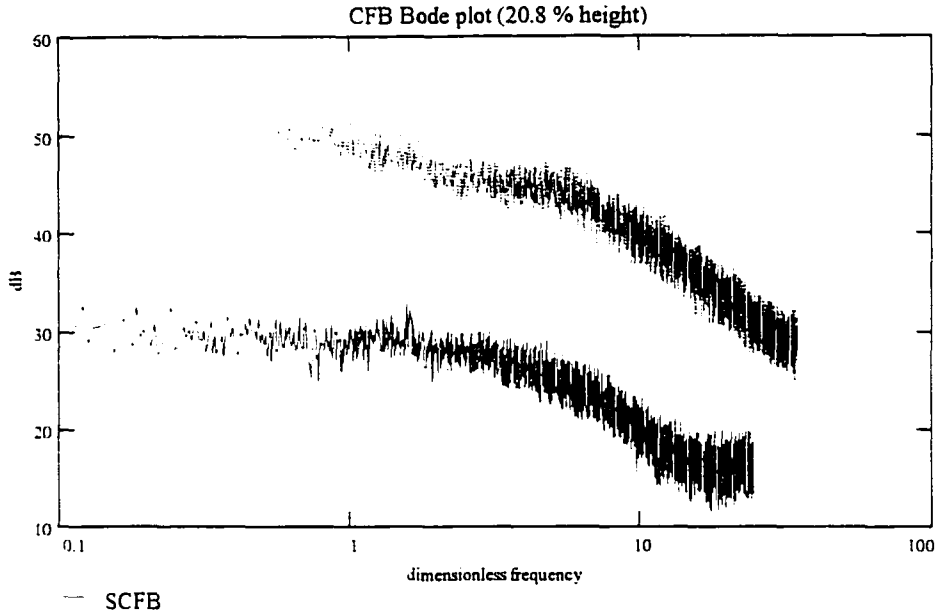
CFB Bode plot (20.8 % height)
60
50
40
30
20
10
dB
0.1
1
10
100
dimensionless frequency
SCFB
LCFB

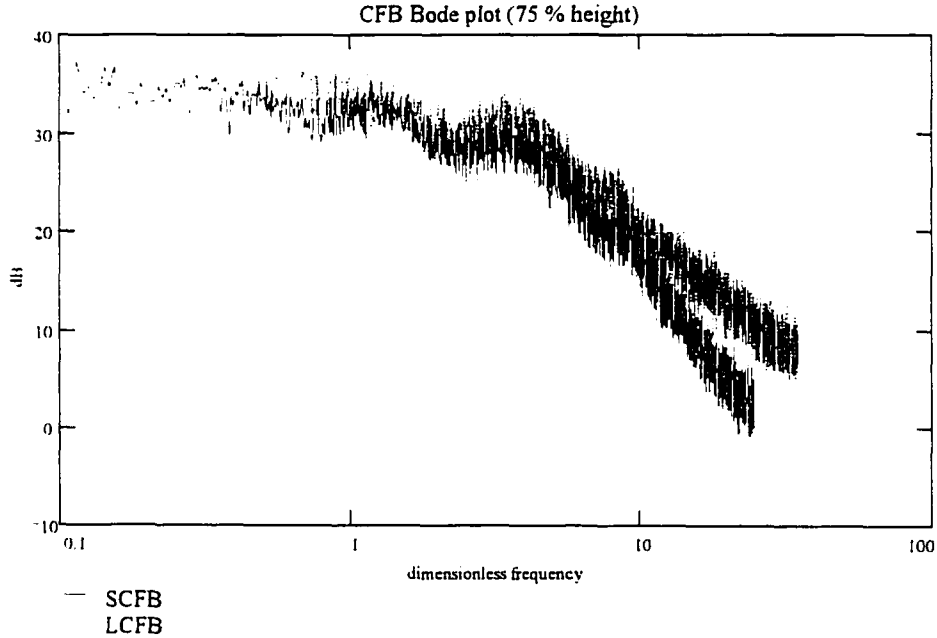
CFB Bode plot (75 % height)
40
30
20
10
0
-10
dB
0.1
1
10
100
dimensionless frequency
SCFB
LCFB

CFB Similitude Experiments - Ethan Brue - ISU - 1995

Dimensionless parameters

(1) denotes LCFB
(2) denotes SCFB

	(+/- Uncertainty)
Fr1 = 10810	UFr1 = 835
Fr2 = 10590	UFr2 = 1455
Rep1 = 114	URep1 = 7
Rep2 = 116	URep2 = 16
Gstar1 = 0.0014	UGstar1 = 0.0002
Gstar2 = 0.0014	UGstar2 = 0.0002
Mstar1 = 2.10	UMstar1 = 0.05
Mstar2 = 2.10	UMstar2 = 0.08
ρratio1 = 2147	Uρratio1 = 73
ρratio2 = 2160	Uρratio2 = 25
Hdp1 = 10160	UHdp1 = 339
Hdp2 = 10160	UHdp2 = 1355
Ddp1 = 339	UDdp1 = 11
Ddp2 = 339	UDdp2 = 45

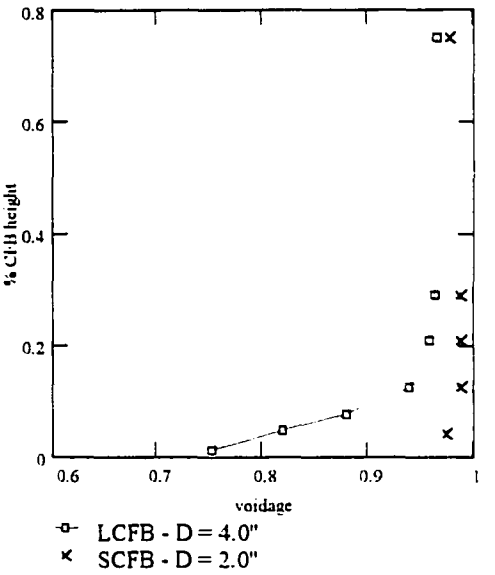

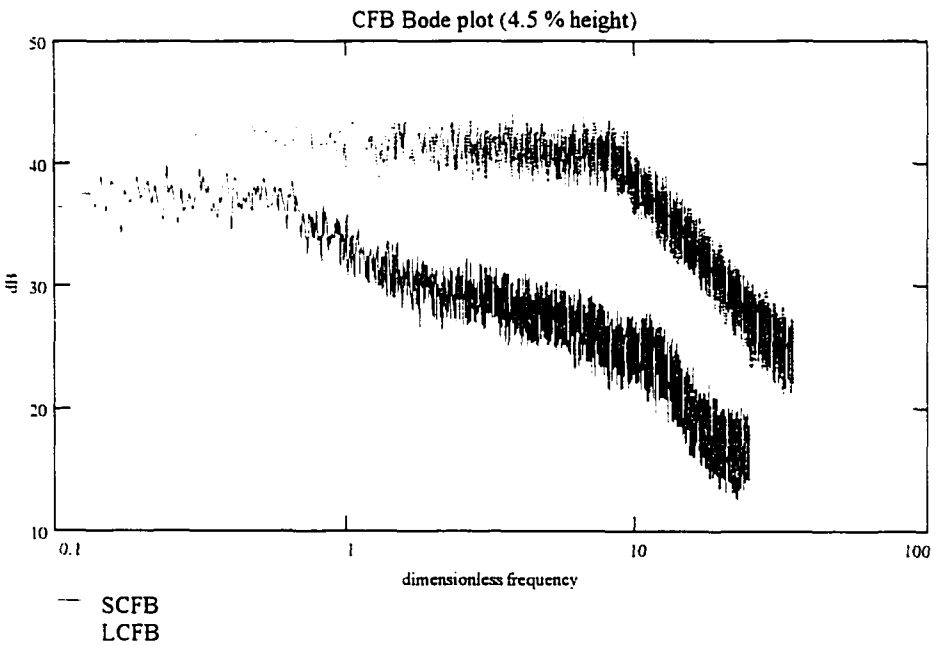

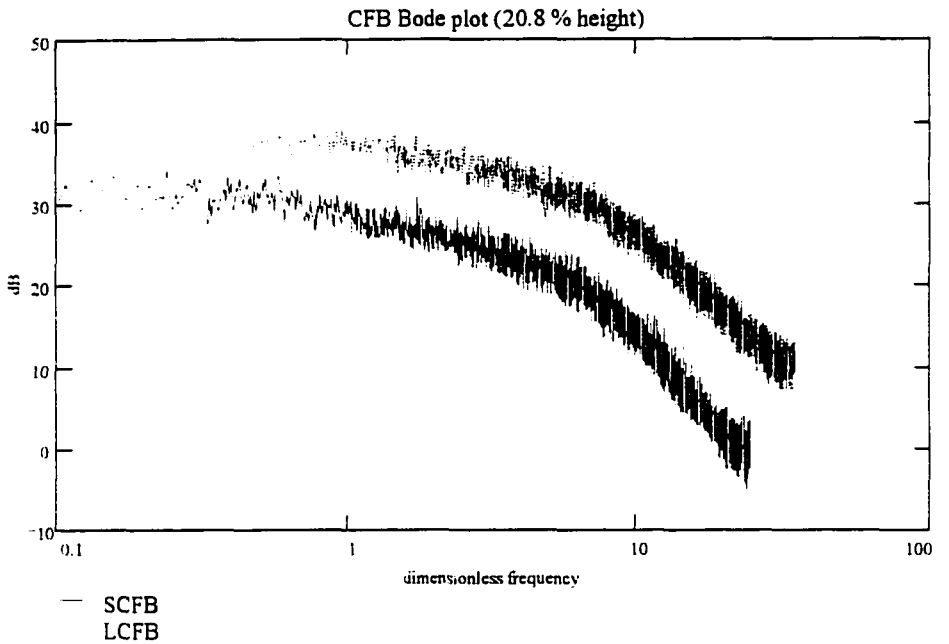
CFB Bode plot (20.8 % height)
50
40
30
20
10
0
-10
dB
0.1
1
10
100
dimensionless frequency
SCFB
LCFB

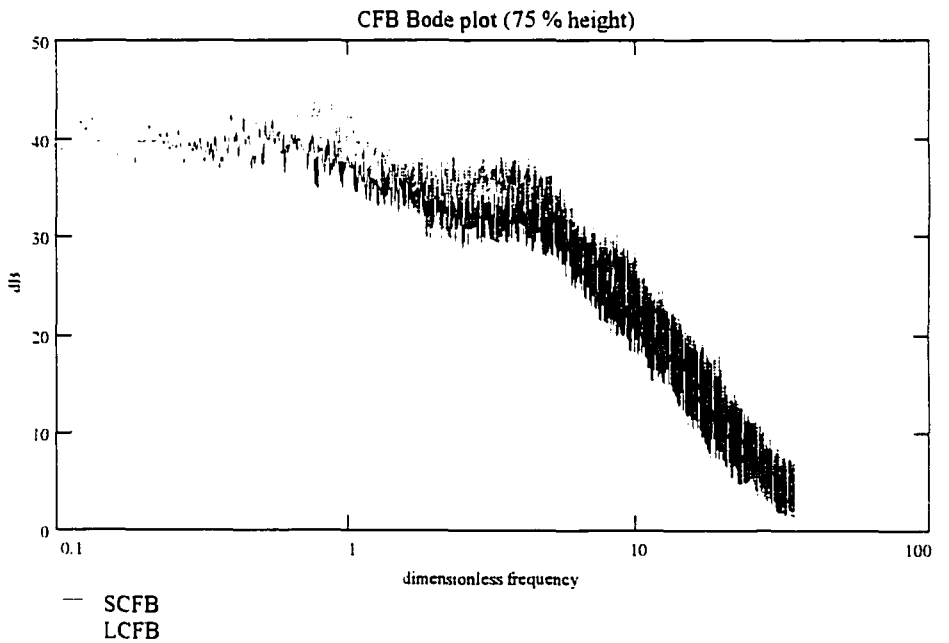
CFB Bode plot (75 % height)
50
40
30
20
10
0
dB
0.1
1
10
100
dimensionless frequency
SCFB
LCFB

CFB Similitude Experiments - Ethan Brue - ISU - 1995

Dimensionless parameters

(1) denotes LCFB
(2) denotes SCFB

	(+/- Uncertainty)
Fr1 = 10650	UFr1 = 823
Fr2 = 10590	UFr2 = 1455
Rep1 = 113	URep1 = 7
Rep2 = 116	URep2 = 16
Gstar1 = 0.0017	UGstar1 = 0.0005
Gstar2 = 0.0017	UGstar2 = 0.0002
Mstar1 = 2.73	UMstar1 = 0.05
Mstar2 = 2.73	UMstar2 = 0.08
ρratio1 = 2147	Upratio1 = 73
ρratio2 = 2160	Upratio2 = 25
Hdp1 = 10160	UHdp1 = 339
Hdp2 = 10160	UHdp2 = 1355
Ddp1 = 339	UDdp1 = 11
Ddp2 = 339	UDdp2 = 45

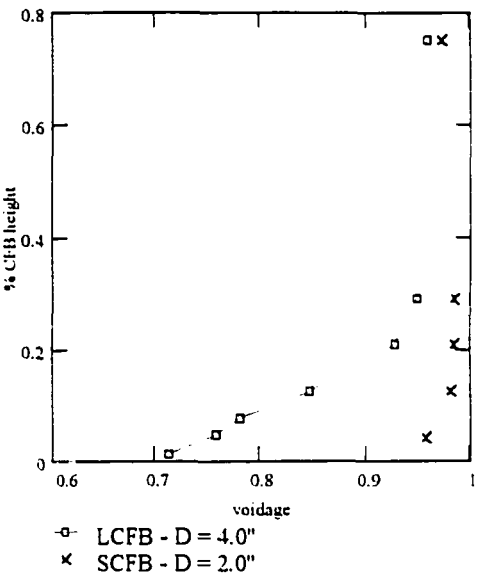

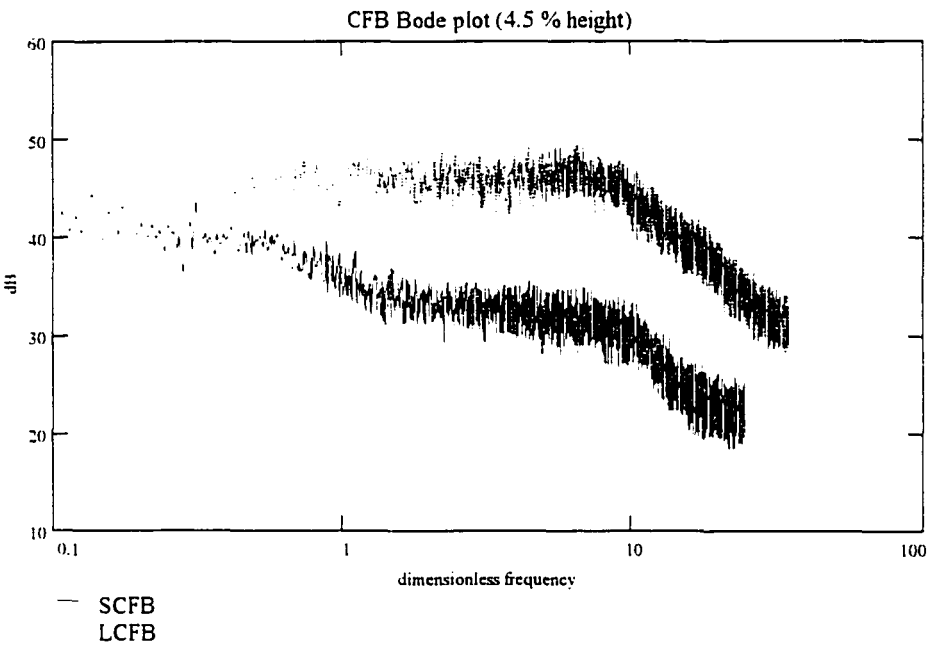

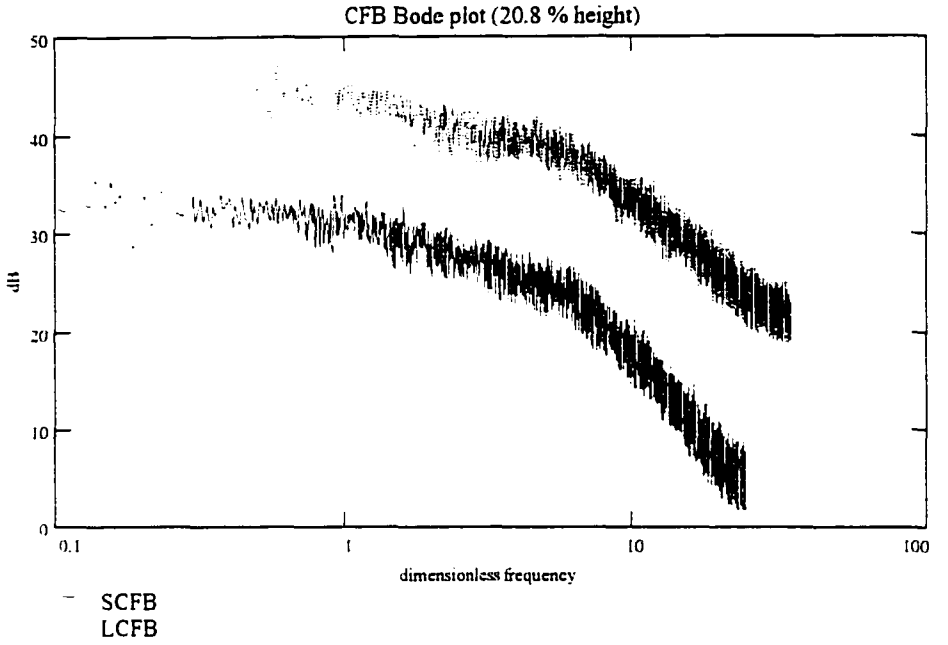
CFB Bode plot (20.8 % height)
50
40
30
20
10
0
dB
0.1
1
10
100
dimensionless frequency
SCFB
LCFB

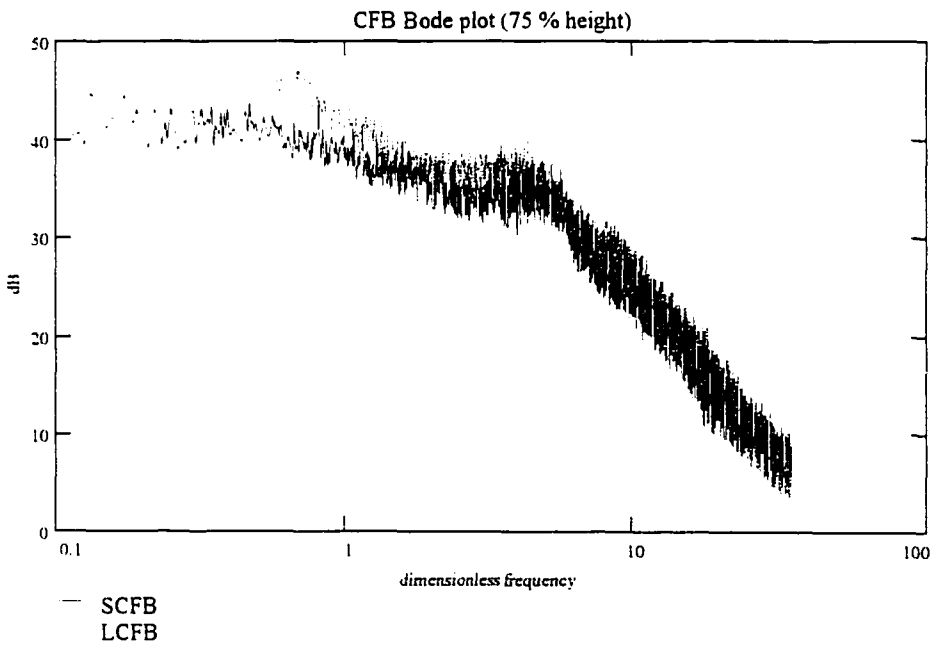
CFB Bode plot (75 % height)
50
40
30
20
10
0
dB
0.1
1
10
100
dimensionless frequency
SCFB
LCFB

CFB Similitude Experiments - Ethan Brue - ISU - 1995

Dimensionless parameters

(1) denotes LCFB
(2) denotes SCFB

	(+/- Uncertainty)
Fr1 = 4073	UFr1 = 304
Fr2 = 3931	UFr2 = 422
Rep1 = 108	URep1 = 6
Rep2 = 109	URep2 = 11
Gstar1 = 0.0010	UGstar1 = 0.0002
Gstar2 = 0.0009	UGstar2 = 0.0001
Mstar1 = 2.10	UMstar1 = 0.05
Mstar2 = 2.10	UMstar2 = 0.08
ρratio1 = 2147	Upratio1 = 73
ρratio2 = 2145	Upratio2 = 25
Hdp1 = 7620	UHdp1 = 191
Hdp2 = 7620	UHdp2 = 762
Ddp1 = 254	UDdp1 = 6
Ddp2 = 254	UDdp2 = 25

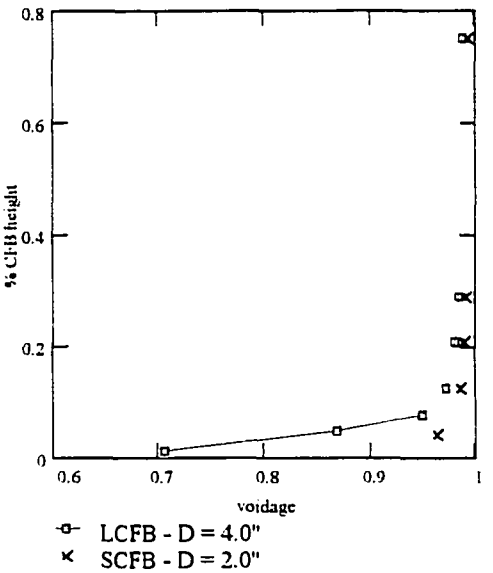

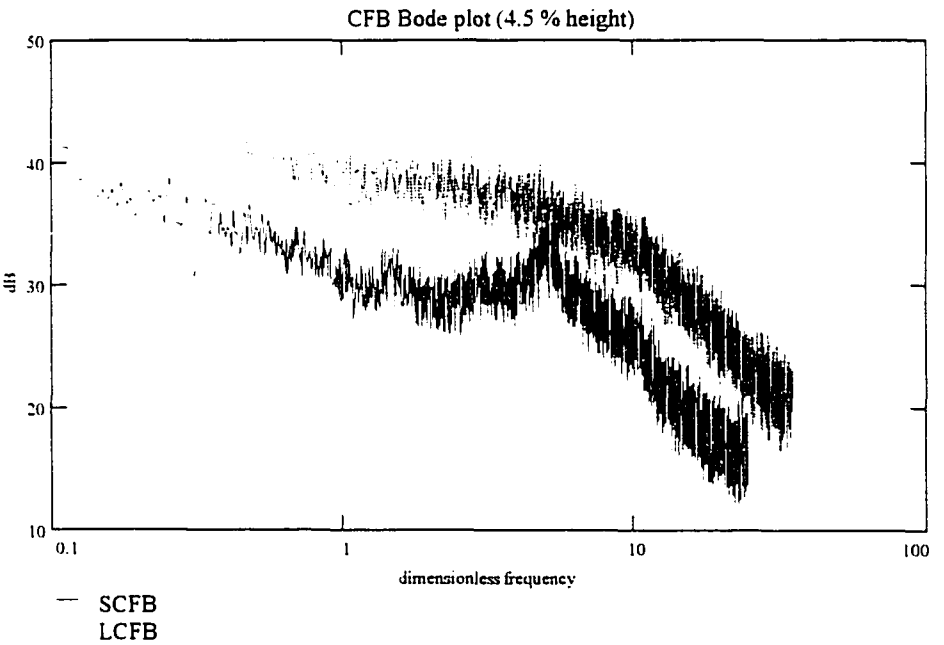

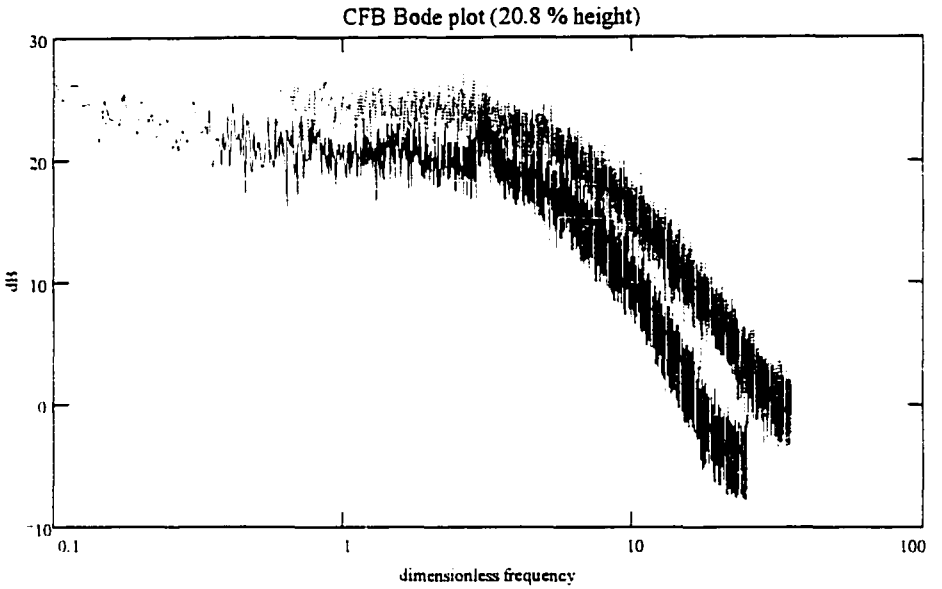
CFB Bode plot (20.8 % height)
30
20
10
0
-10
dB
0.1
1
10
100
dimensionless frequency
SCFB
LCFB

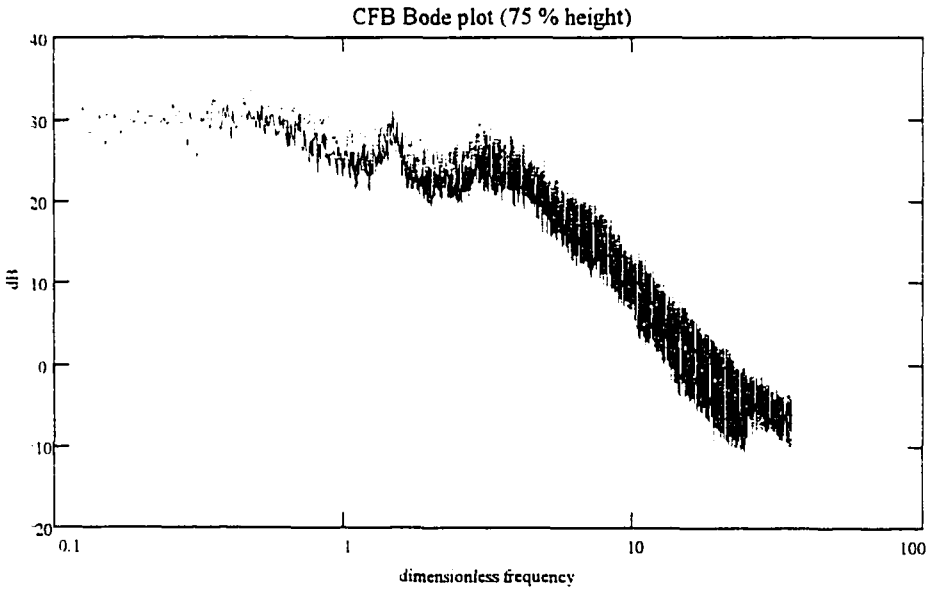
CFB Bode plot (75 % height)
40
30
20
10
0
-10
-20
dB
0.1
1
10
100
dimensionless frequency
SCFB
LCFB

CFB Similitude Experiments - Ethan Brue - ISU - 1995

Dimensionless parameters

(1) denotes LCFB
(2) denotes SCFB

	(+/- Uncertainty)
Fr1 = 5639	UFr1 = 419
Fr2 = 5553	UFr2 = 590
Rep1 = 127	URep1 = 7
Rep2 = 130	URep2 = 13
Gstar1 = 0.0011	UGstar1 = 0.0003
Gstar2 = 0.0012	UGstar2 = 0.0001
Mstar1 = 2.10	UMstar1 = 0.05
Mstar2 = 2.10	UMstar2 = 0.08
pratio1 = 2147	Upratio1 = 73
pratio2 = 2145	Upratio2 = 25
Hdp1 = 7620	UHdp1 = 191
Hdp2 = 7620	UHdp2 = 762
Ddp1 = 254	UDdp1 = 6
Ddp2 = 254	UDdp2 = 25

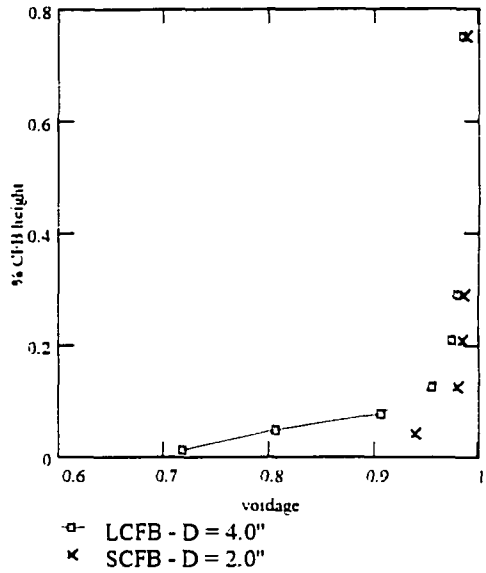

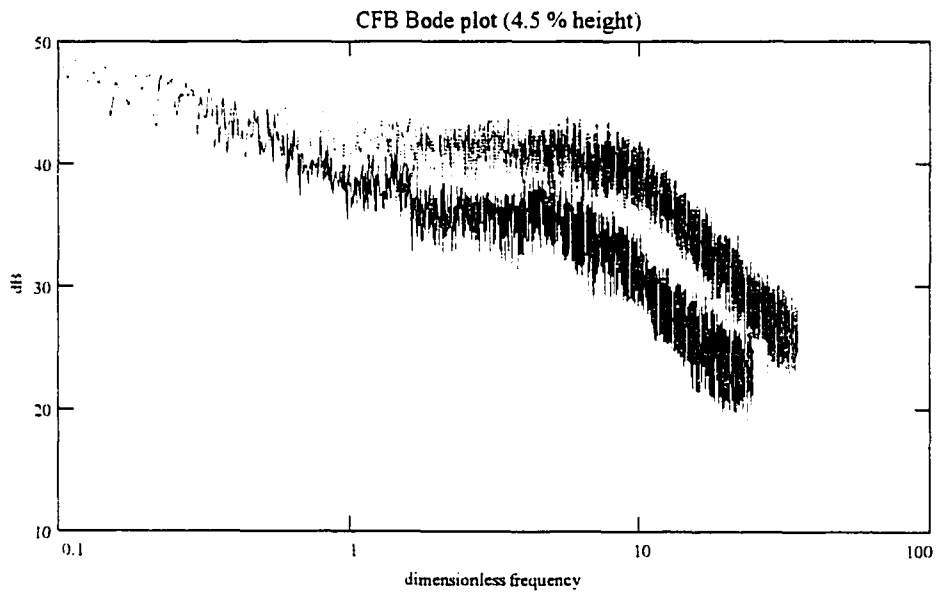

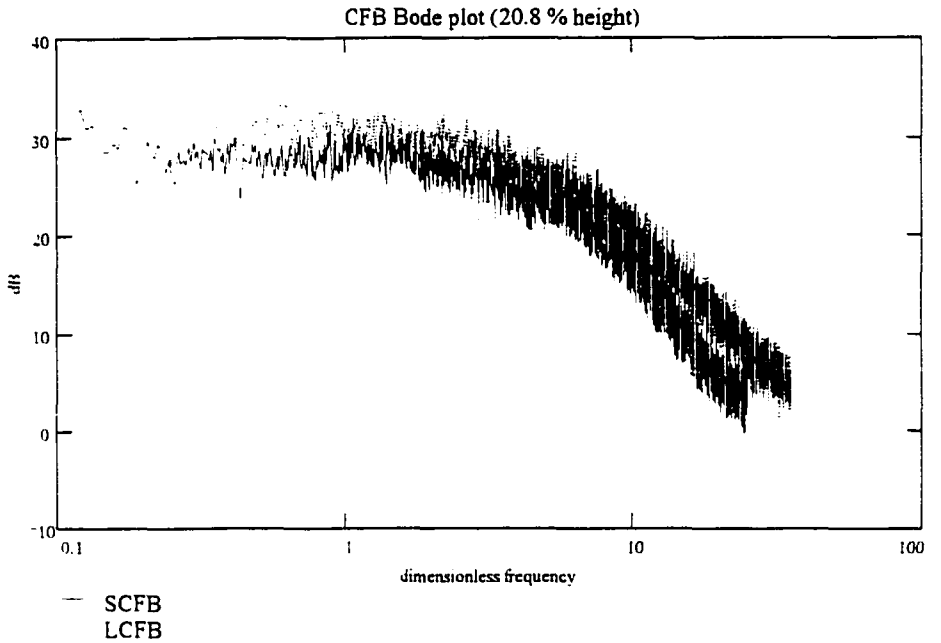
CFB Bode plot (20.8 % height)
40
30
20
10
0
-10
dB
0.1
1
10
100
dimensionless frequency
SCFB
LCFB

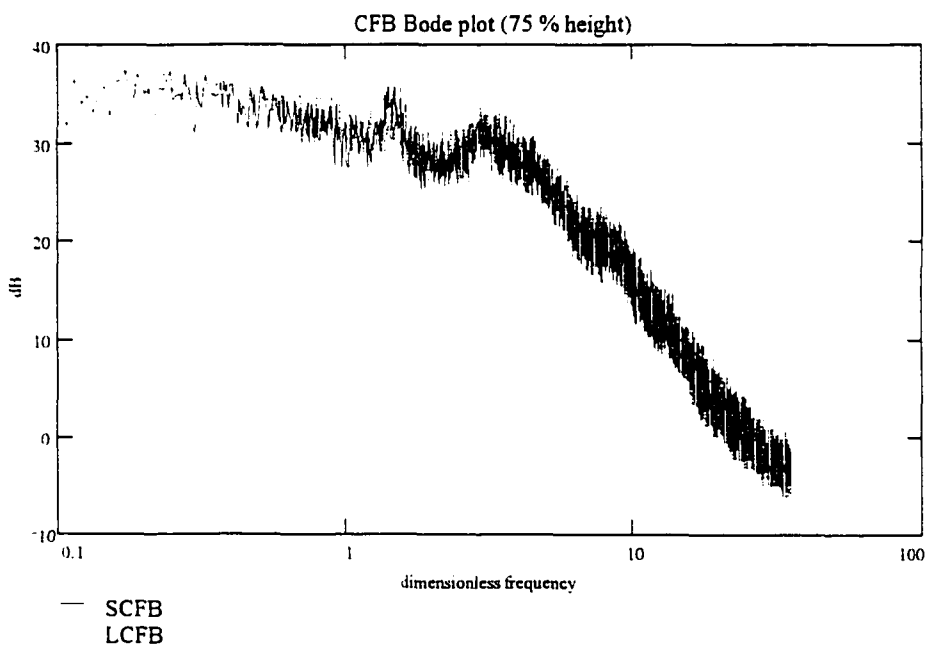
CFB Bode plot (75 % height)
40
30
20
10
0
-10
dB
0.1
1
10
100
dimensionless frequency
SCFB
LCFB

CFB Similitude Experiments - Ethan Brue - ISU - 1995

Dimensionless parameters

(1) denotes LCFB
(2) denotes SCFB

	(+/- Uncertainty)
Fr1 = 5699	UFr1 = 423
Fr2 = 5553	UFr2 = 590
Rep1 = 127	URep1 = 7
Rep2 = 130	URep2 = 13
Gstar1 = 0.0012	UGstar1 = 0.0003
Gstar2 = 0.0016	UGstar2 = 0.0001
Mstar1 = 2.73	UMstar1 = 0.05
Mstar2 = 2.73	UMstar2 = 0.08
ρratio1 = 2147	Uρratio1 = 73
ρratio2 = 2145	Uρratio2 = 25
Hdp1 = 7620	UHdp1 = 191
Hdp2 = 7620	UHdp2 = 762
Ddp1 = 254	UDdp1 = 6
Ddp2 = 254	UDdp2 = 25

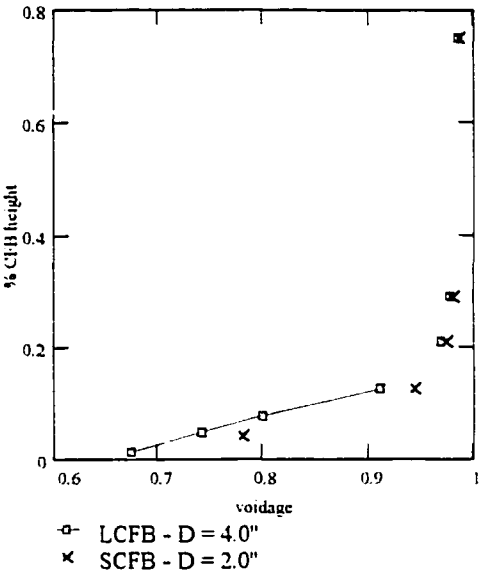

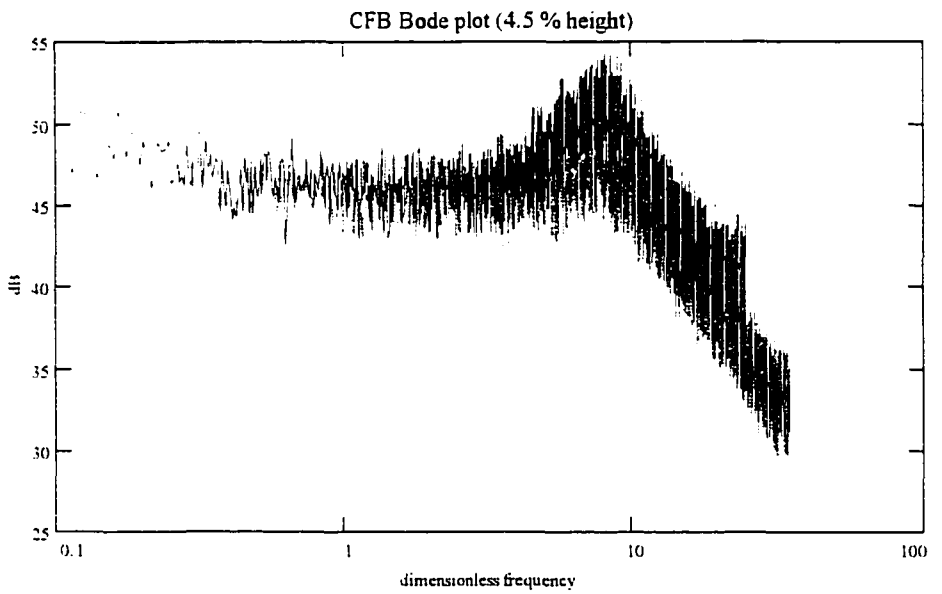

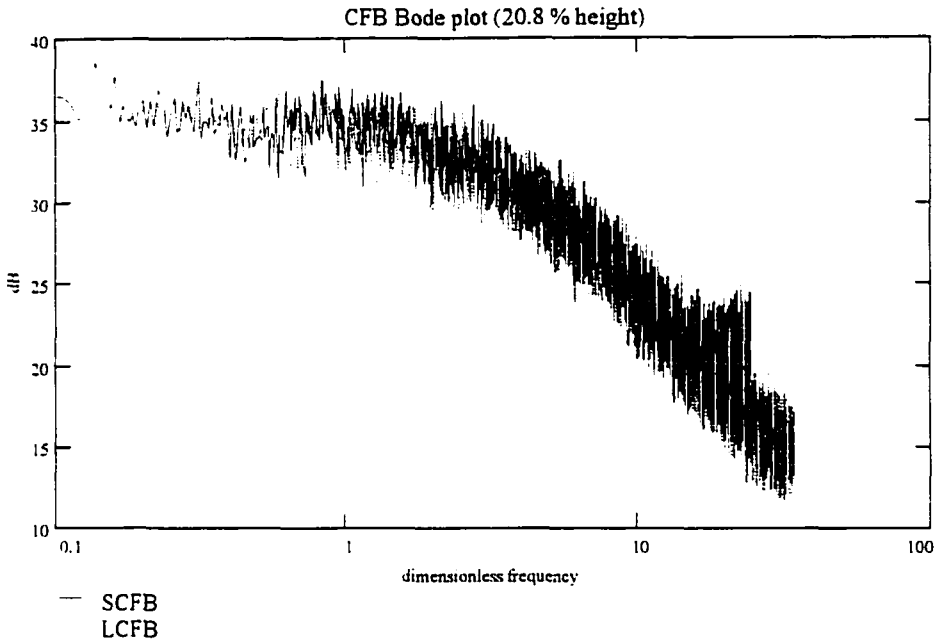
CFB Bode plot (20.8 % height)
40
35
30
25
20
15
10
dB
0.1
1
10
100
dimensionless frequency
SCFB
LCFB

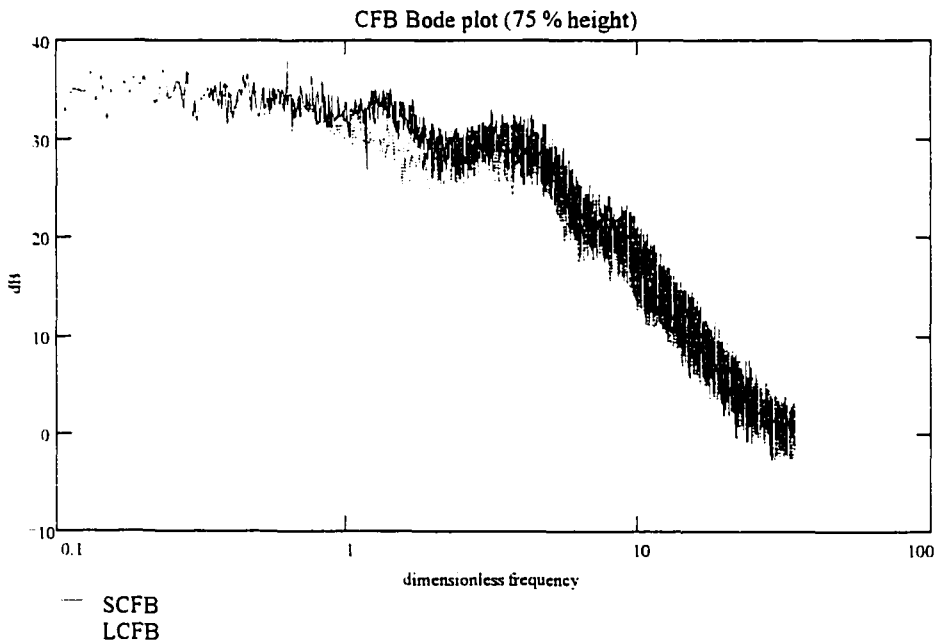
CFB Bode plot (75 % height)
40
30
20
10
0
-10
dB
0.1
1
10
100
dimensionless frequency
SCFB
LCFB

CFB Similitude Experiments - Ethan Brue - ISU - 1995

Dimensionless parameters

(1) denotes LCFB
(2) denotes SCFB

	(+/- Uncertainty)
Fr1 = 8075	UFr1 = 598
Fr2 = 7835	UFr2 = 825
Rep1 = 152	URep1 = 8
Rep2 = 154	URep2 = 16
Gstar1 = 0.0011	UGstar1 = 0.0003
Gstar2 = 0.0014	UGstar2 = 0.0002
Mstar1 = 2.10	UMstar1 = 0.05
Mstar2 = 2.10	UMstar2 = 0.08
ρratio1 = 2147	Uρratio1 = 73
ρratio2 = 2145	Uρratio2 = 25
Hdp1 = 7620	UHdp1 = 191
Hdp2 = 7620	UHdp2 = 762
Ddp1 = 254	UDdp1 = 6
Ddp2 = 254	UDdp2 = 25

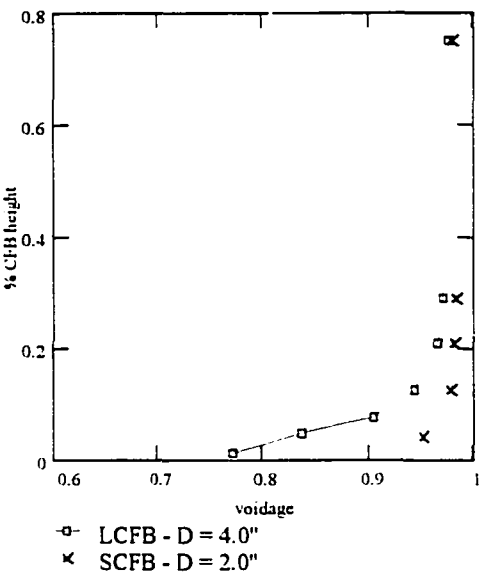

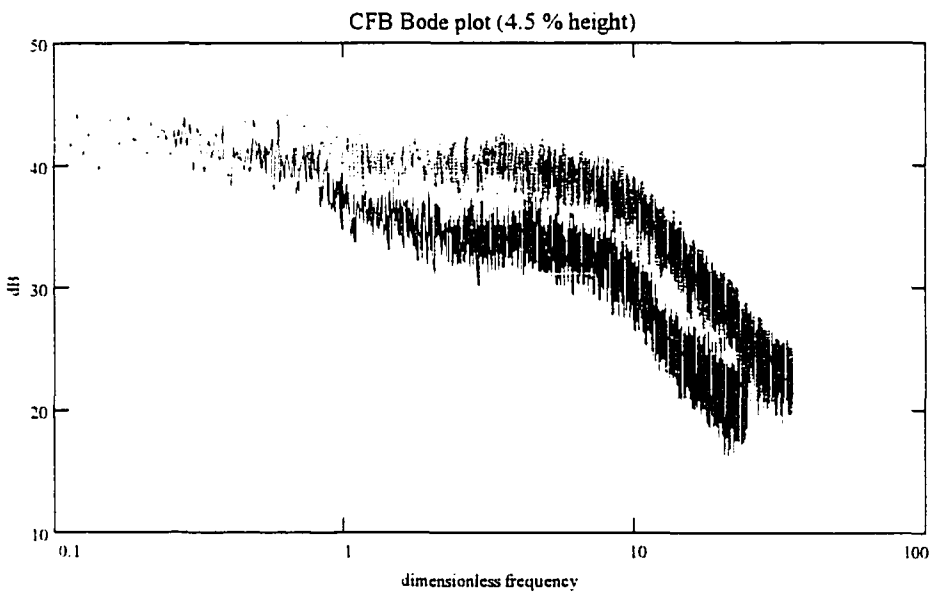

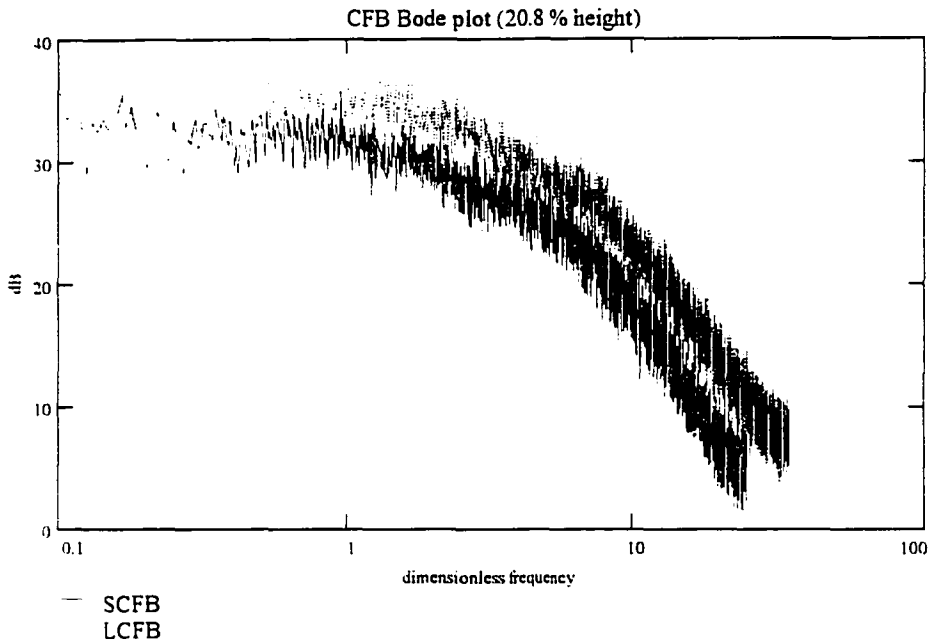
CFB Bode plot (20.8 % height)
40
30
20
10
0
dB
0.1
1
10
100
dimensionless frequency
SCFB
LCFB

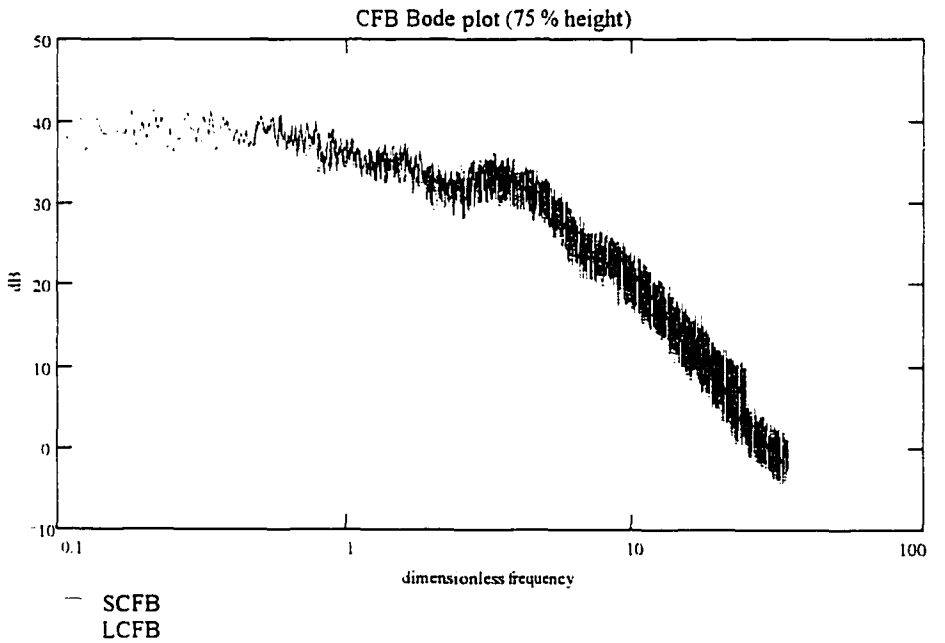
CFB Bode plot (75 % height)
50
40
30
20
10
0
-10
dB
0.1
1
10
100
dimensionless frequency
SCFB
LCFB

CFB Similitude Experiments - Ethan Brue - ISU - 1995

Dimensionless parameters

(1) denotes LCFB
(2) denotes SCFB

	(+/- Uncertainty)
Fr1 = 8075	UFr1 = 598
Fr2 = 7833	UFr2 = 824
Rep1 = 152	URep1 = 8
Rep2 = 154	URep2 = 16
Gstar1 = 0.0012	UGstar1 = 0.0002
Gstar2 = 0.0017	UGstar2 = 0.0003
Mstar1 = 2.73	UMstar1 = 0.05
Mstar2 = 2.73	UMstar2 = 0.08
pratio1 = 2147	Upratio1 = 73
pratio2 = 2145	Upratio2 = 25
Hdp1 = 7620	UHdp1 = 191
Hdp2 = 7620	UHdp2 = 762
Ddp1 = 254	UDdp1 = 6
Ddp2 = 254	UDdp2 = 25

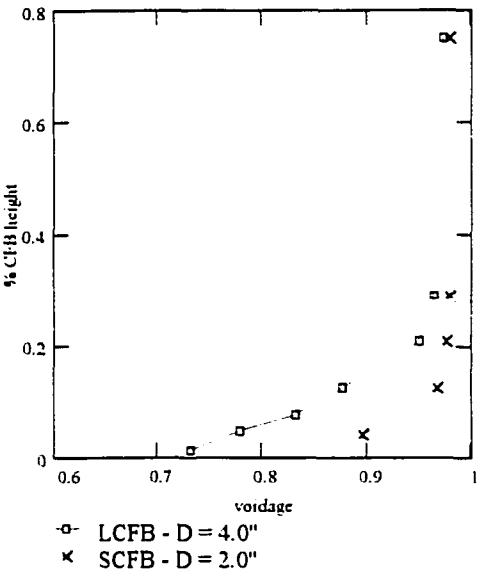

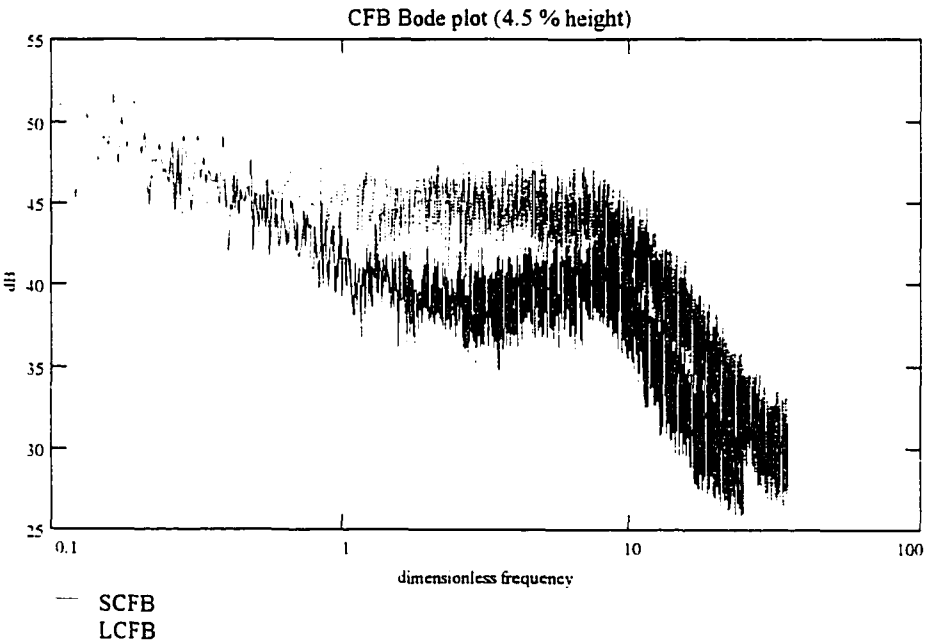

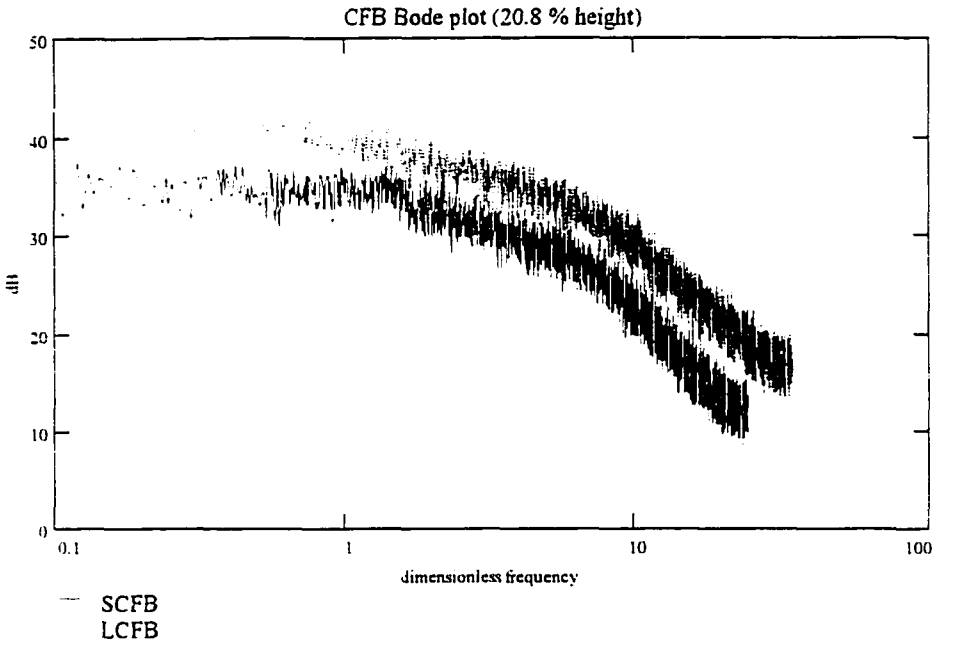
CFB Bode plot (20.8 % height)
50
40
30
20
10
0
dB
0.1
1
10
100
dimensionless frequency
SCFB
LCFB

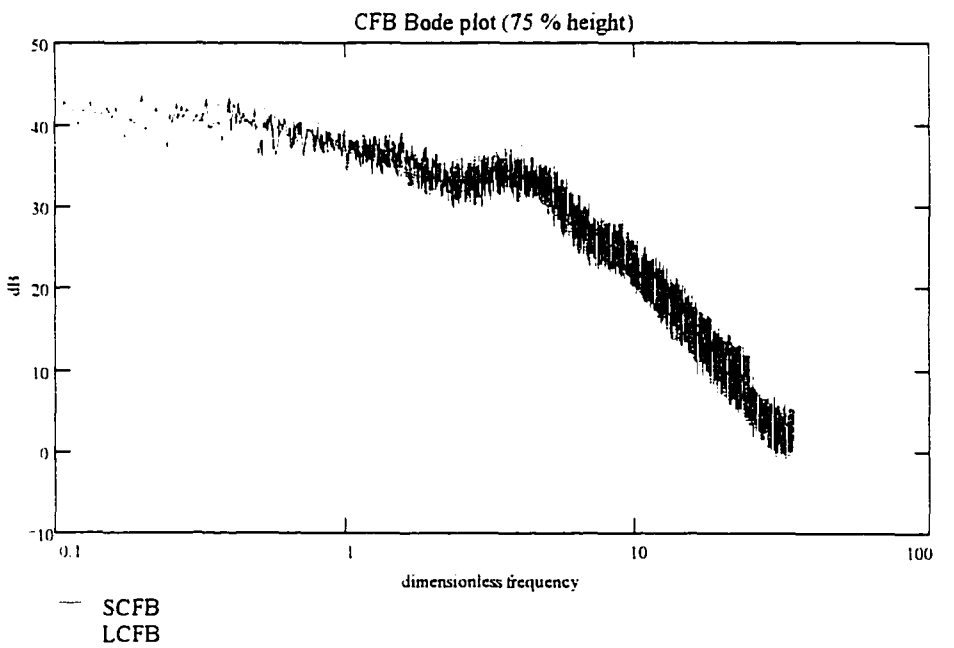
CFB Bode plot (75 % height)
50
40
30
20
10
0
-10
dB
0.1
1
10
100
dimensionless frequency
SCFB
LCFB